

# Chemistry and Enzymology of Vitamin B<sub>12</sub>

Kenneth L. Brown\*

Department of Chemistry and Biochemistry, Ohio University, Athens, Ohio 45701

Received August 25, 2004

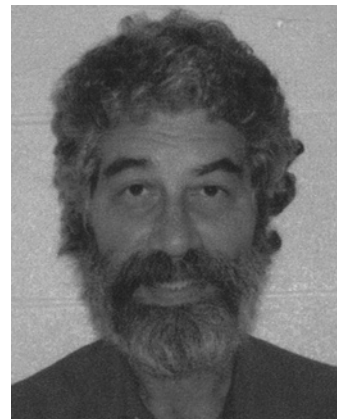
## Contents

1. Introduction	2075
2. Synthesis	2078
3. Structure	2082
4. Solution Chemistry	2086
4.1. Catalysis	2086
4.2. Chemistry of the Carbon–Cobalt Bond	2088
4.3. Ligand Substitution	2092
4.4. Electrochemistry	2095
4.5. Other Reactions	2095
5. Photochemistry	2098
6. Spectroscopy	2099
7. Theory	2101
8. Analysis	2109
9. B <sub>12</sub> Binding Proteins	2109
10. Cobalamins and Nucleic Acids	2110
11. Enzymology	2111
11.1. Coenzyme B <sub>12</sub> -Dependent Enzymes	2111
11.1.1. Class I Mutases	2113
11.1.2. Class II Eliminases	2121
11.1.3. Class II Aminomutases	2134
11.1.4. Other AdoCbl-Dependent Enzymes	2135
11.2. Methyltransferases	2135
11.3. Reductive Dehalogenases	2144
12. Acknowledgment	2145
13. References	2145

## 1. Introduction

The year of this writing, 2004, marks the 70th anniversary of the Noble Prize shared by Whipple, Minot, and Murphy for their discovery that raw liver contained a substance, the “anti-pernicious anemia” factor, that reversed this anemia in dogs and humans. It also marks the 40th anniversary of Dorothy Crowfoot Hodgkin’s Noble prize for her X-ray diffraction work on numerous important biomolecules, including, of course, the landmark crystal structure of vitamin B<sub>12</sub>, and is also the 10th anniversary of her death. It thus seems a fitting time for a review of the chemistry of B<sub>12</sub>.

While a vast amount of work has been done since the initial isolation of crystalline vitamin B<sub>12</sub> (cyanocobalamin, CNCbl, Figure 1) in 1948 simultaneously by Folkers<sup>1</sup> at Merck, Sharpe, and Dohme and by Smith<sup>2,3</sup> at Glaxo, recent years have seen an upsurge in activity in this area due to several recent develop-



Ken Brown was born in Philadelphia, PA. He earned his B.S. degree in Biochemistry from the University of Chicago in 1968 and his Ph.D. degree in Biochemistry from the University of Pennsylvania in 1971. After working as an NIH Postdoctoral Fellow in the Department of Biochemistry and Biophysics at the University of California at Davis in Lloyd Ingraham’s Laboratory, he joined the faculty in the Department of Chemistry at the University of Texas, Arlington, in 1975. In 1990 he moved to Mississippi State University as Professor and Head of the Department of Chemistry, and in 1996 he moved to Ohio University, where he is now Professor and Chair of the Department of Chemistry and Biochemistry.

ments. These include the development and adoption of theoretical approaches to the formidable cobalt corrinoids and the cloning and overexpression of numerous B<sub>12</sub>-dependent enzymes. The latter has led to the crystallization and solution X-ray diffraction structures for several such enzymes and, consequently, to an explosion of work on the enzymology of B<sub>12</sub> coenzymes.

This review will cover the relevant literature from 1999, when a comprehensive review of the topic appeared in the form of the volume *Chemistry and Biochemistry of B<sub>12</sub>*,<sup>4</sup> edited by Ruma Banerjee, through 2003. It will cover the chemistry and enzymology of cobalt corrinoids comprehensively but will not cover theoretical or experimental studies of the mechanism of substrate rearrangements in coenzyme B<sub>12</sub>-dependent enzymes which have no bearing on the coenzyme itself nor will it cover the biosynthesis of B<sub>12</sub>, medical and biological aspects including B<sub>12</sub> uptake and transport and clinical studies of the roll of vitamin B<sub>12</sub> in the suppression of homocysteine levels (of which there have been very many) or the chemistry of simpler model systems. During the period covered by this review, many reviews covering selected topics have appeared including reviews of B<sub>12</sub> enzymology,<sup>5–21</sup> biosynthesis,<sup>22–25</sup> chemical synthesis,<sup>26</sup> theory,<sup>27,28</sup> electrochemistry,<sup>29</sup> carbon–cobalt bond chemistry,<sup>30</sup> and one general review.<sup>31</sup> An excellent volume<sup>32</sup> resulting from the 4th European

\* To whom correspondence should be addressed. Phone: (740) 593-1737. Fax: (740) 593-0148. E-mail: brownk3@ohiou.edu.

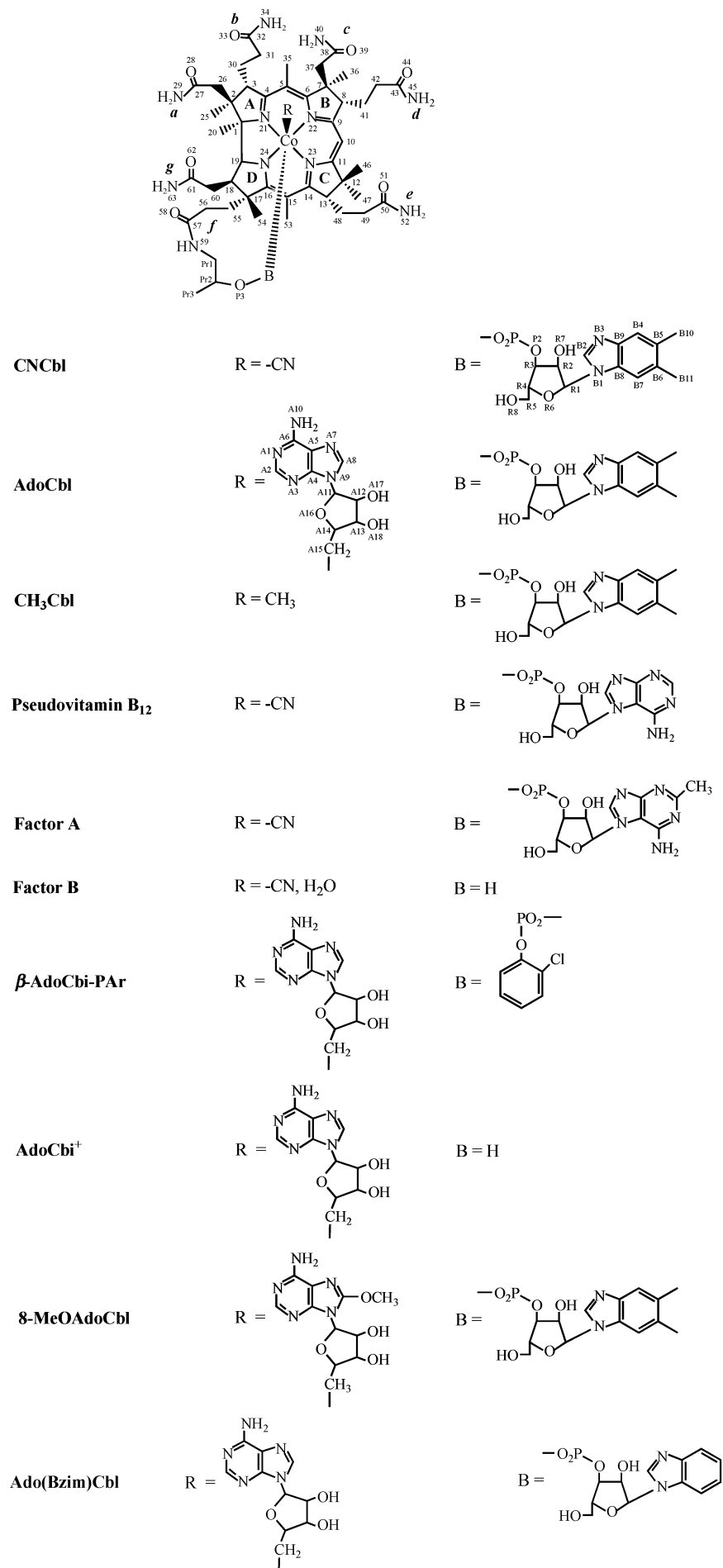


Figure 1.

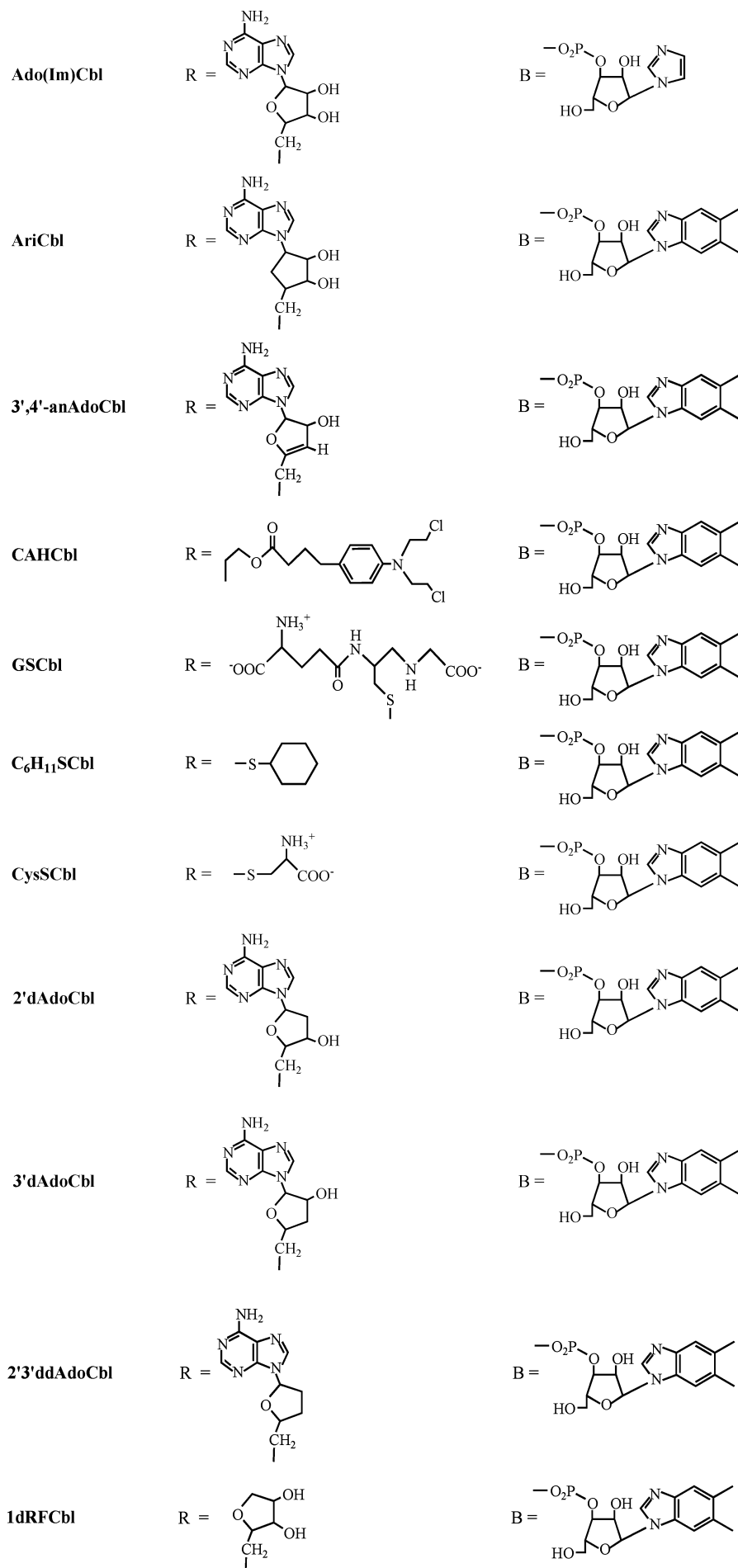
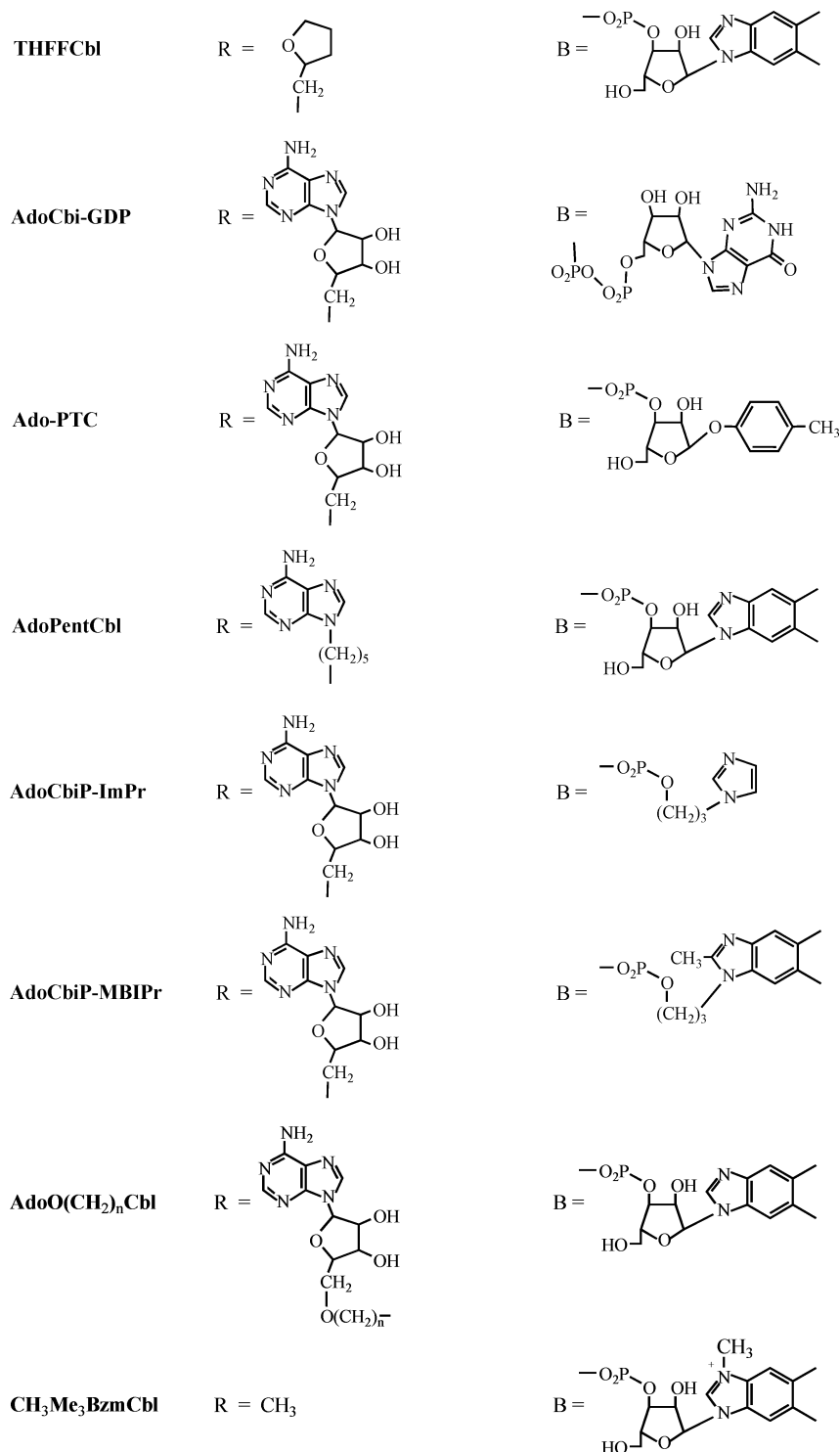


Figure 1 continued.



**Figure 1.** Structure and numbering scheme for cobalt corrinoids referred to in the text.

Symposium on Vitamin B<sub>12</sub> and B<sub>12</sub> Proteins appeared in 1998.

## 2. Synthesis

Brown and co-workers published simplified syntheses of coenzyme B<sub>12</sub> (5'-deoxyadenosylcobalamin, AdoCbl, Figure 1) and a variety of coenzyme analogues altered in the adenosyl ligand (including A10-methyl-, A10,A10-dimethyl-, and A1-methylAdoCbl,

Figure 1) enriched in <sup>13</sup>C in the cobalt-bound carbon.<sup>33,34</sup> The syntheses utilize commercially available [5-<sup>13</sup>C]D-ribose, proceed in good yield (overall yield of 25% for [A15-<sup>13</sup>C]AdoCbl itself), and replace an earlier 11-step synthesis<sup>35</sup> which had an overall yield of <3%.

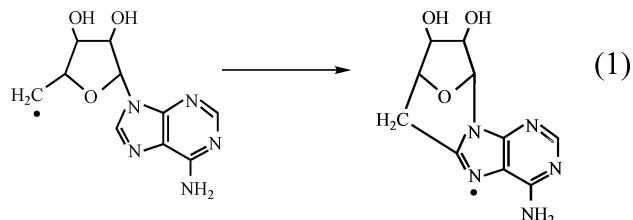
Fonseca and Escalante-Semerena<sup>36</sup> reported an enzymatic synthesis of AdoCbl in which Co(III) corrinoids are reduced with isolated ferredoxin (flavodoxin):NADP<sup>+</sup> reductase and flavodoxin A and subsequently adenosylated with ATP by the ATP:co-

(I)rrinoid adenosyltransferase of *Salmonella enterica*.

Kräutler and co-workers<sup>37</sup> synthesized Ado-13-epiCbl and CH<sub>3</sub>-13-epiCbl, epimers of the normal cobalamins in which the configuration at corrin ring C13 is inverted so that the *e*-propionamide side chain is axially “upward”. For the syntheses CN-13-epiCbl is reduced by controlled potential reduction at  $-1.1$  V for 5.5 h, followed by addition of the alkylating agent, 5'-*O*-tosyladenosine or methyl iodide, and 2 more hours of controlled potential reduction to produce the products in ca. 90% yield. The yield is not a significant improvement over that previously obtained by chemical reduction (with zinc and acetic acid) followed by alkylation with 5'-chloro-5'-deoxyadenosine.<sup>38</sup> Kräutler and co-workers<sup>39</sup> subsequently used a similar electrochemical strategy to synthesize the 5'-deoxyadenosyl derivatives of naturally occurring analogues of vitamin B<sub>12</sub> in which the axial 5,6-dimethylbenzimidazole is replaced by adenine (*Coβ*-cyano-(adenin-7-yl)cobamide, pseudovitamin B<sub>12</sub>, Figure 1) or 2-methyladenine (*Coβ*-cyano-(2-methyladenin-7-yl)cobamide, Factor A, Figure 1) in yields of 70–85%.

White and Finke<sup>40</sup> synthesized 5'-deoxyadenosylcobinamide 2-chlorophenyl phosphate ( $\beta$ -AdoCbi-PAr, Figure 1), a zwitterionic analogue of the axial base-free coenzyme analogue 5'-deoxyadenosylcobinamide (AdoCbi<sup>+</sup>, Figure 1). The idea was to obtain a zwitterionic AdoCbi<sup>+</sup> analogue in the hope that such species, unlike the cationic RCbi<sup>+</sup>s, might be crystallizable and lead to an X-ray crystal structure, a feat which has never been accomplished for an RCbi<sup>+</sup>. The method employed treatment of Factor B (a mixture of diastereomeric aquacyanocobinamides, Figure 1) with a 5-fold molar excess of 2-chlorophenyl phosphodi(1,2,4-triazolide) in dry CH<sub>3</sub>CN/pyridine and afforded the desired coenzyme analogue in 25% yield. Attempts to crystallize the analogue were reported as in progress; however, there have been no further reports to date.

Finke and co-workers<sup>41</sup> also reported the synthesis of 8-methoxy-5'-deoxyadenosylcobalamin (8-MeO-AdoCbl, Figure 1), a coenzyme analogue which upon Co–C bond homolysis produces an analogue of the 5'-deoxyadenosyl radical (Ado•) which cannot undergo the rapid cyclization ( $k \approx 5 \times 10^5 \text{ s}^{-1}$  at 110 °C in ethylene glycol)<sup>41</sup> characteristic of the Ado• radical<sup>42</sup> (eq 1). The analogue was obtained by treatment of



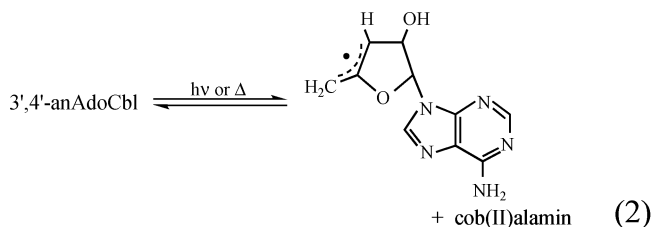
8-bromoadenosine with excess sodium methoxide followed by tosylation, and the 5'-*O*-tosyl-8-methoxyadenosine was then used to reductively alkylate aquacobalamin (H<sub>2</sub>OCbl<sup>+</sup>). The 8-methoxy substitution was shown to have a minimal effect on the thermal homolysis of the carbon–cobalt bond. Oddly,

the photolysis of this analogue was not studied. Unlike AdoCbl itself, 8-MeOAdoCbl would be expected to be quite stable to photolysis in the absence of oxygen and other radical scavengers, as, for example, CH<sub>3</sub>Cbl is. This is because the bimolecular recombination of the solvent-separated radicals produced by photolysis is under diffusion control and consequently very rapid. Thus, in the absence of radical scavengers, CH<sub>3</sub>Cbl is quite photostable. However, because of the competing unimolecular cyclization of the Ado• radical, AdoCbl is very photolabile even in the absence of scavengers.

To begin to address the role, if any, of the axial base in the enzymatic acceleration of Co–C bond homolysis in AdoCbl Brown and co-workers<sup>43</sup> synthesized analogues of AdoCbl with benzimidazole (Ado(Bzim)Cbl, Figure 1) or imidazole (Ado(Im)Cbl, Figure 1) as the axial base. The relevant vitamin B<sub>12</sub> analogues, CN(Bzim)Cbl and CN(Im)Cbl, were obtained by “guided biosynthesis”<sup>44</sup> by fermentation of *Propionibacterium shermanii* on media supplemented with either benzimidazole or imidazole and then reductively adenosylated with 5'-chloro-5'-deoxyadenosine.

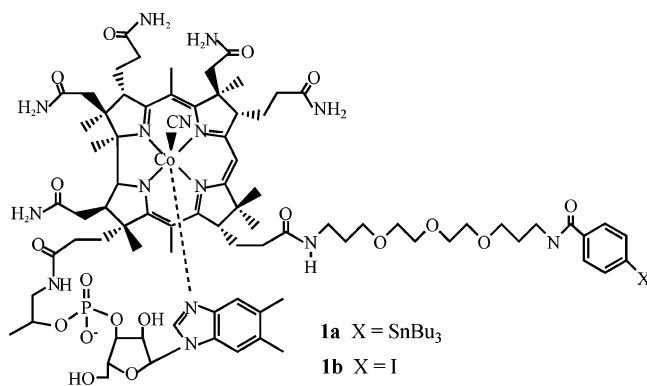
Rétey and co-workers<sup>45</sup> designed a vastly improved synthesis of enantiomerically pure aristeromycylcobalamin (AriCbl, Figure 1), the carbocyclic analogue of AdoCbl, which allows for the facile incorporation of <sup>13</sup>C into the cobalt-bound carbon. Commercially available (1*S*,4*R*)-*cis*-acetoxycyclopent-2-ene-1-ol is coupled to chloropurine and then treated with benzoyl chloride, and the <sup>13</sup>C label was introduced by reaction of the product with phenylsulfonyl[<sup>13</sup>C]-nitromethane, synthesized from sodium phenylsulfonate and [<sup>13</sup>C]nitromethane. After several more steps, enantiomerically pure (2'*S*,3'*R*,4'*R*)-(-)-aristeromycin was obtained along with its 2',3'-bis-epi isomer. After chlorination with thionyl chloride in HMPA, it was used to reductively alkylate HOCbl.

Magnusson and Frey<sup>46</sup> reported the synthesis 3',4'-anhydro-5'-deoxyadenosylcobalamin (3',4'-anAdoCbl, Figure 1). Homolysis of the Co–C bond of this coenzyme produces the 5'-deoxy-3',4'-anhydroadenosine-5'-yl radical (eq 2), an allylically stabilized version of the Ado• radical. The coenzyme analogue was synthesized by reductive alkylation of HOCbl with 3',4'-anhydroATP catalyzed by the ATP:corrinoid adenosyltransferase (CobA).<sup>47,48</sup> 3',4'-anAdoCbl is thermally unstable and sensitive to oxygen and consequently cannot be obtained in high purity. Interestingly, it is stable to anaerobic photolysis in the absence of radical traps, apparently due to the stability of the 3',4'-an Ado• radical and its inability to undergo the cyclization reaction that the Ado• radical suffers (eq 1).

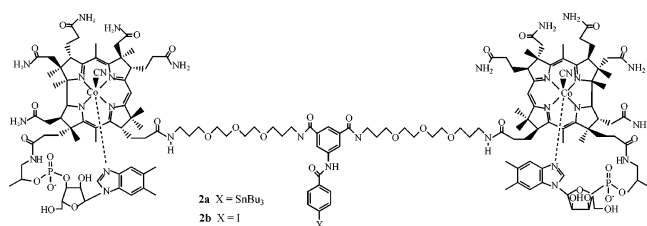


There has been much interest lately in bioconjugates of B<sub>12</sub> as diagnostic and therapeutic agents for cancer. This is because solid malignant tumors require prodigious amounts of B<sub>12</sub> for growth and analogues conjugated to fluorescent probes or drugs can be taken up as their transcobalamin II (TCII) complexes by tumor cells. There are many potential linkage points on the B<sub>12</sub> molecule, including the side chain amides (or their free acids), the 2'- and 5'-hydroxyls on the lower axial ligand, and even the phosphate (i.e., for phosphate triesters). Grissom and co-workers<sup>49</sup> synthesized chlorambucil-hydroxyethylcobalamin (CAHCbl, Figure 1) in which chlorambucil is esterified to the  $\beta$ -hydroxyl of 2-hydroxyethylCbl. The reagent is taken up by leukemia cells via receptor-mediated endocytosis and is nontoxic until the drug is released from the cobalamin.

Wilber and co-workers<sup>50</sup> synthesized radioiodinated cobalamins by conjugation to the *e*-side chain. CNCbl was hydrolyzed to produce a mixture of the *b*-, *d*-, and *e*-monocarboxylates, and the latter was reacted with 4,7,10-trioxa-1,3-tetrafluorophenyl (TFP) ester to give the adduct **1**. This analogue can be cross-linked with a stannylbenzoylaminoisophthalate di-TFP ester to give the dimeric analogue, **2** (the racemic structure in the original report is incorrect). The conjugates **1a** and **2a** were radioiodinated by reaction with *N*-chlorosuccinamide and Na<sup>[125I]</sup> in methanol with radiochemical yields of 17–42%. The

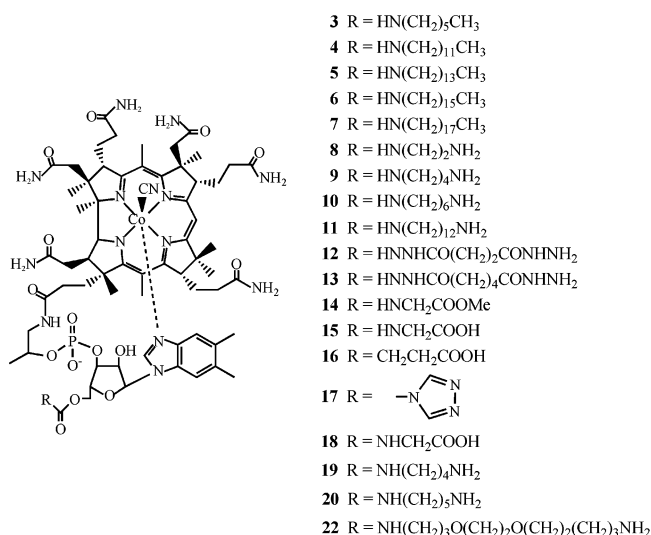


dimer was found to bind to transcobalamin II (TCII), a serum B<sub>12</sub> binding protein, as tightly as unmodified CNCbl itself, although the monomer bound less tightly. Size exclusion chromatography showed that in dimer binding 30% of the dimer had two molecules of TC II bound.



Other bioconjugates have been made with attachments at the axial benzimidazole nucleoside ribose C5'. McEwan et al.<sup>51</sup> activated the ribose 5' hydroxyl of CNCbl with 1,1'-carbonyldiimidazole, 1,1'-carbo-

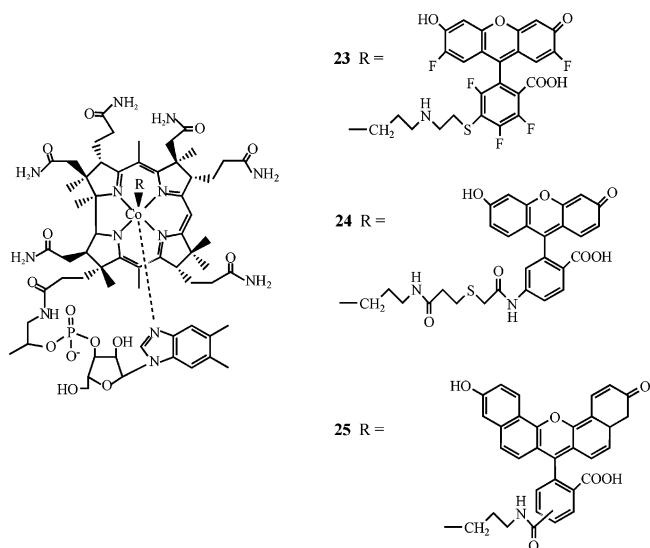
nyldi(1,2,4-triazole), or di(1-benzotriazolyl)carbonate and then added aminoalkanes, diaminoalkanes, or alkanedihydrazides to produce analogues **3–16**.



These derivatives are said to have affinity for intrinsic factor (IF) similar to that of the CNCbl *e*-monocarboxylate (CNCbl-*e*-COO<sup>-</sup>) and affinity for haptocorrin (Hc) similar to or higher than CNCbl itself. This, however, is a puzzling observation since Hc is known to bind Cbls axial nucleotide “down” with the upper axial ligand position inaccessible to the solution but the lower axial ligand position inaccessible. It thus seems highly unlikely that derivatives with bulky modifications at the ribose 5' carbon would bind to Hc as tightly as CNCbl. A possible explanation is that the competition assay used to determine the analogue binding relative to that of CNCbl does not come to equilibrium on the time scale of the experiments but is in fact a kinetic competition assay due to the very large binding constant for CNCbl to Hc ( $5 \times 10^{16} \text{ M}^{-1}$ )<sup>53</sup> and the consequent very slow dissociation rate. Grissom and co-workers<sup>54</sup> synthesized **17–22** using similar chemistry and characterized the derivatives by <sup>13</sup>C and DEPT NMR.

Hogenkamp et al.<sup>55</sup> reported the synthesis of the *nido*-carborane-cobalamin conjugates CNCbl-*b-nido*-carborane, CNCbl-*d-nido*-carborane, and CNCbl-*b,d*-bis-*nido*-carborane by reaction of *o*-carboranoyl chloride with 1,4-diaminobutane to produce *nido*-carboranoyl(4-amidobutyl)amine, which was then coupled to CNCbl-*b*-COO<sup>-</sup>, CNCbl-*d*-COO<sup>-</sup>, or CNCbl-*b,d*-(COO<sup>-</sup>)<sub>2</sub>. One boron atom is eliminated during the synthesis as demonstrated by mass spectrometry and <sup>11</sup>B NMR. The *nido*-carborane conjugates were found to bind to TCII in human serum, giving rise to the possibility that <sup>10</sup>B *nido*-carborane-cobalamins could be useful in cancer therapy via neutron capture therapy.

Finally, fluorescent B<sub>12</sub> derivatives **23–25** have been synthesized by treating 3-aminopropylCbl<sup>56</sup> with commercially available *N*-hydroxysuccinimide



esters of Oregon Green, fluorescein, and naphthofluorescein.<sup>57</sup>

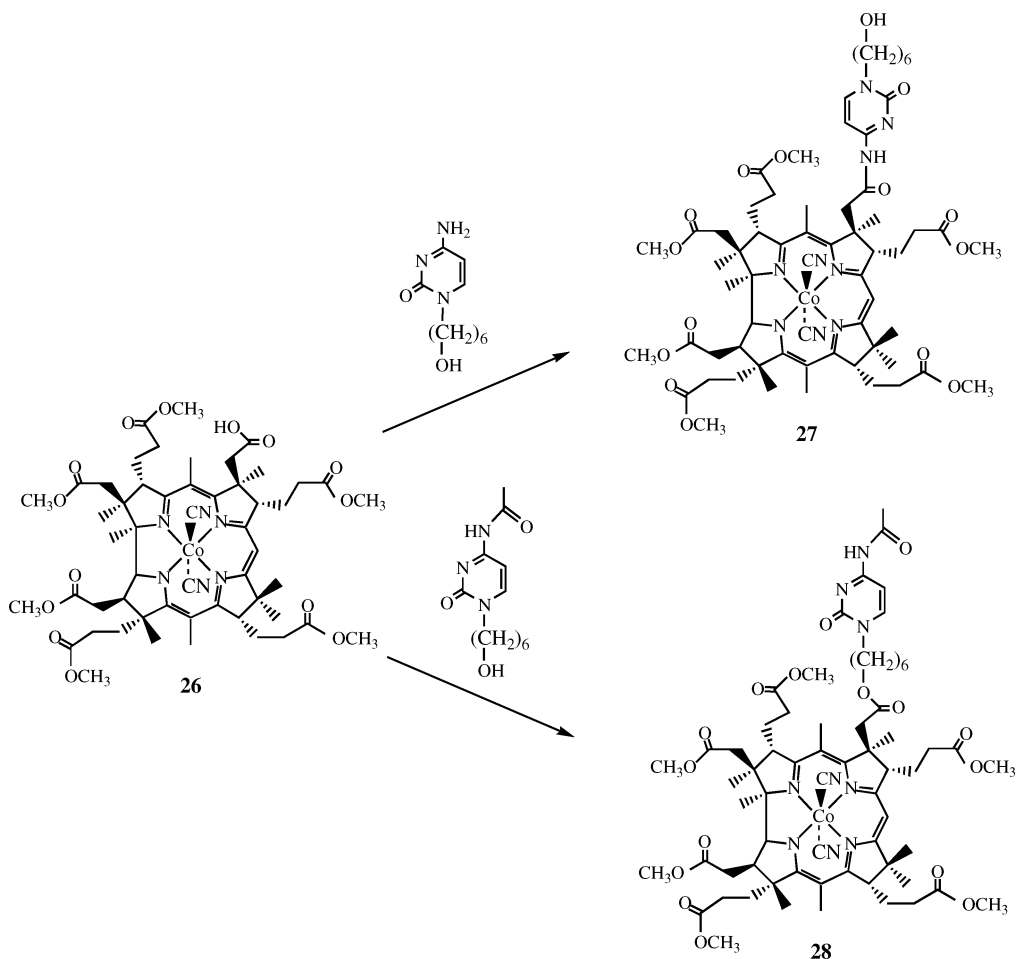
There has also been interest in cobalamins with thiolato ligands, both because of the existence of the naturally occurring glutathionylcobalamin ( $\gamma$ -glutamylcysteinylglycylcobalamin GSCbl, Figure 1),<sup>58,59</sup> which may be the *in vivo* precursor of AdoCbl, and because of the possibility that Cbl-cysteine residue complexes might be involved in AdoCbl-dependent enzyme reactions or their inhibition by H<sub>2</sub>O<sub>2</sub>Cbl<sup>+</sup>. Finke and

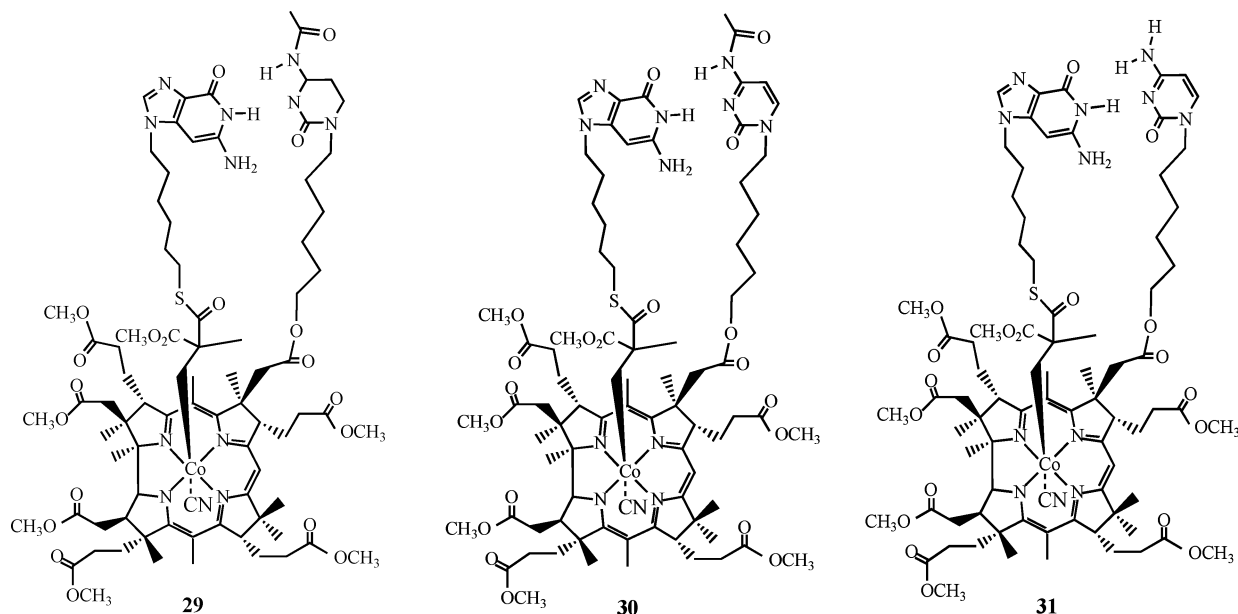
co-workers<sup>60</sup> described the preparation of cyclohexylthiolatocobalamin (C<sub>6</sub>H<sub>11</sub>SCbl, Figure 1) and cysteinylcobalamin (CysSCbl, Figure 1) by addition of ca. 1 equiv of the thiol to H<sub>2</sub>O<sub>2</sub>Cbl<sup>+</sup> in MeOH or water. C<sub>6</sub>H<sub>11</sub>SCbl is unstable in anaerobic aqueous solution, apparently decomposing to a cyclohexylthiyl radical and cob(II)alamin with a half-life of about 6 h. CysSCbl was even more unstable ( $t_{1/2} \leq 10$  s).<sup>61</sup>

GSCbl, on the other hand, is far more stable than C<sub>6</sub>H<sub>11</sub>SCbl or CysSCbl. Seeking the reason for the additional stability of GSCbl, Finke and co-workers<sup>61</sup> synthesized the two dipeptide cysteinylcobalamins,  $\gamma$ -glutamylcysteinylcobalamin ( $\gamma$ -GluCysCbl) and cysteinylglycylcobalamin (CysGlyCbl). The latter proved to be more stable than CysSCbl but more than 100-fold less stable than GSCbl, while  $\gamma$ -GluCysCbl was as stable as GSCbl. The crystal structure of  $\gamma$ -GluCysCbl was also reported (see below).

Keese and co-workers<sup>62</sup> synthesized B<sub>12</sub> analogues with cytosine or *N*-acetylcytosine attached to a side chain. Dicyanocob(III)yrinic acid-*a,b,d,e,f,g*-hexamethyl ester (cobester-*c*-acid, **26**, Scheme 1) was treated with 1-(6-hydroxyhexyl)-cytosine or 1-(6-hydroxyhexyl)-*N*<sup>4</sup>-acetylcytosine in the presence of *N*-(3-(dimethylamino)propyl)-*N'*-ethylcarbodiimide hydrochloride (EDC·HCl) to give analogues **27** and **28** (Scheme 1), respectively. The structures serve as a starting point for the synthesis of a model for the AdoCbl-dependent methylmalonylCoA mutase reaction in which a

**Scheme 1**





model substrate radical will be held in close proximity to the metal atom by a G–C base pair.

The model was completed by Sun and Darbre,<sup>63</sup> who synthesized the organocobalt derivatives **29**–**31** from **28**. These complexes have an organic ligand with a dimethylmalonate-like group (which models the substrate for the methylmalonylCoA mutase reaction) bound to cobalt via the carbon analogous to the radical-bearing carbon of the methylmalonyl-CoA mutase reaction and also tethered to a guanine residue to allow G–C base pairing to hold the “substrate” radical formed by photolysis in the proximity of the metal. Surprisingly, photolysis of the models does not produce any “succinate”-like rearranged products despite the fact that an earlier model using A–T base pairing showed substantial rearrangement.<sup>64</sup> The authors speculated that in the A–T model Hoogsteen base pairing occurred, which is not possible in the G–C base pair, or that the C6 alkyl chain at the G N(9) somehow prevents the intramolecular G–C interaction and that intermolecular G–G interaction prevailed; however, little or no evidence was available for either hypothesis.

Fraga and Keese<sup>65</sup> also described the synthesis of a cobester analogue with dipyrrole side chain. Reaction of 2,2-bis(6-*N*-pyrrylhexyl)ethanol with cobester-*c*-acid in the presence of EDC·HCl (Scheme 2) gives the dipyrrole analogue **32** in 74% yield. The deriva-

tive is to be used to prepare conductive polypyrrole films bearing a B<sub>12</sub> derivative on platinum electrodes.

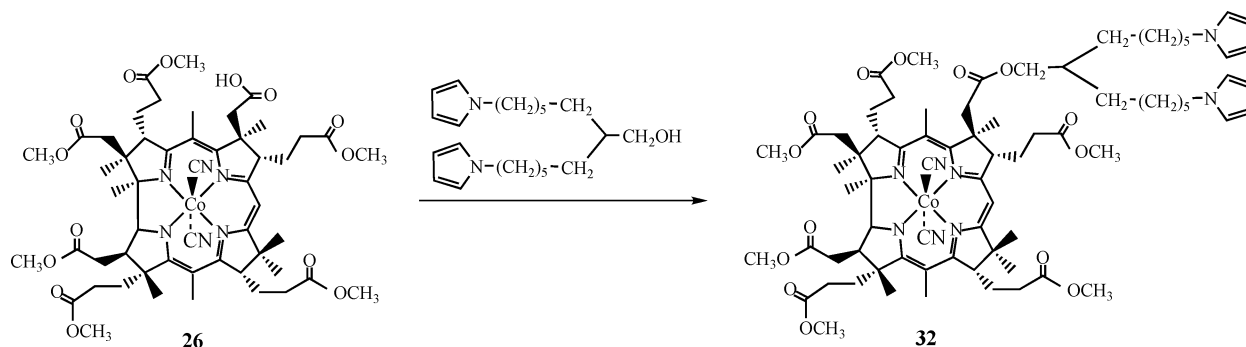
Hisaeda and co-workers<sup>66</sup> synthesized dicyanoheptapropylcobyrinate (**33**) and dicyanoheptaocylcobyrinate (**34**) by refluxing dicyanoheptamethylcobyrinate in the appropriate dry alcohol with added H<sub>2</sub>SO<sub>4</sub>. The dicyano–Co(III) and –Co(II) were studied in lipid monolayers by surface pressure molecular area isotherms. The heptaocyl derivative appeared to be face-on oriented with a molecular area of about 3 nm<sup>2</sup>, but the heptapropyl derivative gave unstable monolayers which collapsed even at low pressures. However, mixing the heptapropyl Co(II) derivative with a lysine-functionalized lipid significantly stabilized the monolayer, presumably by coordination of the lysine amino group to the Co(II) center.

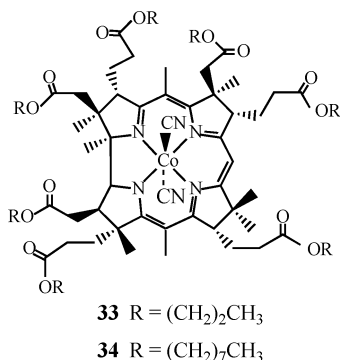
Finally, Hisaeda and co-workers<sup>67</sup> reported the preparation of a B<sub>12</sub> derivative conjugated to a crown ether. Dicyanoheptamethylcobyrinate (**35**) was nitrated at C10 with nitronium tetrafluoroborate, and the nitro group was reduced to an amine with NaBH<sub>4</sub> (Scheme 3). Reaction with 4-formyl-benzo-18-crown-6 gave the derivative **36**. Binding of K<sup>+</sup> to the B<sub>12</sub>–crown ether conjugate was demonstrated by NMR.

### 3. Structure

The molecular structure of cobalt corrinoids is well known. Generally, they crystallize in the orthorhom-

Scheme 2





tric space group  $P2_12_12_1$  with four molecules per unit cell. The coordination geometry is tetragonally distorted pseudo-octahedral, with four equatorial nitrogen donors from the corrin ring. The corrin ring is quite flexible and folds upward about the C10–Co axis. This fold is quantified as the fold angle, defined as the angle between the normal to the least-squares planes through N21–C4–C5–C6–N22–C9–C10 and through C10–C11–N23–C14–C15–C16–N24.<sup>68</sup> One important finding from structural studies of RCbl's is the so-called "inverse trans effect"<sup>69</sup> for alkylCbl's in which increasing  $\sigma$ -donation from R leads to an increase in the length of both the upper ( $\beta$ ) Co–L bond and the lower ( $\alpha$ ) Co–NB3 bond despite expectations to the contrary. Much activity in the period covered by this review is the result of the increased use of synchrotron radiation to produce high-resolution structures of these rather large molecules and the continued use of NMR-based methods to determine solution structures.

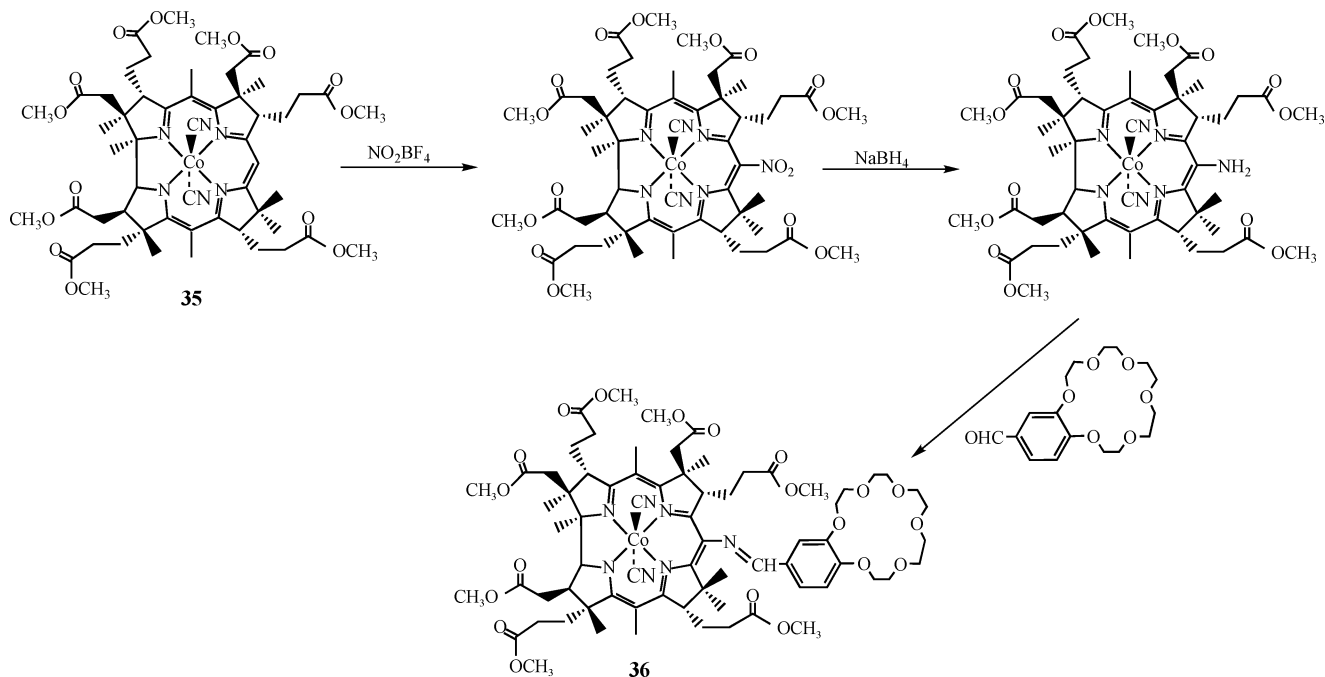
Randaccio and co-workers<sup>70</sup> obtained crystals of NO<sub>2</sub>Cbl·2LiCl and NO<sub>2</sub>Cbl·NaCl by the hanging drop method in the presence of either LiCl or NaCl and PEG400 as the precipitant. NCSCbl and NCSeCbl were crystallized by addition of acetone to aqueous solutions. In NO<sub>2</sub>Cbl·2LiCl (but *not* NO<sub>2</sub>Cbl·NaCl)

the NO<sub>2</sub> group is disordered with two orientations that differ by rotation about the Co–N bond by about 60°. Crystals of NCSCbl contained both N- and S-bound linkage isomers with occupancies of about 0.55 and 0.45, respectively. However, NCSeCbl contained only the Se-bound isomer. From the Co–NB3 bond distances the trans effect of SCN and NO<sub>2</sub> is very similar (1.992(6), 2.014(5), and 1.994(4) Å for NO<sub>2</sub>Cbl·2LiCl, NO<sub>2</sub>Cbl·NaCl, and NCSCbl, respectively), but SeCN has a slightly larger trans effect (Co–NB3 2.020(5) Å).

Randaccio and co-workers<sup>71</sup> also reported the first structures of Cbl's with sulfur donor ligands, i.e., sulfitoCbl and thioureaCbl. Crystals of SO<sub>3</sub>Cbl(NH<sub>4</sub>) and [(NH<sub>2</sub>)<sub>2</sub>CS]Cbl were grown by the hanging drop method from solutions containing LiCl and ammonium sulfate, but the crystals did not contain LiCl. The Co–S bond lengths for the two complexes were very similar (SO<sub>3</sub>Cbl(NH<sub>4</sub>), 2.231(1) Å; [(NH<sub>2</sub>)<sub>2</sub>CS]Cbl, 2.216(7) Å), but the Co–NB3 bond lengths are significantly different (SO<sub>3</sub>Cbl(NH<sub>4</sub>), 2.134(7) Å; [(NH<sub>2</sub>)<sub>2</sub>CS]Cbl, 2.01(1) Å), suggesting that sulfite has a stronger trans influence (similar to CH<sub>3</sub>) than thiourea based on the inverse trans effect in RCbl's.

The X-ray crystal structures of SCNCbl, NCSeCbl, and NO<sub>2</sub>Cbl as well as NaS<sub>2</sub>O<sub>3</sub>Cbl have also been reported by Perry et al.<sup>72</sup> The SCNCbl crystals contained only N-bound complex, although <sup>13</sup>C NMR measurements in solution showed a mixture of linkage isomer. In NaS<sub>2</sub>O<sub>3</sub>Cbl the Co–S bond is 2.286(1) Å, slightly longer than those in SO<sub>3</sub>Cbl(NH<sub>4</sub>) and [(NH<sub>2</sub>)<sub>2</sub>CS]Cbl, the NB3–Co–S angle is 167.05(9)°, and the Co–NB3 distance is 2.078(3) Å. The coordinated S<sub>2</sub>O<sub>3</sub><sup>2-</sup> ligand is hydrogen bonded to the a side chain amide (through one O atom) and the c side chain amide (through the donor S atom). SCNCbl has a very large corrin ring fold angle (22.4°), while the other complexes had more normal fold angles (NCSeCbl, 13.7°; NO<sub>2</sub>Cbl, 14.5°; NaS<sub>2</sub>O<sub>3</sub>Cbl, 17.2°). The

### Scheme 3



large difference in fold angle between SCNCbl and NCSeCbl is attributed to a large difference in Co–X–C angles which causes the axial ligand in NC–SeCbl to make van der Waals contact with C46 and C54, flattening the southern quadrant of the corrin ring, and to the short Co–NB3 bond length in SCNCbl (<2.0 Å), which increases the steric interactions between the axial Bzm and the corrin ring.

The first crystal structure of a thiolatoCbl was also reported during the period covered in this review.<sup>61</sup>  $\gamma$ -Glu-CysCbl (Figure 1) has a Co–S bond length (2.267(2) Å) slightly longer than sulfitoCbl and thio-ureaCbl<sup>71</sup> and an axial Co–NB3 bond length of 2.049(6) Å, nearly the same as CNCbl. Disorder in the  $\gamma$ -Glu-Cys ligand was resolved by two conformations of roughly equal occupancy. The fold angle is an enormous 24.4°, the largest ever observed in a complete cobalamin. With a Co–NB3 distance of 2.049 Å,  $\gamma$ -Glu-CysCbl falls well outside the correlation of fold angle with Co–NB3 distance (see below<sup>73</sup>). The structure provides no obvious reasons for the much greater stability of  $\gamma$ -Glu-CysCbl and GSCbl relative to CysSCbl and CysGlyCbl (see above). Of the possibilities listed by the authors, the most likely are (1) the  $\gamma$ -NH<sub>3</sub><sup>+</sup> group in CysSCbl and CysGlyCbl forms a hydrogen-bonded intermediate with S, leading to more rapid Co–S bond cleavage, and (2) the Glu  $\alpha$ -amino group is H-bonded to the *f* side chain carbonyl O (O58), as suggested from an earlier solution NMR study of GSCbl,<sup>74</sup> but this H-bond was not seen in either conformation of the  $\gamma$ -Glu-CysCbl crystal structure.

In an important paper Randaccio and co-workers<sup>73</sup> report the synchrotron radiation X-ray crystal structures of CH<sub>3</sub>Cbl, CNCbl·2LiCl, and CNCbl·KCl, redeterminations of earlier structures (CH<sub>3</sub>Cbl,<sup>75</sup> CNCbl<sup>44,68</sup>). The crystals were grown by the hanging drop method from solutions containing KF, LiCl, or KCl, with PEG400 as the precipitant, although CH<sub>3</sub>-Cbl crystallized with no salt. Using 12 accurately determined (usually synchrotron radiation) structures the authors calculated new values<sup>76</sup> of the mean bond lengths of the corrin nucleus. These show approximately 2-fold symmetry relative to a line passing through Co and C10. A previous observation<sup>77</sup> of a decrease in the corrin ring fold angle with increasing Co–NB3 bond length is confirmed (Table 1, Figure 2), although there is significant scatter.

An X-ray crystal structure of difluoromethylcobalamin, CF<sub>2</sub>HCbl, has also appeared.<sup>78</sup> Its Co–NB3 bond length, 2.187(7) Å, was originally stated to be almost identical to that of CH<sub>3</sub>Cbl, referring to the older CH<sub>3</sub>Cbl structure.<sup>75</sup> However, the more accurate Randaccio structure<sup>73</sup> of CH<sub>3</sub>Cbl has a Co–NB3 bond length of 2.162(4) Å, so that the axial Co–NB3 bond length in CF<sub>2</sub>HCbl is surprisingly longer than that in CH<sub>3</sub>Cbl. Since the Co–C bond length in CF<sub>2</sub>HCbl (1.949(7) Å) is shorter, as expected, than that for CH<sub>3</sub>Cbl (1.979 Å), CF<sub>2</sub>HCbl fails to follow the inverse trans effect for alkylCbl's. Interestingly, CF<sub>3</sub>Cbl<sup>79</sup> ( $d_{\text{Co-NB3}} = 2.047(10)$  Å,  $d_{\text{Co-C}} = 1.878(12)$  Å) does follow the inverse trans effect with respect to both CF<sub>2</sub>HCbl and CH<sub>3</sub>Cbl. The data in Table 1, along with the data for CF<sub>3</sub>Cbl, can be used to nicely

**Table 1. Axial Bond Lengths and Corrin Ring Fold Angles for XCbl's**

X	Co–X, Å	Co–NB3, Å	fold angle, deg
H <sub>2</sub> O <sup>a</sup>	1.952(2)	1.925(2)	18.7
Cl <sup>b</sup>	2.252(1)	1.981(3)	17.9
NO <sub>2</sub> <sup>c</sup>	1.896(5)	1.989(5)	16.7
N <sub>3</sub> <sup>b</sup>	1.980(3)	1.995(3)	16.8
CN <sup>d</sup>	1.858(10)	2.011(10)	18.0
CN(KCl) <sup>e</sup>	1.868(8)	2.029(6)	14.1
(NH <sub>2</sub> ) <sub>2</sub> CS <sup>f</sup>	2.300(2)	2.032(5)	14.8
CN(LiCl) <sup>e</sup>	1.886(4)	2.041(3)	18.7
CF <sub>3</sub> Cbl <sup>f</sup>	1.878(12)	2.047(10)	15.6
$\gamma$ -Glu-CysCbl <sup>g</sup>	2.267(2)	2.049(6)	24.4
SO <sub>3</sub> <sup>h</sup>	2.231(1)	2.134(4)	16.3
CH <sub>3</sub> <sup>e</sup>	1.979(4)	2.162(4)	14.7
CF <sub>2</sub> H <sup>i</sup>	1.949(8)	2.187(7)	15.6
Ado <sup>j</sup>	2.023(10)	2.214(9)	13.3

<sup>a</sup> Kratky, C.; Färber, G.; Gruber, K.; Deuter, Z.; Nolting, H. F.; Konrat, R.; Kräutler, B. *J. Am. Chem. Soc.* **1995**, *117*, 4654. <sup>b</sup> Randaccio, L.; Geremia, S.; Furlan, M.; Slouf, M. *Inorg. Chem.* **1998**, *37*, 5390. <sup>c</sup> Reference 70. <sup>d</sup> Reference 44. <sup>e</sup> Reference 73. <sup>f</sup> Reference 79. <sup>g</sup> Reference 61. <sup>h</sup> Reference 71. <sup>i</sup> Reference 78. <sup>j</sup> Reference 80.

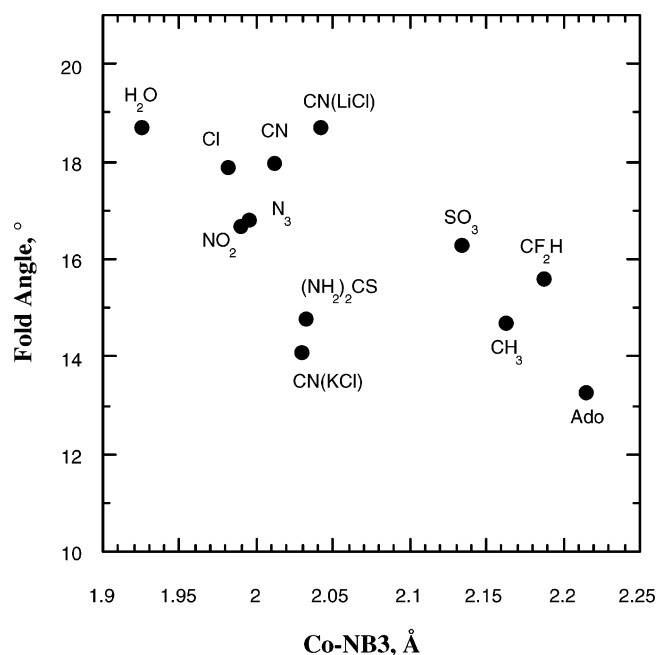


**Figure 2.** Plot of the corrin ring fold angle for XCbl's vs the axial Co–NB3 bond length.

show the inverse trans effect for alkylCbl's but not for XCbl's in general (Figure 3). The structure of CF<sub>2</sub>-HCbl also displays a fold angle of 15.6° (almost identical to that for CH<sub>3</sub>Cbl) and an interaction between the *c*-amide and the organic ligand with a F2–O39 contact of 3.11 Å.

B<sub>12</sub> derivatives catalyze both the enzymatic and nonenzymatic reductive dechlorination of perchloroethylene (PCE) and trichloroethylene (TCE) to ethylene and acetylene (see below). The X-ray structure of *cis*-chlorovinylCbl, suspected to be an intermediate in the nonenzymatic process, has been reported,<sup>80</sup> the first X-ray crystal structure of an RCbl with an sp<sup>2</sup>-hybridized carbon ligand. Reaction of cob(I)alamin with chloroacetylene readily forms *cis*-chlorovinylCbl in 89% yield. The Co–C bond length, 1.953 Å, is shorter than that in CH<sub>3</sub>Cbl (1.979 Å<sup>73</sup>) and AdoCbl (2.023 Å<sup>81</sup>) but longer than that in CF<sub>2</sub>HCbl (1.949-

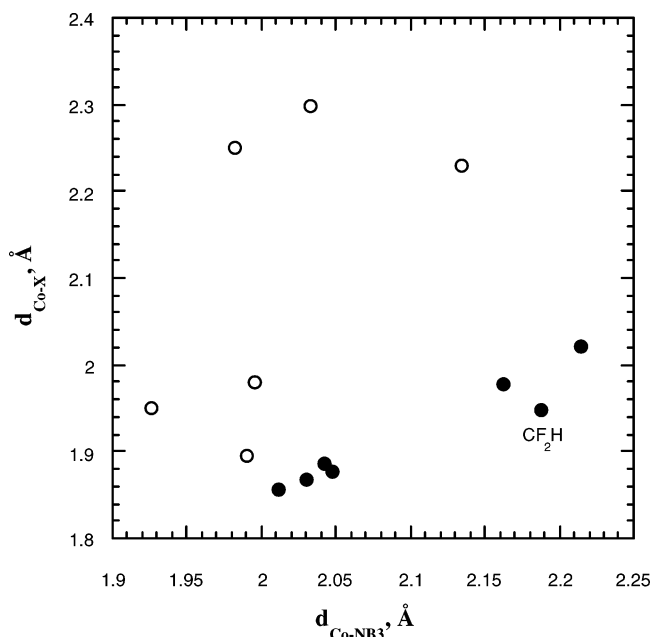


**Figure 3.** Plot of the upper axial Co–X bond length vs the lower axial Co–NB3 bond length for XCbl's. The filled symbols indicate alkylCbl's, while the open symbols are inorganic XCbl's. CF<sub>2</sub>HCbl, which fails to follow the inverse trans effect for alkylCbl's is labeled.

(7) Å<sup>73</sup>) and CF<sub>3</sub>Cbl (1.878(12) Å<sup>79</sup>). The axial Co–NB3 bond length is 2.128 Å compared to 2.162(4) Å for CH<sub>3</sub>Cbl<sup>73</sup> and 2.047(10) Å for CF<sub>3</sub>Cbl,<sup>79</sup> providing another example of the inverse trans effect, although the data for *cis*-chlorovinylCbl does not fall on the same line as the data for the alkylCbl's with sp<sup>3</sup>-hybridized cobalt-bound carbons.

The cobamide cofactor isolated from purified tetrachloroethene reductive dehalogenase from *Dehalospirillum multivorans* is the major corrinoid in this organism. Spectral characterization including 1- and 2-D <sup>1</sup>H, <sup>13</sup>C, and <sup>15</sup>N NMR identifies it as a close analogue of pseudovitamin B<sub>12</sub> (*Coβ*-cyano-7'-adeninylcobamide (Figure 1) which is missing the methyl group at the Pr2 carbon of the nucleotide loop 2-propanolamine moiety (i.e., missing the Pr3 methyl) and has been dubbed norpseudovitamin B<sub>12</sub>.<sup>82</sup> X-ray crystal structures of pseudovitamin B<sub>12</sub>, norpseudovitamin B<sub>12</sub>, and Factor A (redetermining an older structure<sup>83</sup>) were determined using synchrotron radiation and represent the first high-resolution structures of cobamides with adenine axial bases instead of Bzm. The effects of this axial ligand replacement on the inner coordination sphere are small. Substitution of Ade or 2-Me-Ade for Bzm in CNCbl causes a small (0.01–0.02 Å) decrease in the Co–N<sub>ax</sub> and Co–C bond lengths (0.03–0.04 Å). The corrin ring fold angles are slightly larger in pseudovitamin B<sub>12</sub> and norpseudovitamin B<sub>12</sub> and about the same in Factor A as in CNCbl. Pseudovitamin B<sub>12</sub> and norpseudovitamin B<sub>12</sub> have very similar conformations, as expected, the only major difference being the conformation of the *c*-side chain at corrin C7.

Kratky and co-workers<sup>84</sup> redetermined<sup>85</sup> the crystal structure of cob(II)alamin crystallized from *d*<sub>6</sub>-acetone/D<sub>2</sub>O using neutron Laue diffraction with 1.8–8.0 Å neutrons. The difference maps were compared to those obtained from monochromatic neutron diffrac-

tion and high-resolution synchrotron X-ray diffraction data (at 0.9 Å) for the same crystal. The new Laue method allows data collection in 10-fold less time than monochromatic neutron diffraction but with a decrease in resolution (1.43 Å compared to 1.0 Å for monochromatic neutrons) and a poorer signal-to-noise ratio. Laue neutron data enabled the location of many hydrogen and deuterium positions.

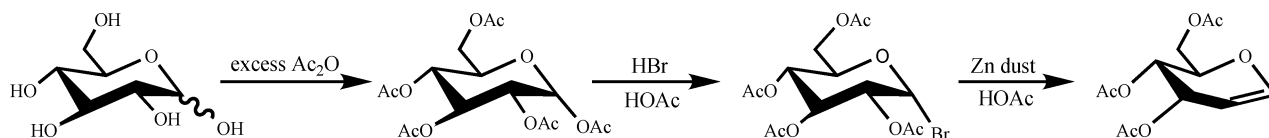
The identity of the native corrinoids from *Clostridium cochlearium* has been determined by NMR methods.<sup>86</sup> Two of three corrinoids obtained as cyano derivatives in a 3:1:1 ratio were identified as pseudovitamin B<sub>12</sub> (Figure 1), about 60%, and Factor A (*Coβ*-cyano-7'-[2-methyl]adeninylcobamide, Figure 1), about 20%, by spectroscopic means. Authentic pseudovitamin B<sub>12</sub> was obtained by guided biosynthesis<sup>44</sup> fermenting *Propionibacterium shermanii* on adenine and characterized by UV-vis, CD, MS, and complete assignment of <sup>1</sup>H, <sup>13</sup>C, and <sup>15</sup>N NMR spectra. The third corrinoid, which proved to be an isomer of Factor A by mass spectrometry, is thought to be *Coβ*-cyano-7'-[6-methyl]adeninylcobamide.

The solution structure of AdoCbl and AdoCbi<sup>+</sup> (Figure 1) were determined by NMR-restrained molecular dynamics (MD) and simulated annealing (SA).<sup>87</sup> The nOe cross-peaks for both compounds are consistent with two solution conformations, one in which the Ado ligand lies over the C ring, as in the crystal structure (the “southern” conformation), and one in which the Ado ligand is over C10 (the “eastern” conformation). Two-state modeling allowed calculation of consensus structures for each compound. The consensus structure for the southern conformation agrees well with the solid-state structure and has a very similar fold angle (13.5° vs 13.3°) and inner-sphere geometry. The corrin ring is much more rigid in AdoCbl than in AdoCbi<sup>+</sup> or other RCbl's studied by these methods. The rigidity is attributed to the presence of two bulky axial ligands in AdoCbl (the Ado and the Bzm) vs other structures with only one bulky ligand. The fold angle in the AdoCbi<sup>+</sup> model (9.0°) is significantly smaller than that in AdoCbl (13.3°).

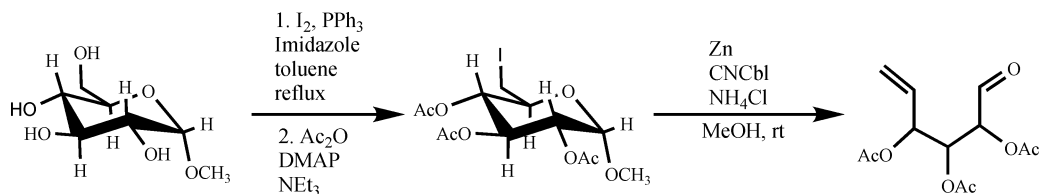
An NMR-based solution structure of Ado-13-epiCbl<sup>37</sup> generally agrees with an earlier NMR-restrained molecular modeling structure.<sup>38</sup> The most important difference was the observation of nOe's that are compatible with a *syn* conformation of the Ado ligand being significantly populated. These nOe's were not observed in the earlier study.

Finally, Kräutler and co-workers<sup>88</sup> reported an NMR-based solution structure of CH<sub>3</sub>Cbl using nOe distance restraints and dihedral angles derived from coupling constants. The principle finding is that the nucleotide loop conformation is significantly different from the solid state structure available at the time,<sup>75</sup> as previously seen in an nOe-restrained molecular modeling study.<sup>89</sup> However, the new, more accurate crystal structure of CH<sub>3</sub>Cbl<sup>73</sup> shows the solution and solid-state nucleotide loop conformations to be more similar.

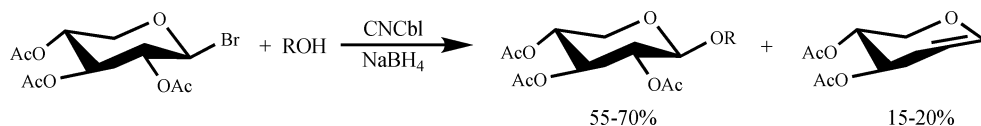
## Scheme 4



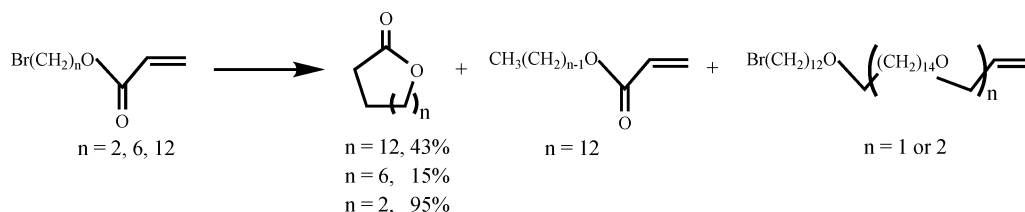
## Scheme 5



## Scheme 6



## Scheme 7



## 4. Solution Chemistry

## 4.1. Catalysis

$B_{12}$  derivatives have long been exploited as useful and often efficient catalysts. Their catalytic utility results from the ready availability of three oxidation states, the ease of formation of alkyl-Co derivatives by a variety of mechanisms at all three oxidation states, and lability of the Co-C bond which is easily cleaved thermally or photolytically. Thus, cobalt corrinoids have been employed effectively as electrochemical catalysts as well as covalent catalysts. In most cases mechanistic studies have not been pursued rigorously, and much in the way of catalytic mechanism in this area remains highly speculative. Nonetheless, there has been active research on the utility of cobalt corrinoids as catalysts during the period covered by this review.

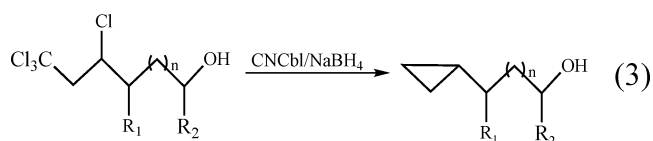
For example, Forbes and Franck<sup>90</sup> used CNCbl to improve the Fischer-Zach synthesis of glycols, unsaturated sugars with a C1-C2 double bond (Scheme 4). Using CNCbl and zinc dust with ammonium chloride in methanol for the final step they both avoided the acidic conditions and improved the yield to as high as 95%. They speculate that the mechanism involves reduction of CNCbl to cob(I)-alamin followed by alkylation of Cbl with the brominated sugar derivative and reductive elimination to give the glycal. This mechanism is actually quite reasonable considering the fact that cyclohexylCbl<sup>91</sup> and secondary alkylCbl's<sup>92</sup> are metastable compounds

in neutral solution (but are stabilized in acid as their base-off forms) and that isopropylCbl decomposes to form propylene. Other mechanisms are, of course, possible.

Similarly, Jäger and co-workers<sup>93</sup> used CNCbl with Zn/ $NH_4Cl$  for the fragmentation of 6-deoxy-6-iodopyranosides to  $\omega$ -unsaturated hexose derivatives, as shown in Scheme 5, for example, for  $\alpha$ -D-glucopyranoside.

Again, Petrovic et al.<sup>94</sup> treated 1-bromo- $\beta$ -D-xylose peracetate with linear alcohols (C1-C8) in the presence of catalytic (2 mol %) cob(I)alamin (by reduction of CNCbl with  $NaBH_4$ ) to obtain alkyl- $\beta$ -D-xylopyranosides in 55-70% yield (Scheme 6) along with xylal reductive elimination products. Again, the anticipated organoCbl derivative was postulated to be the catalytic intermediate.

Petrovic and co-workers<sup>95</sup> also used CNCbl/ $NaBH_4$  to catalyze the reduction of tetrachloroalkanols to cyclopropane alkanols (eq 3). Yields of ca. 70% were obtained for five examples.

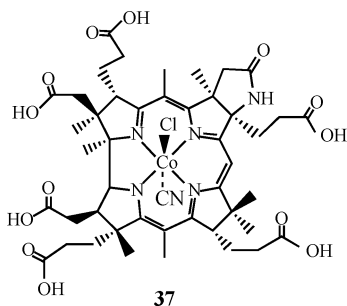


Electrolysis of bromoalkyl acrylates in DMF in the presence of heptamethylcob(II)yrinic acid produces cyclic lactones in moderate yield (Scheme 7).<sup>96</sup> The reaction is severely inhibited by the spin

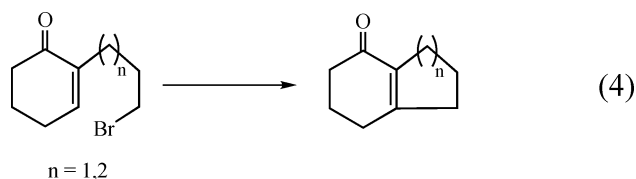
trapping agent  $\alpha$ -phenyl-*N*-(*tert*-butyl) nitron. A photosensitive intermediate with a Co–C bond was characterized by electronic spectroscopy and electrospray mass spectrometry and found to be the expected product from alkylation of heptamethylcob(II)yrinic acid with the bromoalkyl acrylate. This result supports a mechanism in which the Co(II) catalyst is electrochemically reduced to Co(I), alkylated by the bromoalkyl acrylate and the alkylcobalt corrinoid intermediate is reductively decomposed to form the alkyl acrylate radical.

Electrochemical reduction ( $-1.45$  V vs SCE, 3 h) of methylene chloride mediated by CNCbl in the presence of styrene in DMF has been found to give cyclopropylbenzene in quantitative yield.<sup>96</sup> The reaction is solvent sensitive with significant amounts of  $\gamma$ -chloropropylbenzene formed in DMF/H<sub>2</sub>O mixtures. A plausible mechanism is advanced involving the intermediate formation of ClCH<sub>2</sub>Cbl and its reductive decomposition to form the chloromethyl radical, but no evidence for such an intermediate is presented.

Rusling and co-workers<sup>97</sup> covalently linked poly-L-lysine to carbon electrodes and formed amide links from the polylysine to the B<sub>12</sub> derivative chlorocyanohexacarboxy-8-aminocobyrinic acid *c*-lactam (**37**). The stable films showed reversible electron transfer for the Co(II)/Co(I) couple (ca.  $-0.7$  V vs SCE). They were excellent electrochemical catalysts in microemulsions for the reduction of vicinal dihalides to olefins, for the dechlorination of CCl<sub>3</sub>COOH, and for alkylation of the activated olefin 2-cyclohexen-1-one. CV experiments with the alkyl halides suggested the formation of alkyl–cobalt intermediates in these processes.



Similarly,<sup>98</sup> these films were used to cyclize *n*-bromoalkyl-2-cyclohexenones in microemulsions in yields up to 60% (eq 4). Turnover was 30–85-fold higher for the films than for the dissolved corrinoid catalyst. An organocobalt corrinoid intermediate is suggested from CV evidence.



A sol–gel electrode containing heptapropylcobyrinate trapped in an indium tin oxide electrode has been fabricated by dip coating.<sup>99</sup> The film thickness

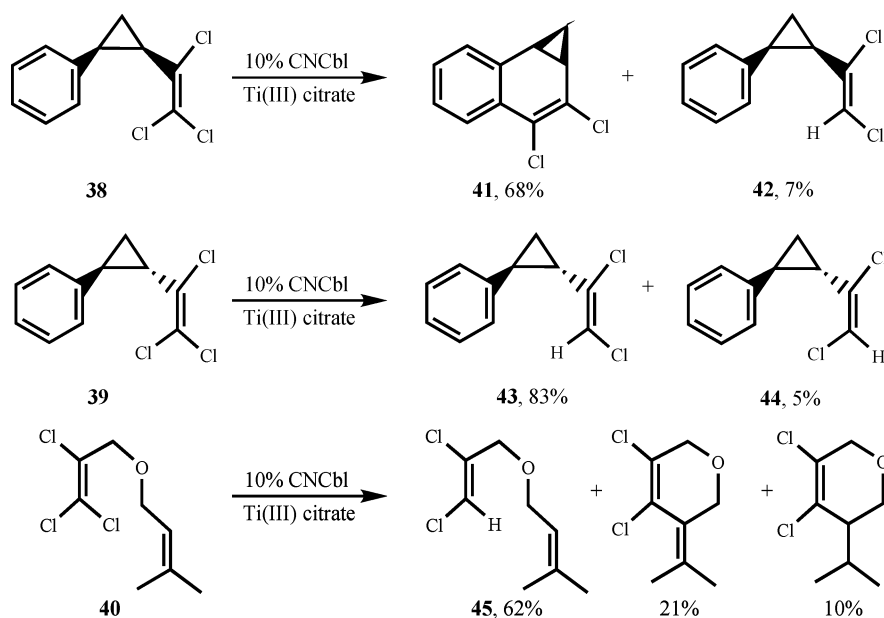
was controlled by dipping withdrawal speed, and the films contained about  $1.8 \times 10^{-13}$  mol of heptapropylcobyrinate per cm<sup>2</sup> per nm of thickness. Cyclic voltammetry showed the Co(II)/Co(I) couple at  $-0.42$  V (vs Ag|AgCl). Using these electrodes, controlled potential reduction ( $-1.2$  V) of benzyl bromide in anaerobic aqueous solution with concomitant irradiation with a 500 W tungsten lamp gave mostly bibenzyl with a small amount of toluene with a turnover number of  $>1000$ .

CO<sub>2</sub> photoreduction is catalyzed by cobalt corrinoids in CH<sub>3</sub>CN/MeOH solution with *p*-terphenyl as a photosensitizer and triethylamine as a reductive quencher.<sup>100</sup> Irradiation with visible light gives carbon monoxide, formic acid, and some hydrogen. The rate of product production was higher for HOCbl, CNCbl, and Factor B than for cobalt *m*-tolylporphyrin. A bizarre (and unlikely) mechanism is suggested which involves a one-electron reduction of cob(I)-alamin to cob(0)alamin followed by its protonation to form a hydrido species and reaction with the CO<sub>2</sub><sup>-</sup> radical anion to form a formylcob(I)alamin species. Evidence presented for this mechanism includes the pulse radiolysis of chemically produced cob(I)alamin in aqueous solution, which showed decay of the e<sub>aq</sub><sup>-</sup> absorption and formation of a new species with a rate constant of ca.  $1 \times 10^{10}$  M<sup>-1</sup> s<sup>-1</sup>.

The electrolyrocatalytic oxidation and reduction of nitric oxide has been observed using CNCbl absorbed onto glassy carbon.<sup>101</sup> In the absence of NO, cyclic voltammograms showed a single, two-electron reduction of CNCbl to cob(II)alamin.<sup>102</sup> The addition of NO at pH 9.0 causes the voltammogram to split so that individual one-electron waves are observed. NO was oxidized at 1.21 V vs Ag|AgCl. The reduction of NO led to ammonia and hydroxylamine.

There remains much interest in the reductive dehalogenation of polychlorinated ethylenes catalyzed by B<sub>12</sub> derivatives as these ubiquitous pollutants are among the most commonly found volatile organics in ambient groundwater in the United States. To distinguish mechanisms involving the intermediate formation of organocobalamins in this process from those which do not, Shey and van der Donk<sup>103</sup> employed radical trap, labeling, and stopped flow spectrophotometric studies to examine the possible involvement of radical anions or vinyl radicals. *cis*-Cyclopropane **38** gave **41** with a small amount of reduction product **42** (Scheme 8), while the *trans* isomer, **39**, gave only reduction products upon reduction with CNCbl/Ti(III)citrate. Reaction of **40** gave ring-closed and reduced products. Only 6-( $\pi$ -endo)-exo cyclization was observed, and no conjugated products were observed. The source of the vinyl hydrogen in **42**–**45** was investigated by labeling experiments. When **39** was reduced with CNCbl/Ti(III)citrate in 1:1 H<sub>2</sub>O and (CH<sub>3</sub>)<sub>2</sub>CDOH, an almost equal mixture of protio- and deuterio-reduction product was observed. In 1:1 D<sub>2</sub>O and (CH<sub>3</sub>)<sub>2</sub>CHOD, mostly protio-reduction product was obtained. Consequently H-atom transfer provides a significant amount of the reduced product. In stopped flow experiments mixing cob(I)alamin with PCE showed clean formation of cob(II)alamin with isosbestic points. The results are

Scheme 8



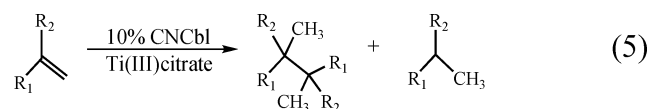
consistent with a mechanism in which cob(I)alamin reduces PCE to a radical anion which subsequently eliminates chloride ion and acquires a hydrogen atom to form TCE. However, they do not rule out other mechanisms. For example, the stopped flow results are also consistent with the formation and decomposition of an organocobalamin intermediate if these processes were too rapid to be detected on the stopped flow time scale, which certainly could be the case.

Van der Donk and co-workers<sup>80</sup> also found that *cis*-chlorovinylCbl, a suspected alkylCbl intermediate in the latter stages of the reductive dechlorination of PCE and TCE, is stable in solution but decomposes when treated with Ti(III)citrate under anaerobic conditions. The reaction features a lag time, and after completion, vinylcobalamin was isolated in 50% yield. However, when *cis*-chlorovinylCbl was treated with Ti(III) citrate and catalytic cob(I)alamin, the lag was abolished and the initial rate of reaction varied with the initial cob(I)alamin concentration, leading to the conclusion that the reduction of *cis*-chlorovinylCbl by Ti(III) citrate leads to formation of cob(D)alamin in an autocatalytic reaction. VinylCbl, however, was stable to these reduction conditions. The cob(I)-alamin-induced reduction of *cis*-chlorovinylCbl is surprising since the reduction potentials of alkylCbl's ( $< -1.5$  V vs NHE) are much more negative than the Co(II)/Co(I) couple ( $-0.61$  V) or the Ti(III)citrate potential (ca.  $-0.6$  V).

Kim and Carraway<sup>104</sup> studied the reductive dechlorination of PCE and TCE with zinc or iron as the bulk reductant and catalytic CNCbl. Spectrophotometric measurements suggested that zinc reduces CNCbl to cob(I)alamin (with intermediate formation of cob(II)-alamin) while iron reduces CNCbl to cob(II)alamin only, consistent with the redox potential for Zn and Fe and the Co(III)/Co(II) and Co(II)/Co(I) couples of B<sub>12</sub>. The apparently one-electron reduction leading to cob(II)alamin in the Zn reduction is likely to be the result of the rapid disproportionation of cob(I)-alamin formed by the two-electron reduction by Zn

with remaining cob(III)alamin. Both Zn and Fe slowly reduced PCE and TCE. For the Zn reduction addition of CNCbl dramatically increased the reduction of both PCE and TCE, while addition of CNCbl to the Fe reductions only enhanced PCE reduction, suggesting that cob(I)alamin can reduce both PCE and TCE but that cob(II)alamin can reduce only PCE. The proposed mechanism involves chlorinated vinyl-radical anion  $\pi$ -complexes with cob(II)alamin, the evidence for which is minimal.

Finally, van der Donk and co-workers<sup>105</sup> observed the dimerization of arylalkanes catalyzed by CNCbl and Ti(III)citrate (eq 5) along with some reduction product. Monosubstituted arylalkanes were found to give pairs of diastereomeric products, but disubstituted arylalkanes gave products with two quaternary carbons in very good yield (70–85%). Although reactions of substituted benzylCbl's gave good dimerization yields, no direct evidence for intermediate formation of alkylCbl's could be obtained; however, evidence for the intermediacy of free radicals was obtained using dienes with intramolecular radical traps.

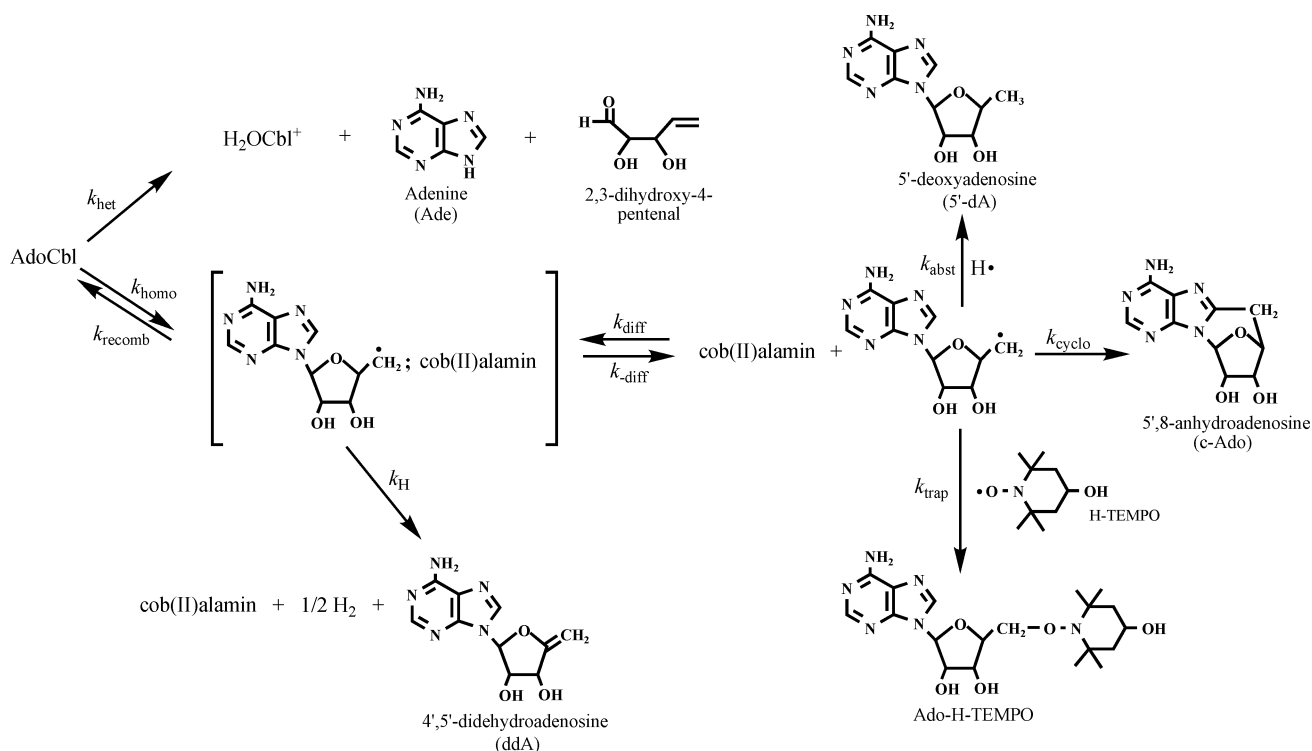


## 4.2. Chemistry of the Carbon–Cobalt Bond

The pathway for AdoCbl thermal decomposition is well known (Scheme 9).

Like all organocobalt complexes with  $\beta$ -oxygen substituents, AdoCbl undergoes specific acid (and general acid, including solvent) catalyzed heterolysis to give  $\text{H}_2\text{OCbl}^+$ , adenine, and 2,3-dihydroxy-4-pentenal. In competition, Co–C bond homolysis leads to a caged Ado•:cob(II)alamin radical pair, the fate of which is dependent upon conditions. An in-cage electron-transfer process leads to 4',5'-didehydroadenosine and competes with escape of the radicals from the solvent cage. After cage escape the Ado• free rad-

## Scheme 9



ical can undergo rapid cyclization to 5',8-anhydroadenosine, abstract a solvent hydrogen to give 5'-deoxyadenosine, or be trapped by a suitable radical trap.

Brown and Zou<sup>106</sup> studied the thermolysis of AdoCbl in the temperature range 30–85 °C in order to determine if extrapolation of kinetic constants from a higher temperature regime from prior measurements<sup>107</sup> was appropriate. The motivation for the work was an earlier NMR study<sup>108</sup> which found evidence for additional conformations of AdoCbl at elevated temperatures which are not populated at room temperature. Under the conditions employed (aqueous solution, 150-fold molar excess of the radical trap H-TEMPO), the only Ado-derived products observed were adenine and the trapped Ado• radical, Ado-H-TEMPO, indicating that the radical trap is kinetically competent to prevent both reentry of the solvent-separated radicals into the solvent cage and the cyclization of the Ado• radical and that the solvent cage is not sufficiently robust to promote the in-cage electron-transfer reaction. Using high specific activity [ $\text{A}2\text{-}^3\text{H}$ ]AdoCbl and the method of initial rates, rate constants for AdoCbl decomposition could be measured down to 30 °C ( $k_{\text{obs}} = 1.16 \times 10^{-8} \text{ s}^{-1}$ ,  $t_{1/2} = 1.9 \text{ year}$ ). Measurement of product ratios permitted deconvolution of the homolysis and heterolysis rate constants, which were corrected for the (minor) presence of the base-off species of AdoCbl. The resulting activation parameters ( $\Delta H^\ddagger = 33.8 \pm 0.2 \text{ kcal mol}^{-1}$ ,  $\Delta S^\ddagger = 13.5 \pm 0.7 \text{ cal mol}^{-1} \text{ K}^{-1}$ ) were not significantly different from those obtained by Hay and Finke<sup>107</sup> in the 85–115 °C temperature range, indicating that the AdoCbl conformers populated at higher temperatures do not significantly affect the homolysis of the Co–C bond. Heterolysis, on the other hand, had a much smaller enthalpy of activation ( $\Delta H^\ddagger = 18.5 \pm 0.2 \text{ kcal mol}^{-1}$ ) and a negative

entropy of activation ( $\Delta S^\ddagger = -34.0 \pm 0.7 \text{ cal mol}^{-1} \text{ K}^{-1}$ ). As a result, the Eyring plots for each process cross, so that homolysis is the dominant pathway at high temperatures while heterolysis predominates at lower temperatures.

As a model for the first steps of the ribonucleoside triphosphate reductase reaction, in which AdoCbl undergoes Co–C bond homolysis followed by hydrogen transfer from an active site cysteine residue to form 5'-deoxyadenosine and a thiyl radical, Sirovatka and Finke<sup>109</sup> studied the thermolysis of AdoCbl in the presence of 2-mercaptoethanol (2-ME). At 100 °C in excess thiol the products (obtained in 90% yield) were cob(II)alamin, 5'-deoxyadenosine, and the disulfide of 2-ME and the heterolysis products cob(II)alamin, adenine, and 2,3-dihydroxy-pentenal (Scheme 9) were obtained in 10% yield. The reaction was first order in AdoCbl but zero order in 2-ME, suggesting that homolysis of AdoCbl is the rate-determining step. Indeed, a temperature-dependent study showed that the observed activation parameters were within experimental error of those previously determined for the trapped homolysis of AdoCbl in the absence of thiol.<sup>107</sup>

In an important, but now quite controversial, paper, Sirovatka and Finke<sup>110</sup> extended their earlier studies<sup>111,112</sup> on the effects of added exogenous bases on the thermolysis of AdoCbl<sup>+</sup> (Figure 1), the axial nucleotide-free base-off analogue of AdoCbl, to investigate the effects of bulky axial bases such as 1,2-dimethylimidazole, 2-methylpyridine, and 2,6-dimethylpyridine. They reported that no evidence could be found for binding of these bulky bases to AdoCbl<sup>+</sup> ( $K_{\text{assoc}} \leq 0.03 \text{ M}$ ) but that bulky bases did bind to cob(II)inamide, the product of homolysis of AdoCbl<sup>+</sup>. However, kinetic studies of thermolysis of AdoCbl<sup>+</sup> in the presence of excess bulky base dem-

onstrated that these bases accelerated Co–C bond homolysis by at least 200-fold. This led to the conclusion that the bulky bases must be involved in the rate-determining step for homolysis and that the “dominant effect of the bulky base is at the Co–C cleavage transition state”.<sup>110</sup> In retrospect, this conclusion was necessarily incorrect. In solution, the homolysis of Ado–cobalt corrinoids is known to be diffusion controlled,<sup>4,113</sup> and consequently, the rate-limiting step is the diffusion step. The prior Co–C bond cleavage step is a simple bond dissociation reaction for which the reaction coordinate is a Morse potential function which has no local maximum and consequently no transition state. As a result, the effect of bulky bases on the homolysis of AdoCbi<sup>+</sup> might well have been a stabilization of the cob(II)-inamide product by coordination, which would lead to a lowering of the reaction free energy barrier.

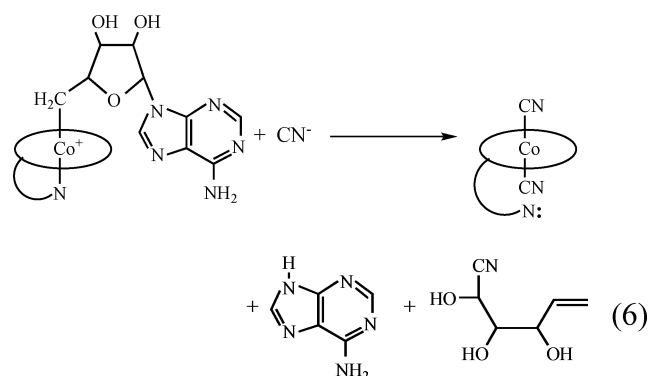
However, Trommel et al.<sup>114</sup> found that 2-methylpyridine and other hindered bases do not coordinate to cob(II)inamide and that previous observations of such associations were due to less hindered impurities in the bulky bases preparations. No evidence of complexation could be found in up to 8 M 2-methylpyridine as long as the base was first purified by a novel Co(III)-affinity distillation procedure which removes traces of less hindered impurities. The effects of such bulky bases on AdoCbi<sup>+</sup> observed by Sirovatka and Finke<sup>110</sup> thus seemed also to be due to trace impurities in the bases. However, more recently, Doll and Finke<sup>115</sup> provided evidence that these effects are actually due to formation of the solvent anion (ethylene glycolate), which can coordinate to AdoCbi<sup>+</sup> in the presence of very large amounts of added base.

Magnusson and Frey<sup>46</sup> studied the thermolysis of 3',4'-anAdoCbl (Figure 1) in ethylene glycol using the radical trap TEMPO in 30-fold excess. The only observed nucleoside-containing products were the anticipated isomers 5'-TEMPO-3',4'-anhydroadenosine and 3'-TEMPO-3',4'-anhydroadenosine. The observed activation parameters were  $\Delta H^\ddagger = 29.5 \pm 0.4$  kcal mol<sup>-1</sup> and  $\Delta S^\ddagger = 27 \pm 2$  cal mol<sup>-1</sup> K<sup>-1</sup>. However, no correction was made for the occurrence of any base-off 3',4'-anAdoCbl, which was assumed to be wholly base-on at the relatively low temperatures studied (12–32 °C). Using the solvent cage correction<sup>116</sup> and the enthalpy for viscous flow for ethylene glycol, the bond dissociation energy (BDE) of 3',4'-anAdoCbl was estimated to be  $24 \pm 2$  kcal mol<sup>-1</sup>, 6 kcal mol<sup>-1</sup> lower than that for AdoCbl.<sup>41</sup> The entropy of activation for 3',4'-anAdoCbl is nearly twice that for AdoCbl, so that at 25 °C 3',4'-anAdoCbl is nearly 7 orders of magnitude (8.8 kcal mol<sup>-1</sup>) more reactive than AdoCbl, a rate enhancement that must be considered to be due to allylic stabilization of the product radical. This provides a nice example of enhanced reactivity by product stabilization of a bond dissociation reaction. However, the reasons for the large increase in the entropy of activation are not at all clear.

Rates and mechanisms of decomposition in acid media of AdoCbl, 2',5'-dideoxyadenosylcobalamin (2'dAdoCbl, Figure 1), 3',5'-dideoxyadenosylcobalamin (3'dAdoCbl, Figure 1), 2',3',5'-trideoxyadenosylcobalamin (2',3'ddAdoCbl, Figure 1), 1',5'-dideoxy-

ribofuranosylcobalamin (1dRFCbl, Figure 1), and tetrahydrofurfurylcobalamin (THFFCbl, Figure 1) have been studied by Jensen and Halpern<sup>117</sup> at 20 (2',3'ddAdoCbl, 1dRFCbl, THFFCbl) and 90 °C (AdoCbl, 2'dAdoCbl, 3'dAdoCbl). Competing Co–C bond homolysis and acid-induced heterolysis is observed in all cases. Heterolysis occurred by two paths, initial depurination followed by elimination from the remaining RCbl intermediate (predominant in 2'dAdoCbl and 2',3'ddAdoCbl) and ring opening following protonation at the ribose ring oxygen. Both pathways showed strong dependence on the alkyl ligand's functional groups. The most highly substituted complex, AdoCbl, was the most stable, decomposing some 10<sup>4</sup>-fold more slowly than THFFCbl, the most reactive. However, Co–C bond homolysis was insensitive to substituents.

There has also been additional work on the reaction of adenosylcobalt corrinoids with cyanide. The reaction of AdoCbl with cyanide gives dicyanocobalamin ((CN)<sub>2</sub>Cbl), adenine, and 1-cyano-D-erythro-2,3-dihydroxy-4-pentenol (eq 6).<sup>118</sup> The kinetics of formation of (CN)<sub>2</sub>Cbl show saturation with respect to cyanide concentration, suggesting the intermediate formation of an AdoCbl species with an  $\alpha$ -cyanide axial ligand (Ado(CN)Cbl<sup>-</sup>), followed by rate-determining Co–C bond cleavage. Brasch and Haupt<sup>119</sup> were able to obtain direct evidence for the formation of such an intermediate in DMF–D<sub>2</sub>O mixtures using <sup>1</sup>H NMR and UV–vis spectroscopy. In 96% DMF/4% D<sub>2</sub>O the rate constant for decomposition of the Ado(CN)Cbl<sup>-</sup> intermediate was at least 100-fold slower than it was in 100% D<sub>2</sub>O, permitting direct NMR and UV–vis characterization of the intermediate species. Similar studies of the reaction of AdoCbi<sup>+</sup> with CN<sup>-</sup> also permitted the observation and characterization of an intermediate Ado(CN)Cbi species.<sup>120</sup> In this case, the decomposition of the Ado(CN)Cbi intermediate was 400-fold slower in 92% DMF/8% D<sub>2</sub>O than it was in water.



In additional work by Brasch, van Eldik, and co-workers,<sup>121</sup> the temperature and pressure dependence of the reactions of AdoCbl and AdoCbi<sup>+</sup> with cyanide was studied in order to seek evidence that the Co–C bond cleavage step is solvent assisted and occurs with protonation of the ribose oxygen by a solvent molecule. Saturation kinetics were again observed at high cyanide concentration from which an equilibrium constant for formation of the Ado(CN)Cbl<sup>-</sup> intermediate of 0.26 M<sup>-1</sup> was obtained. The activation parameters under saturating cyanide conditions were

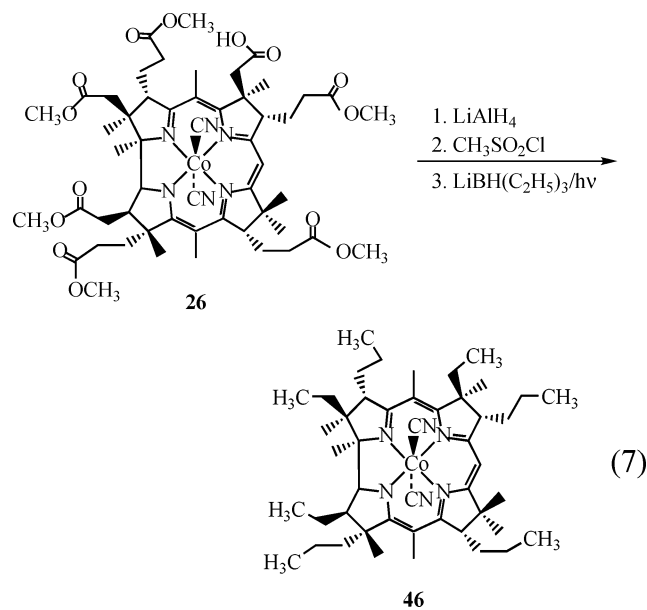
determined to be  $\Delta H^\ddagger = 13.1 \pm 0.2 \text{ kcal mol}^{-1}$ ,  $\Delta S^\ddagger = -23.4 \pm 0.7 \text{ cal mol}^{-1} \text{ K}^{-1}$ , and  $\Delta V^\ddagger = -5.7 \pm 0.3 \text{ cm}^3 \text{ mol}^{-1}$  for AdoCbl. A similar  $\Delta V^\ddagger$  ( $-4.5 \pm 0.4 \text{ cm}^3 \text{ mol}^{-1}$ ) was found for the AdoCbi<sup>+</sup> reaction with cyanide. The negative entropy and volume of activation are taken as evidence for participation of solvent in the transition state for the rate-determining Co–C bond cleavage step, which would otherwise be expected to have positive values for these parameters. It is presumably this solvent participation in the Co–C bond cleavage, at least in part, that enables Brasch's observations<sup>119,120</sup> of the cyanoadenosylcobalt corrinoid intermediates in mixed solvents of reduced water activity. There is also clearly a solvent deuterium isotope effect in DFM/D<sub>2</sub>O solvents<sup>119</sup> and likely a solvent effect as well in order to completely explain the enhanced stability of the intermediates in these solvents.

Photoacoustic calorimetry has been used to determine BDE's for alkylCbl's, although both cases during the period covered by this review involve redeterminations of values previously determined by the kinetic radical trap method. Hung and Grabowski<sup>122</sup> used photoacoustic calorimetry to redetermine<sup>123</sup> the BDE of CH<sub>3</sub>Cbl and determine the BDE of CH<sub>3</sub>Cbi<sup>+</sup>, the axial nucleotide-free "base-off" analogue. Photoacoustic signals were measured at 337 nm in phosphate-buffered neutral solution from  $-1$  to  $40^\circ \text{C}$ . Using measured values for the photolysis quantum yields (0.27 and 0.17 for CH<sub>3</sub>Cbl and CH<sub>3</sub>Cbi<sup>+</sup>, respectively), BDE's of  $36 \pm 4 \text{ kcal mol}^{-1}$  for CH<sub>3</sub>Cbl and  $37 \pm 3 \text{ kcal mol}^{-1}$  for CH<sub>3</sub>Cbi<sup>+</sup> were calculated. The former value is within experimental error of the value determined by Martin and Finke<sup>123</sup> ( $37 \pm 3 \text{ kcal mol}^{-1}$ ) for CH<sub>3</sub>Cbl in ethylene glycol using the kinetic trapping method at much higher temperature. Reaction volumes of  $16 \pm 1$  and  $14 \pm 1 \text{ cm}^3 \text{ mol}^{-1}$ , respectively, were also determined.

Photoacoustic calorimetry has also been used to determine the BDE for 2'dAdoCbl (Figure 1).<sup>124</sup> The measured photolysis quantum yield,  $0.25 \pm 0.02$ , is very close to the literature values for AdoCbl itself, and the BDE ( $31.8 \pm 1.8 \text{ kcal mol}^{-1}$ ) is very close to that previously determined by the kinetic radical trapping method in ethylene glycol<sup>125</sup> and quite close to the value for AdoCbl ( $30 \pm 2 \text{ kcal mol}^{-1}$ ).<sup>107</sup> The activation volume ( $6.5 \pm 0.5 \text{ cm}^3 \text{ mol}^{-1}$ ) is also the same as that previously measured for AdoCbl ( $6 \pm 1 \text{ cm}^3 \text{ mol}^{-1}$ ) by photoacoustic calorimetry.<sup>126</sup>

Keese and co-workers modeled the methyl transfer reactions of the methionine synthase enzyme. The electrochemical methylation of Co(I) by methanol and dimethylaniline under acid conditions has been observed.<sup>127,128</sup> Heptamethylcob(D)yrinic acid in methanol was treated with HClO<sub>4</sub> under controlled potential reduction at  $-0.75 \text{ V}$  for 2 h at  $50^\circ \text{C}$  to give 45% CH<sub>3</sub>–Co complex. With various other acids the yield varied from 20% to 80%. In all cases, both the  $\beta$  diastereomer (with the methyl group "up") and the  $\alpha$  diastereomer (with the methyl group "down") were obtained, with the  $\beta$  diastereomer predominating by 5:1 to 7:1. Substituting ethanol for methanol gave the CH<sub>3</sub>CH<sub>2</sub>–Co complex in 40% yield, but the diastereomeric outcome was not reported. A similar proce-

dure using dimethylaniline in ethanol with H<sub>2</sub>SO<sub>4</sub> gave the CH<sub>3</sub>–Co complex in 11% yield (with no CH<sub>3</sub>–CH<sub>2</sub>–Co formation). Further refinement of this model for the first half-reaction of the methionine synthase enzyme showed that the controlled potential reduction could be substituted by Zn/acetic acid to give a mixture of  $\alpha$ - and  $\beta$ -methylheptamethylcobyrinate in 10% yield plus *N*-methylaniline.<sup>129</sup> When the heptaalkylcorrinato complex, **46** (eq 7), was substituted for heptamethylcobyrinate, the yield of CH<sub>3</sub>–Co complexes was 29%.

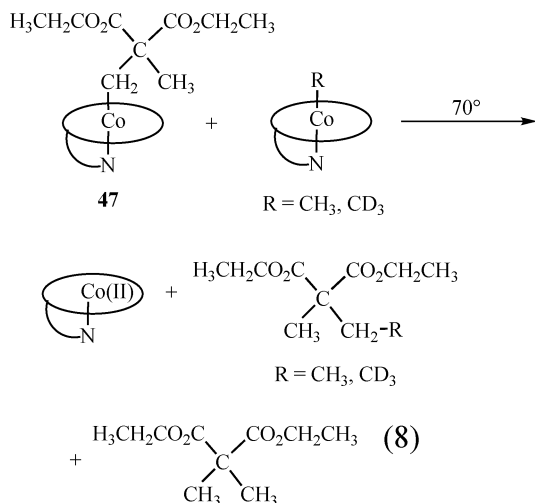


As a model for the second half-reaction of methionine synthase, a mixture of the diastereomeric  $\alpha$ - and  $\beta$ -methylheptamethylcobyrinates was treated with hexane-1-thiol in methanol/pyridine at  $50^\circ \text{C}$  for 24 h, yielding 4% of the hexyl methyl sulfide along with disulfide. Under reflux, the yield improved to 37% and with the addition of ZnCl<sub>2</sub> under reflux it was improved to 69%. With the diastereomeric CH<sub>3</sub>–Co complexes of the peralkylated corrinoid **46**, the methyl sulfide yield was 58% with added ZnCl<sub>2</sub>. The entire model methionine synthase catalytic cycle could then be reconstituted, albeit with disappointing methyl sulfide yields of 5.9%.

Inorganic arsenic can be methylated in mammalian liver, although no such enzyme has been found in human liver. Zakharya and Aposhian<sup>130</sup> found that reaction of CH<sub>3</sub>Cbl and thiols with arsenite forms monomethylarsonic acid along with a small amount of dimethylarsonic acid. Addition of human liver cytosol had no effect on the reaction.

Mosimann and Kräutler demonstrated a most interesting example of methylation of an alkyl radical by CH<sub>3</sub>Cbl.<sup>131</sup> Reaction of 2-bis(ethoxycarbonyl)propylcobalamin (**47**, eq 8) with CH<sub>3</sub>Cbl under anaerobic conditions in the dark at  $70^\circ \text{C}$  produced a 70% yield of a mixture of 2-ethyl-2-methylmalonic acid diethyl ester and 2,2-dimethylmalonic acid diethyl ester in a 4.7:1 ratio. The methyl group in the 2-ethyl ester was shown to be from CH<sub>3</sub>Cbl by use of CD<sub>3</sub>Cbl. The proposed, and quite likely, mechanism involves the thermal homolysis of **47**<sup>132</sup> to form the 2-bisethoxy-

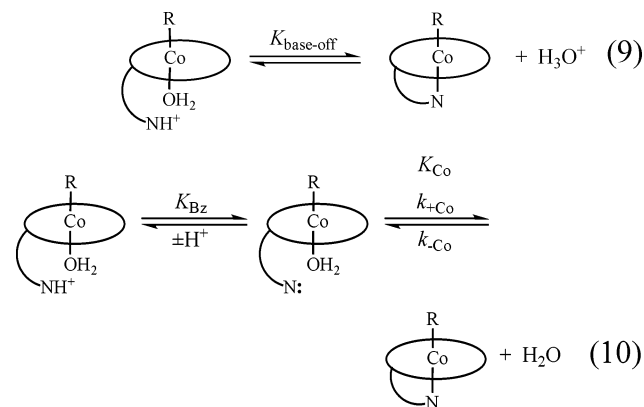
carbonylpropyl radical which abstracts a methyl radical from  $\text{CH}_3\text{Cbl}$ .



### 4.3. Ligand Substitution

Interest in ligand substitution reactions has heightened recently due to the observations that certain enzymes bind AdoCbl and  $\text{CH}_3\text{Cbl}$  in the so-called base-off/His-on mode in which the axial Bzm nucleotide is dissociated and buried in a hydrophobic pocket and the imidazole moiety of an active site His residue becomes the lower axial ligand.

The quintessential Cbl ligand substitution reaction is, of course, the intramolecular dissociation of the Bzm ligand to form the “base-off” species. Thus, in sufficiently strong acid, the dissociated Bzm can be trapped by protonation to form a stable, supposedly (but see below) aqua species (eq 9). This can be seen to be a composite of the consecutive equilibria for deprotonation of the axial Bzm, followed by ligand exchange to form the base-on species (eq 10), and eq 11 relates the observable  $\text{p}K_{\text{base-on}}$  to the equilibria for the proton dissociation from the protonated base-off species and for the ligand exchange step.



$$K_{\text{base-off}} = (1 + K_{\text{Co}})K_{\text{Bz}} \quad (11)$$

Since the value of  $\text{p}K_{\text{Bz}}$  must be the same as that of the detached benzimidazole nucleoside ( $\alpha$ -ribazole,  $\text{p}K_{\text{a}} = 5.56$  at  $25^\circ\text{C}$ ,<sup>133</sup> essentially identical to that of the nucleotide,  $\alpha$ -ribazole-3'-phosphate,  $\text{p}K_{\text{a}} = 5.54$  at  $25^\circ\text{C}$ <sup>134</sup>), values of  $K_{\text{Co}}$  may be calculated directly from measured values of  $\text{p}K_{\text{base-off}}$ . A large number

**Table 2. Values of  $K_{\text{CN}}$  and Related Thermodynamic Constants for RCbl's ( $25^\circ\text{C}$ )**

R	$\text{p}K_{\text{base-off}}^a$	$K_{\text{CN}}, \text{M}^{-1}{}^b$	$K_{\text{Co}}^a$
$\text{CH}_3\text{CH}_2$	4.16	$0.665 \pm 0.066^c$	$2.00 \times 10$
$\text{CH}_3\text{CH}_2\text{CH}_2$	4.10	$1.3 \pm 0.14^c$	$2.37 \times 10$
Ado	$3.67^d$	$0.6 \pm 0.1^e$	$7.25 \times 10$
$\text{CH}_3$	2.90	$0.38 \pm 0.03^f$	$4.52 \times 10^2$
$\text{BrCH}_2$		$0.43 \pm 0.04^f$	
$\text{CF}_3\text{CH}_2$	2.60	$13.0 \pm 1.5^e$	$9.23 \times 10^2$
$\text{CF}_2\text{H}$	2.15	$3.27 \pm 0.11^e$	$2.60 \times 10^3$
$\text{NCCH}_2$	1.81	$63.8 \pm 1.4^e$	$5.62 \times 10^3$
$\text{CF}_3$	1.44	$123 \pm 9^f$	$1.32 \times 10^4$
CN	0.10	$5 \times 10^3^g$	$2.88 \times 10^5$
$\text{H}_2\text{O}$	-2.13		$4.90 \times 10^7$

<sup>a</sup> Equations 9 and 10. Brown, K. L.; Peck-Siler, S. *Inorg. Chem.* **1988**, *27*, 3548. <sup>b</sup> Equation 15. <sup>c</sup> Reference 134. <sup>d</sup> Reference 152. <sup>e</sup> Reference 143. <sup>f</sup> Reference 142. <sup>g</sup> Reference 156.

of such values are available (along with enthalpy and entropy values) as shown for a series of RCbl's in Table 2, which stretches from  $\text{CH}_3\text{CH}_2\text{Cbl}$ ,  $\text{p}K_{\text{base-off}} = 4.16$  and  $K_{\text{Co}} = 20$ , to  $\text{H}_2\text{OCbl}^+$ ,  $\text{p}K_{\text{base-off}} = -2.13$  and  $K_{\text{Co}} = 4.90 \times 10^7$ .

The kinetics of Bzm dissociation in  $\text{NCCH}_2\text{Cbl}$ ,  $\text{CF}_3\text{-Cbl}$ , and  $\text{CNCbl}$  (eq 10,  $k_{-\text{Co}}$ ), i.e., those RCbl's in which it is slow enough to measure, have been studied by “pH-jump” stopped flow measurements in which unbuffered solutions of RCbl are mixed with various concentrations of  $\text{HClO}_4$ .<sup>135</sup> The observed rate constant first decreases and then increases with increasing acidity. The decrease represents the anticipated “titration” of the observed rate constant for Bzm dissociation (eq 12), while the increase represents an acid-catalyzed pathway, presumably via protonation of the coordinated Bzm in the base-on species. The overall rate law is given in eq 13, where  $k_{\text{H}}$  is the rate constant for the acid-catalyzed path. For  $\text{NCCH}_2\text{Cbl}$  at  $5^\circ\text{C}$  a nonlinear least-squares fit to the data gave  $k_{+\text{Co}} = 4.4 \pm 0.3 \times 10^5 \text{ s}^{-1}$ ,  $k_{-\text{Co}} = 83 \pm 13 \text{ s}^{-1}$ , and  $k_{\text{H}} = 913 \pm 71 \text{ M}^{-1} \text{ s}^{-1}$ . From the values of  $k_{+\text{Co}}$  and  $k_{-\text{Co}}$ , a value of 5300 for  $K_{\text{Co}}$  can be calculated, in good agreement with the value obtained (5620) from the measured value of  $\text{p}K_{\text{base-off}}$  via eq 11 (Table 2). Similar measurements for  $\text{CF}_3\text{-Cbl}$  and  $\text{CNCbl}$  showed that the rate constants all followed the trend of  $\text{NCCH}_2\text{Cbl} > \text{CF}_3\text{Cbl} > \text{CNCbl}$ , i.e., decreasing as R becomes more electron withdrawing and  $\text{p}K_{\text{base-off}}$  becomes lower.

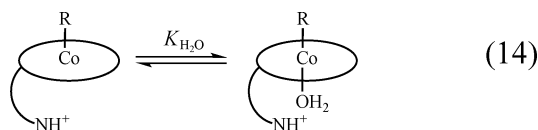
$$k_{\text{obs}} = k_{-\text{Co}} + k_{+\text{Co}}K_{\text{Bz}}/(K_{\text{Bz}} + [\text{H}^+]) \quad (12)$$

$$k_{\text{obs}} = k_{-\text{Co}} + k_{+\text{Co}}K_{\text{Bz}}/(K_{\text{Bz}} + [\text{H}^+]) + k_{\text{H}} \quad (13)$$

Similar results have been obtained for  $\text{NCCH}_2\text{-13-epiCbl}$  and  $\text{CN-13-epiCbl}$ ,<sup>136</sup> the Cbl analogues in which the configuration at corrin ring C13 is inverted so that the *e*-propionamide side chain is axially “upward”. For  $\text{NCCH}_2\text{-13-epiCbl}$  the rate constants were severalfold smaller than those for  $\text{NCCH}_2\text{Cbl}$ , while the results for  $\text{CN-13-epiCbl}$  were quite similar to those for  $\text{CNCbl}$  itself.

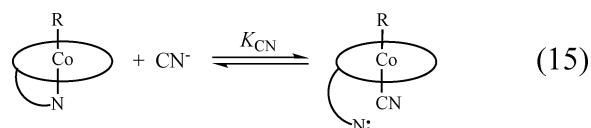
There has long been controversy over the question of whether base-off alkylCbl's and the analogous  $\text{RCbi}^+$ 's exist in solution as a mixture of hexacoordinate aqua (red) species and pentacoordinate (yellow) species (eq 14). The temperature dependence of the

UV-vis spectra and <sup>1</sup>H NMR chemical shift of the C10 hydrogen of such species<sup>137</sup> has been attributed to this equilibrium, but others have argued that a temperature-dependent conformational change of the corrin ring is the cause. Thermodynamic data<sup>138</sup> and EXAFS measurements<sup>139</sup> have provided further evidence, but the concept has been slow to gain acceptance. Hamza et al.<sup>140</sup> provided excellent evidence for the equilibrium of eq 14 from the pressure dependence of the UV-vis spectra of such species. Since conformational changes of the corrin ring would be expected to proceed with little or no volume change, it is unlikely that such pressure-dependent spectral changes could be due to a corrin ring conformational equilibrium. Hamza et al. were able to calculate equilibrium constants,  $K_{\text{H}_2\text{O}}$  (eq 14), for vinylCbi<sup>+</sup> and base-off CH<sub>3</sub>Cbl from the isobestic pressure-dependent spectral changes using limiting spectra for the two forms obtained from the earlier temperature-dependent data.<sup>137</sup> From linear plots of  $\ln K_{\text{H}_2\text{O}}$  vs pressure, volume changes of  $-12.4 \pm 1.0 \text{ cm}^3 \text{ mol}^{-1}$  and  $-12.5 \pm 1.2 \text{ cm}^3 \text{ mol}^{-1}$  were obtained. The absolute values are within experimental error of the calculated activation volume,  $13.1 \text{ cm}^3 \text{ mol}^{-1}$ , for a limiting D ligand substitution mechanism in which a H<sub>2</sub>O ligand is lost from an octahedral complex<sup>141</sup> and consequently provide excellent evidence for the equilibrium of eq 14.

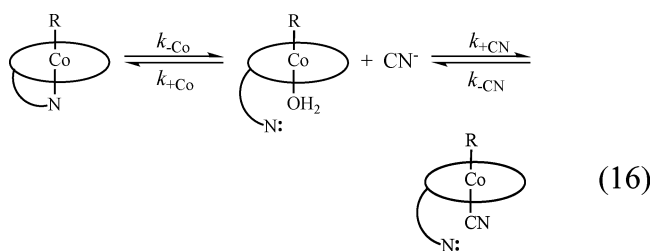


Similar pressure-dependent spectral measurements<sup>135</sup> on other complexes show that the position of the five-coordinate/six-coordinate equilibrium varies widely across the series of RCbl's (Table 2). Thus, the base-off species of AdoCbl and CH<sub>3</sub>CH<sub>2</sub>CH<sub>2</sub>Cbl have spectra characteristic of the high-temperature, low-pressure (i.e., five-coordinate) species and show very small pressure-dependent spectral changes with no isobestic points. These complexes are apparently predominantly five coordinate at ordinary temperatures and all pressures. For base-off CF<sub>3</sub>Cbl, CF<sub>3</sub>Cbi<sup>+</sup>, H<sub>2</sub>O(CN)Cbi<sup>+</sup> (Factor B, a mixture of diastereomers), and (H<sub>2</sub>O)<sub>2</sub>Cbi<sup>2+</sup>, the spectra are characteristic of the low-temperature, high-pressure forms, and again there is little spectral change and no isobestic behavior with increasing pressure. These species are apparently six-coordinate, aqua complexes at ordinary temperatures and all pressures. However, for base-off CF<sub>3</sub>CH<sub>2</sub>Cbl and NCCH<sub>2</sub>Cbl and their respective cobinamide derivatives (as well as for base-off CH<sub>3</sub>Cbl and vinylCbi<sup>+</sup>), significant pressure-dependent spectral changes with isobestic points are observed, indicating that they exist as mixtures of five-coordinate and six-coordinate aqua species at ordinary temperatures.

The reactions of several alkylCbl's with cyanide have been studied.<sup>142–144</sup> Most react to give a stable R(CN)Cbl complex (eq 15), and values for the equilibrium constant,  $K_{\text{CN}}$ , have been measured (Table 2). For CF<sub>3</sub>Cbl, NCCH<sub>2</sub>Cbl, and CNCbl the kinetics of R(CN)Cbl formation were slow enough to measure



by stopped flow methods. The observed rate constant showed saturation kinetics with respect to [CN<sup>-</sup>] suggesting the limiting D mechanism of eq 16. The limiting rate constants,  $k_{-\text{Co}}$ , and activation parameters at high cyanide concentration were  $64.7 \pm 0.7 \text{ s}^{-1}$  (5 °C) for NCCH<sub>2</sub>Cbl ( $\Delta H^\ddagger = 20 \pm 1 \text{ kcal mol}^{-1}$ ,  $\Delta S^\ddagger = 23 \pm 1 \text{ cal mol}^{-1} \text{ K}^{-1}$ , and  $\Delta V^\ddagger = 12.7 \pm 0.5 \text{ cm}^3 \text{ mol}^{-1}$ ),  $8.8 \pm 1.6 \text{ s}^{-1}$  (10 °C) for CF<sub>3</sub>Cbl ( $\Delta H^\ddagger = 18.4 \pm 0.7 \text{ kcal mol}^{-1}$ ,  $\Delta S^\ddagger = 11 \pm 3 \text{ cal mol}^{-1} \text{ K}^{-1}$ , and  $\Delta V^\ddagger = 14.8 \pm 0.8 \text{ cm}^3 \text{ mol}^{-1}$ ), and  $0.042 \text{ s}^{-1}$  (25 °C) for CNCbl ( $\Delta H^\ddagger = 25.1 \pm 0.1 \text{ kcal mol}^{-1}$ ,  $\Delta S^\ddagger = 19 \pm 1 \text{ cal mol}^{-1} \text{ K}^{-1}$ , and  $\Delta V^\ddagger = 13.1 \pm 0.3 \text{ cm}^3 \text{ mol}^{-1}$ ) and are consistent with the limiting D mechanism.



Similar measurements have been made for NCCH<sub>2</sub>-13-epiCbl and CN-13-epiCbl,<sup>136</sup> the Cbl analogues in which the configuration at corrin ring C13 is inverted so that the *e*-propionamide side chain is axially "upward". The kinetic pattern is the same as that for the RCbl's, i.e., saturation behavior of  $k_{\text{obs}}$  with increasing [CN<sup>-</sup>], and also interpreted as indicative of a limiting D mechanism. For the R-13-epiCbl's, whose  $\text{p}K_{\text{base-off}}$  values are  $0.83 \pm 0.14$  units lower than those for the corresponding RCbl's,<sup>138</sup> the values of  $k_{-\text{Co}}$  and  $K_{\text{CN}}$  are lower, suggesting that in the normal RCbl's the coordinated Bzm is crowded by the axially downward *e*-propionamide side chain.

CF<sub>3</sub>CH<sub>2</sub>Cbl and AdoCbl, on the other hand, react with cyanide to give (CN)<sub>2</sub>Cbl, indicating that the R(CN)Cbl adduct is unstable in excess cyanide in the dark.<sup>142,143</sup> For both compounds spectra obtained immediately after mixing with solutions containing cyanide showed clear evidence of cyanide binding, and values of  $K_{\text{CN}}$  (Table 2) were determined using tandem cuvettes. For AdoCbl the kinetics of the cyanide substitution reaction were too fast to follow by stopped flow methods, but a second-order rate constant ( $1.2 \times 10^3 \text{ M}^{-1} \text{ s}^{-1}$ ) for CF<sub>3</sub>CH<sub>2</sub>Cbl was obtained at 3 °C in 0.4 M cyanide at pH 11. As seen in Table 2, values of  $K_{\text{CN}}$  span the range from 0.43 to  $5 \times 10^3 \text{ M}^{-1}$ , increasing as the alkyl group becomes more electron withdrawing. However, the trend is not identical to the trend in  $K_{\text{Co}}$ .

The binding constants for pyridine (Py), *N*-methylimidazole (MeIm), and 4-*N,N*-(dimethylamino)pyridine (4-Me<sub>2</sub>Npy) to CH<sub>3</sub>Cbi<sup>+</sup> have been determined.<sup>145</sup> The values for Py (ca.  $6.5 \text{ M}^{-1}$ ) and MeIm (ca.  $6 \text{ M}^{-1}$ ) agree well with those in the literature and showed little solvent dependence between water (pH 7.2) and ethylene glycol. The value for 4-Me<sub>2</sub>Npy (18

$M^{-1}$  in ethylene glycol) was significantly higher, showing the expected dependence on ligand basicity. Interestingly, the thermodynamic parameters for these association constants differ significantly between the two solvents (e.g., for Py,  $\Delta H = -6.2 \pm 0.4$  kcal mol $^{-1}$  and  $\Delta S = -17 \pm 2$  cal mol $^{-1}$  K $^{-1}$  in ethylene glycol but  $\Delta H = -3.0 \pm 0.5$  kcal mol $^{-1}$  and  $\Delta S = -7 \pm 2$  cal mol $^{-1}$  K $^{-1}$  in water).

There has been substantial controversy over many years regarding the interaction of nitric oxide with B<sub>12</sub> species. Some biological effects of B<sub>12</sub> have been attributed to complexation of NO with H<sub>2</sub>O Cbl<sup>+</sup>, resulting in a decrease in NO availability. Conflicting reports of NO binding to H<sub>2</sub>O Cbl<sup>+</sup> and cob(II)alamin and reports of the lack of such interactions have confused the literature for some time. van Eldik and co-workers<sup>146</sup> have now demonstrated that minor spectral changes seen when NO is added to H<sub>2</sub>O Cbl<sup>+</sup> are the result of trace contamination of NO with nitrite ion and that the species formed has the same UV-vis spectrum and formation kinetics<sup>147</sup> as nitritocobalamin (NO<sub>2</sub>Cbl).

However, gradual addition of NO to solutions of cob(II)alamin produces spectral changes with numerous isosbestic points.<sup>148</sup> The same final spectrum could be generated when a solution of H<sub>2</sub>O Cbl<sup>+</sup> plus NO was irradiated with strong light. The putative NO-cob(II)alamin species has a formation constant of  $1 \times 10^8$  M $^{-1}$  at pH 7<sup>148,149</sup> and undergoes a spectral shift between pH 7 and 4 indicative of a base-on/base-off protonic equilibrium, which has  $pK_{\text{base-off}} = 5.1$ <sup>149</sup> (so that  $K_{\text{Co}}$  (eq 10) is only 1.9!), indicating a very weak Co-NB3 bond. The adduct has been further characterized by resonance Raman<sup>148</sup> and <sup>1</sup>H, <sup>31</sup>P, and <sup>15</sup>N NMR<sup>149</sup> spectroscopies. In the RR spectrum a peak at 514 cm $^{-1}$ , assignable to a Co-N stretching or bending mode, showed the predicted isotopic shift when <sup>14</sup>NO was replaced by <sup>15</sup>NO. The NO-cob(II)alamin complex is believed to be a diamagnetic six-coordinate base-on species (at neutral pH) with a bent Co-nitrosyl bond formally equivalent to a Co(III)-NO<sup>-</sup> species.<sup>148,149</sup>

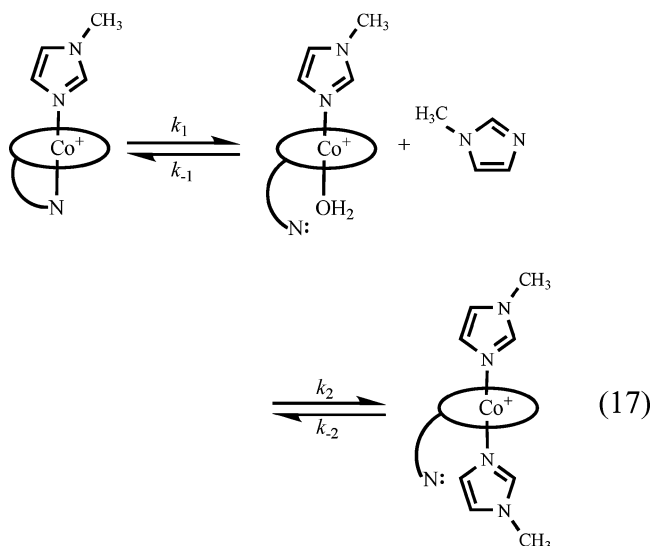
The formation kinetics of the complex were studied by laser flash photolysis and gave  $k_{\text{on}} = 7.4 \pm 0.2 \times 10^8$  M $^{-1}$  s $^{-1}$  (25 °C),  $\Delta H^\ddagger = 5.9 \pm 0.1$  kcal mol $^{-1}$ ,  $\Delta S^\ddagger = 1.7 \pm 0.5$  cal mol $^{-1}$  K $^{-1}$ , and  $\Delta V^\ddagger = 7.4 \pm 0.2$  cm $^3$  mol $^{-1}$ . The kinetics of complex dissociation were studied by stopped flow spectrophotometry by trapping released NO with [Fe<sup>II</sup>(edta)(H<sub>2</sub>O)]<sup>2-</sup> and gave  $k_{\text{off}} = 5.6 \pm 0.2$  s $^{-1}$ ,  $\Delta H^\ddagger = 18.2 \pm 0.2$  kcal mol $^{-1}$ ,  $\Delta S^\ddagger = 6 \pm 1$  cal mol $^{-1}$  K $^{-1}$ , and  $\Delta V^\ddagger = 7.9 \pm 0.5$  cm $^3$  mol $^{-1}$ . The small values of  $\Delta S^\ddagger$  and  $\Delta V^\ddagger$  suggest a dissociative interchange mechanism which is strongly supported by H<sub>2</sub>O exchange kinetics made by observing the effect of temperature and pressure on the <sup>17</sup>O NMR bulk water signal line widths, which provide evidence for water-bound intermediates.

Birke and co-workers<sup>150</sup> also studied the electrochemistry of H<sub>2</sub>O Cbl<sup>+</sup> in the presence of NO and NO<sub>2</sub><sup>-</sup> by cyclic voltammetry and differential pulse voltammetry. They find a thermodynamically favorable reduction of H<sub>2</sub>O Cbl<sup>+</sup> by NO to give cob(II)alamin and NO<sub>2</sub><sup>-</sup> which subsequently react with NO and H<sub>2</sub>O Cbl<sup>+</sup>, respectively, to give NO-cob(II)alamin

and NO<sub>2</sub>Cbl. They suggest that this reaction is slow in solution (to account for the observation that H<sub>2</sub>O Cbl<sup>+</sup> does not react with NO in neutral solution) but catalyzed at the electrode surface. H<sub>2</sub>O Cbl<sup>+</sup> can also catalyze the electrochemical reduction of NO by reaction of cob(II)alamin with NO to form cob(II)alamin and N<sub>2</sub>O, which is subsequently reduced to N<sub>2</sub>. In addition, NO<sub>2</sub><sup>-</sup> can also be catalytically reduced by Cbl's, and NO<sub>2</sub><sup>-</sup> binds to cob(II)alamin with a binding constant of  $3.5 \times 10^2$  M $^{-1}$ .

In contrast, Sharma et al.<sup>151</sup> report a reaction of NO with H<sub>2</sub>O Cbl<sup>+</sup> at low pH to form a complex with the same electronic spectrum as NO-cob(II)alamin at low pH. They postulate that in acid NO reacts with the small amount ( $pK_{\text{base-off}} = -2.1$ <sup>152</sup>) of base-off H<sub>2</sub>O Cbl<sup>+</sup> to form a NO-Co(III) species which undergoes an inner-sphere electron transfer to give cob(II)alamin (and nitronium ion), which then reacts with excess NO to give the observed product. The rate-determining step is said to be the dissociation of the Bzm ligand, which is reasonable given the magnitude of the observed rate constants ( $1.2 \times 10^{-3}$  s $^{-1}$  at pH 1) and the fact that the observed rate constant decreases with increasing pH (see eq 13). They attribute the failure of H<sub>2</sub>O Cbl<sup>+</sup> to react with NO at neutral pH to a negative trans effect of the coordinated Bzm ligand. As evidence, they find that di-aquacobinamide ((H<sub>2</sub>O)<sub>2</sub>Cbi<sup>2+</sup>), the axial base-free analogue of H<sub>2</sub>O Cbl<sup>+</sup>, as well as cob(II)inamide react with NO at all pH's to give a complex whose electronic spectrum is the same as that of NO-cob(II)alamin at low pH. Although the interpretation seems reasonable and could conceivably explain the observation by Zheng and Burke<sup>148</sup> that NO-cob(II)alamin is formed when H<sub>2</sub>O Cbl<sup>+</sup> is treated with NO under strong illumination, there are clearly some problems, the most notable being that the measured dissociation rate of NO from NO-cob(II)inamide (0.02 s $^{-1}$ ) is some 85-fold slower than that from base-off NO-cob(II)alamin (1.7 s $^{-1}$ ). The method of preparation of (H<sub>2</sub>O)<sub>2</sub>Cbi<sup>2+</sup>, exhaustive photolysis of dicyanocobinamide ((CN)<sub>2</sub>Cbi) in acidic solution under argon purge,<sup>153</sup> is fraught with difficulties and leads to an inhomogeneous product, which obviously complicates the interpretation of the observations.

van Eldik and co-workers<sup>154</sup> studied the reaction between MeIm and  $\beta$ -(*N*-methylimidazolyl)cobalamin (MeImCbl) to form bis(*N*-methylimidazolyl)cobalamin ((MeIm)<sub>2</sub>Cbl). The equilibrium constant for the substitution of MeIm for the intramolecularly coordinated Bzm ligand was  $9.6 \pm 0.1$  M $^{-1}$  at 25 °C by NMR measurements. The kinetics for formation of (MeIm)<sub>2</sub>Cbl show an interesting and unusual inverse dependence of  $k_{\text{obs}}$  on MeIm concentration. Although several possibilities are proposed to explain this behavior, the most likely is the mechanism shown in eq 17 in which dissociation of the axial Bzm and its replacement with water (i.e., the aquation of MeImCbl) is followed by substitution of water by MeIm. The associated rate law (eq 18) has a limiting value of  $k_1$  at high [MeIm] and a limiting value of  $k_{-2}$  at low [MeIm]. Thus, the inverse dependence of  $k_{\text{obs}}$  on [MeIm] requires only that  $k_{-2} > k_1$ . Activation parameters at low [MeIm] (i.e., for  $k_{-2}$ ) are  $\Delta H^\ddagger =$



$23.6 \pm 0.5 \text{ kcal mol}^{-1}$ ,  $\Delta S^\ddagger = 9 \pm 1 \text{ cal mol}^{-1} \text{ K}^{-1}$ , and  $\Delta V^\ddagger = 15.0 \pm 0.7 \text{ cm}^3 \text{ mol}^{-1}$ , and at high [MeIm] (i.e.,  $k_1$ ) they are  $\Delta H^\ddagger = 26.1 \pm 0.2 \text{ kcal mol}^{-1}$ ,  $\Delta S^\ddagger = 16.7 \pm 0.7 \text{ cal mol}^{-1} \text{ K}^{-1}$ , and  $\Delta V^\ddagger = 17 \pm 1 \text{ cm}^3 \text{ mol}^{-1}$ .

$$k_{\text{obs}} = (k_1 k_2 [\text{MeIm}] + k_{-1} k_{-2}) / (k_{-1} + k_2 [\text{MeIm}]) \quad (18)$$

The corrin ring clearly exerts a substantial cis effect on the metal ion as ligand substitution in even inorganic cobalamins is fast (stopped flow time scale) despite the usual inertness of  $d^6$  Co(III) complexes to ligand substitution. As part of a study of cis effects in cobalamins, 10-nitrosoaquacobalamin (10-NO-H<sub>2</sub>O-Cbl<sup>+</sup>) has now been studied.<sup>155</sup> The  $pK_a$  for ionization of the coordinated water molecule is  $10.71 \pm 0.04$  (25 °C) compared to 8.1 for H<sub>2</sub>O-Cbl<sup>+</sup> itself.<sup>156</sup> The electron-withdrawing nitroso group deactivates the metal for ligand substitution to the point that the coordinated water cannot be displaced by pyridine (1.2 M) or azide (0.7 M) over a 72 h period despite the fact that H<sub>2</sub>O-Cbl<sup>+</sup> itself reacts with these ligands with binding constants of 1.5 and  $2 \times 10^4 \text{ M}^{-1} \text{ s}^{-1}$ , respectively.

The substitution of iodine ion in iodocobalamin (ICbl) by imidazole (Im), azide, and thiosulfate ion has also been studied.<sup>155</sup> Azide and Im show saturation kinetics, while thiosulfate does not. The limiting rate constants were substantially different ( $11.5 \text{ s}^{-1}$  for Im and  $70 \text{ s}^{-1}$  for N<sub>3</sub><sup>-</sup>), so that the mechanism cannot be limiting D but must be a dissociative interchange. From the temperature dependence of the limiting (i.e., interchange) rate constant, activation parameters consistent with the mechanism assignment were determined.

#### 4.4. Electrochemistry

van der Donk and co-workers<sup>80</sup> studied the electrochemistry of *cis*-chlorovinylCbl by cyclic voltammetry. In DMF an irreversible cathodic peak was observed at  $-1.23 \text{ V}$  which resulted in Co–C bond cleavage as indicated by the fact that the return and second forward scans both showed the presence of the Co(I)/Co(II) couple of unalkylated Cbl's ( $-0.80 \text{ V}$  in DMF). The reduction wave for *cis*-chlorovinylCbl became quasi-reversible at scan rates of  $1 \text{ V/s}$ . This

was surprising since reduced RCbl<sup>-</sup> species are highly unstable and require ultrafast scan rates to achieve reversible redox behavior.<sup>157</sup> The results suggest that the Co–C bond in *cis*-chlorovinylCbl is significantly stronger than in RCbl's with  $sp^3$ -hybridized cobalt-bound carbons.

Kräutler et al.<sup>82</sup> determined the redox potentials for norpseudovitamin B<sub>12</sub> and pseudovitamin B<sub>12</sub> by UV-vis potentiometry at pH 7 to be  $-0.49$  and  $-0.48 \text{ V}$  (vs SHE), respectively, for the Co(II)/Co(I) couple and  $-0.14$  and  $-0.01 \text{ V}$ , respectively, for the CN–Co(III)/Co(II) couple. The latter values compare to ca.  $-0.23 \text{ V}$  for the CNCbl/cob(II)alamin couple under the same conditions.<sup>102</sup> UV-vis spectra of the partially reduced norpseudovitamin B<sub>12</sub> (at  $-0.273 \text{ V}$ , i.e., the Co(II) state) confirmed the presence of the Co(II) oxidation state, and comparison to the pH-dependent spectra of cob(II)alamin<sup>102</sup> suggested that the Co(II) species of norpseudovitamin B<sub>12</sub> is predominantly base-off at pH 7 in contrast to cob(II)alamin itself which is base-on in neutral solution ( $pK_{\text{base-off}} = 3.10 \pm 0.01$ <sup>158</sup>).

Several Cbl's (H<sub>2</sub>O-Cbl, GSCbl, (H<sub>2</sub>O)<sub>2</sub>Cbi<sup>2+</sup>, and acetatocobalamin) have been adsorbed onto edge pyrolytic graphite electrodes with or without the B<sub>12</sub> binding proteins IF and Hc and studied by cyclic voltammetry.<sup>159</sup> For the adsorbed corrinoids densities of  $3.7 \times 10^{-10} \text{ mol mm}^{-2}$  were obtained, and the reduction potentials for adsorbed corrinoids were very similar to those in solution. When acetatocobalamin bound to IF (density  $2.6 \times 10^{-13} \text{ mol mm}^{-2}$ ) or Hc was adsorbed onto the electrodes, the cyclic voltammograms showed very little change from those for adsorbed corrinoids alone.

Mimica et al.<sup>160</sup> also studied modified pyrolytic graphite electrodes. When AdoCbl was adsorbed on such electrodes (density  $1.7 \times 10^{-10} \text{ mol cm}^{-2}$ ) the first potential scan led to the reductive loss of the Ado ligand (as expected) at ca.  $-1.1 \text{ V}$ , following which the electrode behaved the same as one on which H<sub>2</sub>O-Cbl<sup>+</sup> had been adsorbed. Such electrochemically activated AdoCbl electrodes are highly active as redox catalysts for L-cysteine oxidation and reduction, while the bare electrodes are completely inert. However, the electrodes were not active until the adsorbed AdoCbl had been electrochemically reduced to give cob(II)alamin. The best reversibility was observed at pH 7.4, and the only product obtained from exhaustive controlled potential oxidation was L-cystine.

#### 4.5. Other Reactions

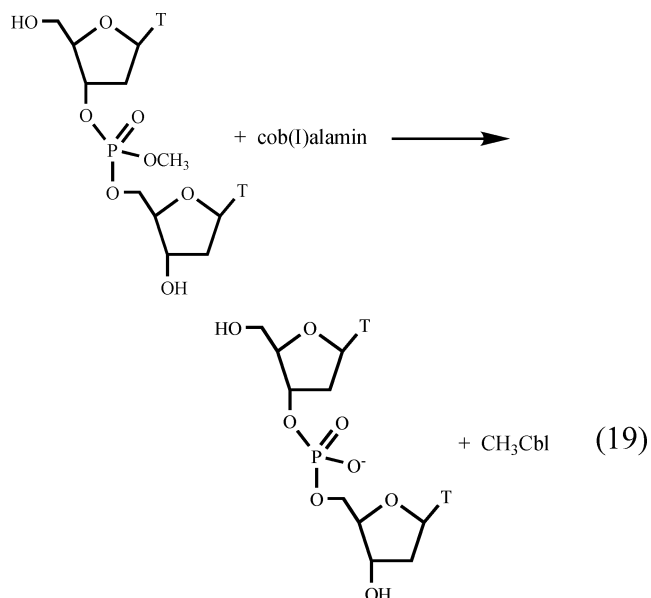
Meskers and Dekkers<sup>161,162</sup> studied the complexes of CNCbl, H<sub>2</sub>O-Cbl<sup>+</sup>, and (CN)<sub>2</sub>Cbi with enantiomeric lanthanide(III) tris(pyridine-2,6-dicarboxylate),  $\Delta$ - and  $\Lambda$ -Ln(DPA)<sub>3</sub><sup>3-</sup>. Using Tb(DPA)<sub>3</sub><sup>3-</sup> the lanthanide-induced shifts (LIS) in the <sup>1</sup>H NMR spectra of the corrinoids were used to determine the position and orientation of the magnetic axis of the Tb(DPA)<sub>3</sub><sup>3-</sup> in the complexes. The LIS also provide values of the average association constants,  $K_{\text{ave}}$ , for the pair of diastereomeric complexes formed when the enantiomeric Tb(DPA)<sub>3</sub><sup>3-</sup> complexes bind to the chiral corrinoids. The values for CNCbl and (CN)<sub>2</sub>Cbi were  $4 \pm 0.5$  and  $0.8 \pm 0.2 \text{ M}^{-1}$ , respectively, but the much

larger values for  $\text{H}_2\text{OCbl}^+$  were strongly dependent on ionic strength ( $K_{\text{ave}} = 70 \pm 1 \text{ M}^{-1}$  at  $I = 0.007$ ) and decrease with increasing ionic strength. The corrinoids bind the enantiomers of racemic  $\text{Nd}(\text{DPA})_3^{3-}$  differentially, thus inducing circular dichroism in the electronic transitions of the lanthanide, an example of the Pfeiffer effect.<sup>163</sup> The dependence of the induced circular dichroism on the concentration of the corrinoid permits determination of the differential binding constant,  $K_{\Delta} - K_{\Lambda}$ , for the two diastereomers of the lanthanide complex and from these the binding enantioselectivity,  $E_b$ , defined as  $(K_{\Delta} - K_{\Lambda})/2 K_{\text{ave}}$ . The values of  $E_b$  obtained were  $-0.5 \pm 0.2$ ,  $-0.7 \pm 0.2$ , and  $-0.7 \pm 0.3$  for  $\text{H}_2\text{OCbl}^+$ ,  $\text{CNCbl}$ , and  $(\text{CN})_2\text{Cbi}$ , respectively. NMR-based molecular models of the diastereomeric complexes suggest hydrogen bonding between the  $\alpha$ - and  $g$ -side chain amide proton and the carboxylate oxygen of two DPA ligands.

Enantioselective dynamic quenching of the luminescence of the enantiomeric  $\Delta$ - and  $\Lambda$ - $\text{Tb}(\text{DPA})_3^{3-}$  and  $\Delta$ - and  $\Lambda$ - $\text{Eu}(\text{DPA})_3^{3-}$  by corrinoids has also been demonstrated.<sup>162,164</sup> For  $\text{Tb}(\text{DPA})_3^{3-}$  the average diastereomeric quenching rate constants were 1.0, 2.9, and  $0.53 \times 10^8 \text{ M}^{-1} \text{ s}^{-1}$  for  $\text{CNCbl}$ ,  $(\text{CN})_2\text{Cbi}$ , and dicyanoheptamethylcobyrinate, respectively, and the degree of enantioselectivity was  $-0.24$ ,  $-0.20$ , and  $+0.01$ , respectively. The quenching by  $\text{H}_2\text{OCbl}^+$  was strongly dependent on ionic strength and pH, suggesting that  $\text{H}_2\text{OCbl}^+$  and  $\text{HOCbl}$  have different quenching rates. Assuming that the quenching involves a preequilibrium formation of a complex between the lanthanide and the corrinoid, for those complexes for which ground-state formation constants and enantioselectivities were determined,<sup>161,162</sup> the average rate of energy transfer  $((k_{\text{et}}^{\Delta} + k_{\text{et}}^{\Lambda})/2)$  can be calculated. The quenching enantioselectivity is lower than that for the ground-state complexation, so that  $k_{\text{et}}^{\Delta}/k_{\text{et}}^{\Lambda}$  is about 0.3 for  $\text{CNCbl}$ ,  $\text{H}_2\text{OCbl}^+$  (pH 6.7), and  $(\text{CN})_2\text{Cbi}$ .

Meskers and Dekkers<sup>162</sup> also showed that the luminescence quenching of  $\text{Ln}(\text{DPA})_3^{3-}$  by  $\text{CNCbl}$  can be used to monitor the binding of corrinoids to proteins. Addition of an anti- $\text{CNCbl}$  monoclonal antibody (Ab) to solutions of the  $\text{Tb}(\text{DPA})_3^{3-}$  complex with  $\text{CNCbl}$  causes an increase in the quenching rate simultaneously with a change in enantioselectivity. The equivalence point occurs at a  $[\text{CNCbl}]/[\text{Ab}]$  ratio of  $\sim 2$ , a result of the two identical binding sites on IgG antibodies. The higher quenching rate for the  $\text{CNCbl}$ -Ab complex relative to free  $\text{CNCbl}$  and the change in enantioselectivity imply that  $\text{CNCbl}$  is still accessible to ions in solution when bound to the Ab but that the binding covers up the  $\alpha$ - and  $g$ -side chain binding site for the lanthanide complex on  $\text{CNCbl}$ . In contrast, addition of Hc to solutions of the  $\text{Tb}(\text{DPA})_3^{3-}$  complex with  $\text{CNCbl}$  causes a strong decrease in the quenching rate with an equivalence point at  $[\text{CNCbl}]/[\text{Hc}] \approx 1$ , since Hc has a single binding site for  $\text{B}_{12}$ . For solutions in which quenching still remains (i.e., those in which insufficient Hc has been added to bind all of the  $\text{CNCbl}$ ), the quenching enantioselectivity is unchanged, so that the unbound  $\text{CNCbl}$  is the main quencher in this case.

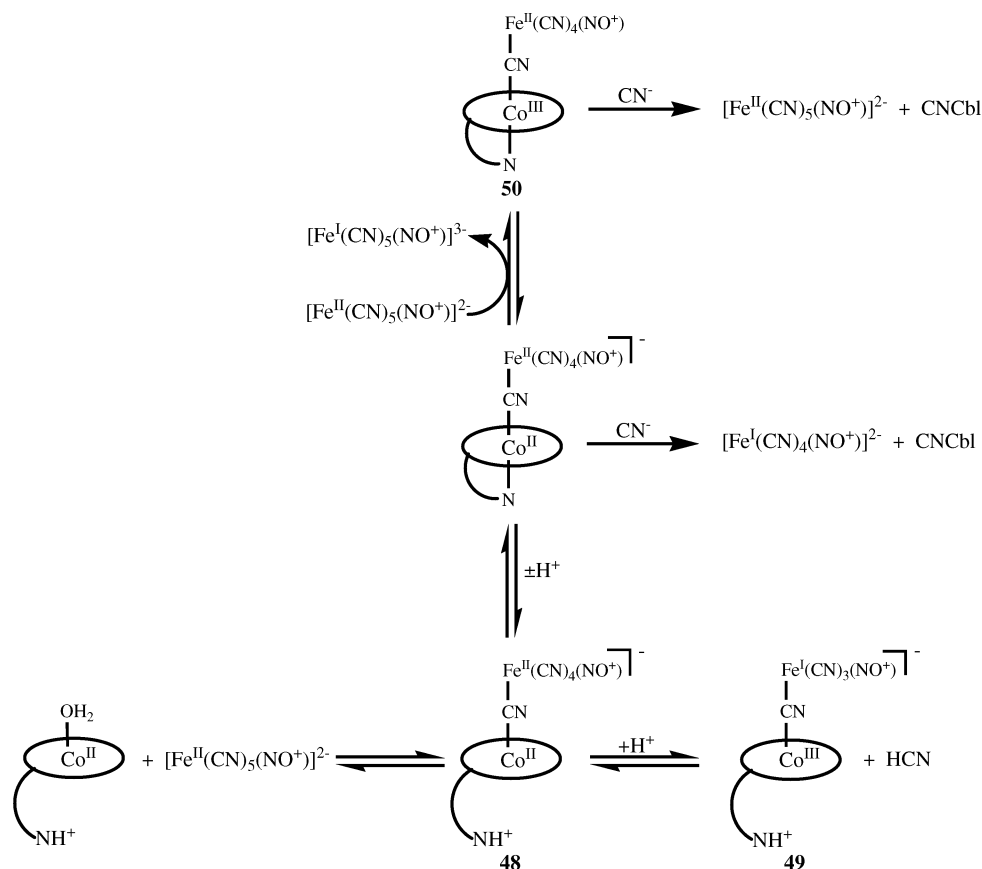
Cob(I)alamin has been used to dealkylate phosphotriesters, including trimethyl phosphate, methylated and ethylated thymidine dinucleotides, and methylated DNA (eq 19).<sup>165</sup> The second-order rate constants using cob(I)alamin were some 2000- to 4700-fold higher than those for thiosulfate, which had previously been used for phosphotriester demethylation, but dimethyl phosphate was unreactive. This appears to be the first report of the alkylation of a cobalt corrinoid with a phosphotriester.



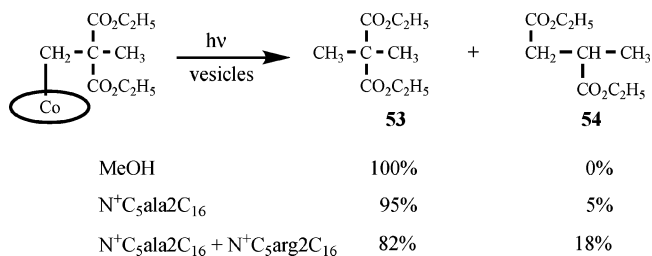
The complicated reaction of cob(II)alamin with nitroprusside (NP) has been studied by UV-vis,  $^1\text{H}$  NMR, and EPR spectroscopies as well as cyclic voltammetry, differential pulse voltammetry, and stopped flow kinetics.<sup>166</sup> The reaction follows two pathways of different order in NP depending on the pH and ratio of NP to cob(II)alamin. At low pH ( $< 3$ ) and low NP ( $[\text{NP}]/[\text{cob(II)alamin}] \approx 1$ ), an initial NP-cob(II)alamin adduct (**48**, Scheme 10) undergoes an inner-sphere electron-transfer process to release cyanide and form the final product  $[(\mu\text{-NC})\text{-Fe}^{\text{I}}(\text{CN})_3(\text{NO}^+)\text{Cbl}]^-$  (**49**). At higher pH the cyanide released in this step attacks the base-on form of the initial adduct to form  $\text{CNCbl}$  and  $[\text{Fe}^{\text{I}}(\text{CN})_4(\text{NO}^+)]^{2-}$ . The pH dependence results from the effect of pH on the nucleophilicity of cyanide. At higher NP concentrations the initial adduct, **48**, reacts with excess NP to give  $[(\mu\text{-NC})\text{-Fe}^{\text{II}}(\text{CN})_4(\text{NO}^+)\text{Cbl}]^-$ , **50**, and reduced nitroprusside, and **50** then reacts with cyanide to give  $\text{CNCbl}$  and NP. In addition, the release of NO by reduction of NP by cob(II)alamin was measured and suggests how Cbl's may effect the pharmacological action of nitroprusside.

A 2,2-bis(ethoxycarbonyl)-1-propyl heptaethylcobyrinate has been incorporated into highly stable hybrid vesicles formed from an alanine-based lipid,  $\text{N}^+\text{C}_5\text{-ala}2\text{C}_{16}$  (**51**), and a novel arginine-based lipid,  $\text{N}^+\text{C}_5\text{-arg}2\text{C}_{16}$  (**52**), to create a model for the AdoCbl-dependent enzyme methylmalonylCoA mutase.<sup>167</sup> When the alkylcorrinoid was photolyzed anaerobically in methanol, only the reduction product of the alkyl ligand, **53**, was formed (Scheme 11). However, in the mixed vesicles, 18% of the rearranged product

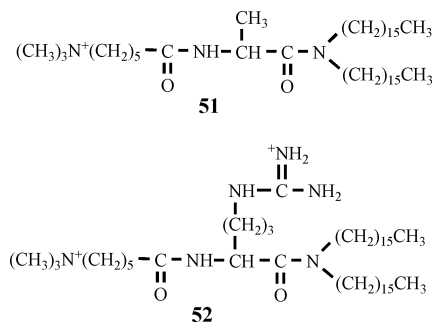
Scheme 10



Scheme 11

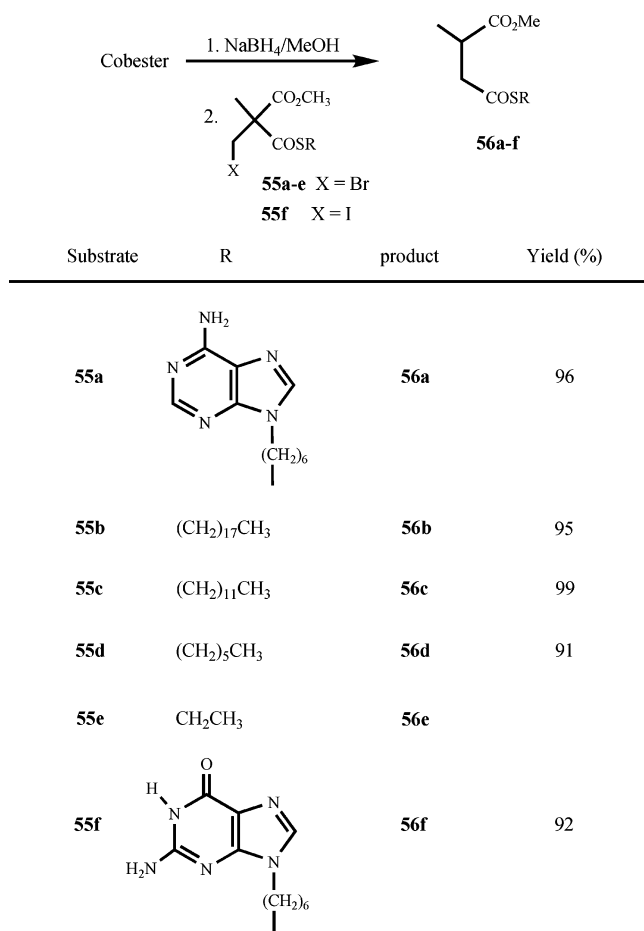


(**54**, formed by 1,2-migration of an ethoxycarbonyl group) was formed, more than three times as much as previously found in vesicles made of N<sup>+</sup>C<sub>5</sub>ala2C<sub>16</sub> only.<sup>168</sup> Fluorescence and differential scanning calorimetry experiments suggested that the corrinoid is in a nonpolar domain of the vesicles, close to the amino acid residues. The authors suggest, with no evidence, that an interaction between the arginine residue of the lipid and an ester of the alkyl moiety enhances the rearrangement.



Sun and Darbre<sup>169</sup> reported a very intriguing set of experiments aimed at modeling the methylmalonylCoA mutase rearrangement. The synthesis of alkylcobalt corrinoids is normally carried out by treating reduced cobalt corrinoids with a large molar excess of alkylating agent (frequently halides). These authors found that when heptamethylcob(II)yrinate perchlorate (“cobester”) was treated with an excess of NaBH<sub>4</sub> in methanol, but *stoichiometric* alkyl halides bearing thioester methylmalonylCoA-like moieties, no alkylated product is formed, but a rapid rearrangement to succinate-like products ensued in very high isolated yields (Scheme 12). Only the thioester migrates under these conditions since a carbomethoxy analogue gave only reduced products. The alkylated products could be isolated if reduced cobester was treated with 3–5 equiv of the halides. A similar reaction with HOCl and **55b** gave the succinate **56b** in 49% yield. The chiral substrate, *S*-**55e**, gave a racemic mixture of the succinates *S*-**56b** and *R*-**56b**. Experiments using controlled potential reduction of cobester demonstrated that excess reducing agent was not responsible for the observed rearrangements. Experiments in CD<sub>3</sub>OD and CH<sub>3</sub>OD showed that a single deuterium is incorporated into the rearranged products and no undeuterated product is formed in CH<sub>3</sub>OD, indicating protonation of an anionic rearrangement product. This is very provocative work considering the fact that it is now generally accepted that the carbon skeleton rearrangements catalyzed by AdoCbl-dependent enzymes occur via radical rearrangements

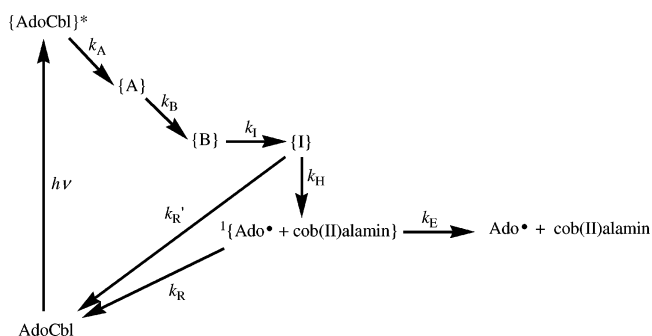
Scheme 12



while the rearrangement mechanism in play here evidently goes via an anion.

Hannak et al.<sup>170</sup> raised a monoclonal antibody to AdoCbl. The antibody binds AdoCbl strongly ( $K_d = 10 \mu\text{M}$ ) and CNCbl less tightly ( $K_d = 65 \mu\text{M}$ ) but binds the nucleotide loop-free (CN)<sub>2</sub>Cbi weakly ( $K_d = 740 \mu\text{M}$ ), suggesting that it recognizes base-on cobamides. The antibody did not bind benzimidazole or 2-aminoisopropylribazole phosphate. PseudoAdoCbl and adenosyl Factor A, which are mostly base-off in solution, were bound well but not as strongly as AdoCbl ( $K_d = 68$  and  $29 \mu\text{M}$ , respectively). Binding of PseudoAdoCbl and Ado-Factor A to the antibody caused large changes in their UV-vis spectra which strongly resembled the spectrum of base-on AdoCbl. For AdoFactor A <sup>1</sup>H nOe NMR experiments confirmed the base-on binding by enhancements of the cross-peaks between the N8 hydrogen of the 2-methyladenine axial base and the *e*- and *f*-side chains. Since the reactivity of the Co-C bond depends strongly on the trans axial ligand, the antibody may regulate the reactivity of such corrinoids. A 90% reduction in the reactivity of an Ado-cobalt corrinoid with cyanide when bound to the antibody is cited as an example. However, since the reaction of cyanide with AdoCbl requires the preequilibrium replacement of the axial Bzm by cyanide before Co-C bond heterolysis, the observation could be the result of blocked access to the lower axial ligand position in the antibody complex, as is known to be the case with corrinoid complexes to the B<sub>12</sub> binding protein Hc.<sup>171</sup>

Scheme 13



## 5. Photochemistry

The primary photochemistry of AdoCbl, CH<sub>3</sub>Cbl, CH<sub>3</sub>CH<sub>2</sub>Cbl, and CH<sub>3</sub>CH<sub>2</sub>CH<sub>2</sub>Cbl has been investigated by transient absorbance spectroscopy at 400 and 520–530 nm.<sup>172–174</sup> For AdoCbl the photochemistry is wavelength-independent, a cob(II)alamin-like spectrum develops rapidly (picosecond time scale), and the quantum yield is essentially determined by the competition between diffusive separation of the caged radical pair and in-cage recombination. The rate constant for pseudo-unimolecular recombination is  $1.4 \times 10^9 \text{ s}^{-1}$ , essentially identical to previous reports,<sup>175–177</sup> and the calculated fractional cage efficiency,  $F_c$ , was  $0.71 \pm 0.05$  in water at room temperature.

The solvent effect on the photolysis of AdoCbl has also been studied in ethylene glycol, water, and mixtures of these solvents.<sup>173</sup> In water excitation produces several excited states with spectra evolving from cob(III)alamin-like to cob(II)alamin-like, which decay sequentially on the 100 fs, 1–3 ps, and 14–37 ps times scales to form the intermediate state {I} (Scheme 13).

Intermediate {I}, which has a cob(II)alamin-like spectrum, can either return to the ground state or relax to the caged radical pair. The small change in the spectrum of {I} on evolution to the caged radical pair is consistent with a relaxation of the corrin ring. There are differences in ethylene glycol which may represent either a change in the nature of {I} (possibly to a base-off species) or differences in the ratio  $k_R/k_H$ , but in ethylene glycol-water mixtures, the mechanism more closely resembles that in water than that in ethylene glycol. The measured rate constant for radical pair recombination was independent of solvent composition and had an average value of  $1.39 \pm 0.06 \times 10^9 \text{ s}^{-1}$ , while the rate constants for cage escape had the expected dependence on viscosity. Surprisingly the linear dependence of  $k_E$  on viscosity had a finite intercept, which is consistent with (but does not prove) the possibility of an intersystem crossing of the caged radical pair from a singlet to triplet state. The data permit the calculation of the cage efficiency in ethylene glycol (0.92) at 20 °C.

The primary photochemistry of the other RCbl's is considerably different. CH<sub>3</sub>CH<sub>2</sub>Cbl and CH<sub>3</sub>CH<sub>2</sub>CH<sub>2</sub>Cbl undergo prompt homolysis to generate a cob(II)-alamin species at 400 nm. At 520 nm slower homolysis occurs with formation of a cob(III)alamin-like intermediate which subsequently converts to cob(II)-

alamin. In contrast, when CH<sub>3</sub>Cbl is excited at 400 nm, two processes are observed, prompt Co–C bond homolysis (25%) and formation of a metastable cob(III)alamin-like product (75%). Recombination of CH<sub>3</sub>• and cob(II)alamin is not observed (i.e.,  $F_c = 0$ ). At 520 nm (the region of the  $\alpha\beta$  band) only the metastable cob(III)alamin-like product is formed, and regardless of the wavelength of excitation, it partitions between homolysis to form caged cob(II)alamin + CH<sub>3</sub>• radical pairs (14%) and conversion back to the ground state (86%). The quantum yield for CH<sub>3</sub>-Cbl photolysis is thus wavelength dependent (0.14 at 520 nm and 0.34 at 400 nm). For all three of these RCbl's the metastable cob(III)alamin-like product appears to be a metal-to-ligand charge transfer (MLCT) state on the pathway to homolysis. For CH<sub>3</sub>-CH<sub>2</sub>Cbl and CH<sub>3</sub>CH<sub>2</sub>CH<sub>2</sub>Cbl the more electron-donating alkyl groups destabilize the carbanion character of the MLCT, leading to a shorter lifetime than that observed for CH<sub>3</sub>Cbl, so that the lifetime for this state varies inversely with the size of the alkyl ligand. The rate constants for recombination of the caged radical pairs for all four of the RCbl's ( $0.76\text{--}1.4 \times 10^9 \text{ s}^{-1}$ ) vary within a narrow 2-fold range. In contrast, the rate constant for diffusive escape of the radicals from the cage varies by 8-fold with the size of the alkyl radical. The calculated efficiencies of  $F_c$  are  $0.22 \pm 0.14$  for CH<sub>3</sub>Cbl,  $0.38 \pm 0.09$  for CH<sub>3</sub>CH<sub>2</sub>Cbl,  $0.57 \pm 0.16$  for CH<sub>3</sub>CH<sub>2</sub>CH<sub>2</sub>Cbl, and  $0.72 \pm 0.13$  for AdoCbl, which increase, as expected, with the size of the alkyl radical.

An FT-EPR study of pulsed laser photolysis of CH<sub>3</sub>-Cbl and AdoCbl<sup>178</sup> shows chemically induced dynamic electron polarization (CIDEP) in the spectra of the alkyl radicals generated by photolysis in neutral aqueous solution at 11 °C. For example, the time dependence of the CH<sub>3</sub>• spectrum shows a biphasic decay with the faster phase having the same time constant as the spin–lattice relaxation time of the CH<sub>3</sub>• radical in aqueous solution, indicating that the radical is formed with spin polarization larger than thermal equilibrium. Before reaching thermal equilibrium the four-line spectrum differs significantly from the 1:3:3:1 thermal equilibrium pattern with the low-frequency part of the spectrum enhanced relative to the high-frequency part. Furthermore, the CIDEP is wavelength dependent, evidence of the development of the spin state in a precursor radical pair, in agreement with the findings of Sension et al.<sup>173–175</sup> regarding two reaction paths for CH<sub>3</sub>Cbl photolysis. The spectrum of the Ado• radical formed from AdoCbl photolysis, a triplet of doublets of doublets, also shows CIDEP but is wavelength-independent, again consistent with the Sension et al. finding of only a single reaction path for AdoCbl photolysis.

## 6. Spectroscopy

Extensive solid-state <sup>59</sup>Co, <sup>13</sup>C, <sup>15</sup>N, and <sup>31</sup>P NMR studies at natural abundance have been reported<sup>179</sup> for CNCbl recrystallized from different solvents and under different conditions. Two polymorphs are found which presumably correspond to the “wet”<sup>180</sup> and “dry”<sup>181</sup> CNCbl structures of Hodgkin and co-workers. The <sup>59</sup>Co NMR spectra consisted of a 200 kHz wide

pattern characterized by an isotropic chemical shift of  $4650 \pm 100$  ppm (downfield from saturated K<sub>3</sub>[Co(CN)<sub>6</sub>], chemical shift anisotropy and asymmetry parameters of  $-635 \pm 100$  ppm and  $0.2 \pm 0.1$ , respectively, Euler angles of  $45 \pm 20^\circ$ ,  $40 \pm 20^\circ$ , and  $20 \pm 20^\circ$ , and quadrupole coupling constants  $e^2qQ/h = 27.8 \pm 0.3$  MHz,  $\eta_q = 0.1 \pm 0.1$  for the “wet” polymorph and  $26.1 \pm 0.4$  and  $0.1 \pm 0.1$  for the “dry” polymorph). Excellent high-resolution <sup>13</sup>C CPMAS spectra were obtained with average line widths of ca. 0.25 ppm. Spectral assignments were made based on the assigned solution spectra and spectral editing methods based on solid-state dipolar couplings, although the entire <sup>13</sup>C spectrum could not be unambiguously assigned. The two polymorphs differed in chemical shifts in the carbonyl and methylene regions, as expected from the differences seen in side chain conformation in the X-ray structures, but also differed at a number of corrin ring carbons, including C10, and in the axial nucleotide B5, B7, and R1 resonances, possibly indicating corrin ring conformational differences. The <sup>15</sup>N CPMAS spectra showed only the amide side chain and nucleotide NB1 resonances, suggesting that the five missing resonances, which are all directly bonded to the cobalt atom, are so strongly coupled to the metal as to broaden their signals beyond detection. The <sup>31</sup>P CPMAS resonance was identical for the two polymorphs and displayed chemical shift anisotropies similar to those of nucleoside monophosphates.

Brasch and Finke<sup>182</sup> suggested the use of the aromatic region of the <sup>1</sup>H NMR spectrum of cobalamins as a method for assessing the purity of Cbl preparations, but HPLC would seem to be a more sensitive and practical method.

van Doorslaer et al.<sup>183</sup> investigated heptamethylcob(II)yrinate (cob(II)ester<sup>+</sup>) and its oxygenated complexes by cw X-band EPR and various pulse EPR and ENDOR techniques in toluene and methanol. They report **g** and **A**<sup>Co</sup> matrixes and the direction of their principal axes as well as temperature-dependent cw EPR measurements for cob(II)ester, its oxygenated complex, O<sub>2</sub>-cob(II)ester<sup>+</sup>, and complexes of the oxygenated complex with Py and MeIm (O<sub>2</sub>-(Py)cob(II)ester<sup>+</sup> and O<sub>2</sub>-(MeIm)cob(II)ester<sup>+</sup>, which show a strong influence of a nitrogenous base on the O<sub>2</sub> binding equilibrium. The cobalt hyperfine interactions of the oxygenated cob(II)ester are much less anisotropic than for cob(II)ester itself, presumably due to the electron withdrawal by the O<sub>2</sub>, and are independent of the nature of the axial base. These observations agree with the superoxide formulation, Co(III)-O<sub>2</sub><sup>-</sup>, rather than the spin-pairing model for Co(II)-O<sub>2</sub> complexes. The ENDOR line widths permit calculation of the maximum cobalt nuclear quadrupole couplings of 700 kHz for O<sub>2</sub>-cob(II)ester<sup>+</sup> and 400 kHz for the Py and MeIm adducts. For the latter the hyperfine interaction of the axial base coordinating nitrogen is dominated by the isotropic part ( $\alpha_{\text{iso}} = 3.6$  or  $3.5$  MHz, respectively) with only a small dipolar part. In contrast, the corrin ring nitrogen's hyperfine interactions for all of the oxygenated complexes have a negative isotropic part ( $\alpha_{\text{iso}} = -0.9$  MHz) and a significant dipolar part ( $-0.4, -0.4, 0.8$

MHz for  $O_2$ -cob(II)ester<sup>+</sup> and  $-0.3$ ,  $-0.3$ ,  $0.6$  MHz for the Py and MeIm complexes) which correspond to distances of  $2.4 \pm 0.4$  and  $2.7 \pm 0.4$  Å, respectively, between the nitrogens and the unpaired electron. The X-ray structure of  $O_2$ -cob(II)alamin<sup>185</sup> shows an average distance of  $2.7$  Å between the coordinated oxygen and the corrin nitrogens and  $2.9$  Å between the closest corrin nitrogens and the second oxygen ( $3.8$  Å for the farthest corrin nitrogens). These distances and the orientation of the hyperfine principal axis again support the Co(III)- $O_2^-$  model of the oxygenated complexes.

Similarly, interactions of the nitrogens in solid cob(II)alamin powder (diluted in HOcbl powder) with the unpaired electron have been studied by X- and Q-band HYSCORE EPR.<sup>185</sup> The use of two frequencies allowed the determination of the **A** matrixes and **Q** tensors for the corrin ring nitrogens and the remote (i.e., *N*-glycosidic) nitrogen of the Bzm ligand. For the remote nitrogen the anisotropy is consistent with a point-dipole interaction of the nitrogen with the metal at a distance of  $3.8$  Å (the X-ray distance is  $4.0$  Å<sup>85</sup>). It was not possible, based on these data, to tell if the corrin ring nitrogens are inequivalent. For the ring nitrogens the hyperfine matrixes have the **A**<sub>1</sub> axes toward the metal and at  $25^\circ$  below the plane of **g**<sub>1</sub> and **g**<sub>2</sub>, and the hyperfine principal values are negative.

Van Doorslaer et al.<sup>186</sup> also studied the cw and pulsed EPR and pulsed ENDOR at different frequencies of cob(II)ester<sup>+</sup>ClO<sub>4</sub><sup>-</sup> and base-off cob(II)alamin<sup>+</sup>, species which are frequently assumed to be four-coordinate, in various solvents to investigate the axial ligation. The *g* and cobalt hyperfine values of cob(II)ester<sup>+</sup>ClO<sub>4</sub><sup>-</sup> in toluene suggest axial ligation of a weak donor, presumed to be the expected ion pair with ClO<sub>4</sub><sup>-</sup>, in agreement with the X-ray structure of cob(II)ester<sup>+</sup>ClO<sub>4</sub><sup>-</sup>,<sup>187</sup> which shows an axially coordinated perchlorate ion with a Co-O distance of  $2.31$  Å. However, the *g* and cobalt hyperfine values of cob(II)ester<sup>+</sup> in methanol and methanol/water mixtures and of base-off cob(II)alamin<sup>+</sup> in methanol/water indicate axial coordination with a stronger donor, i.e., water or methanol, and this is confirmed by comparison of the ENDOR and HYSCORE spectra with those obtained in deuterated solvents. However, in methanol below the phase transition temperature of  $100$  K the EPR parameters clearly indicate six coordination, although in methanol/water only the five-coordinate forms are detected for both cob(II)ester<sup>+</sup> and base-off cob(II)alamin<sup>+</sup> at all temperatures. The ring nitrogens are also sensitive to the state of axial ligation, and the coordination number is reflected in the anisotropy of the hyperfine interaction. The ENDOR experiments (with complimentary DFT calculations) show that the C19 proton has the strongest hyperfine interaction and carries the highest spin density of all of the corrin ring protons.

In an important paper, Trommel et al.<sup>114</sup> studied the effect of exogenous axial ligands on the EPR hyperfine splitting of cob(II)inamide. The study was motivated, in part, by the fact that early X-ray crystal structures of Ado-Cbl-dependent enzymes reconstituted with CNCbl, H<sub>2</sub>OCbl<sup>+</sup>, CH<sub>3</sub>Cbl, or AdoCbl

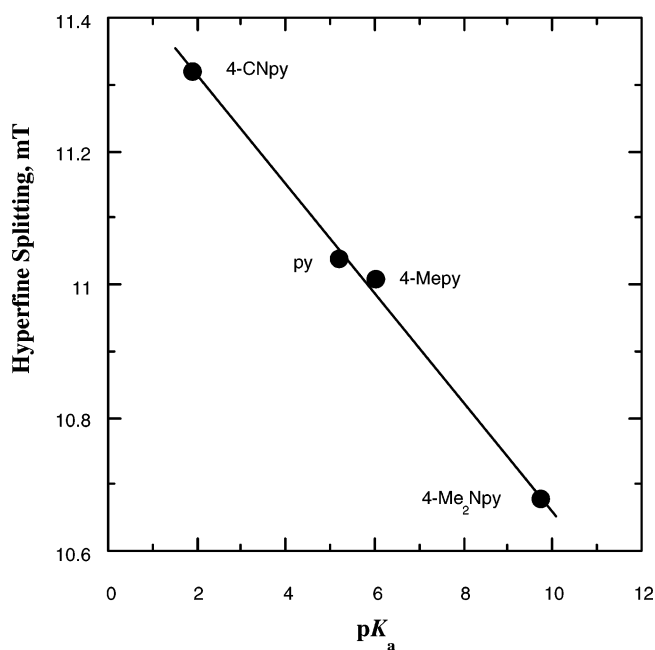


**Figure 4.** Plot of the EPR hyperfine splitting of (4-XPY)-cob(II)inamide adducts vs the pK<sub>a</sub> of the 4-XPY axial ligand. The solid line is a linear regression, slope =  $-0.0816 \pm 0.0034$  mT, intercept =  $11.48 \pm 0.021$  mT,  $r^2 = 0.997$ .

showed surprisingly long axial Co-NB<sub>3</sub> or Co-N<sub>His</sub> bonds (on the order of  $2.50$  Å),<sup>188,189</sup> which had led to much speculation regarding the possible manipulation of axial bond length by enzymes as a mechanism for catalysis of Co-C bond homolysis. EPR theory requires that Co(II) hyperfine splitting increases as electron donation from an axial N-donor decreases, but earlier observations found similar hyperfine splitting for both the Py and the 2-methylpyridine (2-MePy) adducts of cob(II)inamide,<sup>190</sup> despite the fact that the 2-MePy adduct must surely have a longer axial Co-N bond. Trommel et al.<sup>114</sup> found that for adducts of cob(II)inamide with 4-substituted pyridines (4-XPY) the hyperfine splitting increased linearly with the decrease in 4-XPY basicity, in agreement with theory (Figure 4). No adduct could be detected for sterically hindered axial bases including 2-MePy (up to  $8$  M) as long as unhindered impurities were first removed by an affinity distillation (see above), thus explaining the earlier observations of similar hyperfine coupling in cob(II)inamide in the presence of excess Py and 2-MePy as being due to unhindered impurities in the latter. Most importantly, in the five AdoCbl-dependent enzymes for which EPR hyperfine splittings of bound cob(II)alamin have been observed, three show no significant difference from that of free cob(II)alamin ( $d_{Co-NB_3} = 2.13$  Å)<sup>85</sup> while the other two show  $0.3$ – $0.5$  mT lower hyperfine splitting than free cob(II)inamide, suggesting that, if anything, the enzyme-bound species has a shorter axial Co-NB<sub>3</sub> bond. The hyperlong Co-NB<sub>3</sub> bonds observed in early enzyme X-ray structures thus appear to be artifacts of mixed redox and ligand states in the crystals.

In another important paper on this subject Champloy et al.<sup>191</sup> used XAS spectroscopy to address the question of the hyperlong axial Co-NB<sub>3</sub> bonds observed in some AdoCbl-dependent enzyme X-ray

structure studies. XAS spectra were observed for H<sub>2</sub>Ocbl<sup>+</sup>, CNCbl, CH<sub>3</sub>Cbl, AdoCbl, and cob(II)alamin in water/glycerol and water/trehalose glasses at 100 K, both free and bound to glutamate mutase and both before and after irradiation with 7.76 keV X-rays for 10 min. The XAS spectra are unchanged for cob(II)-alamin, CH<sub>3</sub>Cbl, and AdoCbl both before and after radiation for both free and protein-bound species. However, the H<sub>2</sub>Ocbl<sup>+</sup> and CNCbl spectra change significantly after irradiation and resemble each other and the spectrum of cob(II)alamin. Since X-ray radiolysis of water produces free electrons, the authors conclude that H<sub>2</sub>Ocbl<sup>+</sup> and CNCbl are reduced to Co(II) species by this treatment. In a glass matrix (or in the active site of an enzyme) the upper axial ligand would have little freedom to diffuse away from the metal, so the species formed should resemble a six-coordinate cob(II)alamin, while cob(II)alamin is normally five-coordinate. Although six-coordinate Co(II) species are rare, existing examples of such species are characterized by axial Co–N bonds as long as 2.44 Å.<sup>192</sup> Thus, the long Co–NB3 bonds observed in enzymes reconstituted with CNCbl or H<sub>2</sub>Ocbl<sup>+</sup> are likely to be the result of X-ray-induced photoreduction to cob(II)alamin species that are essentially six coordinate. For those enzymes reconstituted with CH<sub>3</sub>Cbl, the observation of long Co–NB3 bonds could well be due to visible light photolysis followed by X-ray photoreduction of the resulting H<sub>2</sub>Ocbl<sup>+</sup>.

Brunold et al.<sup>193</sup> used UV–vis, circular dichroism (CD), magnetic circular dichroism (MCD), and resonance Raman spectroscopies, in conjunction with time-dependent density functional theory calculations, to assign the electronic absorption spectra of CH<sub>3</sub>Cbl, AdoCbl, H<sub>2</sub>Ocbl<sup>+</sup>, CNCbl, and AdoCbi<sup>+</sup>. Most inorganic Cbl's display "typical" UV–vis spectra dominated by the  $\alpha/\beta$  bands in the visible and a prominent  $\gamma$  band in the UV. In contrast, most alkylCbl's display "unique" spectra in which the  $\beta$  band is more prominent than the  $\alpha$  band and the  $\gamma$  band intensity is distributed over several bands in the UV. The "unique" spectra have never been completely assigned, and the differences between the "unique" and "typical" spectra have not been explained. In the "typical" spectra the  $\alpha/\beta$  bands correspond to the origin and first member of a progression in a corrin mode involving stretches of the C=C bond oriented along the C5–C15 vector ( $\nu_{LA}$ ) involving the HOMO–LUMO transition polarized along this vector. The prominent  $\gamma$  band is also a corrin  $\pi \rightarrow \pi^*$  transition originating in the HOMO and terminating in the corrin  $\pi^*$  orbital with the same symmetry as the HOMO, giving a transition moment oriented approximately along the Co–C10 axis (Figure 5, left). Since cyanide is a stronger donor than water, the cobalt 3d<sub>z<sup>2</sup></sub>-based molecular orbital is higher in energy in CNCbl and consequently makes a larger contribution to the HOMO. This explains the trend in the "typical" spectra of XCbl's for a shift of the  $\alpha/\beta$  and  $\gamma$  bands to lower energy as the donor strength of X increases.

In the RCbl's with "unique" spectra the greatly increased donor power of the R ligand destabilizes the cobalt 3d orbitals so that the occupied 3d orbitals

are much closer in energy to the HOMO (Figure 5, right). This increases the number of donor orbitals available for transitions and allows for mixing of the 3d and corrin  $\pi$  orbitals. The  $\alpha/\beta$  bands are again assigned to the HOMO  $\rightarrow$  LUMO transition polarized along the C5–C15 axis, but now the HOMO has Co–C  $\sigma$ -bonding character which is lost on excitation, giving rise to distortions on the  $\nu_{LA}$  and  $\nu_{Co-C}$  coordinates in the excited state and, consequently, the enhanced  $\beta$  band relative to the  $\alpha$  band. The mixing of the cobalt 3d and corrin  $\pi$  orbitals is then responsible for the multiple transitions in the  $\gamma$  region. The much stronger inductive effect of CH<sub>3</sub> (relative to CN) further increases the 3d<sub>z<sup>2</sup></sub> character of the HOMO, causing a stronger Co–NB3 antibonding effect, explaining why the Co–NB3 bond lengths increase from H<sub>2</sub>Ocbl<sup>+</sup> to CNCbl to CH<sub>3</sub>Cbl (i.e., the inverse trans effect).

The effect of removing the axial Bzm (and, presumably, replacing it with a water molecule) on the RCbl spectra is to shift the low-energy bands to the blue. Here, the lower donor power of the H<sub>2</sub>O ligand eliminates the  $\sigma$ -antibonding interaction between the cobalt 3d<sub>z<sup>2</sup></sub> orbital and the HOMO, which is consequently lowered in energy by ca. 0.2 eV. However, the nature of the Co–C bond is said to be unchanged since a Mayer population analysis shows a decrease in the calculated Co–C bond order by only 1% on going from CH<sub>3</sub>Cbl to CH<sub>3</sub>Cbi<sup>+</sup>. Although this would seem to contradict the measured BDE's of AdoCbl<sup>107</sup> and AdoCbi<sup>+</sup>,<sup>194</sup> which show an increase of  $4.5 \pm 2.7$  kcal mol<sup>-1</sup>, the authors claim that there is no contradiction since the Co–C bond strength is a function of the curvature of the Co–C bond potential at its minimum while the BDE is the difference between minimum potential energy and the potential of the final (Ado• + cob(II)alamin) products. Thus, according to this analysis changes in the upper axial ligand donor strength significantly affect the trans axial Co–L bond strength but changes in the lower axial ligand do not significantly change the Co–C bond strength. If this is correct, then it provides evidence against mechanisms for enzymatic catalysis of Co–C bond homolysis invoking the lower axial ligand and supports those that invoke stabilization of the cob(II)alamin cleavage product.

## 7. Theory

There has been an explosion in the use of theory to describe the cobalt corrins, for the most part due to the application of density functional theory (DFT), which permits ab initio calculations on relatively large systems with reasonable calculation efficiency. Most such calculations are still performed on simplified models of cobalt corrins, the consequences of which are not yet completely clear. There is great potential for theory in this area, particularly as a guide to the direction of experimental research. However, when theoretical results deviate badly from experiment, as they sometimes do, little confidence in the methodology is generated among empiricists and conclusions must be carefully drawn and appropriately examined in order to avoid widespread skepticism.

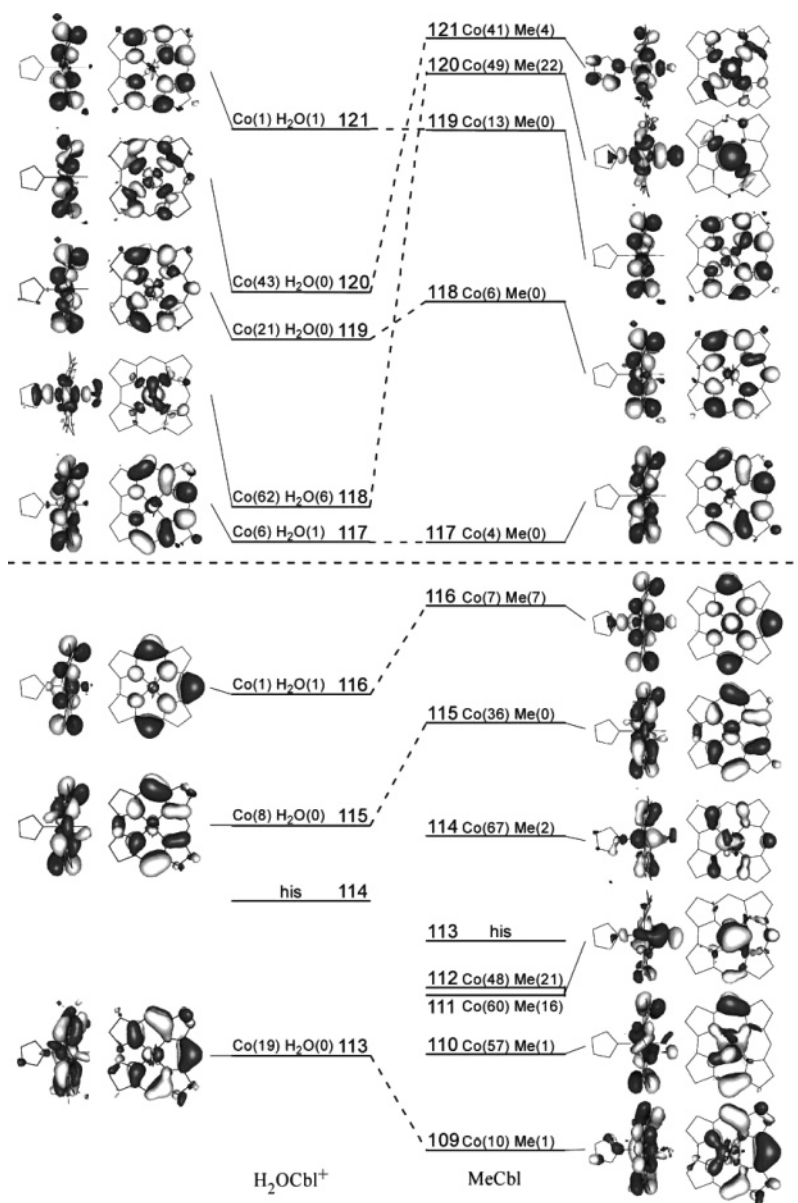


**Figure 5.** Isosurface plots of the relevant MOs of  $\text{H}_2\text{OCbl}^+$  (left) and  $\text{CH}_3\text{Cbl}$  (right). MOs are arranged according to their calculated energies with the doubly occupied orbitals shown below the horizontal dashed line (note that the HOMO/LUMO gap is not drawn to scale). The percent contributions from the Co 3d orbitals and the 2s and 2p orbitals of the coordinating atom from the upper axial ligand to each MO are given in parentheses. (Reprinted with permission from ref 193. Copyright 2003 American Chemical Society.)

Kozłowski and co-workers<sup>195,196</sup> used DFT (at the B3LYP level with 6-31G(d) (H, C, N) on VTZ (Co) basis sets) to calculate the structures and energies of simple models of a variety of alkylcobalt corrinoids. The models used a naked corrin with a cobalt atom, a detached axial base (Bzm, Im, or water), and a variety of upper axial ligands including cyano, ethynyl, methyl, ethyl, Ado, isopropyl, *tert*-butyl, trifluoromethyl, chloromethyl, aminomethyl, and triaminomethyl. The calculated structures routinely overestimate the length of the Co–NB<sub>3</sub> bond by 0.10–0.16 Å but are successful in predicting an increase in Co–C bond length as the trans axial Co–L bond length increases for all three axial bases (i.e., the inverse trans effect). However, a predicted correlation between Co–C bond length and corrin ring fold angle does not agree with experimental results. The main conclusion from the work is that electron donation

to the alkyl group (by substituents or from an externally applied electric field) controls the reactivity of the Co–C bond and that sterics are unimportant.

Jensen et al.<sup>197</sup> also used DFT methods to study the structure and energetics of RCbl models. Using the B3LYP/lacv3p\*\*:<sup>\*</sup>B3LYP/lacvp\*\* method the models contained a naked corrin ring with a cobalt atom, an alkyl ligand, and a detached axial base and included RCo(corrin)Bzm<sup>+</sup>, R = methyl, ethyl, cyano, Ado, isopropyl, and *tert*-butyl, and  $\text{CH}_3(\text{corrin})\text{L}^+$ , L = NH<sub>3</sub> and Im. Once again, Co–N<sub>ax</sub> bond lengths of the RCo(corrin)Bzm<sup>+</sup> models overestimate the length of the Co–NB<sub>3</sub> bond in RCbl's by 0.10–0.14 Å, but the Co–C bonds are more accurately calculated (to <0.01 Å for the CNCbl model, 0.012 Å for the CH<sub>3</sub>-Cbl model, but only 0.029 Å for the AdoCbl model). The steric effect of the R group is found to increase the length of the Co–C bond in the RCo(corrin)Bzm<sup>+</sup>

series in the order methyl < ethyl < isopropyl < *tert*-butyl from 1.97 to 2.11 Å and similarly, although less regularly, increase the length of the trans Co–N<sub>ax</sub> bond from a badly overestimated 2.33 Å for R = methyl to an impossible 2.77 Å for R = *tert*-butyl. This progressive loss of the Co–N<sub>ax</sub> bond is found to decrease the energy of the HOMO, which is delocalized into both axial bonds, by ca. 3 kcal mol<sup>-1</sup> across the series. Using eight N–Co–N–C torsion angles around the corrin ring as an indication of corrin ring distortion, the authors conclude that RCo(corrin)-Bzm<sup>+</sup> series all have similar corrin folding, in contrast to the X-ray structures of the analogous RCbl's in which the corrin ring fold angle changes from 13.3° to 18.0° across the series R = Ado, CH<sub>3</sub>, CN and clearly show the effect of the steric bulk of R on the fold angle (Table 1). Changing the axial base in the CH<sub>3</sub>Co(corrin)L<sup>+</sup> series has a surprisingly small effect on the Co–N<sub>ax</sub> bond length (L = NH<sub>3</sub> and Im are essentially the same (2.27 Å) but L = Bzm is 0.05 Å longer) and essentially no effect on the Co–C bond length or the corrin ring folding, again in contrast to experiment. In AdoCo(corrin)Bzm<sup>+</sup> the HOMO is raised by 5.4 kcal mol<sup>-1</sup> relative to that in CH<sub>3</sub>Co(corrin)Bzm<sup>+</sup>, which renders the AdoCbl more likely to undergo homolytic Co–C bond cleavage, and the LUMO is also higher making AdoCo(corrin)Bzm<sup>+</sup> less susceptible to heterolysis, in concert with the known biochemical mechanisms for Co–C bond cleavage in these two coenzymes. In general, the calculations suggest that elongation of the axial Co–N bond should destabilize the Co–C bond, in contrast to other calculations.

Randaccio et al.<sup>198</sup> used DFT methods, using the local density approximation applied to the VWN parametrization and a basis set of Slater-type orbitals, to calculate the structure of a series of simplified models consisting of a naked cobalt–corrin, a detached axial Bzm ligand, and a β-ligand, X (X(corrin)-Bzm), of cobalamins for which accurate X-ray structures are available (X = H<sub>2</sub>O, Cl, CN, CF<sub>3</sub>, CH<sub>3</sub>, SC(NH<sub>2</sub>)<sub>2</sub>, and SO<sub>3</sub>) and others for which X-ray structures are not available (X–C(CH<sub>3</sub>)<sub>3</sub> and SCH<sub>3</sub>). Co–X bond distances are, in general, predicted to within ca. 0.06 Å, most being underestimated (except for X = CF<sub>3</sub> and SO<sub>3</sub>). Unlike almost all other DFT studies, all but one (X = SO<sub>3</sub>) Co–N<sub>ax</sub> bond distance is *underestimated*, generally by about 0.04–0.06 Å, suggesting that the consistent overestimation of Co–N<sub>ax</sub> bond lengths by much larger amounts is the result of the application by others of the B3LYP method (see below). The long calculated axial bond distances in the SO<sub>3</sub>Cbl<sup>-</sup> model are attributed to a calculation artifact due to the high negative charge concentrated on the oxygen atoms of the sulfite ligand without the possibility of charge delocalization by interaction with solvent. Trends of axial bond lengths within the series (except for X = SO<sub>3</sub>) reproduce the trends from the X-ray structures very well. A rough, inverse correlation of the Mullikan populations of the NB3 atom of the Bzm ligand with Co–N<sub>ax</sub> bond length is found, but no correlations exist for the Mullikan populations on the Co atom or liganding atom of X. For the calculated structures of models

with S-bonded X ligands the Co–N<sub>ax</sub> bond length decreases as the Co–S bond length increases, exhibiting a normal trans effect as opposed to the inverse trans effect found for alkylcobalamins. For this group of compounds the Mullikan populations on the Co atom decrease as the Co–N<sub>ax</sub> bond distance increases, while for the alkylCbl's, which follow the inverse trans effect, the positive charge on the metal increases with the increase in both the Co–N<sub>ax</sub> and Co–C bonds.

Semiempirical calculations have also been used to study cobalt corrinoids. Jensen and Mikkelsen<sup>199</sup> performed PM3(tm) semiempirical calculations on AdoCbl, CH<sub>3</sub>Cbl, their analogues with Im as an axial ligand (it is not clear if these are R(Im)Cbl species, i.e., with Im as part of the nucleotide loop, or if they are R(Im)Cbl<sup>+</sup> species), and cob(II)alamin as well as simple models containing a cobalt–corrin, an alkyl ligand (methyl, isopropyl, Ado), and an axial base (NH<sub>3</sub>, histidine (His), or Bzm) both with (i.e., RCo(corrin)L<sup>+</sup>) and without (i.e., RCo(corrin)L) the proper charge to compare electron affinities of the models. For both the AdoCbl and CH<sub>3</sub>Cbl models as well as their R(corrin)L<sup>+</sup> counterparts the calculated Co–C bond lengths agree well with the X-ray data for AdoCbl and CH<sub>3</sub>Cbl (Table 1), but the Co–N<sub>ax</sub> bonds are underestimated by ca. 0.17 Å for R = CH<sub>3</sub>, 0.23 Å for R = Ado, and 0.26 Å for the cob(II)alamin model, demonstrating that the problems associated with calculated Co–N<sub>ax</sub> bond lengths are not restricted to DFT methods. Although both their own results and the X-ray structures demonstrate a shortening of the axial Co–N bond by about 0.1 Å upon homolysis of AdoCbl, the authors somehow conclude that “the homolysis coordinate includes an elongation of the Co–N(ax) bond”. In addition, the calculated structures of the complete cobalamins show a longer Co–N<sub>ax</sub> bond for CH<sub>3</sub>Cbl than for AdoCbl, contrary to experiment (Table 1), so that even trends within a series of compounds calculated by these methods are not reliable. Comparison of the full cobalamin models to the simplified models suggests that the side chains and nucleotide loop have little effect on the corrin ring geometry. There is a significant cis steric effect which lengthens the Co–C bond in response to steric repulsions between the alkyl ligand and the corrin ring but little or no trans steric effect, which calls mechanochemical triggering mechanisms into question.

Comparison of the RCo(corrin)L<sup>+</sup> and RCo(corrin)L structures shows almost no change in the Co–C and Co–N<sub>ax</sub> bond lengths, despite the fact that one-electron reduction of RCbl's is known to lead to highly unstable RCbl<sup>-</sup> species which dealkylated extremely rapidly. From calculated heats of reaction the authors calculate that the cob(II)alamin model (i.e., Co<sup>II</sup>(corrin)L) with Bzm as the axial ligand is stabilized by 59 kcal mol<sup>-1</sup> relative to one with an ammonia ligand, which they refer to as a delocalization effect of the Bzm ligand, a highly unlikely result. In addition, they calculate that the preference of AdoCbl for a His ligand over a Bzm ligand is 27 kcal mol<sup>-1</sup> greater than this preference in CH<sub>3</sub>Cbl. This is in direct contradiction to experiment since the binding

constants for MeIm to  $\text{CH}_3\text{Cbi}^+$  ( $4.9 \pm 0.2 \text{ M}^{-1}$ )<sup>145</sup> and  $\text{AdoCbi}^+$  ( $0.5 \pm 0.1 \text{ kcal mol}^{-1}$ )<sup>112</sup> which together with the values for  $K_{\text{Co}}$  for these species (eq 10 and Table 2) permit calculation of the equilibrium constants for substitution of MeIm for Bzm in  $\text{CH}_3\text{Cbl}$  and  $\text{AdoCbl}$ . The results show that the selectivity of  $\text{AdoCbl}$  for Im is actually slightly higher than that of  $\text{CH}_3\text{Cbl}$  but only by  $0.27 \text{ kcal mol}^{-1}$ .

Several groups have also used DFT methods to calculate Co–C BDE's, an effort which has not seen great success. Kozłowski and co-workers<sup>200</sup> used gradient-corrected DFT calculations at the B3LYP level to estimate the BDE's of alkylcobalt corrinoid models. Again, the models consisted of a naked cobalt–corrin, a detached base (Bzm, Im, or  $\text{H}_2\text{O}$ ), and an alkyl ligand (methyl, ethyl, Ado, isopropyl, and *tert*-butyl). BDE's were estimated as the difference in the DFT-optimized energy between the alkylcobalt model complex and the Co(II) and alkyl radical dissociations products plus a correction for the vibrational zero-point energy. The calculated BDE's consistently underestimate experimental values (for  $\text{CH}_3\text{Cbl}$ ,<sup>123</sup>  $\text{AdoCbl}$ ,<sup>107</sup> and  $\text{AdoCbi}^{+194}$ ) by 12–13.5  $\text{kcal mol}^{-1}$  or 32–40%. However, if trends within the series of compounds are reliable, as the authors insist, then the linear correlation they find between Co–C BDE and Co–C bond lengths is of interest. The slope of this correlation is  $-168 \text{ kcal mol}^{-1} \text{ \AA}^{-1}$ , a potentially useful metric in attempting to quantify the effects of mechanochemical triggering from MM studies on Co–C bond strength (see below). The authors conclude that the BDE's "do not depend on the axial base", and yet there is a 1–4  $\text{kcal mol}^{-1}$  increase in calculated BDE when Bzm is substituted by water, which is consistent with experiment. Strangely, the authors also conclude that "elongation of the Co–NB bond does not influence the Co–CR bond and vice versa" when their earlier work<sup>195,196</sup> clearly showed (in agreement with experiment) that the Co–BN3 bond length is strongly dependent on the Co–C bond length (i.e., the inverse trans effect).

Maseras and co-workers<sup>201</sup> also studied the structure and BDE's of Cbl models using DFT calculations at the B3LYP level. The models again consist of a naked cobalt–corrin, a detached Bzim axial ligand (i.e., no methyl groups), and a methyl ligand and include  $\text{CH}_3\text{Co}(\text{corrin})\text{Bzim}$ ,  $\text{Co}(\text{corrin})\text{Bzim}$  (evidently  $\text{Co}^{\text{II}}$  and a model for cob(II)alamin), and the base-off models  $\text{CH}_3\text{Co}(\text{corrin})$  and  $\text{Co}(\text{corrin})$ , although it is not specified if the base-off models have an axial water ligand. The models reproduce the inner-sphere geometry of the real Cbl's quite well except for the Co– $\text{N}_{\text{ax}}$  bond lengths in the base-on models which overestimate the X-ray Co–NB3 bond lengths in  $\text{CH}_3\text{Cbl}$ <sup>73</sup> and cob(II)alamin<sup>85</sup> by 0.12 and 0.17  $\text{\AA}$ , respectively, which the authors suggest may be due to the missing nucleotide loop side chain. The overall geometry of the corrin is not significantly changed by homolysis of the Co–C bond (i.e., comparing  $\text{CH}_3\text{Co}(\text{corrin})\text{Bzim}$  to  $\text{CH}_3\text{Co}(\text{corrin})$ ), in agreement with experiment.<sup>85</sup> The Co–C BDE for the  $\text{CH}_3\text{Cbl}$  model is calculated to be  $22.9 \text{ kcal mol}^{-1}$ , fully 60% below the experimental value,<sup>122,123</sup> attributed by the authors, at least in part, to solvation

effects in the experimental determinations which are absent in the gas-phase calculations. However, this seems unlikely as the solvent effect on Co–C bond homolysis is known to be very small by experiment and theory (see below). To probe the effects of the Co– $\text{N}_{\text{ax}}$  bond length on the Co–C BDE, the BDE calculation was repeated with fixed Co– $\text{N}_{\text{ax}}$  bond distances between 1.8 and 2.8  $\text{\AA}$ . The effect is to increase the BDE regardless of whether the Co– $\text{N}_{\text{ax}}$  bond is shortened or lengthened, but the effect is very small, with a 0.5  $\text{\AA}$  change in Co– $\text{N}_{\text{ax}}$  bond length leading to only a 1  $\text{kcal mol}^{-1}$  increase in BDE. However, the geometry changes associated with changing the Co– $\text{N}_{\text{ax}}$  bond length suggest a normal trans effect (i.e., the Co–C bond shortens as the Co– $\text{N}_{\text{ax}}$  bond lengthens). The authors also computed a Co– $\text{N}_{\text{ax}}$  BDE of  $2.2 \text{ kcal mol}^{-1}$ , fully 7.3-fold lower than the available experimental estimate,<sup>112</sup> and again attributed it to solvation effects.

These authors also attempted to calculate the kinetics of Co–C bond homolysis in the  $\text{CH}_3\text{Co}(\text{corrin})\text{Bzim}$  model using a broken symmetry approach to avoid the inconvenient spin-crossing problem. They find no transition state on the reaction pathway, which is correct. Amazingly, the results, which do not vary significantly as the Co– $\text{N}_{\text{ax}}$  bond distance is altered, give a much more realistic activation energy of ca.  $30 \text{ kcal mol}^{-1}$  but completely contradict their BDE calculations since the activation energy and BDE for a vacuum bond dissociation must be the same.

Similar calculations have been carried out on a more realistic  $\text{AdoCbl}$  model containing a tetrahydrofuran– $\text{CH}_2$  alkyl ligand with similarly poor results. The Co–C bond length is underestimated by 0.05  $\text{\AA}$ , the Co– $\text{N}_{\text{ax}}$  bond length is overestimated by a whopping 0.22  $\text{\AA}$ , the calculated Co–C BDE is 25% too low, and the calculated Co– $\text{N}_{\text{ax}}$  BDE of  $<1 \text{ kcal mol}^{-1}$  is impossible. Substitution of Im for Bzim in the  $\text{CH}_3\text{Co}(\text{corrin})\text{L}$  and  $\text{Co}(\text{corrin})\text{L}$  models had little effect other than to shorten the Co– $\text{N}_{\text{ax}}$  bond in the former by 0.057  $\text{\AA}$  to a much more realistic but still too long 2.23  $\text{\AA}$ .

Jensen and Ryde<sup>202</sup> also carried out B3LYP DFT calculations on Cbl models consisting of a naked cobalt–corrin, i.e.,  $\text{RCo}(\text{corrin})\text{L}$ , with  $\text{R} = \text{CH}_3$  or 5'-deoxyriboseyl (rib), and  $\text{L} = \text{Bzm}$ , Im, or imidazolate ( $\text{Im}^-$ ), as well as cob(II)alamin models  $\text{Co}^{\text{II}}(\text{corrin})\text{L}$  with the same axial ligands, L. The impetus for studying the  $\text{Im}^-$  ligand is the fact that in all enzymes utilizing the base-off/His-binding mode a conserved aspartate residue is H-bonded to the His ligand, possibly inducing a partial imidazolate character to this ligand. While the Co–C bond length of  $\text{CH}_3\text{Cbl}$  is well reproduced, the Co–C bond length of the  $\text{AdoCbl}$  model is less so, and as usual, the Co– $\text{N}_{\text{ax}}$  bonds are all overestimated by about 0.17  $\text{\AA}$  relative to the X-ray structures of the Cbl's they model. In addition, the fold angles of the  $\text{AdoCbl}$  and  $\text{CH}_3\text{Cbl}$  models, which are 5–6° smaller than those from the X-ray studies, are poorly reproduced. However, a reduction in the fold angle upon replacement of Bzm by Im of several degrees is in agreement with experiment.<sup>44</sup> When Im is replaced by  $\text{Im}^-$  as the

axial ligand, the Co–C bond elongates slightly (ca. 0.03 Å) but the axial Co–N bond shortens dramatically (0.16–0.18 Å) according to these models. Calculation of the potential energy well for the Co–N<sub>ax</sub> bonds in these models shows that for Bzm and Im the potential is quite flat and the force constant (ca. 24 kcal mol<sup>-1</sup> Å<sup>-2</sup>) is 5- or 6-fold smaller than that for the much stiffer Co–C bond (ca. 140 kcal mol<sup>-1</sup> Å<sup>-2</sup>). For the Im<sup>-</sup> ligand the bond potential is steeper and the force constant about 72 kcal mol<sup>-1</sup> Å<sup>-2</sup>. The shallow potentials for the Co–Bzm and Co–Im bonds are considered by these authors to be the cause of the large errors in the calculated Co–N<sub>ax</sub> bond lengths, as errors of this magnitude account for only about 1 kcal mol<sup>-1</sup> bond energy difference. For the Co<sup>II</sup>(corrin)L corrin models the potential energy curves for the Co–N<sub>ax</sub> bond are very close to those for the RCo(corrin)L models, suggesting that manipulation of the Co–NB3 bond of AdoCbl by the AdoCbl-dependent enzymes is not a viable mechanism for activation of the Co–C bond for homolysis. In addition, a study of the corrin ring fold angle of the RCo(corrin)L models, in which the Co–N<sub>ax</sub> bond length is fixed at various values, shows that the fold angle increases as the Co–N<sub>ax</sub> bond length is shortened and that this effect is smaller when L = Im than when L = Bzm, exactly as found in MM studies (see below). Similarly, compression of the axial Co–N bond leads to elongation of the Co–C bond, also as seen in the MM studies. Calculated Co–C BDE's (without a zero-point correction) are about 40% lower than experimental values, and incredibly, for the RCo(corrin)L models with L = Im or Bzm, the Co–C BDE's *increase* as the Co–N<sub>ax</sub> bond is compressed, despite the fact that such compression *lengthens the Co–C bond!* Similarly, the Co–C BDE's of the Im<sup>-</sup> complexes are larger (by 2–4 kcal mol<sup>-1</sup>) than those of the Im and Bzm complexes despite the fact that the former have the longer (by 0.03 Å) Co–C bonds.

Jensen and Ryde<sup>203</sup> directly addressed the question of why DFT calculations consistently underestimate the BDE's of RCbl's by substantial amounts. The models considered consist of a naked cobalt–corrin, a detached axial ligand, and an alkyl ligand, including CH<sub>3</sub>Co(corrin)Im, CH<sub>3</sub>Co(corrin)Bzm, and ribCo(corrin)Im. Using the B3LYP method six different basis sets produced values for the CH<sub>3</sub>Co(corrin)Im BDE of 20.5–26 kcal mol<sup>-1</sup>, far below the experimental value of 37 kcal mol<sup>-1</sup> for CH<sub>3</sub>Cbl,<sup>123</sup> and improvement of the basis set actually increases the discrepancy. Inclusion of a relativistic correction improved the BDE estimate for five of the basis sets by about 1.4 kcal mol<sup>-1</sup>. The basis set superposition error was investigated using the largest basis set and found to decrease the calculated BDE by <1 kcal mol<sup>-1</sup>. Solvation effects were also simulated using the polarizable continuum model with both high and low dielectric constants. The solvation energies of CH<sub>3</sub>Co(corrin)Im and Co<sup>II</sup>(corrin)Im were quite similar, as expected, so that the methyl radical provides all of the very small solvation correction, which increased the BDE by about 1.4 kcal mol<sup>-1</sup>. Alternative use of the COSMO model *decreased* the BDE by an inconsequential 0.2 kcal mol<sup>-1</sup>. Zero-point energy correc-

tions decreased the calculated BDE by 5 kcal mol<sup>-1</sup>, while thermal corrections (the experimental data are collected in the 120–140 °C temperature range) increased the calculated BDE by 1.4 kcal mol<sup>-1</sup>. Using all corrections the best estimate is 20.6 kcal mol<sup>-1</sup>, 1.2 kcal mol<sup>-1</sup> lower than the calculated value without corrections and 30% below the experimental value.

These authors then considered if the method itself is the problem. Using 10 different methods without the corrections results varied widely, but two methods, BP86 (BDE = 37.2–38.2 kcal mol<sup>-1</sup>) and MP2 (BDE = 37.3 kcal mol<sup>-1</sup>), duplicated the experimental value extremely well, leading to the conclusion that the B3LYP method itself is responsible for the poor results obtained previously. The authors also considered if the B3LYP geometries were responsible for the poor BDE results but conclude that they are not. Geometries were calculated for several models using various methods (but only one basis set). For the ribCo(corrin)Bzm model of AdoCbl the Co–C and Co–N<sub>eq</sub> distances are well reproduced but the calculated Co–N<sub>ax</sub> distances are overestimated by all methods, with the BP86 method being the best (ca. 0.05 Å error). For the CH<sub>3</sub>Co(corrin)Im model (relative to the CH<sub>3</sub>Cbl X-ray structure) the BP86 method gives an excellent Co–C bond length and comes within 0.03 Å of the Co–N<sub>ax</sub> bond length while the MP2 method duplicates the Co–N<sub>ax</sub> bond well but underestimates the Co–C bond length by 0.09 Å. All methods overestimate the Co–N<sub>ax</sub> bond length of the cob(II)alamin model, the best method (BP86) by 0.07 Å. While the BP86 method gave the best overall geometries, calculating the CH<sub>3</sub>Co(corrin)Im BDE with the B3LYP method but using the BP86 geometry does not improve the B3LYP BDE very much. The result is general since the calculated BDE's for the other models (R = CH<sub>3</sub> or ribosyl, L = Im or Bzm) are all about 13 kcal mol<sup>-1</sup> lower via the B3LYP method than via the BP86 method. The latter is, however, far from a panacea since it overestimates the AdoCbl BDE (i.e., the ribCo(corrin)Bzm model) by 5.4 kcal mol<sup>-1</sup>.

Dybala-Defratyka and Paneth<sup>204</sup> used semiempirical and DFT methods to model the active site of methylmalonylCoA mutase (MMCM) and calculate kinetic deuterium isotope effects for the initial Co–C homolysis and hydrogen-atom transfer events considering both stepwise (i.e., Co–C bond homolysis followed by H-atom abstraction from the substrate by the Ado• radical) and concerted pathways. The study was prompted by Banerjee's observations (see below) of kinetic isotope effects (KIE's) in the MMCM reaction considerably surpassing the classical limit, suggesting hydrogen-atom tunneling is important. Their "large model" consisted of the substrate, methylmalonylCoA, the coenzyme, and all of the amino acid residues within 15 Å of the cobalt atom (2320 atoms), while the "core model" consisted of a coenzyme with a naked corrin ring and a ribosyl alkyl group with an Im axial base and a substrate in which the –SCoA moiety is truncated to –SEt (93 atoms). Because of the essential nature of an arginine residue (Arg207) which is H-bonded to the substrate's carboxyl group, two other models were created, one in

which the substrate carboxyl is protonated (94 atoms) and one in which Arg207 is H-bonded to the substrate carboxyl (119 atoms). Models of the second step in the stepwise process consisted of these models minus the cobalt–corrin and Im axial ligand. Strangely, the initial model of the 119-atom model, both by semiempirical and DFT methods, overestimates the Co–C bond length by 0.18 Å but *underestimates* the Co–N<sub>ax</sub> bond length by a prodigious 0.30 Å. This model, however, gives an activation energy for the concerted route within 1 kcal mol<sup>-1</sup> of the measured value. Calculated deuterium KIE's using the zero-curvature tunneling method gave reasonable values, although they consistently overestimated the experimental values by 27–39%. The models for the second step in the stepwise version gave calculated KIE's that corresponded very closely to the experimental values as long as the substrate carboxyl was either protonated or H-bonded to the Arg residue. From the calculated and observed activation energies the authors estimate that the enthalpy of the Co–C bond dissociation in the stepwise process must be about 7 kcal mol<sup>-1</sup>, i.e., some 23 kcal mol<sup>-1</sup> lower than that for free AdoCbl, indicating an unexpected and underappreciated extent of catalysis by the enzyme. The authors conclude that both the concerted and stepwise pathways are consistent with the observed deuterium KIE's.

Maseras and co-workers<sup>205</sup> also used B3LYP DFT methods to calculate the structures of coenzyme models with naked cobalt–corrins, detached Bzim (i.e., no methyl groups) and Im axial ligands including CH<sub>3</sub>Co(corrin)Bzim<sup>+</sup>, CH<sub>3</sub>Co(corrin)Im<sup>+</sup>, RCH<sub>2</sub>-Co(corrin)Bzim<sup>+</sup> (R = tetrahydrofuran), and the possible homolytic and heterolytic cleavage products, Co<sup>II</sup>(corrin)Bzim<sup>+</sup>, Co<sup>I</sup>(corrin)Bzim, and Co<sup>III</sup>(corrin)-Bzim<sup>2+</sup> (there is no indication if the latter model includes a water ligand—it does not seem to). The Co–C bond length of the CH<sub>3</sub>Cbl model is quite close to that of CH<sub>3</sub>Cbl itself, but the Co–N<sub>ax</sub> bond lengths in CH<sub>3</sub>Co(corrin)Bzim<sup>+</sup> and Co<sup>II</sup>(corrin)Bzim<sup>+</sup> are overestimated relative to the X-ray structures by 0.13 and 0.17 Å, respectively.<sup>85,73</sup> The structure of Co<sup>II</sup>(corrin)Bzim<sup>+</sup> does, however, reproduce the displacement of the metal from the mean equatorial plane toward the Bzim but overestimates it by 0.05 Å.<sup>85</sup> The cob(I)alamin model is found to be four coordinate with the cobalt in the mean equatorial plane and the equatorial Co–N bonds shortened by 0.02–0.04 Å relative to CH<sub>3</sub>Co(corrin)Bzim<sup>+</sup>. In the Co<sup>III</sup>(corrin)-Bzim<sup>2+</sup> model the Co–N<sub>ax</sub> bond is appropriately shortened to 1.93 Å but the cobalt is massively displaced from the mean equatorial plane by 0.36 Å toward the Bzim (likely due to the apparent lack of an upper axial ligand—a very unrealistic model).

The energetics of the heterolytic cleavage of CH<sub>3</sub>-Co(corrin)Bzim<sup>+</sup> to form Co<sup>I</sup>(corrin)Bzim and CH<sub>3</sub><sup>+</sup> has been studied as a function of the Co–N<sub>ax</sub> distance, which was fixed at values between 1.8 and 2.8 Å. The absolute values of the enthalpy change for this reaction are very large and positive because of the formation of the isolated CH<sub>3</sub><sup>+</sup> carbonium ion. Lengthening of the Co–N<sub>ax</sub> bond leads to a dramatic decrease in the enthalpy (ca. 10 kcal mol<sup>-1</sup> per 0.5 Å

increase), suggesting that increasing the Co–NB<sub>3</sub> bond length in CH<sub>3</sub>Cbl would favor this kind of heterolysis over Co–C bond homolysis. The effect is essentially entirely due to stabilization of the Co<sup>I</sup> product by axial bond elongation. In contrast, a similar study of the heterolysis of CH<sub>3</sub>Co(corrin)-Bzim<sup>+</sup> to form Co<sup>III</sup>(corrin)Bzim<sup>2+</sup> and CH<sub>3</sub><sup>-</sup> shows that elongation of the Co–N<sub>ax</sub> bond increases the (positive) enthalpy change dramatically (by ca. 24 kcal mol<sup>-1</sup> per 0.5 Å). Substitution of Im for Bzim had minor effects in both heterolysis reactions. The results for both types of heterolysis were also quite similar for the AdoCbl model, RCH<sub>2</sub>Co(corrin)Bzim<sup>+</sup> (R = tetrahydrofuran). The authors attribute these trends to changes in the Mullikan populations of the cobalt d<sub>z2</sub> orbital, which are 1.06 for CH<sub>3</sub>Co(corrin)-Bzim<sup>+</sup>, 1.10 for Co<sup>II</sup>(corrin)Bzim<sup>+</sup>, 1.85 for Co<sup>I</sup>(corrin)-Bzim, and 0.69 for Co<sup>III</sup>(corrin)Bzim<sup>2+</sup>.

Similarly, Jensen and Ryde<sup>206</sup> modeled the methionine synthase half-reaction, in which homocysteine is methylated by CH<sub>3</sub>Cbl, using a simple model with a naked cobalt–corrin, methyl and Im ligands (i.e., CH<sub>3</sub>Co(corrin)Im), and CH<sub>3</sub>S<sup>-</sup> as the substrate. Unfortunately, the B3LYP method was used with the 6-31G(d) basis set for geometries and the large triple- $\zeta$  6-311+G(2d,2p) basis set for energies. The optimized geometry of the CH<sub>3</sub>Co(corrin)Im accurately reproduces the Co–C bond length but overestimates the Co–N<sub>ax</sub> bond length by 0.09 Å. The transition state contains only one imaginary vibration frequency which represents an axially directed S<sub>N</sub>2 reaction with significant displacement of S, CH<sub>3</sub>, Co, and N<sub>ax</sub> coordinates. Solvation effects were accounted for using a conductor-like screening model with a high dielectric constant (80) to simulate water and a low dielectric (4) to simulate an enzyme-like environment. In solution the reaction is exothermic by 11 kcal mol<sup>-1</sup>. The free energy of activation at 25 °C was calculated to be 24.9 kcal mol<sup>-1</sup> at 25 °C, the same as the estimated value for the nonenzymatic reaction of 24.9 kcal mol<sup>-1</sup> (the enzyme-catalyzed barrier is 14.6 kcal mol<sup>-1</sup>).<sup>207</sup> The transition state is found to be very early, the Co–N<sub>ax</sub> bond elongates as the Co–C bond is stretched, and there is no evident distortion of the corrin ring in the transition state. The reaction is characterized by a large transport of charge, with the Im ligand accepting 0.17e and the corrin ring 0.86e. The effect of deprotonation of the thiol substrate is large, with the activation barrier being 47 kcal mol<sup>-1</sup> for CH<sub>3</sub>SH as substrate.

The electronic structure and absorption spectra of Cbl's have also been investigated by DFT methods. Kozłowski and co-workers<sup>208</sup> used time-dependent DFT calculations of models consisting of a naked cobalt–corrin with a cyanide and an Im ligand (CNCo(corrin)Im) and a naked cobalt–corrin with two cyanide ligands ((CN)<sub>2</sub>Co(corrin)) to analyze the absorption spectra of CNCbl and (CN)<sub>2</sub>Cbi, respectively. In the optimized geometry of CNCo(corrin)-Im the Co–C bond length is essentially identical to that in the X-ray structure of CN(Im)Cbl<sup>44</sup> but the Co–N<sub>ax</sub> bond length is overestimated by 0.12 Å. For both models the 30 lowest energy transition states and transition dipole moments were calculated. The

calculated excitation energies consistently overestimate the experimentally observed values by about 0.5 eV or 10–20%. After applying an empirical correction of about this magnitude, the calculated energies agreed reasonably well with the experimental spectra. In both models the lowest energy transition, assigned to the  $\alpha$  band, is the HOMO  $\rightarrow$  LUMO, with the HOMO described as a  $\pi$  orbital located on the corrin with strong mixing of the  $\sigma$  orbitals of the two axial ligands but essentially no participation of the Co 3d<sub>z<sup>2</sup></sub> orbital. In contrast, the LUMO is described as a corrin  $\pi^*$  orbital with no participation of axial ligand orbitals and a small contribution from the Co 3d<sub>z<sup>2</sup></sub>. This transition thus shifts electron density from the axial ligands to the corrin and is consequently sensitive to the identity of the axial ligands and shifts ca. 0.3 eV when the Im ligand is replaced by CN<sup>-</sup>. The other prominent bands of the absorption spectra are similarly assigned.

Ouyang and co-workers carried out first-principle calculations of the electronic structure of CNCbl<sup>209</sup> and CH<sub>3</sub>Cbl,<sup>210</sup> considered as intact molecules, using the orthogonalized LCAO method based on DFT. The HOMO and LUMO are found to be dominated by C–N and C–C interactions in the corrin in both complexes, and the HOMO–LUMO gap is 1.96 eV for CNCbl and 2.09 eV for CH<sub>3</sub>Cbl. In CH<sub>3</sub>Cbl the HOMO, but not the LUMO, has participation of the cobalt 3d orbitals, while in CNCbl, orbitals involving the CN ligand are far from the gap but states involving the cobalt 3d orbitals are slightly above and below the HOMO and LUMO. In both complexes orbitals involving the upper axial ligand are far from the gap. Surprisingly, in both complexes several MO's from the phosphate in the nucleotide loop fall within the HOMO–LUMO gap, although these isolated localized states do not interact with any corrin or Co states. Compared to calculations on simplified models (CNC<sub>o</sub>(corrin)Bzm<sup>197,209</sup> and CNC<sub>o</sub>(corrin)Im)<sup>208</sup> the HOMO–LUMO gap for the intact CNCbl molecule is much lower, and simplified models omitting the side chains and particularly the nucleotide loop cannot explain the electronic spectrum of the complexes. The authors also used these results to interpret the X-ray emission (XES) and X-ray photoelectron (XPS) spectra of CNCbl and CH<sub>3</sub>Cbl.<sup>210</sup> The coincidence of the Co L<sub>3</sub> emission with the first feature of the C K <sub>$\alpha$</sub>  emission for CNCbl demonstrates that the Co–C bond is strong, while the minimal overlap of the N K <sub>$\alpha$</sub>  XES with the Co L<sub>3</sub> emission indicates a weak axial Co–N bond. Comparison to the XES of CH<sub>3</sub>Cbl shows that the Co–C bond is weaker in this complex than in CNCbl.

Koslowski and co-workers<sup>211</sup> also developed a vibrational force field and used the scaled quantum mechanical method to refine DFT force constants at the B3LYP level. Preliminary work on a simplified model consisting of a naked cobalt–corrin, a detached Im base, and a CH<sub>3</sub> or CD<sub>3</sub> ligand focused on vibrational analysis of the Co–C and Co–N<sub>ax</sub> bonds in simulated off-resonance Raman spectra. A prominent band at 535 cm<sup>-1</sup> is assigned to the Co–C stretch, which shows a deuterium isotopic shift of 35 cm<sup>-1</sup> and overestimates the experimental results (for

CH<sub>3</sub>Cbl and CD<sub>3</sub>Cbl) by ca. 30 and 7 cm<sup>-1</sup>, respectively. The calculated <sup>12</sup>CH<sub>3</sub>  $\rightarrow$  <sup>13</sup>CH<sub>3</sub> isotopic shift of 12 cm<sup>-1</sup>, however, agrees well with the experimental value of 13 cm<sup>-1</sup>. Additional Co–CH<sub>3</sub> modes identified include a torsion at 120 cm<sup>-1</sup>, wagging modes at 195, 215, 296, and 335 cm<sup>-1</sup>, and two CH<sub>3</sub> rocking modes at 816 and 826 cm<sup>-1</sup>, which shift by 200 cm<sup>-1</sup> upon deuterium substitution. The Co–N<sub>ax</sub> stretch was found at 128 cm<sup>-1</sup>, approximately 100 cm<sup>-1</sup> lower in energy than expected.

These authors expanded this study<sup>212</sup> to a similar model with a corrin ring with all peripheral substituents truncated to methyl groups and obtained very similar results for interligand vibrational modes, except that the calculated Co–C stretching frequency more closely matched experiment due to adjustment of a scaling factor. The analysis also permits a semiquantitative description of some of the crowded and low-intensity corrin vibrational modes in the 1300–1600 cm<sup>-1</sup> region. A corrin ring breathing mode was identified at 353 cm<sup>-1</sup>, about 70 cm<sup>-1</sup> below the experimental value. About 20 weak modes were identified in the 850–1100 cm<sup>-1</sup> region, with those in the 900–950 cm<sup>-1</sup> region having major pyrroline C <sub>$\beta$</sub> –C <sub>$\beta$</sub>  stretching components. In the 1300–1400 cm<sup>-1</sup> region the model predicts 11 medium intensity modes, most of which are H wagging modes. Four modes in this region are corrin modes with the most intense at 1354 cm<sup>-1</sup> (exp. 1351 cm<sup>-1</sup>) being a stretching mode of N2–C6 and N4–C14, with contributions from C3–C4 and C16–C17. In the 1430–1600 cm<sup>-1</sup> range the model predicts six in-plane corrin modes mainly involving C–C bond stretches within the delocalized  $\pi$ -system. The most intense, at 1497 cm<sup>-1</sup>, is assigned to an in-phase stretching mode of the C=C bond along the longer corrin axis.

Warncke and co-workers<sup>213</sup> calculated <sup>14</sup>N nuclear quadrupole coupling (NQC) constants,  $\chi$  and asymmetry parameters,  $\eta$ , using DFT at a variety of theory levels and basis set sizes for a series of substituted imidazoles and benzimidazoles as free molecules in the solid state and solution as well as in AdoCbl and cob(II)alamin. While NQC constants could be accurately calculated in the gas phase and quantitative predictions could be made for substituted benzimidazoles, calculated asymmetry parameters were not accurate and only trends across a series were useful. NQC parameters could also be reasonably well calculated for the solid state using a trimer model. In solution, short-range effects are very important and hydrogen-bonded solvent molecules had to be explicitly included, although second shell solvent molecules also affect the results. Cobalt–ligand interactions were simulated using truncated models of AdoCbl and cob(II)alamin, which consisted of a complete Bzm, four equatorial ammonia molecules, and, for the AdoCbl model, an axial methyl group. For both models the asymmetry parameter of the axially coordinated nitrogen is greatly increased from the gas phase, while the NQC constant is 1.5-fold smaller. The coordinated nitrogen in the Bzm ligand of cob(II)alamin is predicted to have  $\chi = 2.7$  MHz and  $\eta = \text{ca. } 0.8$ .

Parrinello and co-workers<sup>214</sup> used DFT to study the structure and electronic properties of the Co–corrole, Co–corrin, and Co–porphyrin cores, optimizing the structures without symmetry constraints to the spin states 0, 1, and 2 for Co–corrin and Co–corrole and 1/2, 3/2, and 5/2 for Co–porphyrin. The lowest energy spin states were  $S = 1$  for Co–corrole but low-spin states  $S = 0$  and  $S = 1/2$  for Co–corrin and Co–porphyrin, respectively. The Co–corrole and Co–porphyrin structures are planar ( $C_{2v}$  and  $D_{4h}$ , respectively), but the Co–corrin is nonplanar with  $C_2$  symmetry. For Co–porphyrin the calculated structure agreed very well with the X-ray structure of Co–octaethylporphyrin.<sup>215</sup> The nonplanar conformation of the corrin ring in Co–corrin was similar to that in AdoCbl,<sup>81</sup> leading to the conclusion that the structure of the Co–corrin core itself is the major cause of distortions of the corrin ring in Cbl's rather than steric interactions with axial ligands, in contrast to most thinking on this subject.

Jensen and Ryde<sup>216</sup> similarly studied iron and cobalt porphyrins and corrins using simplified models with naked tetrapyrrole macrocycles and detached axial ligands with the B3LYP DFT method for geometries and the BP86 method for single-point energies. The central cavity of the corrin ring is smaller than that of the porphyrin, which favors the low-spin cobalt states in all oxidation states. Although the aqueous  $\text{Co}^{\text{III}}$  ion is more easily reduced than  $\text{Fe}^{\text{III}}(\text{aq})$ , in the tetrapyrrole macrocycles this tendency is reversed so that cobalt corrins have potentials 0.1–0.3 eV lower than those for iron porphyrins. The  $\text{CH}_3\text{Co}(\text{corrin})\text{Im}^+$  model, in which the  $\text{Co}-\text{N}_{\text{ax}}$  bond length is overestimated by 0.09 Å, has the highest Co–C BDE (37.6 kcal mol<sup>-1</sup>) of the four organometallic complexes modeled.

Several Gaussian analyses of Cbl electronic spectra have appeared,<sup>72,193,217</sup> which are useful in locating the positions of electronic transitions. Perry et al.<sup>72</sup> fitted the spectra of  $\text{H}_2\text{OCbl}^+$  and  $\text{NO}_2\text{Cbl}$  with 11 Gaussian functions,  $\text{S}_2\text{O}_3\text{Cbl}^-$ ,  $\text{SeCNCbl}$ , and  $\text{SO}_3\text{Cbl}^-$  with 12 functions, and  $\text{CH}_3\text{Cbl}$  with 13 and used the calculated band positions to explore cis and trans effects in XCbl's and RCbl's. They find a weak ( $r^2 = 0.58$ ) direct correlation between the position of the  $\gamma$  band and the axial  $\text{Co}-\text{NB3}$  bond length. The mean of the three components of the  $\alpha\beta$  band envelope also shifts to longer wavelengths as the  $\text{Co}-\text{NB3}$  bond length increases ( $r^2 = 0.81$ ).

The universal force field (UFF) and the MM2 force field developed for cobalt corrins<sup>218</sup> have been used for molecular mechanics (MM) modeling of the mechanochemical triggering mechanism for enzymatic catalysis of AdoCbl Co–C bond homolysis.<sup>219,220</sup> In this mechanism, an ideal subject for MM modeling, compression of the (long) axial  $\text{Co}-\text{NB3}$  bond of AdoCbl is envisioned to increase the upward fold of the corrin ring, putting steric pressure on the Ado ligand and weakening the Co–C bond. The MM2 model reproduced the structure of AdoCbl very accurately (e.g., at a  $\text{Co}-\text{NB3}$  bond length equal to that of the neutron structure,<sup>81</sup> modeled fold angle = 14.9–(1.3)°, neutron structure, 14.6°, modeled Co–C bond length = 2.041(7) Å, neutron structure, 2.04 Å,

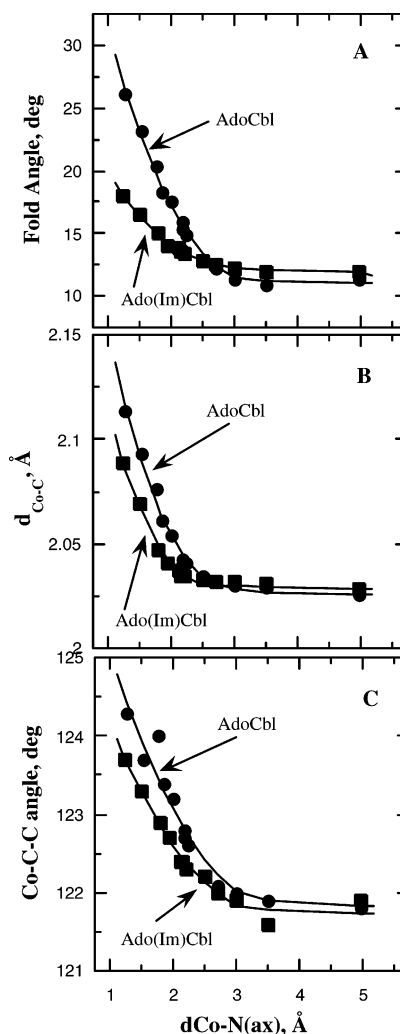


**Figure 6.** Dependence of (A) the corrin ring fold angle, (B) the Co–C bond length, and (C) the Co–C–C bond angle on the axial  $\text{Co}-\text{NB3}$  bond length in AdoCbl (●) and Ado(Im)Cbl (■) by molecular mechanics calculations.

modeled Co–C–C bond angle = 122.6(1.7)°, neutron structure, 123°). MM calculations do indeed show that compression of the axial  $\text{Co}-\text{NB3}$  bond increases the corrin ring fold angle, the Co–C bond length, and the Co–C–C bond angle (Figure 6). In models in which the axial 5,6-dimethylbenzimidazole ligand is replaced by imidazole (Ado(Im)Cbl<sup>219</sup> or Ado(MeIm)Cbl<sup>+ 220</sup>) the same kinds of effects are seen but the increase in the fold angle, Co–C bond length, and Co–C–C bond angle obtained by shortening the  $\text{Co}-\text{N}_{\text{ax}}$  bond are smaller, indicating that, as expected, the mechanochemical triggering effect is a steric phenomenon. However, the effects induced on the Co–C bond of AdoCbl by axial  $\text{Co}-\text{NB3}$  bond compression appear to be too small to account for the lowering of the free energy of activation for Co–C bond homolysis by enzyme catalysis. Compression of the axial  $\text{Co}-\text{NB3}$  bond from 2.23 (its normal value<sup>81</sup>) to 1.75 Å requires 19 kcal mol<sup>-1</sup> of energy to overcome the steric strain. However, this is feasible as proteins are well known to be capable of binding Cbl's extremely tightly,<sup>53,106</sup> thus making available large amounts of binding energy (as much as 23 kcal mol<sup>-1</sup>).<sup>53</sup> Such compression results in a 0.035 Å shortening of the Co–C bond, which, if Kozłowski's

calibration<sup>200</sup> of the effect of Co–C bond length on bond strength is correct, could lower the BDE by as much as 5.9 kcal mol<sup>-1</sup>, far short of the observed 13–17.5 kcal mol<sup>-1</sup> of AdoCbl activation.<sup>18,106,221,222</sup> However, calculations of the effect of shortening the axial Co–N bond on the Co–C bond length and BDE of a model CH<sub>3</sub>(corrin)Bzim species<sup>201</sup> predict a much smaller change in Co–C BDE of ca. 1 kcal mol<sup>-1</sup> for a 0.035 Å shortening of the Co–C bond.

Brown and Marques<sup>219</sup> also considered another version of mechanochemical triggering in which Co–NB3 bond compression in the transition state for Co–C bond homolysis stabilizes this species electronically by increasing orbital overlap between the NB3 and the cobalt atom. However, as it is now clear that the homolysis of AdoCbl at an enzyme active site is a simple bond dissociation process, devoid of a maximum on the reaction coordinate, there is no transition state, and this kind of “transition state” mechanochemical triggering cannot be correct.

Finally, Marques et al.<sup>223</sup> developed parameters for the AMBER force field for MM modeling of cobalt corrinoids using statistical analyses of the known X-ray structures. The modified AMBER force field reproduces bond lengths, bond angles, and torsion angles to within 0.01 Å, 0.8°, and 4.0°, respectively, reproducing the corrinoid structures as accurately as the MM2 corrinoid force field,<sup>218</sup> although it does tend to underestimate the corrin ring fold angle. Preliminary modeling of the active site of methylmalonylCoA mutase, including all residues within 20 Å of the cobalt atom, was performed, comparing the results to an early X-ray structure, reconstituted with AdoCbl and displaying an anomalously long (2.5 Å) Co–N<sub>ax</sub> bond (to the active site histidine residue, see below). In the MM structure the Co–N<sub>ax</sub> bond is a much more reasonable 2.23 Å, the Co–C bond length is very close to the crystal structure value for AdoCbl, and the very wide Co–C–C bond angle in the enzyme crystal structure (135°) has closed to a more reasonable 121.6°. Interestingly, in the MM-minimized structure the Ado ligand is rotated counterclockwise to a northeastern conformation, between the B ring and C10, although rotation about the Co–C bond found other, more stable, conformations in which the adenine remains near the B ring and the ribose has adopted other conformations to accommodate the rotation.

## 8. Analysis

Baker and Miller-Ihli<sup>224</sup> used capillary electrophoresis inductively coupled plasma mass spectrometry, including both capillary zone electrophoresis (CZE) and micellar electrokinetic chromatography (MEKC) methods, to determine Cbl's. CZE provided the best separation of CNCbl, HOCbl, CH<sub>3</sub>Cbl, AdoCbl, and (CN)<sub>2</sub>Cbi at pH 2.5 in either 20 mM phosphate or 20 mM formate buffers. It should be noted, however, that formate reduces HOCbl<sup>225</sup> and probably other cobalt corrin species and should be avoided as a buffering species. The detection limit was approximately 50 ng/mL. MECK provided a rapid method for separating CNCbl from free cobalt.

Sharma and co-workers<sup>226</sup> used a newly discovered B<sub>12</sub> binding protein (Gm protein, see below) obtained from the culture medium of the marine phytoplankton, *Thalassiosira pseudonana*, to improve the radioassay for Cbl's based on mammalian IF. When Gm protein was used in place of IF in the standard CNCbl radioassay, the limit of detection approached 5 pg/mL, 20-fold lower than the standard assay with IF.<sup>227</sup>

## 9. B<sub>12</sub> Binding Proteins

Nexø and co-workers<sup>228</sup> cloned bovine transcobalamin (TC) cDNA and expressed it in the yeast *Pichia pastoris*. The recombinant bovine TC had 414 amino acid residues and bound Cbl's and bound to human placental TC receptor similarly to natural bovine TC. Sequence alignment with intrinsic factor (IF) and TC's from other species revealed four conserved clusters of amino acid residues which might be required for Cbl binding. Bovine TC has no free cysteine residues but three disulfide bonds which are required for Cbl binding as dialysis against dithiothreitol released bound B<sub>12</sub>. The H<sub>2</sub>OCbl<sup>+</sup>–TC complex reacted with azide ion in solution to give N<sub>3</sub>Cbl but more slowly than free H<sub>2</sub>OCbl<sup>+</sup> and with a smaller binding constant (1.2 × 10<sup>3</sup> M<sup>-1</sup> compared to 2.2 × 10<sup>4</sup> M<sup>-1</sup> for free H<sub>2</sub>OCbl<sup>+</sup>).

These workers also reported<sup>229</sup> the isolation of human TC cDNA from a commercial human kidney cDNA library and its expression in yeast. The sequence of the recombinant TC was the same as a published sequence for human TC<sup>230</sup> except for a Ser → Leu substitution at position 376. The ligand-free protein apo-TC could be obtained from B<sub>12</sub>-saturated TC by extensive incubation in guanidinium chloride. The Cbl and TC receptor binding characteristics of the recombinant TC were similar to those of human and bovine TC. Binding of H<sub>2</sub>OCbl<sup>+</sup>, CNCbl, and N<sub>3</sub>Cbl to apo-TC caused an enhancement of the γ-band absorbance and a small red shift of the γ-band, which was greatest for H<sub>2</sub>OCbl<sup>+</sup> (11 nm). This enabled the binding of these Cbl's to apo-TC and apo-human haptocorrin (Hc) to be studied by stopped flow spectrometry. Kinetic measurements were made at 20 and 37 °C at pH 7.5. For apo-Hc all three Cbl's displayed a single kinetic phase with second-order rate constants of 9 × 10<sup>7</sup> (CNCbl), 1.2 × 10<sup>8</sup> (N<sub>3</sub>Cbl), and 6 × 10<sup>7</sup> M<sup>-1</sup> s<sup>-1</sup> (H<sub>2</sub>OCbl<sup>+</sup>) at 20 °C. For apo-TC at 20 °C CNCbl and N<sub>3</sub>Cbl bound in a single kinetic phase with rate constants of 1 × 10<sup>8</sup> and 1.3 × 10<sup>8</sup> M<sup>-1</sup> s<sup>-1</sup>, respectively. All of these binding rate constants are likely to be at or near the diffusion-controlled limit. However, the binding of H<sub>2</sub>OCbl<sup>+</sup> displayed two kinetic phases, a rapid one ( $k = 3 \pm 0.6 \times 10^7 \text{ M}^{-1} \text{ s}^{-1}$ ,  $E_a = 7 \pm 2 \text{ kcal mol}^{-1}$ ) and a much slower one which was independent of H<sub>2</sub>OCbl<sup>+</sup> concentration ( $k = 0.02 \text{ s}^{-1}$ ,  $E_a = 29 \pm 2 \text{ kcal mol}^{-1}$ ). The authors interpret the difference in kinetic behavior between H<sub>2</sub>OCbl<sup>+</sup> and the other two Cbl's as being due to a subsequent conformational change of the initially formed H<sub>2</sub>OCbl<sup>+</sup>–TC complex to form a “closed” species in which the axial water ligand of the bound Cbl has undergone substitution by an amino acid residue. This ligand substitution does not

occur for the CNCbl and  $N_3$ Cbl complexes which remain in an “open” state. This would be consistent with the enhanced shift of the  $\gamma$ -band of bound  $H_2O$ Cbl<sup>+</sup> compared to the spectral changes for CNCbl and  $N_3$ Cbl upon binding.

Studies of ligand substitution in bound  $H_2O$ Cbl<sup>+</sup> showed that when  $H_2O$ Cbl<sup>+</sup>–TC was reacted with excess cyanide, the kinetics showed a saturating increase in  $k_{obs}$  to a limiting value of  $5 \times 10^{-4} s^{-1}$  at 37 °C. Reaction of  $H_2O$ Cbl<sup>+</sup>–TC with excess azide displayed a decrease in rate constant with increasing  $[N_3^-]$  but also saturated to a limiting value of  $5.5 \times 10^{-4} s^{-1}$ . These observations are consistent with the model of a “closed”  $H_2O$ Cbl<sup>+</sup>–TC complex which must undergo a rate-limiting conformational change (i.e., with a rate constant of  $5 \times 10^{-4} s^{-1}$ ) to an “open” form before ligand substitution can occur. They also permit the estimation of the equilibrium constant for this conformational change of ca. 40.

These workers subsequently expanded this work<sup>231</sup> to include studies with IF and AdoCbl and an unfortunately unspecified cobinamide (“Cbi”). Only the binding of  $H_2O$ Cbl<sup>+</sup> and “Cbi” to TC displayed biphasic kinetics, with the rate constant for the slow phase with “Cbi” being slower ( $4.3 \times 10^{-3} s^{-1}$  at 20 °C) than with  $H_2O$ Cbl<sup>+</sup>, but the significance of the observations with “Cbi” is unknown since the liganded state of the cobinamide is unspecified. On the basis of spectral comparisons the authors suggest that the slow phase in the binding of  $H_2O$ Cbl<sup>+</sup> to TC results in the formation of a His-liganded Cbl. The authors report rate constants for the binding of His to free  $H_2O$ Cbl<sup>+</sup> of  $0.92 M^{-1} s^{-1}$  and  $2.2 \times 10^{-4} s^{-1}$  for the reverse reaction with a binding constant of  $4.2 \times 10^3 M^{-1}$  at pH 7.5 and 20 °C. Addition of His to solutions of the complex of  $H_2O$ Cbl<sup>+</sup> with Hc or IF caused spectral changes similar to those for the slow phase of  $H_2O$ Cbl<sup>+</sup> binding to TC. Reaction of “Cbi” with His showed spectral changes similar to those of the slow phase of “Cbi” binding to TC; however, addition of excess His to the “Cbi”–TC complex caused further spectral changes. Again, these observations are un-interruptible without knowing the axial ligands of the cobinamide employed. Rate constants for the binding of  $H_2O$ Cbl<sup>+</sup>, CNCbl, and AdoCbl to IF were slower than the rate constants for binding to TC by 2.5–13-fold. AdoCbl bound to IF, TC, and Hc with rate constants of  $4.5 \times 10^6$ ,  $5.7 \times 10^7$ , and  $1.4 \times 10^8 s^{-1}$ , respectively, while the values for “Cbi” were  $2.1 \times 10^7 s^{-1}$  for IF and TC and  $6.1 \times 10^7 s^{-1}$  for Hc. Dissociation rate constants for corrinoids from their protein complexes were measured in chase experiments in which the protein–Cbl complex was incubated with a 4-fold excess of CNCbl. However, it is unclear if this small excess is sufficient to drive the replacement reaction to completion, and binding constants for the Cbl’s to the proteins calculated from the binding and dissociation rate constants measured here differ from previously reported values by as much as 2–3 orders of magnitude. Consequently, these dissociation rate constants may not be reliable. The authors also find that IF, Hc, and TC slow the formation of  $H_2O$ Cbl<sup>+</sup> from protein-bound AdoCbl by aerobic photolysis by 7-, 15-, and 17-fold relative to

free AdoCbl. However, interpretation of such results is complicated by questions relating to solvent cages, diffusion barriers, and radical recombination rates for such macromolecular photodissociations. Nonetheless, it seems clear that binding of  $H_2O$ Cbl<sup>+</sup> to TC results in a conformational change in the protein and a substitution of the axial water ligand by a group on the protein.

Sharma and co-workers<sup>226</sup> investigated the possibility that high-affinity Cbl binding proteins exist in marine animals as a result of the fact that many such organisms require Cbl’s and the concentration of Cbl’s in seawater is very low (10 pg/mL at the most). They discovered a new  $B_{12}$  binding protein in the growth medium (Gm protein) of *Thalassiosira pseudonana* that has high affinity ( $K = 2 \times 10^{11} M^{-1}$ ) for CNCbl and high specificity for complete corrinoids over Cbi’s and an unusual oligomeric composition. The protein is halophilic and only stable in water containing 2–10% NaCl. It could be purified to homogeneity only as the CNCbl complex, the apo-protein being too unstable. The native molar mass from gel filtration was  $\geq 400$  kDa, while SDS–PAGE showed eight dissimilar subunits, only one of which contained bound CNCbl, suggesting the possibility of a large binding protein with only a single Cbl binding site and an unusual octameric structure.

## 10. Cobalamins and Nucleic Acids

Several interesting studies have appeared recently involving the direct interactions of Cbl’s with nucleic acids. While an RNA aptamer that specifically binds CNCbl is an artificial construct, there is now increasing evidence that Cbl’s interact directly with RNA in vivo as part of the regulation of the expression of genes involved in Cbl uptake, biosynthesis, and function.

Wilson and co-workers<sup>232–234</sup> determined the X-ray crystal structure of a 35 nucleotide pseudoknot RNA aptamer which specifically binds CNCbl.<sup>235</sup> The aptamer, which requires 1 M lithium chloride for binding and proper folding, binds CNCbl with an association constant of  $1.1 \times 10^7 M^{-1}$ , binds  $(CN)_2$ -Cbi 200-fold less strongly, and fails to bind AdoCbl. Unlike other RNA aptamers the  $B_{12}$  binding pseudoknot does not bind its ligand by “adaptive binding”, in which an initially unstructured RNA strand folds around its ligand, coupling binding to the folding process. Instead, secondary structure elements form a stable tertiary structure which provides an accessible binding site for the ligand in the manner of protein–ligand interactions. Evidence for this includes the observation that nucleotides in the core of the aptamer are protected from chemical modification even in the absence of the  $B_{12}$  ligand while those which are solvent accessible in the crystal structure are readily modified. The first helix of this two-helix pseudoknot is nested in a large triplex, one end of which contacts the bound CNCbl and is stabilized by a novel three-stranded zipper featuring nucleotide intercalation. This end of the triplex is defined by the pairing of strand 1 with the major groove of strands 2 and 3, while the other end is defined by the pairing of strand 3 with the minor groove of strands 1 and

2. Five nucleotides cap the perpendicular helix and triplex forming a hydrophobic patch that provides the CNCbl binding site. Interactions between the aptamer and CNCbl include hydrophobic packing, hydrogen bonding, and electrostatic interactions. The nucleosides of the aptamer create a hydrophobic surface complementary to the Cbl. While the corrin ring substituents prevent direct contact between the RNA and the corrin ring, seven of the substituents make hydrophobic contacts with bases and ribose rings on the aptamer. The amide side chains make numerous H-bonded contacts with the RNA backbone and the bases. The coordinated cyanide of the bound Cbl lies in a pocket at the end of the triplex created by three residues whose unsatisfied hydrogen-bond donors create an electrostatic potential which compliments the strong dipole created by the cyanide lone pair. Strangely, only the  $\beta$ -face of CNCbl contacts the aptamer, so that the Bzm faces the solution and does not participate in the binding interactions, making the observation that (CN)<sub>2</sub>Cbi binds significantly more weakly than CNCbl difficult to rationalize.

The activity of methionine synthase in cell culture is known to be enhanced by media supplementation with B<sub>12</sub>, which had been thought to result from enhanced conversion of the apoenzyme to the holoenzyme. Banerjee and co-workers<sup>236</sup> showed that five different cell lines displayed increases in methionine synthase activity by 2–14-fold when the growth media was supplemented with B<sub>12</sub>. However, cell-free extracts of these cultures showed no increase in the proportion of holoenzyme regardless of whether the medium was supplemented or not. The increase in activity could be detected as soon as 2 h after supplementation and reached a plateau in 24–48 h. Northern analysis of methionine synthase mRNA levels as a function of time showed that the level of mRNA was unchanged during the time during which the enzyme activity increased 2.5-fold. However, Western analysis showed directly that the increase in activity is due to an increase in methionine synthase protein. The authors conclude that the regulation must be exerted posttranscriptionally, suggesting that B<sub>12</sub> may directly interact with methionine synthase mRNA.

Expression of the *btuB* gene in *E. coli*, which codes for the outer membrane Cbl transporter, is suppressed by growth on B<sub>12</sub>. The effect is known to be due to regulation at the translational level, specifically by AdoCbl.<sup>237</sup> Nou and Kadner<sup>238</sup> studied the binding of *E. coli* ribosomes to *btuB* mRNA using a primer extension-inhibition assay. Binding of the 30S ribosomal subunit to the *btuB* mRNA start site was reduced in the presence of AdoCbl (5  $\mu$ M), although once the mRNA-ribosome complex had been formed in the absence of AdoCbl subsequent addition of AdoCbl had no effect. Inhibition of binding of the 30S subunit to *btuB* mRNA was half-maximal at about 0.3  $\mu$ M AdoCbl, but 10-fold higher CH<sub>3</sub>Cbl was required for inhibition, and CNCbl, H<sub>2</sub>OCbl<sup>+</sup>, and (CN)<sub>2</sub>Cbi had no effect at 30  $\mu$ M. Mutations in the *btuB* mRNA leader regions that were known to affect translational regulation also affected ribosome binding and its sensitivity to AdoCbl. The authors con-

clude that suppression of *btuB* translation by AdoCbl is the result of direct binding of AdoCbl to *btuB* mRNA, although they could not demonstrate such binding with Ado[<sup>57</sup>Co]Cbl.

Breaker and co-workers<sup>239</sup> further studied the interaction of AdoCbl with *btuB* mRNA. They subjected an RNA composed of the first 202 residues of the 5'-untranslated region of *btuB* mRNA to "in line probing" by spontaneous RNA cleavage. In the presence of AdoCbl the distinct pattern of cleavage products, which suggests a stable conformational state, was altered at eight positions. The level of spontaneous cleavage at the six most prominent modulation sites correlated with the concentration of AdoCbl, and all gave similar  $K_D$  values of about 0.3  $\mu$ M, the value previously found for half-maximal inhibition of ribosome binding to *btuB* mRNA by AdoCbl by Nou and Kadner.<sup>238</sup> These authors directly detected AdoCbl binding to the *btuB* mRNA leader using equilibrium dialysis and [A15-<sup>3</sup>H]AdoCbl. The specificity of the binding of AdoCbl was studied using the in-line cleavage assay and various Cbl's including structural analogues of AdoCbl. A 5'-deoxyadenosyl-like  $\beta$ -axial ligand was absolutely necessary for activity. Modification of the adenine moiety (*N*<sup>6</sup>-methyl-AdoCbl, *N*<sup>1</sup>-methyl-AdoCbl, 3-deaza-AdoCbl) generally decreased the activity. However, 2'-deoxy-AdoCbl was fully active, while Ado-13-epiCbl was totally inactive in the in-line assay as well as in the in-vivo regulation of *btuB* expression. Mutations in the *btuB* leader region had parallel effects on in-vitro binding of AdoCbl and in-vivo regulation of *btuB* transcription.

## 11. Enzymology

The last 5 years have seen an explosion of work on the enzymes that utilize B<sub>12</sub> cofactors. In part this has been fueled by the widespread availability of cloned and overexpressed enzymes, which has enabled many complex experiments requiring large amounts of enzyme. However, it has also been fueled by the successful crystallization and solution of the X-ray crystal structures of a number of enzymes, which has engendered much mechanistic speculation, hypotheses, and experimentation.

### 11.1. Coenzyme B<sub>12</sub>-Dependent Enzymes

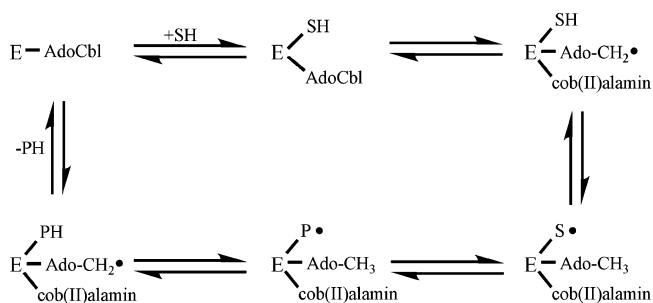
The AdoCbl-dependent enzymes, with one exception, catalyze intramolecular 1,2-rearrangements in which a group X and a hydrogen on adjacent carbon atoms exchange places. These enzymes fall into three classes, distinguished by the nature of the migrating group and the nature of the substituent on the carbon atom to which this group migrates.<sup>240,241</sup> The Class I enzymes are mutases, catalyzing carbon skeleton rearrangements in which the migrating group is a carbon fragment (2-glycinyll, 2-acrylate, or formyl-CoA) so that a C–C bond is cleaved and the receiving carbon has two hydrogens. These enzymes include glutamate mutase (GluM, EC 5.4.99.1), 2-methyl-eneglutamate mutase (MGM, EC 5.4.99.4), methyl-malonylCoA mutase (MMCM, EC 5.4.99.2), and isobutyrylCoA mutase (ICM, EC 5.4.99). The Class

II enzymes, with one exception, are eliminases which catalyze the migration and subsequent elimination of a hydroxyl or amino group, so that a C–O or C–N bond is cleaved and the receiving carbon bears a hydroxyl substituent. These include propanediol dehydratase (diol dehydratase, DD, EC 4.2.1.28), glycerol dehydratase (GD, EC 4.2.1.30), ethanolamine ammonia lyase (EAL, EC 4.3.1.7), and ribonucleoside triphosphate reductase (RTPR, EC 1.17.4.2), which catalyzes the reduction of ribonucleoside triphosphates to 2'-deoxyribonucleoside triphosphates with no rearrangement. The Class III enzymes are the aminomutases, which catalyze the migration of an amino group to an adjacent carbon which bears two hydrogens, so that a C–N bond is cleaved. These enzymes are distinguished by an additional requirement for pyridoxal phosphate (PLP) and include  $\beta$ -lysine-5,6-aminomutase (LAM, EC 5.4.3.3) and D-ornithine-4,5-aminomutase (OAM, EC 5.4.3.4).

While this classification is based on the specifics of the migrating group and the receiving carbon there are several other interesting differences among the classes of AdoCbl-dependent enzymes. The first is the mode of coenzyme binding. The Class I mutases bind AdoCbl in a base-off conformation, with the  $\alpha$  axial ligand position occupied by the imidazole of a histidine residue at the active site and the nucleotide loop buried in a hydrophobic pocket, known as "base-off/His-on" binding. They all contain the consensus sequence, Asp-x-His-x-x-Gly, in their binding subunits, which provides the axial His residue. This mode of coenzyme binding was first discovered for CH<sub>3</sub>Cbl in the X-ray crystal structure of the Cbl binding domain of methionine synthase.<sup>242</sup> This suggests the possibility of an evolutionary relationship between the Class I AdoCbl-dependent enzymes and the CH<sub>3</sub>Cbl-dependent methionine synthase. In stark contrast, the Class II enzymes all bind AdoCbl base-on with the axial Bzm ligand remaining coordinated to the metal. Both Class III enzymes are now known to bind AdoCbl in the base-off/His-on mode (see below). This dichotomy of binding modes could never have been imagined just a few years ago, prior to the advent of the "X-ray crystallography age" of B<sub>12</sub> enzymology.

A second interesting difference between the Class I and Class II enzymes is the specificity for AdoCbl. The Class II enzymes are remarkably promiscuous in tolerating structural variations in the coenzyme.<sup>243</sup> Many coenzyme analogues with structural alterations in the adenine and its ribose, the corrin ring and its substituents, and the axial nucleotide are partially active coenzymes for the Class II enzymes (although some are inactive inhibitors). In contrast, the Class I mutases are much more specific for AdoCbl itself. While there is significant tolerance for alterations in the axial base<sup>244</sup> (and see below), there is an almost absolute requirement for an intact 5'-deoxyadenosyl  $\beta$ -axial ligand,<sup>244,245</sup> the single known exception being GluM for which 3-IsoAdoCbl (Figure 1) displays 50% of the activity of AdoCbl itself. These important differences in binding mode and coenzyme specificity among the AdoCbl-dependent enzyme classes suggest the very real possibility that the

#### Scheme 14



primary bioinorganic event in the catalytic cycle of these enzymes, the homolysis of the Co–C bond of the coenzyme, might be catalyzed by more than one mechanism, another possibility that could not have been imagined only a short time ago.

A third difference between Class I and Class II enzymes is the character of the biradical spectrum obtained by cryotrapping the enzymes during normal turnover. For the Class I enzymes the EPR spectrum is characterized by showing Co<sup>II</sup> hyperfine coupling and a zero-point crossing  $g$  value between the Co<sup>II</sup> and organic radical  $g$  values. These spectra result from relatively strong spin–spin coupling between the cobalt unpaired spin and that of the organic radical. In contrast, the Class II enzymes exhibit weak coupling so that the Co<sup>II</sup> and organic radical features are resolved. The Co<sup>II</sup> is generally broad and featureless at  $g \approx 2.2$ , and a sharper organic radical feature appears near  $g = 2$ .

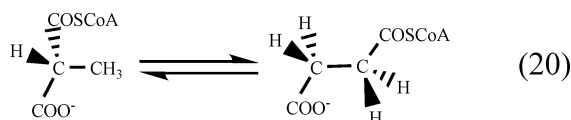
The generally accepted skeleton reaction scheme for the AdoCbl-dependent enzymes is shown in Scheme 14. After binding the coenzyme and substrate (SH) the Co–C bond of the coenzyme is cleaved homolytically in a step known as the "activation" of AdoCbl. The Ado• radical formed in this process then abstracts the migrating hydrogen from the substrate to produce a substrate radical and 5'-deoxyadenosine. As it is now generally accepted that the intramolecular rearrangements occur at the radical level; the substrate radical is next envisioned to rearrange into a product radical which then abstracts one of three now equivalent hydrogens from 5'-deoxyadenosine to form the product. Release of the substrate then completes the catalytic cycle. In this skeleton mechanism the cob(II)alamin formed by coenzyme homolysis plays only the role of spectator (although, of course, it provides a very valuable probe of the active site during catalysis). The means by which these enzymes catalyze the simple dissociation of the Co–C bond of AdoCbl by 10<sup>9</sup>- to nearly 10<sup>14</sup>-fold<sup>18,106,221,222</sup> remains unknown and a topic of intense research.

It must be pointed out that although the X-ray structures of AdoCbl-dependent enzymes have been extremely valuable in guiding mechanistic hypotheses and experimentation, some of the structures contain artifacts which show anomalously long Co–NB3 axial bonds in enzyme-bound Cbl's (see below).<sup>188</sup> Unfortunately, some EXAFS on MMCM<sup>246</sup> similarly predicted a long axial Co–NB3 bond. These observations led to erroneous mechanistic speculations about the possibility of enzymatic manipulation of the axial Co–N bond as a means to foster the

homolysis of the Co–C bond. The erroneous EXAFS results have subsequently been attributed to Fourier filtering and the reliance on first-shell analysis only (see below).<sup>247</sup> As above, the X-ray crystal structure anomalies are now known to be due to X-ray-induced photoreduction of protein-bound Cbl's leading to mixed oxidation and coordination state species with anomalously long axial Co–N bonds.<sup>114,191</sup>

### 11.1.1. Class I Mutases

MethylmalonylCoA mutase (MMCM) catalyzes the rearrangement of (2*R*)-methylmalonylCoA ((2*R*)-MMCoA) to succinylCoA (eq 20) via exchange of a hydrogen atom from the methyl group for the carbonyl–CoA group on the adjacent carbon. The most frequently studied enzyme, from *P. shermanii*, is a dimer of dissimilar subunits of 69.5 and 80.1 kDa mass. It is the only AdoCbl-dependent enzyme that occurs in both mammals and bacteria. The reaction is a crucially important step in the metabolism of odd chain fatty acids, and the absence of a functional protein is the basis for the human metabolic disease methylmalonic acidemia.



Watanabe and co-workers<sup>248</sup> purified MMCM from methanol utilizing bacterium *Methylobacterium extorquens* NR-1 to homogeneity (specific activity 15.9 U mg<sup>-1</sup>) in 6.9% yield. The enzyme has an apparent molar mass of 150 kDa by gel filtration and is composed of subunits of molar mass 85 and 70 kDa (by SDS gel electrophoresis). N-Terminal amino acid analysis of both subunits showed no homology to the enzyme from other species.  $K_m$  values were 15.4  $\mu\text{M}$  for (2*R*)-MMCoA, 0.29 mM for succinylCoA, 30.9 nM for AdoCbl, and 5.6  $\mu\text{M}$  for AdoCbi<sup>+</sup>, the last of which, in contrast to MMCM from *P. shermanii* (see below), was an active coenzyme with a  $V_{\text{max}}$  ca. 28% of that for AdoCbl. Other Cbl's investigated were competitive inhibitors including CNCbl ( $K_i = 0.12$  mM), CH<sub>3</sub>Cbl ( $K_i = 1.2$   $\mu\text{M}$ ), and H<sub>2</sub>OCbl<sup>+</sup> ( $K_i = 12$   $\mu\text{M}$ ).

Mancia and co-workers<sup>249</sup> solved the X-ray crystal structures of *P. shermanii* MMCM reconstituted with AdoCbl and the substrate, (2*R*)-MMCoA, and two inhibitors, 3-carboxypropylCoA, a product analogue, and (2*R*)-carboxypropylCoA, a substrate analogue. The three refined structures were very similar to each other and to the structure of the enzyme reconstituted with desulfo–CoA,<sup>188</sup> suggesting that the rearrangement occurs without any major conformational change in the enzyme, in contrast to substrate binding which causes large conformational change in the protein. As was the case for the desulfo–CoA complex, none of the enzyme complexes showed any electron density for a cobalt-bound adenosyl group, suggesting that the Ado ligand is lost during crystallization and the Cbl is cob(II)alamin. However, for the substrate complex electron density was found for partial occupancy of a 5'-deoxyadenosine not bonded to cobalt with its nitrogens and hydroxyls close to H-bond donors and acceptors (or

waters) and its 5' carbon near the substrate. Compared with a previous structure with AdoCbl but no substrate, which has an intact AdoCbl,<sup>250</sup> the Ado has moved away from the metal and sits in the only open space in the active site with its adenine ring perpendicular to the corrin. Several residues in the active site, including Arg $\alpha$ 207, His $\alpha$ 244, and Tyr $\alpha$ 89, are suspected of positioning and stabilizing the substrate radical. The geometry of the complex with 3-carboxypropylCoA seems to explain both the preference for the enzyme to abstract the H<sub>Re</sub> hydrogen from carbon 3 of succinylCoA and the fact that it sometimes selects the other hydrogen. Thus, apparent flexibility in the C2,C3 torsion angle allows for a situation where the succinyl group spends some of its time in a conformation in which the H<sub>Re</sub> hydrogen is much closer to the adenosyl radical than the H<sub>Si</sub> hydrogen but some time in a conformation in which there is much less difference between the distances from H<sub>Re</sub> and H<sub>Si</sub> to the radical. The position of Tyr $\alpha$ 89 seems to explain the stereospecificity for (2*R*)-methylmalonylCoA since migration of the methyl to form the 2*S* enantiomer would clash with this residue.

Banerjee and co-workers<sup>251</sup> used cryogenic resonance Raman (RR), which prevents laser-induced AdoCbl photolysis, to study MMCM and its complexes with substrates and inhibitors. Since product dissociation is rate limiting and the equilibrium favors the succinylCoA product, complexes with the normal substrate, methylmalonylCoA (MM–CoA), or product, succinylCoA (S–CoA), resemble the product state (P state) while those with inhibitors, cyclopropylcarbonyl–CoA carboxylate (CPC–CoA), or slow substrates, ethylmalonylCoA (EtM–CoA) or glutaryl–CoA (G–CoA), resemble the substrate state (S state). The high-frequency modes of the corrin ring of AdoCbl are shifted to higher frequency when AdoCbl binds to MMCM, suggesting a possible flattening of the corrin ring, but remain at these positions upon binding substrate or the inhibitor CPC–CoA. Isotope editing of the AdoCbl–MMCM complex with [A15-<sup>13</sup>C]AdoCbl allowed the assignment of bands at 424 cm<sup>-1</sup> to the Co–C stretching mode ( $\nu_{\text{Co-C}}$ ) and at 567 cm<sup>-1</sup> to a A15-coupled ribose ring deformation mode ( $\delta_{\text{ribose}}$ ). Deuteration of the coenzyme at A15 shifts these two modes more than <sup>13</sup>C substitution and also allows the assignment of two other modes, the Co–C–C bending mode ( $\delta_{\text{CoC5'C4'}}$ ) at 363 cm<sup>-1</sup> and a band at 420 cm<sup>-1</sup> which is suggested to be a hindered rotation about the Co–C bond ( $\tau_{\text{Co-CH2R}}$ ). When AdoCbl binds to MMCM, the Co–C stretching frequency shifts from 430 to 424 cm<sup>-1</sup>, but when saturating product or substrate is added (P state), it shifts back to 430 cm<sup>-1</sup>, although its intensity is diminished. However, when either of the slow substrates or the inhibitor are added (S state), both  $\nu_{\text{Co-C}}$  and  $\tau_{\text{Co-CH2R}}$  disappear but  $\delta_{\text{ribose}}$  remains, ensuring that AdoCbl remains intact. However, the  $\delta_{\text{CoC5'C4'}}$  mode, which is barely detectable in the free coenzyme, intensifies in the AdoCbl–MMCM complex and intensifies further when the inhibitor or a slow substrate (S state) is added but is missing the complex with substrate (P state). Two other low-frequency corrin modes, suggested to be Co–N<sub>eq</sub>

stretching modes, at 423 and 437  $\text{cm}^{-1}$  are downshifted when substrate is added (P state). Taken together, the authors suggest that these changes imply a small amount of tilting of the Ado ligand in the AdoCbl–MMCM complex, which is enhanced in the S state but reversed in the P state. The tilting is suggested to contribute to Co–C bond activation, and the downshift of the low-frequency corrin frequencies in the P state suggests a possible displacement of the Co from the mean equatorial plane.

Chowdhury and Banerjee<sup>222</sup> studied the kinetics of the formation of cob(II)alamin at the active site of MMCM as a function of substrate concentration. In this enzyme AdoCbl homolysis is coupled to hydrogen-atom transfer from the substrate to the Ado• radical (see below). The kinetics show saturation behavior with respect to MMCoA concentration and permit the determination of the rate of cob(II)alamin formation,  $k_f$ , and the substrate binding constant,  $K_i$ , between 5 and 20 °C, above which the reaction becomes too fast to study by stopped flow spectroscopy. The substrate binding constant,  $8 \pm 1 \times 10^3 \text{ M}^{-1}$  at 20 °C, is characterized by a small negative enthalpy change,  $-2.0 \pm 0.1 \text{ kcal mol}^{-1}$ , and a surprisingly large positive entropy change,  $9.4 \text{ cal mol}^{-1} \text{ K}^{-1}$ , suggesting that association of the substrate with the enzyme is accompanied by release of bound solvent since substrate binding does not cause protein conformational changes.<sup>249</sup> Activation analysis for  $k_f$  gives  $\Delta H^\ddagger = 18.8 \pm 0.8 \text{ kcal mol}^{-1}$  and  $\Delta S^\ddagger = 18.2 \pm 0.8 \text{ cal mol}^{-1} \text{ K}^{-1}$ , and extrapolation to 37 °C gives  $k_f = 3.34 \times 10^3 \text{ s}^{-1}$ . Compared to the rate constant for nonenzymatic homolysis of AdoCbl at 37 °C ( $8.9 \times 10^{-9} \text{ s}^{-1}$ <sup>158</sup>), the latter value gives an enzymatic rate enhancement for the activation of AdoCbl by MMCM of  $3.8 \times 10^{11}$ -fold or  $16.4 \text{ kcal mol}^{-1}$ . Compared to the activation parameters for nonenzymatic AdoCbl homolysis,<sup>106</sup> the enzyme catalyzes AdoCbl homolysis by lowering the enthalpy of activation by  $15.0 \text{ kcal mol}^{-1}$  and increasing the entropy of activation by  $4.7 \text{ cal mol}^{-1} \text{ K}^{-1}$ . Thus, at 37 °C the enzymatic activation of AdoCbl is predominantly (91%) enthalpic in nature.

Following an earlier approximate estimation<sup>252</sup> of the primary deuterium kinetic isotope effect (KIE) for the formation of cob(II)alamin at the MMCM active site which had a value of  $\geq 20$  at 25 °C, Chowdhury and Banerjee<sup>253</sup> investigated the temperature dependence of the KIE by studying the dependence of the rate constant for cob(II)alamin formation on the concentration of MMCoA (5–20 °C) and  $[\text{C3-}^2\text{H}_3]\text{MMCoA}$  (5–37 °C). The measured KIE's are very large, indeed, varying from 49.9 at 5 °C to 35.6 at 20 °C, far above the semiclassical limit. An Arrhenius analysis according to eq 21 (Figure 7) gave  $0.078 \pm 0.009$  for the Arrhenius preexponential factor,  $A_{\text{H}}/A_{\text{D}}$ , and  $3.41 \pm 0.07 \text{ kcal mol}^{-1}$  for the difference in activation energies,  $E_{\text{a(D)}} - E_{\text{a(H)}}$ . These values are far outside the semiclassical limits of  $0.7 \leq A_{\text{H}}/A_{\text{D}} \leq 1.0$  and  $E_{\text{a(D)}} - E_{\text{a(H)}} = 1.15 \text{ kcal mol}^{-1}$ , strongly indicating the involvement of hydrogen-atom tunneling in this process.

$$\ln(k_{\text{f(H)}}/k_{\text{f(D)}}) = \ln(A_{\text{H}}/A_{\text{D}}) + (E_{\text{a(D)}} - E_{\text{a(H)}})/RT \quad (21)$$

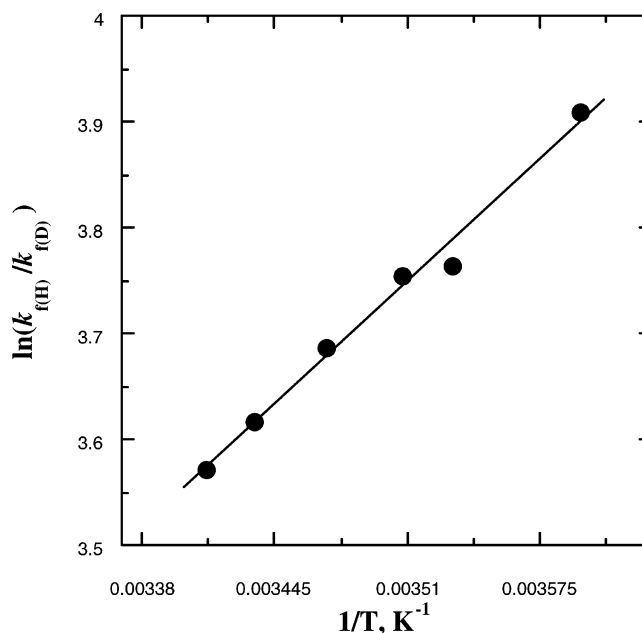
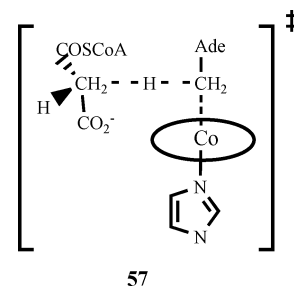


**Figure 7.** Plot of the natural logarithm of the primary deuterium kinetic isotope effect for methylmalonylCoA mutase vs  $1/T$ .

It should be noted that this kind of kinetic coupling of Co–C bond cleavage to H-atom transfer can contribute to the energetics of enzymatic activation of AdoCbl. If the processes are concerted, then the net activation reaction has a transition state, which may be depicted as in 57.



This transition state can be stabilized by the partial transfer of a hydrogen atom from the MMCoA substrate methyl to the emerging Ado• radical methylene by an amount which must be something less than the difference in stability of the Ado• radical and the MMCoA radical, which could be as high as 8  $\text{kcal mol}^{-1}$ .<sup>254</sup>

Finke and co-workers<sup>255</sup> used these observations regarding H-atom tunneling to design a clever series of experiments to test the Klinman hypothesis regarding enzymes in which quantum mechanical tunneling occurs during hydrogen-atom transfers, i.e., that such enzymes have evolved to increase the probability of tunneling as part of their catalytic mechanism. Studying the nonenzymatic counterpart of the closely related diol dehydratase reaction, these workers thermolyzed AdoCbl at 80–100 °C in ethylene glycol or ethylene glycol- $d_4$  in the absence of a radical trap. Under these conditions the only possible fates of the Ado• radical formed from thermolysis are cyclization to form 5',8-anhydroadenosine (c-Ado, Scheme 9), return to the solvent cage, and abstraction

of a hydrogen atom from the ethylene glycol solvent to form 5'-deoxyadenosine (Ado-H). By determining the ratio c-Ado/Ado-H in ethylene glycol relative to that (i.e., c-Ado/Ado-D) in ethylene glycol-*d*<sub>4</sub>, the primary deuterium KIE for the H-atom abstraction reaction could be determined. From the temperature dependence of the KIE, the zero-point activation energy difference ( $E_D - D_H$ ) was  $3.0 \pm 0.3$  and the preexponential factor ratio ( $A_H/A_D$ ) was  $0.16 \pm 0.07$ , values not significantly different from Banerjee's values for methylmalonylCoA mutase. These experiments were repeated, with very similar results, with 8-MeOAdoCbl (Figure 1), for which the associated 8-MeO Ado• radical cannot undergo cyclization, to control for the unknown effect of the possible reversibility of the cyclization reaction (eq 1) in the KIE measurements.

To provide a data set in the temperature range relevant to enzymes (where the thermolysis of AdoCbl is much too slow and proceeds mainly via the heterolysis pathway) a similar study was carried out with benzylCbl at 10–40 °C,<sup>256</sup> where it readily homolyzes to form the benzyl radical.<sup>257,258</sup> The results are again quite similar, and in fact, the data from all three studies fall on the same linear plot of  $\ln(\text{KIE})$  vs  $1/T$ . The authors conclude that H-atom tunneling is not enhanced in these B<sub>12</sub>-dependent enzymes.

It must, however, be pointed out that a preliminary report of the estimation of the primary deuterium KIE for formation of cob(II)alamin at the active site of diol dehydratase, the enzyme for which Finke's experiments actually probe the nonenzymatic occurrence of tunneling, has recently appeared.<sup>18</sup> At 4 °C the reaction is very fast ( $k_{\text{obs}} = 8 \pm 1 \times 10^2 \text{ s}^{-1}$  for 1,2-propanediol) but the KIE's for [1,1-<sup>2</sup>H<sub>2</sub>]1,2-propanediol and [1,1,2,2-<sup>2</sup>H<sub>4</sub>]1,2-ethanediol are only  $3.3 \pm 0.6$  and  $4 \pm 2$ , respectively. These results imply either that there is very little kinetic coupling between Co–C bond cleavage and H-atom transfer in this enzyme or that the enzyme does not use H-atom tunneling in its mechanism.

Binding of AdoCbl to MMCM in the base-off/His-on mode causes a large conformational change in the protein. To delineate the role of the nucleotide loop in this conformational change, Chowdhury and Banerjee<sup>259</sup> studied the interactions of AdoCbi<sup>+</sup> and 5'-deoxyadenosylcobinamide methyl phosphate (AdoCbi-PMe) with MMCM. Fluorescence quenching was used to determine the dissociation constant for AdoCbl, and the result ( $0.17 \pm 0.01 \mu\text{M}$ ) agreed extremely well with that determined by equilibrium dialysis using [A15-<sup>3</sup>H]AdoCbl ( $0.16 \mu\text{M}$ ). The measured  $K_d$  values for AdoCbi<sup>+</sup> and AdoCbi-PMe were, surprisingly, only slightly increased,  $0.62 \pm 0.09$  and  $3.33 \pm 0.03 \mu\text{M}$ , respectively. UV–vis spectra of protein-bound AdoCbi<sup>+</sup> and AdoCbi-PMe showed that His610, the active site histidine that becomes the axial ligand for AdoCbl, is *not* coordinated to these enzyme-bound coenzyme analogues missing the axial nucleotide (correcting an earlier misinterpretation<sup>260</sup> that His610 did bind to AdoCbi<sup>+</sup>). AdoCbi<sup>+</sup> could only support detectable catalytic activity when the enzyme concentration was increased 1000-fold over the normal

assay level, and AdoCbi-PMe did not support catalysis even at a 4000-fold increase in enzyme concentration. The kinetics of the fluorescence quenching by AdoCbl binding was also studied, and second-order rate constants varied as a function of pH with an apparent  $pK_a$  of  $7.3 \pm 0.2$ . The authors conclude that the nucleotide loop makes only a minor contribution (ca. 1 kcal mol<sup>-1</sup>) to the affinity of AdoCbl for MMCM. The failure of His610 to coordinate to AdoCbi<sup>+</sup> and AdoCbi-PMe as well as their lack of catalytic activity suggests that the absence of the nucleotide loop results in a failure of the active site to organize into the proper conformation for activity. The authors present a model for the binding of AdoCbl to MMCM in which the base-on to base-off conversion is slow, the base-on species is first bound and then base dissociation (assisted by the enzyme), and protein conformational changes occur in either order followed by coordination of His610, with the observed  $pK_a$  for the rate of fluorescence quenching (7.3) reflecting either a medium effect on  $pK_{\text{base-off}}$  for AdoCbl (solution value 3.7<sup>152</sup>) or the pH dependence of the conformational change. However, given measurements on the rate constants for Bzm dissociation and association in RCbl's,<sup>135,143</sup> it is clear that the rate of equilibration of the base-on and base-off species of AdoCbl must be very fast indeed, despite the fact that very little of the base-off species exists at neutral pH ( $pK_{\text{base-off}}$ , eqs 10 and 11, is 3.67). Thus, although the equilibrium of the base-on/base-off reaction for AdoCbl lies very far toward the base-on species at neutral pH, reequilibration of base-on and base-off species after binding the small fraction of base-off species to the enzyme cannot be a slow process.

Banerjee and co-workers<sup>261</sup> also studied the coenzymic activity of 5'-deoxyadenosylcobinamide-GDP (AdoCbi-GDP, Figure 1), a biosynthetic precursor of AdoCbl which is base-off in solution at all pH's, with MMCM. Binding of AdoCbi-GDP to MMCM does *not* lead to coordination of the active site His610 residue to the coenzyme analogue, as confirmed by the lack of superhyperfine coupling to an axial N-donor in the EPR spectrum. AdoCbi-GDP is a reasonably active cofactor with a  $k_{\text{cat}}$  value ( $18 \text{ s}^{-1}$  at 30 °C) only 4-fold lower than that for AdoCbl, despite the fact that it appears to bind in a base-off/His-off mode. The overall steady-state kinetic deuterium isotope effect ( $7.2 \pm 0.8$ ) is comparable to that of AdoCbl-MMCM ( $5.0 \pm 0.6$ ), demonstrating that suppression of the very large intrinsic KIE associated with the hydrogen-atom transfers is comparable for both coenzymes. This, in turn, suggests that the Co–C bond homolysis step is not affected by the lack of His coordination since the homolysis step is tightly coupled to the H-atom transfer. The binding constant, however, for AdoCbi-GDP ( $2.0 \times 10^5 \text{ M}^{-1}$ ), determined by fluorescence quenching, is 30-fold smaller than that for AdoCbl. Unlike the AdoCbl-holoenzyme, which during turnover exists as a mixture of intact AdoCbl (ca. 80%) and cob(II)alamin (ca. 20%), the AdoCbi-GDP reconstituted enzyme contained predominately intact AdoCbi-GDP during turnover. The activity of AdoCbi-GDP suggests that binding of a nucleotide to the nucleotide binding pocket of MMCM is essential for catalytic

activity but that coordination to axial N-donor is not. This supports the idea that binding of the nucleotide loop in its hydrophobic pocket assists in the conformational changes that the enzyme undergoes when AdoCbl binds and which results in the organization of the active site for catalysis.

In contrast, AdoCbl analogues with altered structure in the adenosyl ligand are not active coenzymes for MMCM. Thus, Rétey and co-workers<sup>45</sup> found that aristeromycylcobalamin (AriCbl, Figure 1) was not an active coenzyme with MMCM but was a weak competitive inhibitor, with  $K_i = 0.83 \pm 0.05 \mu\text{M}$ , about 14-fold higher than  $K_m$  for AdoCbl ( $57 \pm 4 \text{ nM}$ ).

The question of the role of the coordinating His ligand in MMCM has been further evaluated by Banerjee and co-workers<sup>262</sup> in studies in which His610 has been mutated both conservatively to asparagine (H610N) and nonconservatively to alanine (H610A). The conservative H610N mutant displayed steady-state catalytic activity 4000-fold lower than the wild-type enzyme, and the H610A mutant had 5000-fold lower activity than wild type. For both mutants the  $K_m$  value for AdoCbl (difficult to measure due to the low activity) was quite close to that for wild-type enzyme, but the association constants for AdoCbl (unmeasurably low) were reduced by at least  $10^3$ -fold from the value for wild-type enzyme, effects similar to those seen for His mutants in glutamate mutase.<sup>263</sup> Added imidazole was unable to rescue the mutants, and neither mutant displayed a deuterium isotope effect on the overall steady-state reaction (in contrast to wild type, for which the isotope effect is  $5.0 \pm 0.6$ ). The greatly reduced activity of the His mutants of MMCM suggests a change in the rate-determining step (thought to be product release for the wild-type enzyme), and this is supported by the lack of a deuterium isotope effect on steady-state turnover. The sharp difference between the effects of His mutation and the results obtained with the AdoCbl analogue AdoCbi-GDP,<sup>261</sup> which has 25% of the activity of AdoCbl in the steady state but does not coordinate to His610, suggests that the His-off state achieved in the mutants is somehow functionally different from that obtained with AdoCbi-GDP. The authors propose that coenzyme binding is the rate-determining step in the His mutants and that the role of His610 has to do with generating the base-off species of AdoCbl and catalyzing cofactor binding. The observation of an apparent  $pK_a$  of 7.3 associated with AdoCbl binding to wild-type enzyme<sup>259</sup> is certainly consistent with ionization of a His residue.

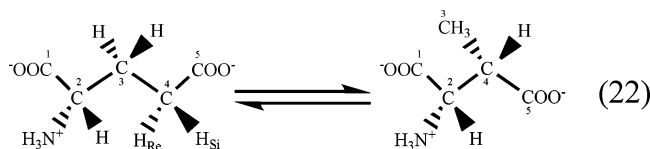
Binding of the substrate to MMCM causes a large conformational change in which a TIM barrel wraps around the CoA moiety.<sup>250</sup> The active site residue undergoing the largest change in position during this conformational change is Tyr89, which moves from a position above the adenine ring of AdoCbl into a position in which it impinges on the Ado binding site and hydrogen bonds with the substrate. Vlasie and Banerjee<sup>264</sup> studied the effect of the conservative mutation of Tyr89 to Phe (Y89F) and the more radical mutation of Tyr89 to Ala (Y89A), which creates a cavity at the active site. The activity of both mutants for conversion of MMCoA to product is reduced by

about  $10^3$ -fold, while the  $K_m$ 's for substrate and AdoCbl show only minor changes. In addition, the deuterium isotope effect on the steady-state reaction is abolished in both mutants. These observations suggest that in the mutants the rate-determining step must occur prior to the isotope-sensitive steps, which are the H-atom transfer steps. The UV-vis spectrum of the mutant holoenzymes during turnover show only the presence of AdoCbl, in contrast to wild-type enzyme which is about 20% cob(II)alamin during turnover.<sup>261</sup> Similarly, cob(II)alamin could not be detected under pre-steady-state conditions, suggesting that Co-C bond homolysis has become rate determining in the mutants. Both mutants retained stereospecificity for the *R* enantiomer of MMCoA despite the loss of the H-bonded contacts with the substrate, and the mutant enzymes were stable, insensitive to oxygen and photolysis. Since in the wild-type enzyme the rate constant for formation of cob(II)alamin (i.e., the coupled processes of Co-C bond homolysis and H-atom transfer from the substrate) is 10-fold faster than turnover and turnover is suppressed by  $10^3$ -fold in the Y89 mutants, the authors estimate that ca.  $10^4$ , or  $5.4 \text{ kcal mol}^{-1}$  (33%), of the ca.  $4 \times 10^{11}$ -fold, or  $16.4 \text{ kcal mol}^{-1}$ , catalysis of cob(II)alamin formation is due to Tyr89, which they refer to as a "molecular wedge". This is an interesting result, and if it is correct that the action of Tyr89 on Co-C bond homolysis is due to a steric displacement of the Ado ligand from its binding site it has consequences regarding the specificity of the enzyme for AdoCbl. Thus, analogues with structural alterations in the Ado portion of the coenzyme, which are, with one exception, reported to be "inactive", should in fact show detectable activity (about 6400-fold below AdoCbl activity) since it is hard to see how the "molecular wedge" action of Tyr89 would be affected by minor alterations of the adenine or ribose of the Ado ligand.

Thus, while much work has been done on the bioinorganic chemistry of MMCM during the period of this review, the details of the method by which it activates AdoCbl remain murky. It is clear that a nucleotide loop, which can have a variety of structures, is necessary for driving conformational changes in the protein which cause the assembly of a catalytically competent active site, but the role of the coordinating His610 residue remains obscure, since its mutation lowers catalytic activity dramatically, but it is not coordinated to coenzyme analogues such as AdoCbi-GDP which nonetheless support catalysis. Banerjee's hypothesis that the role of His610 has something to do with catalyzing the formation of base-off AdoCbl at the active site is plausible but cannot involve catalysis of the Bzm dissociation of AdoCbl which must be very rapid for this Cbl.<sup>135,143</sup>

Glutamate mutase (GluM) catalyzes the conversion of (*S*)-glutamate to (2*S*,3*S*)-3-methylaspartate (eq 22) via an exchange of  $H_{Si}$  on carbon 4 with the glycol fragment on carbon 3, a rearrangement which occurs with inversion of the configuration at C4. The reaction is the first step in the bacterial fermentation of glutamate to acetate and butyrate. The enzyme most often studied is from *Clostridium tetanomorphum*

and is a  $\epsilon_2\sigma_2$  tetramer of molar mass 137 kDa, consisting of an  $\epsilon_2$  dimer (MutE) of mass 107.6 kDa and two monomeric  $\sigma$  subunits (MutS) of mass 14.7 kDa. The latter provides the binding site for the AdoCbl cofactor. The related GluM from *C. cochlearium* has a similar subunit structure, and the large subunit (GlmE) has 94% sequence identity with MutE while the smaller AdoCbl binding subunit (GlmS) has 83% sequence identity with MutS.



Kratky and co-workers<sup>265</sup> reported the X-ray crystal structure of GluM from *C. cochlearium* reconstituted with CNCbl and CH<sub>3</sub>Cbl. Surprisingly, each complex contained a (2*S*,3*S*)-tartrate molecule, derived from the crystallization buffer, at the presumed substrate binding site, although tartrate is a weak inhibitor of GluM, at least at high pH. Both complexes contain one heterodimer  $\epsilon_2\sigma_2$  in the asymmetric unit with two bound Cbl's. The Cbl binding subunit,  $\sigma$ , is folded as an  $\alpha/\beta$  domain consisting of a  $\beta$  sheet of five parallel strands surrounded by six  $\alpha$  helices, very similar to the Cbl binding domains of MMCM,<sup>188</sup> methionine synthase,<sup>242</sup> and the MutS subunit from *C. tetanomorphum* GluM (see below). The  $\epsilon$  subunit is a TIM barrel with one end packed against the  $\beta$  face of the Cbl, forming the active site, and the other capped by an  $\alpha$  helix forming a lid for the barrel. The two  $\epsilon$  subunits have primarily hydrophobic contacts involving two  $\alpha$  helices which form a hydrophobic cavity, but the two  $\sigma$  subunits make no contact, and the two Cbl cobalt atoms are very remote (42.5 Å). The Cbl's bind in the base-off/His-on mode with the nucleotide loop buried in a hydrophobic cavity between the  $\beta$  sheet and two of the  $\alpha$  helices on the  $\sigma$  subunit. The cobalt atom is coordinated by the N $\epsilon$  nitrogen of His16, while the N $\delta$  nitrogen is H-bonded to Asp14 in the signature Asp-x-His-x-x-Gly motif conserved in all enzymes that bind coenzyme in the base-off/His-on conformation. The Co–N<sub>His</sub> bonds are anomalously long (2.28 Å in the CNCbl complex and 2.35 Å in the CH<sub>3</sub>Cbl complex), and the electron density for the “upper” axial ligand is difficult to interpret in both complexes. This is most likely the result of partial reduction to the cob(II)alamin state, so that a reasonable interpretation is that the crystals contain ca. 50% CNCbl or CH<sub>3</sub>Cbl and ca. 50% cob(II)alamin. This conclusion is fortified by observation that the cobalt atom is displaced from the mean equatorial plane toward the lower axial ligand by 0.06–0.07 Å, somewhat less than the out-of-plane displacement seen in the X-ray crystal structure of cob(II)alamin<sup>85</sup> and in the X-ray crystal structure of MMCM.<sup>188</sup> The authors conclude that it is likely that the Co(III) Cbl's bound to the enzyme have normal Co–N<sub>ax</sub> bond lengths, in agreement with recent EXAFS results (see below). The tartrate inhibitor is tightly bound into the presumed substrate binding site by a total of 14 hydrogen bonds.

While the  $\sigma$  subunit has 32% sequence identity with the Cbl binding domain of MMCM, there is only 18% sequence similarity between the  $\epsilon$  subunit of GluM and the TIM barrel domain of MMCM. Nonetheless, the two domains of the two enzymes are remarkably similar in three-dimensional structure, although the relative orientation of the two domains in GluM is somewhat different from that in MMCM, so that superposition of the two molecules requires translation and rotation of the TIM barrel domain. In the GluM structures the volume above the corrin ring is limited and cannot accommodate the adenosyl ligand in the conformation found in its X-ray structures (i.e., the “southern” conformation). The authors suggest a “northern” conformation, which still creates steric clashes and suggests the possibility of a steric mechanism for Co–C bond labilization based on conformational changes induced by substrate binding.

Kratky and co-workers<sup>266</sup> directly addressed the question of long axial Co–N bonds seen in some X-ray structures and some EXAFS studies by investigating the X-ray absorption spectra of CH<sub>3</sub>Cbl and its complexes with *C. cochlearium* GluM with and without the added inhibitor (2*S*,4*S*)-4-fluoroglutamate and with 2-methylglutamate mutase (MGM) from *C. barkeri* using solid CH<sub>3</sub>Cbl and freeze-dried or frozen protein samples. The XANES spectra of all four samples are very similar and quite different from those of cob(II)alamin and H<sub>2</sub>O Cbl<sup>+</sup>. In each case there is a pronounced preedge peak which indicates the presence of a sixth C-ligand, demonstrating the integrity of the samples. The EXAFS spectra were simulated by deriving the amplitude reduction factor, the energy shift, and the Debye–Waller factors without Fourier filtering and maintaining the inner-sphere coordination distances at the values from the X-ray crystal structure of CH<sub>3</sub>Cbl, with the exception of the Co–NB3 distance, which was varied from 1.7 to 2.9 Å. For free CH<sub>3</sub>Cbl the optimization profile shows the deepest minimum at 2.18(9) Å, essentially identical to that in the X-ray structure.<sup>73</sup> An additional minimum occurs at 1.9 Å, the mean Co–N<sub>eq</sub> distance, and a broad minimum occurs at 2.5–2.8 Å. The optimization profiles for the three protein samples were very similar to that for CH<sub>3</sub>Cbl and compatible with the same axial Co–N bond length, although a longer Co–N<sub>ax</sub> bond distance could not be rigorously excluded. The authors conclude that the most likely interpretation is that the Co–NB3 bond lengths in the complexes of CH<sub>3</sub>Cbl with GluM and MGM are normal.

Kratky and co-workers<sup>267</sup> also reported a second X-ray crystal structure of GluM, this time reconstituted with AdoCbl and glutamate. Successful modeling of the ribose moiety of the 5'-deoxyadenosyl fragment required a two-state model and the superposition of two species, one in which the ribose is in a C<sub>2</sub>-endo conformation and one in which the ribose is in a C<sub>3</sub>-endo conformation. These are shifted slightly from each other and display a 25° difference in the glycosidic bond torsion, so that the C5' carbons are 1.7 Å apart. These two states occurred with 40% occupancy of the C<sub>2</sub>-endo conformation and 60%

occupancy of the  $C_3$ -endo conformation in one crystal but in other ratios in other crystals. In these crystals most of the substrate is methylaspartate. In the  $C_2$ -endo state the C5' carbon is 3.2 Å from the cobalt atom and positioned above it, while in the  $C_3$ -endo state this distance is 4.5 Å and C5' is within van der Waals distance of the substrate. The interaction of the 5'-deoxyadenosine fragment with the protein is similar in both conformations and involves hydrogen bonds from adenine to main chain carbonyls and the *c* acetamide side chain of the corrin and to two waters. The authors interpret the two conformations as intermediates along the reaction pathway. The  $C_2$ -endo state can be viewed as an "activated" coenzyme with a very long (3.2 Å) Co–C bond, while the  $C_3$ -endo state represents a 5'-deoxyadenosine resulting from the transfer of a hydrogen atom from the substrate to the Ado• radical. Thus, ribose pseudorotation between the two states represents a low-energy process that constrains the path of the highly reactive C5' radical carbon and, according to the authors, represents a perfect example of the concept of "negative catalysis".<sup>268</sup>

Kräutler and co-workers<sup>269–271</sup> used NMR methods to determine the solution structures of the AdoCbl binding subunits of GluM, including <sup>15</sup>N-enriched apo-GlmS (from *C. cochlearium*) and <sup>13</sup>C- and <sup>15</sup>N-enriched apo-MutS (from *C. tetanomorphum*) and the complex of <sup>15</sup>N-enriched MutS with the extended nucleotide from Cbl's (including the 2-propanolamine "spacer", i.e., O3'-[(1*R*)-aminoprop-2-oxo]phosphoryl]-1'α-(5,6-dimethylbenzimidazol-1-yl)-D-ribofuranoside), which binds to apo-MutS with an association constant of  $150 \pm 20 \text{ M}^{-1}$ . An earlier structure based on <sup>15</sup>N-labeled MutS had already appeared.<sup>272</sup> The secondary and tertiary structures of the Cbl binding subunits are quite similar to each other and to the Cbl binding subunits from the X-ray crystal structures of *C. cochlearium* GluM<sup>265</sup> and MMCM from *P. shermanii*.<sup>188</sup> The apo binding subunits display a tertiary structure which is a variation of the "Rossmann fold" consisting of a twisted β sheet of five strands surrounded by four α helices and a fifth conformationally disordered and highly dynamic "nascent helix" (residues 17–30), which forms the nucleotide binding pocket. The latter is adjacent to the Asp-x-His-x-x-Gly (residues 14–19 in MutS) binding motif characteristic of enzymes which bind Cbl's in the base-off/His-on mode and is disordered in the absence of coenzyme. In the best model the nascent helix represents the equilibration of two states, one with a short helix (residues 26–30) and one with a longer helix (residues 22–30). Consequently, apo-MutS represents an equilibrium between an  $\alpha_5\beta_5$  structure, in which the larger part of the nascent helix is helical, and an  $\alpha_4\beta_5$  structure in which only the C-terminal part of this segment is helical. Overall, apo-MutS is largely preorganized to bind AdoCbl, except for the nascent helix. Most of the protein side chains that will form the hydrophobic binding pocket for the nucleotide loop are in orientations close to those in the crystal structure of holo-GluM, and the side chain of Ser61, which hydrogen

bonds to the axial nucleotide NB3 in the holoenzyme, is already in position to do so.

Apo-MutS binds the nucleotide loop into the hydrophobic pocket of the  $\alpha_5\beta_5$  structure, which stabilizes that topology. However, the residues in the conserved B<sub>12</sub> binding motif, which are conformationally dynamic in the apo-protein, remain so in the holo-protein. As a result, both the protein and the cofactor adopt their structures mutually to the final state during the binding process. In the nucleotide loop–MutS complex solution structure many nOe contacts are seen between the Bzm protons and backbone amide and side chain protons but none are seen for the ribosyl moiety, indicating that the nucleotide loop is not bound as deeply in the binding pocket as it is in the crystal structure of GluM. From relaxations studies the time constant,  $\tau$ , for formation of the  $\alpha_1$  helix from the nascent helix was ca. 30 μs for both apo-MutS and the nucleotide loop–MutS complex, showing that binding AdoCbl shifts the equilibrium for formation of the helix but does not alter the kinetics. The authors propose a multistep binding mechanism for Cbl in which binding of the nucleotide loop of the base-off cofactor stabilizes the  $\alpha_5\beta_5$  conformation and reduces the conformational mobility of the adjacent Asp-x-His-x-x-Gly sequence which may help position the His residue to coordinate the metal of the cobalt–corrinoid portion of the coenzyme. Thus, the structure of the nucleotide loop–MutS complex may resemble an intermediate in the natural binding process of AdoCbl to these binding domains.

As further evidence of the fact that the Class I enzymes can utilize AdoCbl analogues with altered axial nucleotide structure as long as they have an intact Ado ligand, Rétey and co-workers<sup>273</sup> studied the reactivity of the natural cobamide, (Coβ-5'-deoxyadenosin-5'-yl)[1'-O-(*p*-tolyl)cobamide (Ado-PTC, Figure 1), which has a *p*-tolyl axial group in place of Bzm and is consequently base-off under all conditions, with GluM and MGM. Ado-PTC was an active coenzyme for GluM with 10% of the activity of AdoCbl and a  $K_m$  value, 0.2 μM, only twice that of AdoCbl. With MGM, Ado-PTC was an even better coenzyme with 76% of the activity of AdoCbl and, remarkably, a  $K_m$  value (10 nM) 5.4-fold lower than that for AdoCbl.

To probe mechanisms for the activation of AdoCbl by GluM, Marsh and co-workers<sup>274</sup> studied the interconversion of GluM with AdoCbl and the homolysis fragments cob(II)alamin and 5'-deoxyadenosine by a variety of techniques. The equilibrium constant for AdoCbl binding was determined to be  $5.0 \pm 0.5 \times 10^5 \text{ M}^{-1}$  by gel filtration at 25 °C, pH 7, but titration calorimetry showed essentially no enthalpy change for the reaction. The binding is thus entirely driven by the entropy change of about  $+26 \text{ cal mol}^{-1} \text{ K}^{-1}$ , exactly as seen by Brown and Li for ribonucleotide reductase ( $K_b = 2.4 \times 10^4 \text{ M}^{-1}$ ,  $\Delta H^\circ = 0$ ,  $\Delta S^\circ = +20 \text{ cal mol}^{-1} \text{ K}^{-1}$  at 37 °C).<sup>221</sup> In resonance Raman spectra the Co–C stretching frequencies for AdoCbl previously assigned by Spiro and Banerjee<sup>251</sup> were found to be little perturbed by binding to GluM, with the band at 424  $\text{cm}^{-1}$  shifting to 426  $\text{cm}^{-1}$ , although

the intensity of this band was increased. Overall, the ground-state stretching modes of the corrin ring were not changed much by binding to GluM. The UV–vis spectrum of cob(II)alamin is slightly perturbed by binding to GluM with bands in the 600–800 nm region being slightly increased along with shoulders at 380 and 450 nm. Addition of saturating L-glu caused no further change. However, L-threo-3-methylaspartate caused increases in the intensities of the bands at 375 and 535 nm. Addition of 5'-deoxyadenosine to the cob(II)alamin–GluM complex caused more extensive changes including blue shifts of about 6 nm in the 404 and 470 nm bands. Addition of substrates to this ternary complex had no further effect. The EPR spectrum of cob(II)alamin showed only minor sharpening of the superhyperfine structure upon binding to GluM, and addition of 5'-deoxyadenosine or substrates has no further effect. The authors conclude from these observations that the UV–vis spectral changes are not caused by changes in the axial coordination strength but instead are due to a distortion of the corrin ring, which they suggest might disfavor radical recombination at the active site, although this seems an unlikely result for a reaction which is diffusion controlled in water and may be even faster at an enzyme active site. The authors conclude that enzymatic activation of AdoCbl is more likely to be due to stabilization of the products of homolysis than to some kind of mechanochemical destabilization of the coenzyme, an idea which agrees with the molecular modeling work on mechanochemical triggering.

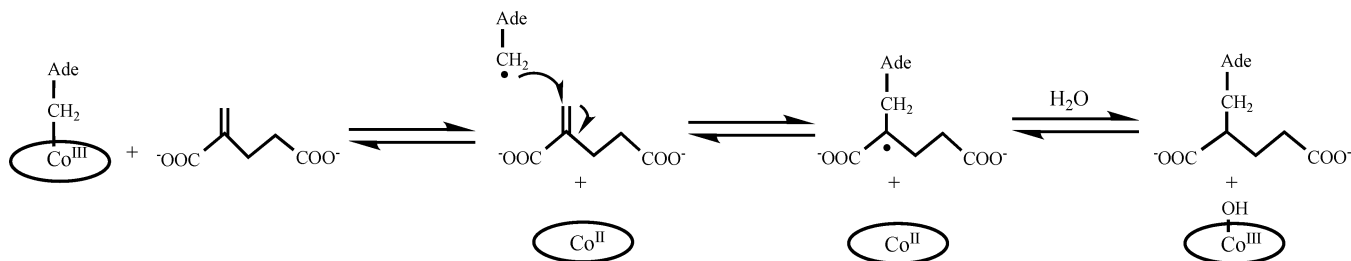
Chih and Marsh<sup>275</sup> studied the partitioning of tritium and tritium isotope effects in GluM using [A15-<sup>3</sup>H]-AdoCbl as the tritium source. Tritium exchange was studied using high concentrations of holoenzyme (45 μM) and saturating concentrations of substrates using the method of initial rates in rapid mix-quenching experiments carried out at 10 °C and pH 7.0. The time dependence of tritium exchange was monitored over the time range of 37–260 ms before quenching with 5% trifluoroacetic acid. The concentration of recovered 5'-deoxyadenosine (5'-dA) was constant throughout the time period but different for each substrate. The rate of tritium loss from 5'-dA was the same for both substrates and close to the rate at which tritium appeared in glutamate and methylaspartate. The appearance of tritium in glutamate and methylaspartate showed a lag, probably due to pre-steady-state kinetics, and then became linear with time. With glutamate as the substrate the rate of appearance of tritium in the substrate and product was identical ( $v_{\text{Glu}}/v_{\text{MeAsp}} = 1.1 \pm 0.2$ ), while with methylaspartate the partitioning ( $v_{\text{Glu}}/v_{\text{MeAsp}} = 1.3 \pm 0.2$ ) slightly favored glutamate, but the differences in partition coefficients are not experimentally significant. The results require that the energy barriers for the transfer of tritium between the coenzyme and the substrate or product radicals must be of very similar energy and the interconversion of the radicals must be fast compared to tritium transfer. The rate of product formation for each substrate showed a lag after which they became linear, and the turnover numbers were calculated to

be  $5.3 \pm 0.5 \text{ s}^{-1}$  for glutamate and  $5.1 \pm 0.5 \text{ s}^{-1}$  for methylaspartate. The calculated tritium isotope effects for H-atom transfer from 5'-dA to the methylaspartate radical is 19, and that for the transfer from 5'-dA to the glutamyl radical is 21. These, in fact, are small compared to the measured tritium isotope effects in diol dehydratase (83)<sup>276</sup> and ethanolamine ammonia lyase (107).<sup>277</sup> These are attributed to H-atom tunneling. However, as pointed out above, the measured deuterium isotope effects on the rate of formation of cob(II)alamin in diol dehydrase are modest,<sup>18</sup> which demonstrates that H-atom transfer is not strongly kinetically coupled to Co–C bond homolysis in this enzyme.

Marsh and co-workers<sup>278</sup> also investigated the interaction of the substrate analogue 2-ketoglutarate (2-KG) with GluM. No inhibition could be detected up to 1 mM 2-KG (the  $K_m$  for L-glu is 0.5 mM), above which the UV absorption of 2-KG interfered with the activity assay. However, 2-KG induced irreversible inactivation of the holoenzyme under aerobic conditions only, with a rate constant of ca.  $1 \times 10^{-4} \text{ s}^{-1}$ , and AdoCbl was degraded with the same kinetics. Addition of 2-KG to the holoenzyme resulted in changes in the UV–vis spectrum of the coenzyme, indicating the formation of about 35% of cob(II)alamin compared with about 45% with L-glu. In addition, GluM catalyzed the transfer of tritium from [A15-<sup>3</sup>H]AdoCbl to C4 of 2-KG (consistent with expectations based on the reaction with L-glu) with a rate constant of  $0.3 \text{ s}^{-1}$ , quite close to the rate constant of  $0.5 \text{ s}^{-1}$  previously measured for <sup>3</sup>H transfer to 3-methylaspartate.<sup>279</sup> However, no turnover to form the product analogue, 3-methyloxalacetate, could be detected; an upper limit of  $5 \times 10^{-5} \text{ s}^{-1}$  could be set for  $k_{\text{cat}}$ , 5 orders of magnitude lower than  $k_{\text{cat}}$  for L-glu. The results show that 2-KG can induce homolysis of AdoCbl at the GluM active site, the only molecule other than the natural substrate and product that is known to do so. The subsequent inactivation presumably results from the reaction of oxygen with radical species at the active site. 2-KG should thus provide a means of studying the kinetics of the activation of AdoCbl and the coupled H-atom transfer in GluM without the kinetic complications of turnover.

Marsh and co-workers<sup>280</sup> also investigated the interaction of 2-methyleneglutarate (2-MG), a substrate analogue for glutamate, with GluM, for which it had previously been reported to be a competitive inhibitor.<sup>281</sup> 2-Methyleneglutarate is the natural substrate for the AdoCbl-dependent 2-methyleneglutarate mutase, which catalyzes its rearrangement to (*R*)-3-methylitaconate (3-MI). Holo-GluM was unable to catalyze the interconversion of 2-MG and 3-MI even during prolonged incubation capable of detecting a single turnover. Similarly, no tritium transfer could be detected from [A15-<sup>3</sup>H]-AdoCbl to either 2-MG or 3-MI. However, UV–vis spectra showed that incubation of 2-MG with holo-GluM resulted in the rapid formation of about 54% cob(II)alamin at the active site (compared to 43% for the natural substrate, L-glutamate). Further incubation leads to formation of enzyme-bound HOcbl with an observed

## Scheme 15



rate constant for  $1.7 \times 10^{-3} \text{ s}^{-1}$ , despite anaerobic conditions. The rapid formation of cob(II)alamin was confirmed by EPR observations of samples of holo-GluM plus 2-MG frozen (115 K) within 20–30 s of mixing. The EPR spectrum was typical of those formed by the reaction of AdoCbl-dependent enzymes with their substrates due to the coupling of the unpaired spin on the metal atom with a carbon-centered radical. When 2-MG, enriched with  $^{13}\text{C}$  at C4 (the normal site for H-atom abstraction) or in the methylene carbon, was reacted with holo-GluM, the EPR spectrum was unchanged, but [ $^{13}\text{C}$ ]-2-MG resulted in an EPR spectrum broadened in the hyperfine region, indicating that the carbon-centered radical is at C2 of 2-MG. Since this carbon has no hydrogen, the radical cannot be formed by H-atom abstraction but could be formed by addition of the Ado• radical to the methylene group to form a tertiary radical.

2-MG causes irreversible inactivation of GluM with a biphasic time course characterized by two exponentials with rate constants of  $1.7 \times 10^{-2}$  and  $1.7 \times 10^{-4} \text{ s}^{-1}$  under anaerobic conditions. This is attributed to “half-of-sites” reactivity, i.e., negative cooperativity due to conformational changes caused by the inhibitor and transmitted to the other active site of the enzyme. The inactivation was not caused by covalent modification of the enzyme by the Ado• radical as the use of [A15- $^3\text{H}$ ]-AdoCbl failed to yield a radioactive protein. The use of [A8- $^{14}\text{C}$ ]-AdoCbl led to degradation of one-half of the AdoCbl and formation of a new  $^{14}\text{C}$ -labeled product, which at longer times converted to a second product. The rate constant for degradation of AdoCbl ( $1.7 \times 10^{-3} \text{ s}^{-1}$ ) agreed well with that for formation of the first product ( $1.8 \times 10^{-3} \text{ s}^{-1}$ ) and with that for formation of HOCbl. The rate constant for conversion of the first product to the second was  $2.7 \times 10^{-4} \text{ s}^{-1}$ . Unfortunately, sufficient amounts of these products for characterization could not be obtained. The authors propose that the reaction of 2-MG with GluM occurs as depicted in Scheme 15. Attack of the Ado• radical on 2-MG leads to an adduct radical which is reduced by the cob(II)alamin and protonated by solvent. The authors do not speculate about the identity of the second product formed from the adduct radical. The biphasic kinetics of irreversible inactivation of GluM are ascribed to the reaction at one active site which generates an enzyme conformation that blocks the reaction at the other active site. If this mechanism is correct, the fact that the Ado• radical attacks 2-MG at the methylene carbon rather than abstracting a hydrogen from C4 implies that 2-MG binds backward in the substrate binding site, so that the methylene

occupies a position equivalent to that of the H<sub>Si</sub> hydrogen of C4 of the normal glutamate substrate.

In the X-ray crystal structure of GluM<sup>267</sup> Glu171 makes a H-bond contact with the amino group of the substrate. Marsh and co-workers<sup>282</sup> consequently examined the kinetics of cob(II)alamin formation in a Glu171Gln mutant by stopped flow spectroscopy at 10 °C under anaerobic conditions. The kinetics of formation of cob(II)alamin for both wild-type and mutant enzymes are biphasic, apparently due to negative cooperativity between the two active sites. For the wild-type enzyme the faster reacting site is nearly complete during the stopped flow dead time, so that only the slower site is observed.<sup>283</sup> For the mutant enzyme the reaction is slower so that both reacting sites are observed, allowing direct comparison of the slow reacting site for the mutant and wild-type enzymes. For the mutant enzyme the substrate binding constants are decreased by 400- and 50-fold for methylaspartate and glutamate, respectively, demonstrating that 2–3 kcal mol<sup>-1</sup> of substrate binding energy is provided by the Glu171 hydrogen bond to the substrate amino group. The mutation, which lowers  $k_{\text{cat}}$  by 50-fold, decreases the rate constant for cob(II)alamin formation by 7-fold when glutamate is the substrate and by 13-fold when methylaspartate is the substrate, a 1–1.5 kcal mol<sup>-1</sup> increase in the free energy of activation. Since Glu171 does not contact the coenzyme, the reduction in the catalysis of Co–C bond homolysis suggests that a substrate-induced conformational change of the enzyme (for which there is as yet no independent evidence for GluM) contributes to the catalysis of Co–C bond homolysis. Given the fact that 2–3 kcal mol<sup>-1</sup> of substrate binding energy is lost in the mutant and Co–C bond homolysis is slowed by 1–1.5 kcal mol<sup>-1</sup>, it would seem that as much as one-half of the substrate binding energy is used to promote homolysis. In the wild-type enzyme formation of cob(II)alamin displays large primary KIE's (35 when methylaspartate is the substrate and 28 when glutamate is the substrate), which are interpreted to mean that, as in MMCM, Co–C bond homolysis is tightly coupled to H-atom transfer, and the latter displays significant quantum mechanical tunneling.<sup>283</sup> In the mutant enzyme these KIE's are reduced to 12 for methylaspartate as substrate and 1 for glutamate. This requires either that the mutation stabilizes the homolysis products sufficiently so that homolysis is no longer coupled to H-atom transfer or that the mutation slows homolysis sufficiently so that it becomes rate determining and although still coupled to H-atom transfer loses most of its sensitivity to isotopic substitution. The latter explanation seems

most likely, especially since the homolysis rate constants are slowed by the mutation.

Finally, Robinson and co-workers<sup>284</sup> cloned, sequenced, and overexpressed in *E. coli* the isobutyryl-CoA mutase (ICM) from *Streptomyces cinnamonensis*. The enzyme, which catalyzes the interconversion of isobutyrylCoA and *n*-butyrylCoA, occurs in aerobic and anaerobic bacteria and plays a key roll in the catabolism of valine and fatty acids. The enzyme is composed of large subunits (IcmA, 65.2 kDa) and small subunits (IcmB, 14.3 kDa), the latter being a 136-residue protein with high sequence similarity to the AdoCbl binding subunits of the other mutases and to the CH<sub>3</sub>Cbl binding domain of methionine synthase and including the consensus sequence Asp-x-His-x-x-Gly indicative of the base-off/His-on binding mode. Like GluM, IcmA is a tightly bound dimer, but IcmB alone is monomeric. IcmA and IcmB expressed separately in *E. coli* were sufficient, with added AdoCbl, to reconstitute holoenzyme, but the subunits bound only weakly in the absence of coenzyme. The holoenzyme is apparently an  $\alpha_2\beta_2$  heterotetramer with two molecules of bound AdoCbl. The equilibrium constant for the reaction is 1.7 in favor of isobutyryl-CoA, the  $K_m$ 's are  $57 \pm 13 \mu\text{M}$  for isobutyrylCoA,  $54 \pm 12 \mu\text{M}$  for *n*-butyrylCoA, and  $12 \pm 2 \mu\text{M}$  for AdoCbl, and  $k_{\text{cat}}$  is  $39 \pm 3 \text{ s}^{-1}$ .

### 11.1.2. Class II Eliminases

Diol dehydratase (DD) and glycerol dehydratase (GD) are isofunctional enzymes that catalyze the conversion of 1,2-propanediol, 1,2-ethanediol, and glycerol to propionaldehyde, acetaldehyde, and  $\beta$ -hydroxypropionaldehyde, respectively (eq 23). The most frequently studied enzymes are from *Klebsiella oxytoca* (DD) and *Klebsiella pneumoniae* (GD), the organisms in which the enzymes were originally discovered. Both enzymes undergo mechanism-based suicide inhibition with glycerol as the substrate, despite the fact that glycerol is a growth substrate for these organisms. The reaction is a 1,2-rearrangement in which the hydroxyl group from C2 migrates to C1 in exchange for a C1 hydrogen. The resulting *gem*-diol is stereospecifically dehydrated by the enzyme. The stereospecificity is lax in that both (*R*)- and (*S*)-1,2-propanediol are substrates (the *S* enantiomer has a lower  $K_m$  but also a lower  $k_{\text{cat}}$ ) with the pro-*S* hydrogen migrating when (*S*)-1,2-propanediol is the substrate and the pro-*R* hydrogen migrating when (*R*)-1,2-propanediol is the substrate.



X-ray crystal structures of *Klebsiella oxytoca* DD reconstituted with CNCbl and 1,2-propanediol,<sup>189,285,286</sup> with adeninylpentylCbl (AdoPentCbl, Figure 1) and 1,2-propanediol,<sup>286</sup> and with CNCbl but no substrate<sup>287</sup> have appeared. The CNCbl complex<sup>189,285</sup> represented the first reported structure of a Class II AdoCbl-dependent enzyme, i.e., one lacking the consensus Asp-x-His-x-x-Gly base-off/His-on binding motif. The enzyme is a dimer of heterotrimers,  $(\alpha\beta\gamma)_2$ , in which only the  $\alpha$  subunits make contact between

the two dimers, and each heterotrimer contains one molecule of Cbl. In the CNCbl complex (determined at 277 K) the CNCbl is bound between the  $\alpha$  and  $\beta$  subunits, but the electron density for the cyano ligand could not be located. The axial Bzm is coordinated to the cobalt, the first time such base-on binding had been demonstrated crystallographically. The  $\alpha$  subunits have a central  $(\beta/\alpha)_8$  TIM barrel with the C-terminal ends of the  $\beta$  strands providing part of the Cbl binding site and the substrate and an essential K<sup>+</sup> ion bound deeply in the barrel. The  $\beta$  subunits have a Rossmann-fold structure surrounded by  $\alpha$  helices and a few antiparallel  $\beta$  strands. The interaction of the Cbl with its binding site is complex. Five of the corrin ring side chain amides form hydrogen bonds to five residues in the  $\alpha$  subunit and three in the  $\beta$  subunit. There is little interaction, however, between the Bzm ligand or the ribose and the protein, although the phosphate group, which is known to be essential for tight binding of the cofactor, participates in three hydrogen bonds as well as a salt bridge to the  $\epsilon$ -amino group of a lysine residue from the  $\beta$  subunit. The axial Co–NB3 bond length is a very long 2.50 Å in the CNCbl-reconstituted enzyme at 277 K, an artifact which is now known to be due to the presence of mixed oxidation and coordination states as a result of irradiation with X-rays (see above), and the corrin ring fold angle is a very small 3°. In the structure determined at 100 K<sup>286</sup> the electron density of the cyano ligand is partly observable and the axial Co–NB3 bond length is only 2.18 Å, still longer than that in free CNCbl (2.01 Å) but indicative of less radiation damage at the lower temperature. The substrate oxygens are each hydrogen bonded to a carboxyl from an  $\alpha$  subunit residue and a histidine residue from the  $\alpha$  subunit, and each is coordinated to the essential K<sup>+</sup> ion, which is heptacoordinate, but the substrate is remote (ca. 9 Å) from the cobalt atom. The authors speculate on a mechanism in which the K<sup>+</sup> ion participates directly in the rearrangement as a Lewis acid to lower the energy of a cyclic transition state.

In the structure with AdoPentCbl (determined at 100 K),<sup>286</sup> an inhibitor which binds to DD more strongly than AdoCbl in which the ribose of the Ado ligand is replaced by a pentamethylene group, the overall form of the heterotrimeric dimer persists. The AdoPentCbl is bound at the interface of the  $\alpha$  and  $\beta$  subunits, as was CNCbl, with its adenine ring parallel to the corrin and lying over the C pyrrole. However, in the complex with DD, the adenine ring  $si_{C(6)}$  face faces the corrin, in contrast to free AdoCbl and the complex of AdoCbl with MMCM.<sup>250</sup> All of the adenine nitrogens are involved in hydrogen bonds with  $\alpha$  subunit residues except A9. The Co–NB3 bond length is 2.22 Å, very close to that in AdoCbl (2.21 Å)<sup>80</sup> and to its close analogue adeninylpropylCbl (2.21 Å),<sup>288</sup> although the corrin ring fold angle is very small (2°). Thus, in the absence of radiation damage (or photolysis during preparation), an intact, six-coordinate Co(III) cobalamin has a normal Co–NB3 bond length when bound to DD. In a crystal that was purposely exposed to visible light before and during data collection, the pentamethylene group is cleaved

from the cobalt atom but the adenine remains firmly bound via hydrogen-bonding interactions.<sup>286,289</sup> In this crystal, presumably containing cob(II)alamin, the Co–NB3 bond length is 2.23 Å, 0.07 Å longer than in free cob(II)alamin.<sup>85</sup>

The authors attempt to explain the outcome of extensive earlier work with AdoCbl analogues of altered structure in the Ado ligand, some of which are active coenzymes and some of which are inhibitors, but with all of the adenine nitrogens participating in hydrogen bonding with the protein, it is difficult, for example, to understand why 3-deaza- and 1-deazaAdoCbl are active coenzymes (with ca. 50% of the activity of AdoCbl) while 7-deazaAdoCbl is a tightly bound inhibitor. Interestingly, a model of the interaction of 3-IsoAdoCbl (Figure 1), an active coenzyme in which the *N*-glycosidic bond of the Ado ligand is to the adenine N3 instead of N9, shows that hydrogen bonds can be maintained to all of the adenine nitrogens if the adenine is bound with the opposite enantio-face (*re*<sub>C(6)</sub>) facing the corrin ring. In an interesting modeling study the authors find that superposition of the adenine ring and the corrin of AdoCbl on these structural features of DD-bound AdoPentCbl leads to a Co–C distance of 3.3 Å and a Co–C–C angle of 153°, suggesting that the active site is designed to bind the fragments of AdoCbl homolysis.

The structure of the substrate-free enzyme (reconstituted with CNCbl and determined at 100 K)<sup>287</sup> shows the same dimer of heterotrimers with a similar structure to the substrate-bound enzymes. However, when the substrate binds to the  $\alpha$  subunit, the  $\beta$  subunit tilts by about 3°, although the contacts between the  $\alpha$  and  $\beta$  subunits are not altered significantly. The Cbl tilts with the  $\beta$  subunit, but its hydrogen-bond contacts are mostly maintained. The electron density of the cyanide ligand is again only partly observed, and the Co–NB3 distance is 2.25 Å, indicating, again, less radiation damage at 100 K. Superposition of the Cbl with that of the substrate-bound form shows little difference (corrin ring atoms rms deviation 0.06 Å, while including the side chains gave 0.27 Å). However, in the substrate-free form the A and D rings are lifted up some 0.1–0.15 Å, resulting in a corrin ring fold angle of 5.1°, larger than that in the substrate-bound form but still considerably smaller than that in free CNCbl (18°). In the substrate-free enzyme the K<sup>+</sup> ion in the TIM barrel remains heptacoordinate and is coordinated by two additional water molecules, each of which is hydrogen bonded to two residues that hydrogen bond to the substrate hydroxyls in the presence of substrate, so that it remains heptacoordinate. The methyl group of the substrate clashes with a Phe and a Gln residue, pushing the Phe residue down and consequently the *g* acetamide side chain of the corrin. This then results in the tilt of the corrin ring and of the  $\beta$  subunit. The authors suggest that the lack of this interaction when 1,2-ethanediol is the substrate may be the cause of the lower activity of DD with this substrate.

In a repeat of the modeling study described above,<sup>286</sup> AdoCbl docked into the enzyme in the presence of

substrate had a Co–C bond length of 3.11 Å and a Co–C–C bond angle of 155.9°. In the absence of substrate the Co–C bond length was 2.98 Å and the Co–C–C bond angle 159.6°. The authors conclude that the Co–C bond of the coenzyme is significantly labilized even in the absence of substrate (despite the fact that the AdoCbl of the holoenzyme is stable in the absence of substrate and oxygen) and that substrate binding causes additional activation and leads to Co–C bond homolysis. While this is an interesting and viable hypothesis, it suggests that a considerable portion of the activation of the Co–C bond for homolysis occurs when the coenzyme binds to the enzyme to form the stable (at least in the absence of oxygen) holoenzyme. This means that it should be possible to find evidence for such ground-state strain in the holoenzyme using resonance Raman or perhaps NMR observations with AdoCbl enriched with <sup>13</sup>C in the cobalt-bound carbon.

Recombinant glycerol dehydratase (GD) from *Klebsiella pneumoniae* has been cloned and overexpressed in *E. coli* and purified to homogeneity in 18% yield.<sup>290</sup> SDS–PAGE showed three bands with molar masses of 61 ( $\alpha$ ), 22 ( $\beta$ ), and 16 kDa ( $\gamma$ ), and nondenaturing gels confirmed a subunit structure  $\alpha_2\beta_2\gamma_2$ . The  $K_m$  for AdoCbl is 8 nM, and while the rate of the reaction is 2.5 times faster with (*R*)-1,2-propanediol than with the *S* enantiomer, the  $K_m$  for the *S* enantiomer was only slightly less than that for the *R* enantiomer, displaying a much smaller preference for the *S* enantiomer than DD. EPR experiments with an active analogue of AdoCbl, adenosylcobinamide-3-imidazolylpropyl phosphate (AdoCbiP–ImPr, Figure 1), in which the axial nucleoside is replaced by a 3-imidazolylpropyl group, with and without <sup>15</sup>N enrichment in the imidazole moiety, suggested that AdoCbl is bound to GD base-on.

This proved to be correct in two X-ray crystal structures of GD from *K. pneumoniae*, one in which the enzyme was reconstituted with CNCbl and 1,2-propanediol<sup>290</sup> and one in which the enzyme was reconstituted with CNCbl but without substrate.<sup>291</sup> The enzyme has the same dimer of heterotetramer structure as DD, and the amino acid sequences of the  $\alpha$ ,  $\beta$ , and  $\gamma$  subunits have 71%, 58%, and 54% identity, respectively. Most of the conserved residues are in the core of the enzyme, and most of the nonconserved residues are on the surface. In the crystal containing substrate the overall structure is very similar to that of DD, with the  $\alpha$  subunit displaying a TIM barrel inside which the substrate and essential K<sup>+</sup> ion bind. The Cbl is bound at the  $\alpha/\beta$  interface, which makes closer contact in GD than in DD, possibly explaining the lower  $K_m$  for AdoCbl with GD. The Cbl is bound base-on, and all of the hydrogen-bonding contacts to the corrin ring side chains in DD are preserved in GD. In addition, a Ser residue from the  $\beta$  subunit is hydrogen bonded to the *g* acetamide amide oxygen in GD. As in DD, no electron density could be located for the cyanide ligand, even though the data were collected at 100 K. The Co–NB3 bond length is again very long (2.48 Å), indicative of the radiation damage to bound CNCbl as discussed above. The corrin ring is again

very flat, with a fold angle of 5.5°. Again, as in DD, the active site K<sup>+</sup> ion is heptacoordinate with both of the substrate hydroxyls coordinated, and each of the substrate oxygens is again hydrogen bonded to two residues from the  $\alpha$  subunit. Although the enzyme was crystallized from racemic 1,2-propanediol, the enzyme-bound species is assigned to the *R* enantiomer (on the bases of smaller residuals). However, GD shows almost equal affinity for both enantiomers, in contrast to DD which prefers the *S* enantiomer by about 3-fold. Glycerol is both a very good substrate and potent suicide inhibitor for both DD and GD, although DD is inactivated by glycerol faster than DD. Since it is known that DD can distinguish between the *R* and *S* binding conformations, with the *R*-glycerol complex primarily producing product and the *S*-glycerol complex primarily leading to inactivation, the authors suggest that the smaller preference of GD for the *S* enantiomer may explain why GD is less susceptible to glycerol inactivation.

The structure of GD reconstituted with CNCbl but without substrate<sup>291</sup> also shows the dimer of heterotrimer motif, with the TIM barrel in the  $\alpha$  subunit containing the active site and the Cbl bound at the  $\alpha/\beta$  subunit interface. Although the structure was determined at 100 K, no electron density could be detected for the cyano ligand, and the Co–NB3 bond lengths were 2.6 and 2.5 Å (there are slight differences between the two  $\alpha\beta\gamma$  trimers), again evidently the result of radiation damage. In the substrate-free enzyme the K<sup>+</sup> ion is hexacoordinate with a single water molecule bound in place of the two substrate hydroxyls, in contrast to substrate-free DD in which two waters are bound and the K<sup>+</sup> ion is heptacoordinate.

Both DD and GD are known to undergo irreversible inactivation by glycerol, a natural substrate for both enzymes, and by O<sub>2</sub> in the absence of substrate. The inactivation results from cleavage of the Co–C bond of the coenzyme to form a modified corrinoid which is not released from the enzyme. Toraya and co-workers previously found that inactivated DD and GD in permeabilized cells of *K. oxytoca* and *K. pneumoniae* could be reactivated by the addition of AdoCbl, ATP, and Mg<sup>2+</sup><sup>292</sup> and subsequently identified two genes (*ddrA* and *ddrB*) on the 3'-flanking side of the *K. oxytoca* DD genes that encode for a putative DD-reactivating factor<sup>293</sup> and two genes (*gdrA* and *gdrB*) in *K. pneumoniae* which code for a putative reactivation factor for GD.<sup>294</sup> These genes have now been cloned and overexpressed in *E. coli*, and the DdrA and DdrB proteins of the DD-reactivating factor<sup>295</sup> and the GdrA and GdrB proteins of the GD-reactivating factor<sup>296</sup> have been co-purified as a tight complex to homogeneity. The proteins have apparent molar masses of 64 (A) and 14 kDa (B) (12 kDa for the GdrB) and form an A<sub>2</sub>B<sub>2</sub> heterotetramer of apparent molar mass of 150 kDa (135 kDa for the GD reactivating factor). Both glycerol- and O<sub>2</sub>-inactivated DD or GD were reactivated in vitro by the appropriate reactivating factor only in the presence of added AdoCbl, ATP, and Mg<sup>2+</sup>. In addition, inactive DD–CNCbl and GD–CNCbl complexes were

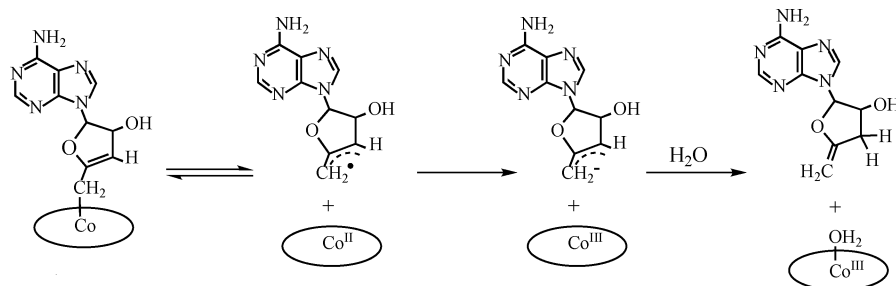
also reactivated under the same conditions. To determine if the reactivating factors were catalyzing an exchange of exogenous coenzyme for the tightly bound modified cobamide in the inactivated enzyme, the enzyme–CNCbl complexes were incubated with the reactivating factor and adenylpentylCbl (AdoPentCbl, Figure 1) in the presence of ATP and Mg<sup>2+</sup>. UV–vis spectra showed that enzyme-bound CNCbl was replaced by AdoPentCbl (although the reverse reaction did not take place), so that the reactivating factor catalyzed the replacement of the modified coenzyme rather than its adenosylation.

Further studies with the DD–CNCbl and GD–CNCbl complexes<sup>293,297</sup> showed that the DD-reactivating factor causes the exchange of enzyme-bound, nonadenosylated corrinoids for exogenous AdoCbl via the intermediate formation of apoenzyme. The reactivating factor has a low ATPase activity and forms a strong complex with apoenzyme in the presence of ADP but not in the presence of ATP. As a result, incubation of the enzyme–CNCbl complex with the reactivating factor and ADP leads to the release of CNCbl and leaves a tight apoenzyme-reactivating factor complex. The latter complex is inactive and does not bind exogenous AdoCbl. However, addition of ATP dissociates the complex freeing apoenzyme, which can then bind AdoCbl. The reactivating reaction thus occurs in two steps: an ADP-dependent release of the nonadenosylated corrinoid followed by ATP-dependent dissociation of the reactivating factor-apoenzyme complex, so that ATP acts as both the source of ADP and the effector that switches the reactivating factor to a form which has low affinity for the enzyme. The authors conclude that the DD reactivating factor is a new kind of molecular chaperone.

In contrast with the Class I enzyme MMCM (see above), aristeromycylcobalamin (AriCbl, Figure 1) is an active coenzyme for both DD and GD<sup>45</sup> with 44% and 38% of the activity of AdoCbl, respectively. Interestingly, the *K<sub>m</sub>* values for AriCbl are essentially the same as those for AdoCbl with both DD and GD, suggesting that the ribose oxygen does not play a role in the mechanism of the activation reaction or in the binding of coenzyme, a conclusion that cannot yet be confirmed by structure analysis as none of the existing X-ray crystal structures of DD or GD contain an intact adenosine fragment.

However, 3',4'-anhydroadenosylcobalamin (3',4'-anAdoCbl, Figure 1), another coenzyme analogue with altered Ado structure, is only slightly active as a coenzyme for DD (0.02% of AdoCbl activity) and GD (0.05% of AdoCbl activity)<sup>46,298</sup> but is also a suicide inactivator with DD. UV–vis spectra show that incubation of DD with 3',4'-anAdoCbl anaerobically in the absence of substrate leads to the rapid (<2 min) formation of cob(II)alamin, which, on longer incubation, is converted to a cob(III)alamin, probably H<sub>2</sub>Ocbl<sup>+</sup>, with a rate constant of  $2.38 \pm 0.03 \times 10^{-3} \text{ s}^{-1}$ . In the presence of substrate both processes are slowed with cob(II)alamin formed with a rate constant of  $5.5 \pm 0.3 \times 10^{-3} \text{ s}^{-1}$  and H<sub>2</sub>Ocbl<sup>+</sup> with a rate constant of  $7.2 \pm 0.2 \times 10^{-4} \text{ s}^{-1}$ . In either case, precipitation of the protein with acid and HPLC

## Scheme 16



separation gives two products,  $\text{H}_2\text{OCbl}^+$  and 3',5'-dideoxyadenosine-4',5'-ene, which is deuterated at the 3' position if the reaction is run in  $\text{D}_2\text{O}$ . The authors propose Scheme 16 to account for the reaction of 3',4'-anAdoCbl with DD. After Co–C bond homolysis the cob(II)alamin at the active site is oxidized by the anhydroadenosyl radical and the resulting allylic anion is protonated by water, with or without the intervention of a protein residue. The slower rate of formation of cob(II)alamin in the presence of substrate is surprising since no cob(II)alamin can be detected in the absence of substrate with AdoCbl as the coenzyme and coenzyme homolysis is induced by substrate binding. This gives rise to the possibility that with AdoCbl homolysis does occur in the absence of substrate but that the equilibrium strongly favors intact coenzyme and is shifted toward the homolysis fragments by substrate binding. This idea would seem to agree with the proposals of Toraya and co-workers for the activation of AdoCbl by DD from modeling studies based on the X-ray crystal structures,<sup>287</sup> and it is experimentally testable. The failure of an active site electron-transfer process to occur between the Ado• radical and cob(II)alamin when the reaction is catalyzed by AdoCbl presumably reflects the rapid reaction of this radical with substrate, unlike the anhydroadenosyl radical, and the need to prevent such electron-transfer processes involving the cobalt atom provides a rationale for the fact that the substrate and product radicals are maintained remotely from the cobalt by these enzymes.

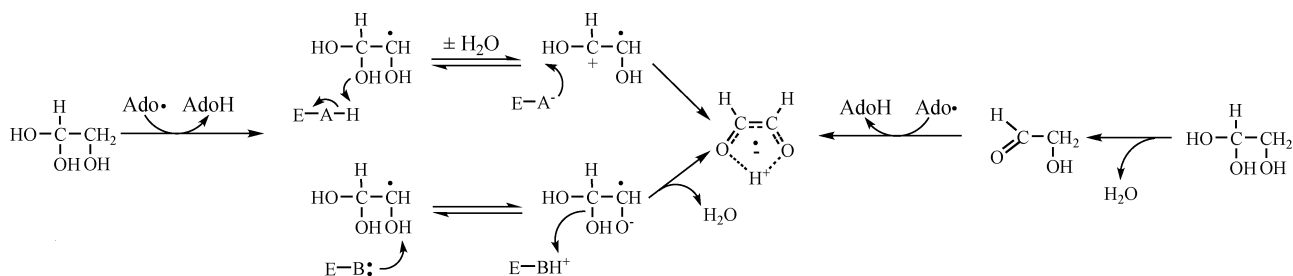
However, a number of hydroxyalkylCbl's and other derivatives which can be considered as models of the substrate and coenzyme proved to be potent competitive inhibitors of DD and GD.<sup>299</sup> Thus,  $\text{HO}(\text{CH}_2)_n\text{Cbl}$ 's ( $n = 2-5$ ) and (*S*)- and (*R*)-2,3-dihydroxypropylCbl's had  $K_i$ 's of 13–25 nM for GD (compared to a  $K_m$  of 12.6 nM for AdoCbl) and 0.72–1.25  $\mu\text{M}$  for DD (compared to a  $K_m$  of 0.72  $\mu\text{M}$  for AdoCbl). None were as good an inhibitor as  $\text{HOCbl}$  ( $K_i = 8.6$  nM for GD and 0.68  $\mu\text{M}$  for DD), and  $\text{CNCbl}$  was about as good an inhibitor as the poorest of the hydroxyalkylCbl's. In contrast, the dihydroxypropyl derivatives of the (*p*-tolyl)cobamide analogues (which are base-off under all conditions, see Ado-PTC, Figure 1, for the structure of the *f* side chain tail) are much poorer inhibitors, and HO-PTC inhibition was barely detectable. The results have been interpreted as being due to interaction of the hydroxyl group(s) on the alkyl ligands of the inhibitors with the substrate binding site or with the portion of the active site that binds the adenine ribose moiety. Although none of the

X-ray crystal structures available contain an adenosine ribose moiety, it is clear that the substrate binding site in these enzymes is too far away from the cobalt corrinoid to interact with the inhibitor hydroxyls, at least for those with the shorter alkyl chains. The fact that the PTC derivatives can bind despite their uncoordinated “tails” shows that the tail can be folded in such a way to fit into the binding pocket for the normal nucleotide loop. The reduced affinity of these analogues is likely due to the entropic effect of the loss of motional freedom of the tail in the binding process.

Toraya and co-workers<sup>300</sup> studied the reactivity of DD with AdoCbl analogues with altered structure in the axial nucleotide loop, including Ado(Bzim)Cbl and Ado(Im)Cbl (Figure 1), and the trimethylene analogues with 2-methylbenzimidazole as the axial base (AdoCbiP-MBIPr, Figure 1), which is base-off under all conditions. AdoCbi-MBIPr was inactive but a good competitive inhibitor with  $K_i = 2.7$   $\mu\text{M}$  (compared to  $K_m$  for AdoCbl of 0.8  $\mu\text{M}$ ). Ado(Bzim)Cbl and Ado(Im)Cbl were active coenzymes with  $K_m$  values very close to that for AdoCbl (0.96 and 1.04  $\mu\text{M}$ , respectively) and 95% and 50% of the activity of AdoCbl. However, both of these coenzymes caused the enzyme to suffer increased rates of suicide inhibition, so the values of  $k_{\text{cat}}/k_{\text{inact}}$  (157 for AdoCbl) decreased to 75 for Ado(Bzim)Cbl and 8.9 for Ado(Im)Cbl. UV-vis spectra indicated that in the presence of 1,2-propanediol DD-bound Ado(Bzim)Cbl and Ado(Im)Cbl both undergo homolysis to generate cob(II)alamin. The kinetics of cob(II)alamin formation were studied using  $[1,1\text{-}^2\text{H}_2]1,2\text{-propanediol}$  (to slow the rate so that measurements could be made) at 4 °C. The observed rate constant for Ado(Bzim)Cbl ( $3.7 \pm 0.3$   $\text{s}^{-1}$ ) was actually slightly larger than that for AdoCbl ( $2.3 \pm 0.2$   $\text{s}^{-1}$ ), while the rate constant for Ado(Im)Cbl ( $2.0 \pm 0.2$   $\text{s}^{-1}$ ) was the same as that for AdoCbl. These results demonstrate that the bulkiness of the axial base is not important for coenzyme activation with DD. The authors conclude that the stability of holo-DD with respect to suicide inactivation is substantially affected by the bulkiness of the axial base, with the bulkier bases giving coenzymes with greater stabilizing effect. However, as the size of the axial base has no effect on the rate of formation of cob(II)alamin at the active site, ground-state mechanochemical triggering is effectively ruled out for this enzyme.

As pointed out above, a preliminary measurement of the primary deuterium KIE's for formation of cob(II)alamin at the active site of DD at 4 °C has appeared.<sup>18</sup> These KIE's are quite modest (3–4, while

## Scheme 17



the deuterium isotope effect on  $k_{\text{cat}}$  is 10) compared to those in MMCM (50 at 5 °C)<sup>252</sup> where Co–C bond homolysis is coupled to H-atom transfer utilizing quantum mechanical tunneling. Since the tritium KIE's for exchange of hydrogens between the coenzyme and the substrate and product in DD are very large,<sup>276</sup> implying that tunneling is important in the H-atom transfers in DD as well, this must mean that Co–C bond homolysis in DD is only weakly coupled to H-atom transfer. At 4 °C the rate constant for cob(II)alamin formation with 1,2-propanediol as the substrate is  $8.00 \pm 1.0 \times 10^2 \text{ s}^{-1}$ . From the temperature dependence of the rate constants for nonenzymatic homolysis of AdoCbl, the nonenzymatic rate constant is  $2.1 \times 10^{-11} \text{ s}^{-1}$  at 4 °C.<sup>106</sup> DD consequently activates the Co–C bond of AdoCbl for homolysis by a factor of  $7 \times 10^{13}$ , or 17.5 kcal mol<sup>-1</sup>, the largest catalytic effect for any AdoCbl-dependent enzyme yet known.

Glycolaldehyde, a substrate analogue for DD, is a known suicide inhibitor which results in the formation of cob(II)alamin, 5'-deoxyadenosine, and a tightly bound product derived from glycolaldehyde which converts to glyoxal after aerobic denaturation of the protein complex.<sup>301</sup> Abend et al.<sup>302</sup> used EPR to identify the enzyme-bound product of glycolaldehyde as *cis*-ethanesemidione. EPR spectra of the inhibited enzyme show an altered cob(II)alamin signal and a signal characteristic of an organic radical near  $g = 2$ . Spectra from samples using either [1-<sup>13</sup>C]glycolaldehyde or [2-<sup>13</sup>C]glycolaldehyde were slightly broadened and identical, while deuterated glycolaldehyde caused collapse of the spectral features, and deuterated glycolaldehyde in D<sub>2</sub>O sharpened the spectrum, indicating the radical contains a solvent-exchangeable proton. The changes in the EPR spectrum upon <sup>13</sup>C enrichment are too small to be due to a carbon-centered radical but suggest a semidione radical in which the unpaired electron is in a  $\pi$ -orbital including p-orbitals from both carbons and both oxygens. Both the organic radical spectrum and the cob(II)alamin spectra show signs of alteration by spin–spin coupling. The observed dipole–dipole interaction (–21 G) leads to a distance estimate of ca. 11 Å between the semidione radical and the cobalt ion. The results suggest that a proton is bound to the semidione radical oxygens in place of the K<sup>+</sup> ion bound to substrate hydroxyls in the X-ray structure of the enzyme. Similar EPR experiments were carried out with ethanolamine ammonia lyase with very similar results, including the distance between the semidione radical and the Co<sup>II</sup> ion, but there is a larger ferromagnetic exchange interaction than in DD. The

formation of the semidione radical (Scheme 17) can be explained either by reaction of the hydrated species of glycolaldehyde (the predominant form in water) with the enzyme to form an initial radical at C1 which then undergoes either an acid/base-catalyzed or base/acid-catalyzed elimination of water or directly by H-atom abstraction from the unhydrated species.

Finally, the genes for DD from *Lactobacillus colinioides* have been cloned and overexpressed in *E. coli*.<sup>303</sup> The *pduC*, *pduD*, and *pduE* genes gave rise to polypeptides of 63, 28, and 22 kDa, respectively, and an active enzyme with subunit structure  $\alpha_2\beta_2\gamma_2$  and a molar mass of 207 kDa.  $K_m$ 's of 8  $\mu\text{M}$  for AdoCbl, 1.6 mM for 1,2-propanediol, 5.5 mM for 1,2-ethanediol, and 8.3 mM for glycerol were reported. The enzyme was inactivated both by glycerol and by added CNCbl.

Ethanolamine ammonia lyase (EAL) catalyzes the conversion of 2-aminoethanol to acetaldehyde and ammonia and the conversion of other vicinal amino alcohols to ammonia and the oxo product. The reactions are 1,2-intermolecular rearrangements in which a hydrogen on the alcohol carbon and the neighboring amino group exchange places, followed by deamination of the resulting carbinolamine. The enzymes studied so far are oligomers containing two dissimilar subunits of ca. 50 and 32 kDa molar mass and an  $\alpha_6\beta_6$  quaternary structure with a molar mass of ca. 500 kDa. Most of the recent mechanistic work has been done on the *Salmonella typhimurium* enzyme, which has been cloned and overexpressed in *E. coli*. With 2-aminoethanol or 2-aminopropanol the *pro-S* hydrogen is preferentially abstracted from C1. 2-Aminoethanol stereospecifically labeled in C2 to produce a chiral methyl group, however, yields acetaldehyde that is racemized at C2. In contrast, when either 2*S*- or 2*R*-2-aminopropanol is the substrate and an isotopic label from the coenzyme is introduced into the product, 2*S*-propionaldehyde is the exclusive product.

Although there has been no X-ray crystal structure of EAL, several experimental methods have been used to determine the mode of coenzyme binding. Rétey and co-workers<sup>273</sup> used *Coβ*-5'-deoxyadenosin-5'-yl[1'-*O*-(*p*-tolyl)cobamide (Ado-PTC, Figure 1), which is base-off under all conditions, as a probe for coenzyme binding mode. Thus, the Class I enzymes GluM and MGM which contain the consensus Asp-x-His-x-x-Gly sequence and bind AdoCbl in the base-off/His-on mode, utilize Ado-PTC as a coenzyme with 10% and 76% of the activity of AdoCbl, respectively (and  $K_m$  values of  $0.2 \pm 0.02 \mu\text{M}$  and  $10 \pm 1 \text{ nM}$ ,

respectively, compared to AdoCbl of  $0.1 \pm 0.02 \mu\text{M}$  and  $54 \pm 4 \text{ nM}$ , respectively). In contrast, Ado-PTC has no coenzymatic activity with EAL and instead is a very good competitive inhibitor, with a  $K_i$  value of  $25 \pm 6 \text{ nM}$  (compared to a  $K_m$  of  $30 \pm 6 \text{ nM}$  for AdoCbl). Similarly, the authors had previously shown<sup>304</sup> that Ado-PTC was an active coenzyme for MMCN but an inhibitor of DD and GD. The authors conclude that EAL binds AdoCbl in the base-on mode, and the activity, or lack thereof, of AdoCbl-dependent enzymes with Ado-PTC is diagnostic of the mode of coenzyme binding.

Rétey and co-workers<sup>305</sup> used EPR to determine the mode of binding of AdoCbl to EAL. Since the superhyperfine structure of the EPR spectrum of cob(II)-alamin results from the coupling of the unpaired spin with the  $^{14}\text{N}$  nucleus ( $I = 1$ ) of the axial ligand, the coupling in base-on cob(II)alamin gives a 1:1:1 triplet. If, on the other hand, the coordinating nitrogen is enriched in  $^{15}\text{N}$  ( $I = 1/2$ ), the coupling is a 1:1 doublet. Thus, if either the axial Bzm of the coenzyme or the His residues of the enzyme are enriched in  $^{15}\text{N}$ , the mode of coenzyme binding can be determined after conversion of the coenzyme to cob(II)alamin. [ $\text{B1}, \text{B3}-^{15}\text{N}$ ]AdoCbl, approximately 50% enriched in  $^{15}\text{N}$ ,<sup>306</sup> was consequently bound to EAL and converted to cob(II)alamin either by photolysis or by incubation with ethanol, a substrate analogue that induces Co-C bond homolysis and irreversibly inhibits the enzyme. In both cases the superhyperfine region of the EPR spectrum was altered from that of natural abundance cob(II)alamin as expected for 50%  $^{15}\text{N}$  enrichment of the axial N donor, and subtraction of the appropriate fraction of the spectrum of unlabeled cob(II)alamin gave the expected doublet coupling for  $^{15}\text{N}$ -enriched cob(II)alamin, leading to the conclusion that EAL-bound cob(II)alamin, at least when formed by processes not on the normal catalytic cycle, is base-on.

Warncke and co-workers<sup>307</sup> used X-band electron spin-echo envelope modulation (ESEEM) spectroscopy to study the cob(II)alamin formed in cryotrapped samples of *S. typhimurium* EAL during steady-state turnover with 2-aminopropanol as the substrate. For free base-on cob(II)alamin two sets of features due to  $^{14}\text{N}$  coupling are found in the ESEEM spectrum. One set could be assigned to the B1 nitrogen of the axial Bzm (i.e., the remote nitrogen), both from studies of free cob(II)inamide and from ESEEM simulations and calculations of the nuclear quadrupole parameters by DFT, and was distinct from the parameters found for enzyme-free cob(II)inamide complexed with imidazole (i.e., (Im)cob(II)alamin). The other set is due to corrin ring equatorial  $^{14}\text{N}$ 's. As a result, the enzyme-bound cob(II)alamin generated during normal turnover, in which the  $^{14}\text{N}$  parameters due to the B1 nitrogen of the Bzm persist but are different from those of free (Im)cob(II)inamide, was found to be bound in the base-on mode. In addition, a 14% increase in the hyperfine coupling of the B1 nitrogen occurs in enzyme-bound cob(II)alamin compared to free cob(II)alamin, indicating increased delocalization of the unpaired spin onto the axial ligand, which would be expected to decrease the

rate of radical recombination at the enzyme active site.

Earlier EPR studies of the radical pair formed by reaction of holo-EAL with natural abundance and selectively labeled 2-aminopropanol have shown that the organic radical formed is the unrearranged substrate radical.<sup>308</sup> Warncke and co-workers<sup>309</sup> used X-band EPR and isotopic labeling to show that the organic radical observed at the active site when aminoethanol is the substrate is actually the product-derived radical. Reaction mixtures consisting of holo-EAL and excess aminoethanol in the steady state (at 273 K) were cryotrapped at 130 K. The typical biradical EPR spectrum consisted of a broad feature at  $g = 2.27$  representing the cob(II)alamin and a weakly coupled organic radical feature at  $g = 2.02$  with a line width of 10.8 mT. The line width of the radical derived from [ $1,1,2,2\text{-}^2\text{H}_4$ ]aminoethanol was narrowed by 0.7 mT, while those derived from [ $2\text{-}^{13}\text{C}$ ] or [ $1,2\text{-}^{13}\text{C}_2$ ]aminoethanol were broadened by 2.4 mT, demonstrating that the organic radical is derived from the substrate rather than the enzyme or coenzyme and that the spin density is located at C2, so that the radical is a rearranged, or product, radical. However, the observations do not discriminate between a rearranged, 1-aminoethanol-2-yl radical, and ethanal-2-yl radical produced by ammonia elimination.

Ke and Warncke<sup>310</sup> further characterized the EAL-bound substrate radical derived from 2-aminopropanol and the EAL-bound product radical derived from aminoethanol using X-band electron spin-echo EPR (ESE-EPR) and ESEEM spectroscopies. In the biradical ESE-EPR spectra from both substrates the organic radical signal near  $g = 2$  is split into a doublet because of isotropic exchange and dipolar interactions with the cobalt radical. For the 2-aminopropanol-1-yl substrate radical the splitting is 11.1 mT, while for the aminoethanol-derived product radical the splitting is 7.1 mT, suggesting that C1 of the product radical is further from the cobalt than C2 of the product radical. The ESEEM spectra of both radicals show that both are coupled comparably to the same  $^{14}\text{N}$  nucleus. The coupling is too weak to be due to the substrate radical or product radical amino group, and the use of  $^{15}\text{N}$ -labeled 2-aminopropanol does not alter the ESEEM spectrum, so the coupled  $^{14}\text{N}$  nucleus must come from the protein or the coenzyme. From the simulated nuclear quadrupole parameters the coupled  $^{14}\text{N}$  nucleus seems most likely to be an amide nitrogen from the polypeptide backbone or the A10 amino nitrogen of the Ado group. Since the  $^{14}\text{N}$  hyperfine coupling parameters are the same for both substrate (C1) and product (C2) radicals, the  $^{14}\text{N}$  nucleus responsible for the interaction must either lie in the plane bisecting the C1-C2 bond of the radicals or move in concert with movement of spin density from C1 to C2 during the rearrangement.

This work has been extended by a detailed simulation of the EPR spectra<sup>310</sup> of aminoethanol-derived (i.e., product) biradical state.<sup>311</sup> The modeling leads to values for the isotropic exchange of  $56.6 \times 10^{-4} \text{ cm}^{-1}$  and a point magnetic dipole-dipole at a dis-

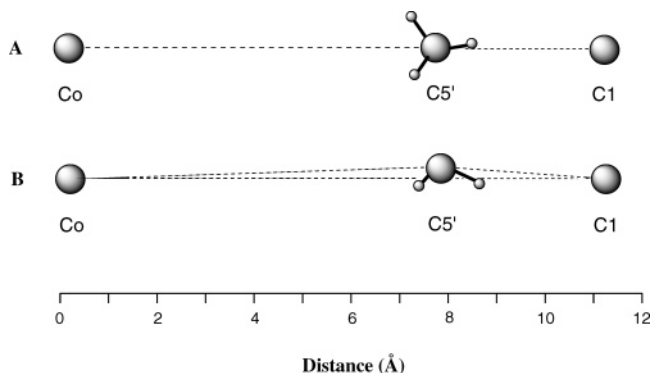


**Figure 8.** Model for the reactant centers in the EAL Co<sup>II</sup>-substrate radical pair state. The Co<sup>II</sup>-C1 axis and distance scale are in the plane of the page. (A) View along a line perpendicular to the Co<sup>II</sup>-C1 axis, with the C5'-C1 axis eclipsed. (B) View after 90° rotation about the Co<sup>II</sup>-C1 axis relative to A.

tance of 9.7 Å and establishes that the product-derived radical obtained from aminoethanol is a  $\pi$ -electron-based radical with principal hyperfine values [16, 16, 100] and [-9, -22, -29] G for the <sup>13</sup>C<sub>1</sub> and <sup>1</sup>H<sub>1</sub> nuclei, respectively.

Canfield and Warncke<sup>312</sup> used ESE-EPR and ESEEM (at four magnetic fields) to determine the geometry of the C5' methylene group of 5'-deoxyadenosine, the C1 (radical carbon) of the substrate radical (from 2-aminopropanol), and the cob(II)-alamin Co<sup>II</sup> ion in the functioning active site of EAL during turnover. The Co<sup>II</sup>-radical exchange and dipolar interactions were determined by simulation of the ESE-EPR line shape and used to calculate a Co<sup>II</sup>-C1 distance of 11.1 Å. Global simulation of the ESEEM at four magnetic fields, which probe the coupling between <sup>2</sup>H in the 5'-methyl group of the 5'-deoxyadenosine fragment, along with the orientation dependence of the EPR line shape, yields a model of the active site geometry (Figure 8). The Co<sup>II</sup>-C1 distance is 11.1 Å, and the C5' group lies nearly on Co<sup>II</sup>-C1 axis at distances of 3.3 Å from C1 and 7.8 Å from Co<sup>II</sup>. The C1-H-C5' angle for the strongly coupled hydrogen is 165°. The results confirm that the C5' radical directly abstracts the H-atom from the substrate and show that the 5' carbon migrates some 6 ± 1 Å from its position in the intact coenzyme to the biradical state. This is significantly larger than the ~1.3 Å of apparent migration of the C5' group in glutamate mutase<sup>267</sup> and suggests that the distance of the Ado• radical carbon migration may be yet another distinguishing feature between Class I and Class II enzymes.

Reed and co-workers<sup>313</sup> also studied the geometry of the steady-state biradical intermediate of EAL containing the substrate-derived radical from 2-aminopropanol using ESE-EPR and pulsed electron nuclear double-resonance (ENDOR) spectroscopy. The ENDOR spectra obtained using [1,1-<sup>2</sup>H<sub>2</sub>]-2-aminopropanol as substrate exhibit a doublet centered at the <sup>2</sup>H Larmor frequency indicative of a statistically favored orientation in which the magnetic field is perpendicular to the electron-nuclear spin vector. An identical splitting (2.26 MHz) is obtained when the substrate is unlabeled but the coenzyme contains deuterium on the A15 carbon

([A15-<sup>2</sup>H<sub>2</sub>]AdoCbl), indicating that regardless of whether deuterium enters the system from C1 of the substrate or A15 of the coenzyme it ends up in the same position relative to the organic radical formed. The ENDOR spectrum for a sample prepared with [U-<sup>13</sup>C-ribosyl]AdoCbl (i.e., [A11,A12,A13,A14,A15-<sup>13</sup>C<sub>5</sub>]AdoCbl) and unlabeled substrate contains a pattern centered at the Larmor frequency for <sup>13</sup>C with an A<sub>⊥</sub> splitting of 1.0 MHz and a weaker peak implying a hyperfine coupling of 0.5 MHz assigned to A<sub>∥</sub>. These results are most likely due to a distance of 3.4 ± 0.2 Å between C5' of the 5'-deoxyadenosine fragment and C1 of the substrate radical, a result essentially identical to that (3.3 Å) from Warncke's ESEEM studies, above.<sup>312</sup> The data lead to the conclusion that the <sup>13</sup>C superhyperfine coupling tensor has a unique axis approximately parallel to the z-axis of the Co<sup>II</sup> and that C1 of the substrate radical lies almost on this z-axis. The model obtained requires a separation of the C5' carbon of 5'-deoxyadenosine and C1 on the substrate of about 12 Å and motion of the C5' carbon by about 7 Å from its position in the bound coenzyme to its steady-state position near the substrate radical. These results are all in excellent agreement with Warncke's ESEEM results,<sup>312</sup> resulting in substantial confidence that they accurately represent the geometry at the EAL active site.

Grissom and co-workers<sup>314</sup> studied the effect of xenon on the steady-state turnover in EAL. Spin-orbit coupling with xenon can increase intersystem crossing in radical pair intermediates in chemical systems. The initial (i.e., cob(II)alamin/5'-deoxyadenosyl) radical pair formed in AdoCbl-dependent enzymes is a singlet, and hyperfine coupling from cob(I)alamin promotes intersystem crossing to partially convert the singlet to a triplet state. Although both the singlet and the triplet states can proceed to productive reaction, only the singlet state can undergo radical recombination. Earlier work<sup>315</sup> had shown that an applied magnetic field (500–2000 G) decreases the rate of intersystem crossing and decreases  $V_{\max}/K_m$  for EAL. Spin-orbit coupling by xenon is expected to have the opposite effect. Steady-state catalysis by EAL was observed using perdeuterated aminoethanol (which maximizes the magnetic field effect) in the presence and absence of a 1500 G magnetic field and in the presence and absence of xenon.  $V_{\max}$  was invariant (0.56 ± 0.03 s<sup>-1</sup>) under all conditions, but  $V_{\max}/K_m$  was increased by 22% in the presence of 40 psi xenon and decreased by 42% by the magnetic field. In the presence of xenon the magnetic field effect was lowered to a 15% decrease. The results are consistent with the radical pair intermediate occurring before the first irreversible step in the catalytic mechanism.

Bandarian and Reed<sup>316</sup> determined the isotope effects on the transient phases of the EAL reaction and the number of exchangeable hydrogens in the holoenzyme. Values of  $k_{\text{cat}}$  and the primary deuterium KIE's were similar to those reported previously. UV-vis spectral measurements during steady-state turnover of *S*-2-aminopropanol indicated that 90% of the active sites (six per  $\alpha_6\beta_6$  oligomer) contained cob-

(II)alamin, and this was unchanged when [1,1-<sup>2</sup>H<sub>2</sub>]-*S*-2-aminopropanol was the substrate. Formation of cob(II)alamin when aminoethanol is mixed with holoenzyme was too fast to be measured by stopped flow methods ( $k > 300 \text{ s}^{-1}$ ); however, a rate constant of  $74 \pm 7 \text{ s}^{-1}$  was measurable when *S*-2-aminopropanol was the substrate. Measurements with [1,1-<sup>2</sup>H<sub>2</sub>]-*S*-2-aminopropanol ( $k = 29 \pm 1 \text{ s}^{-1}$ ) and [1,1-<sup>2</sup>H<sub>2</sub>]ethanolamine ( $k = 24 \pm 1 \text{ s}^{-1}$ ) allowed estimation of the KIE's for cob(II)alamin formation, which were  $3.1 \pm 0.3$  and  $> 10$ , respectively. In experiments with various small molar excesses of substrate the reformation of intact coenzyme (i.e., disappearance of cob(II)alamin) could be observed. The rate constants for coenzyme reformation with unlabeled substrates were independent of the initial substrate concentration and essentially identical to the  $k_{\text{cat}}$ 's for those substrates, consistent with the idea that the rate-determining step(s) occur after cob(II)alamin formation. With the deuterated substrates, however, the rate constants for coenzyme reformation decrease with increasing substrate concentration and reach minima ( $0.057$  and  $19 \text{ s}^{-1}$  for deuterated *S*-2-aminopropanol and aminoethanol, respectively) at a point where ca. 2 equiv of substrate were present initially and the maximal KIE's (ca. 5.7 and 4.5 for deuterated *S*-2-aminopropanol and aminoethanol, respectively) are similar to the KIE's observed for  $k_{\text{cat}}$  for these substrates. These results indicate that the holoenzyme contributes a pool of two exchangeable hydrogen atoms. When the deuterated substrates were used with holoenzyme formed with deuterated coenzyme (i.e., [A15-<sup>2</sup>H<sub>2</sub>]AdoCbl), the minimal rate constant (i.e., the maximal KIE) for coenzyme reformation was observed at all initial substrate concentrations, indicating that the entire pool of exchangeable hydrogens contains deuterium and that the two exchangeable hydrogens contributed by the holoenzyme come from the coenzyme A15 hydrogens. The results rule out obligatory formation of a protein-derived radical on every turnover. The KIE's for the formation of cob(II)alamin suggest that Co–C bond homolysis is either concerted with or coupled to H-atom transfer from the substrate. The former seems unlikely for EAL since a concerted path would require a proximity of the Co–C bond in the intact coenzyme with the substrate C1 which is incompatible with the observed 11–12 Å distance from the cobalt atom to the substrate C1 radical in EAL.<sup>312,313</sup>

Hydroxyethylhydrazine (HEH), an analogue of 2-aminoethanol, has been found to be a mechanism-based inhibitor of EAL.<sup>317,318</sup> Incubation of EAL with excess AdoCbl and HEH leads to rapid loss ( $k = 2.7 \pm 0.3 \text{ s}^{-1}$ ) of activity and the formation of about 6 equiv each of cob(II)alamin, 5'-deoxyadenosine, and acetaldehyde. Although earlier work had suggested that the  $\alpha_6\beta_6$  EAL oligomer had two active sites, the stoichiometry of the reaction of EAL with HEH and AdoCbl indicates six active sites per molecule. The reaction with [1,1,2,2-<sup>2</sup>H<sub>4</sub>]HEH showed a deuterium KIE of  $4 \pm 0.3$ . Inhibition of the enzyme results from irreversible formation of cob(II)alamin and 5'-deoxyadenosine which remain tightly bound to the enzyme. Ammonium sulfate precipitation of the inhibited

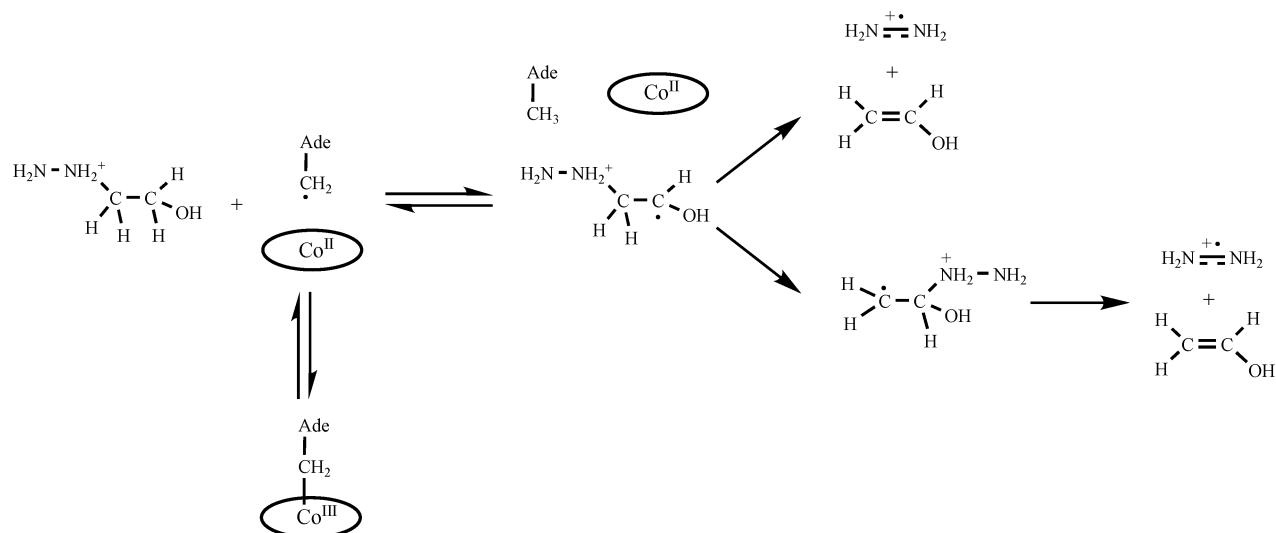
enzyme followed by resuspension and dialysis removed the bound cob(II)alamin and restored ca. 50% of the enzyme's activity. The EPR spectrum of a reaction mixture containing EAL, HEH, and AdoCbl frozen after 20 s confirms that cob(II)alamin is formed and shows the presence of a strong radical signal at  $g \approx 2$ . Surprisingly, the superhyperfine features of the cob(II)alamin spectrum were not the usual 1:1:1 triplets due to coupling of the unpaired electron to the <sup>14</sup>N nucleus of the axial ligand but instead were 1:2:2:1 quartets. This is not due to substitution of the axial ligand but, instead, to magnetic interactions between the unpaired electron and the active site radical which leads to an overlapping doublet of triplets which displays the 1:2:2:1 pattern. Experiments with labeled HEH showed that the active site radical is in the hydrazine portion of HEH. Thus, [1,1,2,2-<sup>2</sup>H<sub>4</sub>]HEH caused no change in the EPR spectrum, but [<sup>15</sup>N]HEH altered the hyperfine splitting pattern. The hyperfine structure in this radical was narrowed when the reaction was run in D<sub>2</sub>O, indicating that a solvent-exchangeable hydrogen resides near the unpaired radical. Simulation of the EPR spectra shows that the unpaired electron is shared equally by both nitrogens of the hydrazine fragment and identifies it as the hydrazine cation radical, produced in 1:1 stoichiometry with cob(II)alamin and located 13 Å from the cobalt unpaired spin.

When the reaction with HEH was run in D<sub>2</sub>O no deuterium was incorporated into the 5'-deoxyadenosine product, indicating that a solvent-exchangeable site on the protein is not involved in the hydrogen-atom transfer step. However, when the reaction was run with [1,1,2,2-<sup>2</sup>H<sub>4</sub>]HEH, all of the 5'-deoxyadenosine product had at least one deuterium atom and a significant amount of 5'-deoxyadenosine had two or three deuteriums, indicating that the hydrogen-atom transfer step is reversible and that, most likely, the 5'-deoxyadenosyl radical directly abstracts a hydrogen atom from HEH (and probably from normal substrates as well). Scheme 18 is consistent with the observations. Thus, reversible homolysis of AdoCbl leads, as always, to cob(II)alamin and the Ado• radical which reversibly abstracts a hydrogen atom from C1 of HEH to form the HEH radical. The latter either directly eliminates the hydrazine cation radical to form the enol of acetaldehyde or, alternatively, undergoes a substrate-like rearrangement and then eliminates the hydrazine cation radical, neither of which can be ruled out based on the experimental observations.

Despite the fact that aristeromycylcobalamin (Ari-Cbl, Figure 1) is an active coenzyme for DD and GD (see above), it is completely inactive with EAL.<sup>45</sup> Instead, it is a strong competitive inhibitor, with a  $K_i$  value ( $16 \pm 2 \text{ nM}$ ) 4-fold lower than the  $K_m$  for AdoCbl. This observation highlights numerous differences in the activity and inhibitory power of AdoCbl analogues among the Class II enzymes, which suggests that even with a single class of AdoCbl-dependent enzymes the mechanism of AdoCbl activation may not be the same.

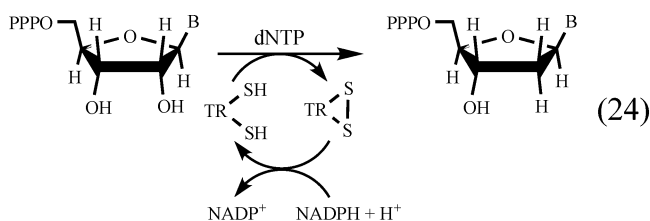
Finally, Toraya and co-workers<sup>300</sup> also studied the reactivity of EAL with the axial-base-altered AdoCbl

## Scheme 18



analogues Ado(Bzim)Cbl and Ado(Im)Cbl. The results were quite similar to those obtained with DD (see above). Ado(Bzim)Cbl was an active coenzyme with a  $K_m$  (74 nM) similar to that for AdoCbl (70 nM) and 91% activity. Ado(Im)Cbl was a much poorer coenzyme with a  $K_m = 950$  nM and only 9% activity. While Ado(Bzim)Cbl did not cause a significant increase in suicide inactivation of EAL, Ado(Im)Cbl rapidly inactivated the enzyme, 23-times more rapidly than AdoCbl, and had a  $k_{cat}/k_{inact}$  value (0.063) 260 times lower than that for AdoCbl. EAL is inherently about 10-fold more susceptible to suicide inactivation with AdoCbl as the coenzyme than is DD. The very high rates of inactivation with Ado(Im)Cbl suggest that the stabilizing effect of the bulky axial base is even more important for EAL than for DD.

Ribonucleoside triphosphate reductase (RTPR) catalyzes the reduction of ribonucleoside triphosphates to 2'-deoxyribonucleoside triphosphates (eq 24). The immediate reductant is a thioredoxin, which is re-reduced by NADPH, although low molecular weight dithiols, such as dithiothreitol, are active reductants. The enzyme from *Lactobacillus leichmannii*, which has been cloned and overexpressed in *E. coli*,<sup>319</sup> has been used for most mechanistic studies. The enzyme is apparently monomeric with a molar mass of 82 kDa. It contains five active site cysteine residues involved in catalysis, four involved in redox transfers and one, Cys408, that is essential for catalysis under all conditions.<sup>320</sup> It represents one of three classes of enzymes that reduce ribonucleotides to deoxyribonucleotides utilizing metal cofactors. Like all ribonucleotide reductases it is allosteric with dNTP's (i.e., the reaction products) as allosteric effectors, and in the case of RTPR, coenzyme binding is very weak in the absence of effectors.



RTPR is unique among AdoCbl-dependent enzymes in a number of ways. It is the only AdoCbl-dependent enzyme that does not catalyze a rearrangement. It is also the only one to be apparently monomeric. It is also the only bisubstrate AdoCbl-dependent enzyme and can catalyze the homolysis of AdoCbl in an incomplete system containing AdoCbl, a dithiol reductant, and an allosteric effector. No other AdoCbl-dependent enzyme can activate AdoCbl in the absence of its substrate. RTPR is also unique in the character of the EPR spectrum of the biradical intermediate, which has been shown to be due to cob(II)alamin and a thiyl radical derived from the essential Cys408 residue at the enzyme active site, when AdoCbl activation is carried out in both the absence and the presence of substrate.<sup>321</sup> Thus, the activation process involves Co–C bond homolysis followed by transfer of a hydrogen atom from Cys408 to the Ado• radical to form 5'-deoxyadenosine and the thiyl radical. The thiyl radical then initiates interaction with the substrate by abstracting a hydrogen atom from the 3' carbon of the substrate ribose moiety. Consequently, RTPR is also the only AdoCbl-dependent enzyme that is known to use AdoCbl to form a radical from an enzyme amino acid residue.

Since the A15 hydrogens of AdoCbl are exchangeable with a solvent-mobile proton on Cys408 at the RTPR active site, RTPR catalyzes the exchange of tritium from [A15-<sup>3</sup>H]AdoCbl with solvent. Stubbe and co-workers<sup>322</sup> studied this exchange and in the presence of a thioredoxin (TR)/thioredoxin reductase (TRR)/NADPH reducing system find  $K_m$ 's of  $60 \pm 9$   $\mu$ M for AdoCbl (as opposed to 0.25  $\mu$ M for substrate turnover) and  $17 \pm 3$   $\mu$ M for dGTP and  $k_{exch} = 0.35$  s<sup>-1</sup>. However, the exchange does not require a reducing system, although it is faster in the presence of one. Mutation of Cys408 to serine eliminated detectable exchange ( $k_{exch} \leq 1.25 \times 10^{-5}$  s<sup>-1</sup>). Mutation of the active site Cys419 and Cys119, which directly deliver the reducing equivalents to the reaction, reduced the exchange rate significantly (0.5–1.5% activity), but mutation of the Cys residues involved in shuttling reducing equivalents into the active site by disulfide exchange, Cys736 and Cys731, had little

effect. The mutant C408S was unable to catalyze formation of cob(II)alamin at the active site as shown by stopped flow spectrometry.

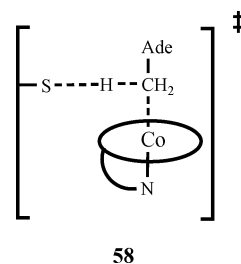
To try to distinguish between stepwise vs concerted Co–C bond cleavage and H-atom transfer pathways, solvent and primary deuterium isotope effects on the kinetics of cob(II)alamin formation were measured. The formation of cob(II)alamin with  $[A15\text{-}^2\text{H}_2]\text{AdoCbl}$  and the TR/TRR/NADPH reductant in  $\text{H}_2\text{O}$  was biphasic, and in the initial phase, 35% more cob(II)alamin was formed (with a rate constant of  $22 \pm 2 \text{ s}^{-1}$ ) than that from unlabeled coenzyme, but in a slower reaction ( $1.3 \pm 0.2 \text{ s}^{-1}$ ), the cob(II)alamin level decayed to the same level as for unlabeled coenzyme. The slower decline is presumably associated with exchange of deuterium from the coenzyme with solvent. With AdoCbl in  $\text{D}_2\text{O}$  the kinetics were also biphasic with rate constants of  $24 \pm 2$  and  $1.0 \pm 0.1 \text{ s}^{-1}$ , with the second phase representing an increase in cob(II)alamin due to deuterium wash-in. Surprisingly, when the reaction is carried out with  $[A15\text{-}^2\text{H}_2]\text{AdoCbl}$  in  $\text{D}_2\text{O}$  the kinetics are still biphasic with rate constants of  $15 \pm 1$  and  $0.5 \pm 0.1 \text{ s}^{-1}$  but with a very small increase in cob(II)alamin in the second phase, possibly due to contaminating protium in the labeled coenzyme.  $\text{D}_2\text{O}$  also causes a shift in the equilibrium for cob(II)alamin formation so that twice as much cob(II)alamin (0.4 equiv) is formed in  $\text{D}_2\text{O}$  as in  $\text{H}_2\text{O}$ . The authors also determined that the binding of coenzyme is rapid relative to cob(II)alamin formation by observations made at low concentrations of RTPR and AdoCbl and that the H-atom transfer step is rapid relative to Co–C bond homolysis on the basis of observing no contribution of the Ado• radical in the EPR spectrum. Simulations and global analysis of the complete set of exchange and cob(II)alamin formation kinetic data and isotope effects (20 parameters for the concerted model) were used to attempt to distinguish the stepwise and concerted mechanisms, and the results best fit the concerted mechanism.

However, Frey and Stubbe and co-workers<sup>323</sup> also addressed the question of stepwise vs concerted mechanisms by studying the epimerization of stereoselectively deuterated  $(A15R)\text{-}[A15\text{-}^2\text{H}_1]\text{AdoCbl}$  ( $A15R/S = 3:1$ ) by wild-type and mutant RTPR using  $^1\text{H}$  NMR. The C408A RTPR mutant was found to bind AdoCbl ( $K_b = 7.6 \pm 0.6 \times 10^3 \text{ M}^{-1}$ ) with similar affinity as wild type by ultrafiltration. Although C408S has been shown not to catalyze substrate reduction, tritium exchange from the A15 hydrogens of coenzyme with water or any detectable formation of cob(II)alamin, both C408S and C408A catalyze the epimerization of  $(A15R)\text{-}[A15\text{-}^2\text{H}_1]\text{AdoCbl}$  in the presence of dGTP and dithiothreitol (DTT) with rate constants of  $0.4 \pm 0.1$  and  $0.28 \pm 0.04 \text{ s}^{-1}$ , respectively. Wild-type enzyme, which catalyzes the exchange of deuterium from solvent into A15 and the exchange of deuterium from  $(A15R)\text{-}[A15\text{-}^2\text{H}_1]\text{AdoCbl}$  into solvent with a rate constant of  $1.5 \text{ s}^{-1}$ , also catalyzed the epimerization but with a rate constant of  $5 \pm 1 \text{ s}^{-1}$ , 12–18-fold faster than the mutant enzymes. While epimerization required the presence of dGTP, a reducing agent was not absolutely re-

quired, although DTT stimulated epimerization considerably, suggesting that the reduced form of the enzyme is responsible for the catalysis although the process does not consume reducing equivalents.

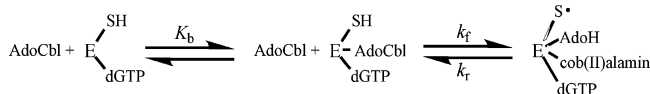
Epimerization of  $(A15R)\text{-}[A15\text{-}^2\text{H}_1]\text{AdoCbl}$  requires cleavage of the Co–C bond and rotation about the A14–A15 bond. While these experiments demonstrate conclusively that Cys408 is not required for Co–C bond cleavage, they do not prove that the processes of Co–C bond cleavage and H-atom transfer are independent, stepwise processes (as the authors agree). The rate constant for epimerization catalyzed by wild-type enzyme is about 10-fold smaller (about  $1.4 \text{ kcal mol}^{-1}$ ) than that for formation of cob(II)alamin. The rate constant for recombination of the cob(II)alamin and the Ado• radical in solution is  $1.2 \times 10^9 \text{ s}^{-1}$ , and that for unhindered rotation about the A14–A15 bond would be expected to be around  $10^{12} \text{ s}^{-1}$ . Thus, reduction in the rate of epimerization relative to that of Co–C bond cleavage would require either an increase in the rate of radical recombination at the active site (possibly from orientation effects) or hindered rotation about the A14–A15 bond or both, so that recombination competed with rotation, slowing net epimerization relative to Co–C bond homolysis. In the case of a stepwise mechanism the fact that the mutants catalyze epimerization 12–18-fold ( $1.5\text{--}1.8 \text{ kcal mol}^{-1}$ ) more slowly than the wild-type enzyme could be due to a slight derangement of the active site due to the presence of the altered amino acid residue.

However, a completely different, and equally reasonable, interpretation of these results is possible. If, in wild-type enzyme, the processes are concerted, then there is a true transition state (structure **58**) which is stabilized by partial transfer of the hydrogen atom from Cys408 to the emerging Ado• radical since the resulting thiyl radical is expected to be about  $6 \text{ kcal mol}^{-1}$  more stable than the Ado• radical. Thus, the ca.  $1.5 \text{ kcal mol}^{-1}$  lowering of the free energy of activation for epimerization upon mutating the C408 residue is consistent with a concerted process in which the migrating hydrogen atom is about 25% transferred from Cys408 to the A15 carbon in the transition state.



Stubbe and co-workers<sup>324</sup> also studied the temperature dependence of the kinetics of formation of cob(II)alamin by RTPR using the TR/TRR/NADPH reductant but no substrate to determine activation parameters for the enzymatic activation of AdoCbl. The results are analyzed assuming a concerted mechanism for Co–C bond homolysis and H-atom transfer (Scheme 19), although this assumption does not affect the analysis of the data. Stopped flow

## Scheme 19



spectroscopy was used to monitor the formation of cob(II)alamin as a function of AdoCbl concentration with AdoCbl in 4–10-fold excess over RTPR. At 37 °C values of  $k_f = 55 \pm 7 \text{ s}^{-1}$ ,  $k_r = 27 \pm 2 \text{ s}^{-1}$ , and  $K_b = 5.1 \pm 1.7 \times 10^3 \text{ M}^{-1}$  and, hence,  $K_{\text{eq}} = k_f/k_r = 2.0 \pm 0.3$  were obtained. The amplitude of the absorbance change for conversion of AdoCbl to cob(II)alamin by RTPR was also used to determine  $K_b$  and  $K_{\text{eq}}$  and gave values at 37 °C of  $2.1 \pm 0.5 \times 10^4 \text{ M}^{-1}$  and  $0.65 \pm 0.05$ , respectively. The temperature dependence of the kinetic and thermodynamic parameters was determined by Eyring plots of  $k_{\text{obs}}$  at a given [AdoCbl], which permitted calculation of  $k_{\text{obs}}$  at any temperature for that [AdoCbl]. The calculated  $k_{\text{obs}}$  values at each temperature were then plotted vs [AdoCbl] to obtain the values of  $K_1$ ,  $k_f$ ,  $k_r$ , and  $K_{\text{eq}}$  at that temperature. Subsequent Eyring and van't Hoff plots of these kinetic and thermodynamic parameters gave  $\Delta H_f^\ddagger = 46 \pm 7 \text{ kcal mol}^{-1}$ ,  $\Delta S_f^\ddagger = 96 \pm 12 \text{ cal mol}^{-1} \text{ K}^{-1}$ ,  $\Delta H_{\text{eq}}^\circ = 20 \pm 8 \text{ kcal mol}^{-1}$ , and  $\Delta S_{\text{eq}}^\circ = 70 \pm 17 \text{ cal mol}^{-1} \text{ K}^{-1}$ .

These results are extraordinary in several regards. Compared to the activation parameters for nonenzymatic homolysis of AdoCbl ( $\Delta H^\ddagger = 33.8 \pm 0.2 \text{ kcal mol}^{-1}$  and  $\Delta S^\ddagger = 13.5 \pm 0.7 \text{ cal mol}^{-1} \text{ K}^{-1}$ ),<sup>106</sup> they suggest that the enzyme “uncatalyzes” the reaction enthalpically by some  $12 \text{ kcal mol}^{-1}$  (a factor of  $2.9 \times 10^8$ ) but catalyzes it entropically by  $83 \text{ cal mol}^{-1} \text{ K}^{-1}$  (at 37 °C, a factor of  $1 \times 10^{18}$ ), a situation which is surely unprecedented in enzymology. The results also contrast those of Banerjee<sup>222</sup> which show that MMCM catalysis of Co–C bond homolysis is 90% enthalpic at 37 °C. Moreover, they are diametrically opposed to earlier results of Brown and Li,<sup>221</sup> who measured  $\Delta H_f^\ddagger = 20 \pm 1 \text{ kcal mol}^{-1}$  and  $\Delta S_f^\ddagger = 13 \pm 4 \text{ cal mol}^{-1} \text{ K}^{-1}$  for RTPR-induced AdoCbl homolysis and consequently concluded that the catalysis was entirely enthalpic (i.e.,  $\Delta\Delta H^\ddagger = 14 \pm 1 \text{ kcal mol}^{-1}$  and  $\Delta S^\ddagger = -0.5 \pm 4 \text{ cal mol}^{-1} \text{ K}^{-1}$ ). While these discrepancies have never been resolved, several observations concerning the differences in results by these two groups should be noted.

Brown and Li found sharp temperature breaks in the Eyring plot of  $k_f$  and the van't Hoff plot of  $K_{\text{eq}}$  at around 31 °C, reminiscent of similar temperature breaks seen previously by Tamao and Blakley<sup>325</sup> in the temperature dependence of the amplitude of the spectral change upon conversion of AdoCbl to cob(II)alamin and in the temperature dependence of the UV difference spectra of RTPR alone and with allosteric effector and reductant, which these authors attributed to a conformational change in the protein at lower temperatures. No such temperature breaks were observed in the Stubbe work. Brown and Li reported the activation parameters for RTPR taken from the part of the Eyring plot above 31 °C as most likely the physiologically significant ones. Most interestingly, the activation parameters taken from the part of the Eyring plot below the temperature break

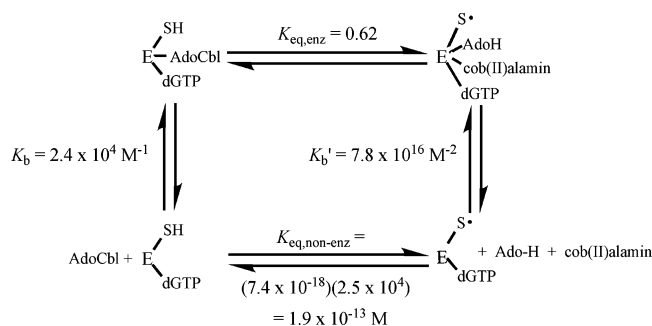
( $\Delta H_f^\ddagger = 42 \pm 4 \text{ kcal mol}^{-1}$  and  $\Delta S_f^\ddagger = 83 \pm 14 \text{ cal mol}^{-1} \text{ K}^{-1}$ ) are experimentally indistinguishable from those reported by Stubbe and co-workers. It would seem that a resolution of the dilemma requires an understanding of the physical changes that give rise to the breaks in the temperature dependence and the reasons that this phenomena was not observed by the Stubbe group.

The discordant results could possibly be explained if the active form of RTPR were actually a dimer,<sup>326</sup> with the dimerization process being strongly entropically driven (note that monomeric allosteric enzymes are rare). Thus, at lower temperatures the enzyme would exist mostly as the inactive monomer and the kinetics of cob(II)alamin formation at the active site would reflect both the thermodynamics of dimer formation and the activation parameters for homolysis. At higher temperatures and at the protein concentrations used by Brown and Li (10–200  $\mu\text{M}$ ) the enzyme would be mostly in the dimer form and the measured activation parameters would reflect the homolysis by the active dimer only. At the lower protein concentrations used by Stubbe and co-workers (3–10 mM) the enzyme might be mostly monomer at some temperatures and mixtures of monomer and dimer at others, so that the activation parameters again reflect both the thermodynamics of dimer formation and the activation parameters for homolysis.

There is, however, no evidence for dimerization of RTPR. Although Brown and co-workers<sup>243,327</sup> consistently found that analogues of AdoCbl which are not active coenzyme are linear, noncompetitive inhibitors, the classical interpretation of which requires two binding sites, the X-ray crystal structure of RTPR (see below) is monomeric, and mass spectral light scattering measurements<sup>326</sup> on highly purified RTPR agree with a monomeric structure. Hence, the discrepancy between the activation parameters for RTPR-induced AdoCbl homolysis between the Brown and Stubbe groups remains unexplained.

The availability of the equilibrium constant for cob(II)alamin formation at the active site of RTPR allows an analysis of the thermodynamics of Co–C bond homolysis on the enzyme. This equilibrium constant ( $0.59 \pm 0.03$ <sup>221</sup> and  $0.65 \pm 0.05$ ,<sup>324</sup> the “kinetic” value of  $2 \pm 0.3$ <sup>324</sup> clearly violates the spectrophotometric measurements) is the product of the equilibrium constants for the coupled processes of Co–C bond homolysis and H-atom transfer from the Cys408 thiol to the Ado• radical. The equilibrium constant for the latter process may be estimated<sup>106</sup> from literature values for the rate constants for H-atom transfer from thiols to carbon-centered radical and for the reverse process to be about  $2.5 \times 10^4$  (range from  $1.0 \times 10^4$  to  $5.1 \times 10^4$ ). This gives an equilibrium constant of  $2.5 \times 10^{-5}$  for RTPR-induced Co–C bond homolysis. Since the rate constant for AdoCbl nonenzymatic homolysis at 37 °C ( $8.9 \times 10^{-9} \text{ s}^{-1}$ ) has been measured<sup>106</sup> and the rate constant for the reverse process, the recombination of cob(II)alamin and the Ado• radical, is known ( $1.2 \pm 0.2 \times 10^9 \text{ s}^{-1}$ ), the equilibrium constant for the nonenzymatic homolysis of AdoCbl is  $7.4 \times 10^{-18}$ . The enzyme thus shifts the

## Scheme 20



equilibrium toward homolysis products by  $2.4 \times 10^{12}$ . Combined with the  $2.5 \times 10^4$  “pull” by the subsequent H-atom transfer step, the enzyme is thus able to form a stoichiometrically significant concentration (ca. 0.38 equiv) of radical at the active site, despite the fact that the reaction is triggered by a hopelessly unfavorable bond homolysis.

The only way the enzyme can shift the equilibrium for Co–C bond homolysis in this fashion is by differential binding of AdoCbl to the native enzyme and the net products of homolysis and H-atom transfer, cob(II)alamin and 5′-deoxyadenosine, to the thiyl radical form of the enzyme. Since the binding constant for AdoCbl to the enzyme is known,<sup>221,324,328</sup> the binding constant for cob(II)alamin and 5′-deoxyadenosine to the thiyl radical form of the enzyme can be calculated from the thermodynamic cycle in Scheme 20. The result,  $7.8 \times 10^{16} \text{ M}^{-2}$ , is consistent with the very high affinity of B<sub>12</sub> binding proteins for Cbl’s<sup>53</sup> and explains why it is not possible to demonstrate a mass action effect of exogenous cob(II)alamin on the equilibrium between AdoCbl and the homolysis fragments at the enzyme active site. It also makes it tempting to suggest the possibility that the intrinsic binding of AdoCbl to the enzyme is much stronger than appears from the measured binding constant but that substantial amounts of binding energy are used to somehow effect catalysis, simultaneously providing catalytic power and setting up the differential binding that forces the homolysis equilibrium toward radicals.

Stubbe and co-workers<sup>329</sup> used a clever series of experiments to show that AdoCbl is released from RTPR after each turnover and consequently that the Co–C bond is reformed during each catalytic cycle. Thus, the  $K_{\text{m}}$  for AdoCbl was  $0.2 \mu\text{M}$  and  $k_{\text{cat}}$  was  $2 \text{ s}^{-1}$  for both ATP and CTP reduction using the coupled assay of the TR/TRR/NADPH reducing system under standard Michealis–Menton conditions with  $[\text{AdoCbl}] \gg [\text{RTPR}]$ . However, when  $[\text{RTPR}] > [\text{AdoCbl}]$  such that all of the AdoCbl was bound to enzyme, the rate of ATP reduction with dGTP as the allosteric effector showed saturation behavior in  $[\text{AdoCbl}]$  with a limiting rate of  $10 \text{ s}^{-1}$ , five times faster than under MM conditions. Similar results were obtained for CTP reduction with dATP as the effector; the maximal rate was  $8.5 \text{ s}^{-1}$ , 4.5-fold higher than under normal conditions. This can only occur if each molecule of AdoCbl is able to undergo several turnovers before the rate-determining step, and the simplest interpretation is that the limiting rate,  $\sim 10 \text{ s}^{-1}$ , is the rate of AdoCbl dissociation. In addition, the kinetics of

tritium exchange from  $[\text{A15-}^3\text{H}]\text{Cbl}$  to water during the reduction of ATP was studied. dATP was formed with an apparent rate constant of  $55 \pm 10 \text{ s}^{-1}$ , demonstrating that nucleotide reduction is not rate limiting (i.e., the apparent rate constant is faster than the maximal turnover rate). The apparent rate constant for tritium washout from the labeled coenzyme was  $0.6 \text{ s}^{-1}$ , comparable to that previously determined ( $0.3 \text{ s}^{-1}$ ) in the absence of substrate,<sup>322</sup> and the ratio of  $^3\text{H}_2\text{O}$  to dATP formed increased with time. If a single Co–C bond dissociation resulted in multiple turnovers, the amount of  $^3\text{H}_2\text{O}$  formed would be expected to be very low compared to the amount of product, since failure of the Co–C bond to reform would limit the opportunity for tritium washout from other molecules of AdoCbl. Modeling of the turnover including an obligatory dissociation of AdoCbl vs AdoCbl remaining bound for multiple turnovers strongly suggests that the Co–C bond is reformed after every turnover, i.e., that the radical chain length is one (1).

Stubbe and Rétey and co-workers<sup>330</sup> studied the interaction of the substrate analogue 2′-deoxy-2′-methylcytidine-5′-triphosphate (MdCTP) with RTPR to determine the mode of coenzyme binding. When MdCTP was mixed with RTPR, AdoCbl, dATP, and the TR/TRR/NADPH reducing system, rapid inactivation (complete in 3 min) of the enzyme occurred. Stopped flow and rapid freeze quench EPR measurements showed that cob(II)alamin was formed with a rate constant of  $10 \text{ s}^{-1}$ . The EPR spectrum contained a well-resolved signal for cob(II)alamin which permitted determination of the nature of the axial ligand (and hence the mode of coenzyme binding) by isotopic substitution. Thus, when the reaction was run using  $[\text{U-}^{15}\text{N}]\text{RTPR}$ , the superhyperfine coupling in the cob(II)alamin EPR signal was unperturbed (i.e., the triplet splitting due to  $^{14}\text{N}$  axial coordination persisted), demonstrating that the axial ligand position was not occupied by a group from the protein. In contrast, when  $[\text{B1,B3-}^{15}\text{N}_2]\text{AdoCbl}$  (50% enriched in each nitrogen) was used, the superhyperfine coupling was altered in a way that was successfully simulated assuming 50%  $^{15}\text{N}$  and 50%  $^{14}\text{N}$  axial coordination. Thus, the cob(II)alamin was bound to the enzyme base-on.

Rétey and Finke and co-workers<sup>331</sup> investigated the inhibition of RTPR by a series of  $[\omega\text{-(adenosin-5′-O-yl)alkyl}]\text{cobalamins}$  ( $\text{AdoO}(\text{CH}_2)_n\text{Cbl}$ ’s, Figure 1), analogues of AdoCbl with an oligomethylene chain ( $n = 3\text{--}7$ ) inserted between the cobalt atom and the adenosine 5′ oxygen, as models for the “posthomolysis” state. All five of analogues were competitive inhibitors with the best inhibitor being the  $n = 5$  analogue ( $K_{\text{i}} = 7.7 \pm 0.2 \mu\text{M}$ , compared to  $K_{\text{m}} = 1.5 \mu\text{M}$  for AdoCbl). This same pattern of inhibition had previously been observed for the Class II enzymes DD and GD,<sup>332</sup> but for Class I MMCM, the best inhibitor was the  $n = 6$  analog.<sup>333</sup> The enzyme was also competitively inhibited by cob(II)alamin alone ( $K_{\text{i}} = 20.8 \pm 0.2 \mu\text{M}$ ) and by equimolar cob(II)alamin and adenosine ( $K_{\text{i}} = 14.3 \mu\text{M}$ ). Interestingly, adeninylpentylCbl (AdoPentCbl, Figure 1) was a pure non-competitive inhibitor with the lowest  $K_{\text{i}}$  ( $1.3 \mu\text{M}$ ). The

results suggest that the active site geometry of the homolysis products may be different in the Class I and Class II enzymes. Using literature values the authors also demonstrated another difference between the Class I and Class II enzymes, namely, that the  $\gamma$ -band of enzyme-bound cob(II)alamin is shifted to longer wavelengths (by 2–7 nm) in the Class II enzymes but to shorter wavelengths (by 3–8 nm) in the Class I enzymes.

Brown and co-workers<sup>43</sup> studied the kinetics of the RTPR-induced formation of cob(II)alamin analogues from AdoCbl analogues with altered axial nucleotides, including the benzimidazole analogue (Ado(Bzim)Cbl, Figure 1) and the imidazole analogue (Ado(Im)Cbl, Figure 1). Both analogues were highly active coenzymes with  $V_{\max}$  unaltered from that for AdoCbl, although the  $K_m$  for Ado(Bzim)Cbl ( $0.14 \pm 0.01 \mu\text{M}$ ) was essentially the same as that for AdoCbl ( $0.18 \pm 0.01 \mu\text{M}$ ), the  $K_m$  for Ado(Im)Cbl ( $13 \pm 1 \mu\text{M}$ ) was nearly 100-fold higher. AdoCbi<sup>+</sup> was not an active coenzyme but instead a pure uncompetitive inhibitor with  $K_i = 30 \pm 4 \mu\text{M}$ . As was the case for AdoCbl itself,<sup>221</sup> the observed rate constant for the RTPR-induced formation in the presence of a dithiothreitol reductant was independent of the concentration of enzyme (at constant coenzyme analogue concentration) and had an average value of  $k_{\text{obs}} 24.1 \pm 1.4 \text{ s}^{-1}$  for Ado(Bzim)Cbl and  $7.9 \pm 0.8 \text{ s}^{-1}$  for Ado(Im)Cbl. However, as was also the case for AdoCbl, the extent of formation of the Co<sup>II</sup> derivative (i.e., the spectral change observed) showed saturation with respect to [RTPR], indicative of perturbation of the coenzyme binding equilibrium ( $K_b$ , Scheme 19). Fits of these data to binding isotherms permitted evaluation of  $K_b$  and of the maximal amount of Co<sup>II</sup> derivative formed when the coenzyme is “saturated” with enzyme. From the latter the equilibrium constant ( $K_{\text{eq}} = k_f/k_r$ , Scheme 19) for formation of the Co<sup>II</sup> species could be calculated and consequently the forward ( $k_f$ ) and reverse ( $k_r$ ) rate constants since  $k_{\text{obs}} = k_f + k_r$ . The binding constant for Ado(Bzim)Cbl ( $1.7 \pm 0.2 \times 10^4 \text{ M}^{-1}$ ) is quite close to that for AdoCbl ( $2.7 \pm 0.5 \times 10^4 \text{ M}^{-1}$ ), but that for Ado(Im)Cbl ( $3.3 \pm 0.5 \times 10^3 \text{ M}^{-1}$ ) is considerably smaller, suggesting that the axial base is a significant binding determinant. The forward rate constant for formation of the Co<sup>II</sup> species from Ado(Bzim)Cbl ( $9.8 \pm 0.8 \text{ s}^{-1}$ ) is ca. 70% of that for AdoCbl ( $14 \pm 1 \text{ s}^{-1}$ ) but that for Ado(Im)Cbl ( $0.8 \pm 0.1 \text{ s}^{-1}$ ) is reduced by 17-fold. The results suggest some importance of the bulk of the axial base in the activation of AdoCbl by RTPR; however, this cannot be assessed without knowledge of the intrinsic nonenzymatic reactivity of Ado(Im)-Cbl.

RTPR is a member of one (Class II) of three classes of ribonucleotide reductases, all of which use an active site radical as a crucial intermediate. The Class I enzymes, which occur in eukaryotes, bacteria, and viruses, use a diiron–tyrosyl radical, while the Class III enzymes from anaerobic bacteria use an FeS cluster and *S*-adenosylmethionine to generate a glycy radical. Drennan and co-workers<sup>334</sup> have now determined the X-ray crystal structure of RTPR both as the apoenzyme and complexed with adeninylen-

tylcobalamin (AdoPentCbl, Figure 1). The structure features a 10-stranded  $\alpha/\beta$  barrel with two parallel five-stranded  $\beta$  sheets oriented antiparallel to each other. The barrel contains a RNR finger-loop with the essential Cys408 residue (which provides the thiyl radical) at the fingertip. This global fold is surprisingly similar in all three classes of RNR's despite the low sequence identity (<10%) among them. A number of active site residues are also conserved in all three structures, including the radical-bearing Cys408 residue, Glu410 and its hydrogen-bonding partner, Asn406, and the active site redox couple Cys119/Cys419. There is also a surprising similarity between the substrate binding region of the Class I enzyme from *E. coli* and RTPR considering the fact that the Class I enzymes use nucleoside diphosphates as substrates while the Class II enzymes use triphosphates. In the structure crystallized with AdoPentCbl the Cbl is bound base-on but, unfortunately, electron density for the adenine moiety is ambiguous, although the pentamethylene segment is clearly bonded to the cobalt. Comparison with the structure of the apoenzyme shows concerted movement of about 100 residues as a result of coenzyme binding, most of the motion being in three  $\beta$  strands, while two  $\alpha$  helices make smaller adjustments. The coenzyme binding domain shows no structural similarity to other B<sub>12</sub> binding domains, even that of DD, which also binds coenzyme in the base-on form, but is similar to related regions in the Class I RNR's instead. The result of the coenzyme-induced structural changes is to form a more closed structure that also brings Cys408 into closer position for hydrogen-atom transfer, although this structure is probably not completely closed as the Co-to-Cys408 sulfur distance is 10 Å (compared to the 5.5–7.5 Å distance from EPR studies,<sup>335</sup> possibly due to the lack of an allosteric effector). The “hinge” for this motion is at the base of two  $\beta$  strands in the coenzyme binding site, near a bound anion which has been modeled as a sulfate ion.

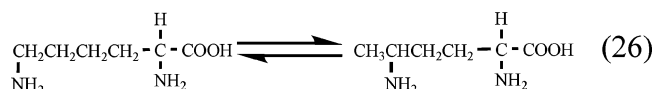
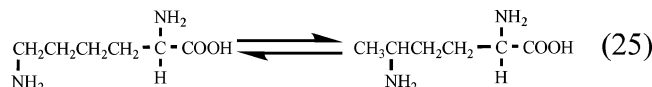
The effector binding site has been assigned to the top of a four-helix bundle, in a similar position to the corresponding site in the Class I enzyme from *E. coli*. However, in the Class I enzyme the effector binding site is created at a dimer interface, while in the monomeric RTPR structure a 130-residue insertion maintains the essence of the interface binding site. The authors consequently consider the RTPR structure as a paradigm for the simplest structure capable of carrying out allosterically sensitive ribonucleotide reduction.

Finally, Finke and co-workers<sup>336</sup> reported an improved and shortened purification of RTPR. The initial step is a two-phase extraction using a bottom phase of high molecular weight dextran solution and a top phase of PEG 8000, which extracts most of the protein. The PEG phase is applied directly to a DEAE-Sepharose column, and after washing the RTPR is eluted with a potassium phosphate gradient. The pooled RTPR fractions are directly loaded onto a dGTP–C<sub>6</sub>–Sepharose affinity column,<sup>337</sup> and after washing with buffer the RTPR is eluted with dATP. The procedure takes less than 10 h and results in a

48% yield of enzyme with 20–30% increased specific activity compared to the usual protocol and a purity of >98% (by SDS–PAGE). Electrospray MS gave values of  $81855 \pm 24$  and  $81865 \pm 55$  kDa (on two separate preparations), while MALDI-TOF gave  $81\ 800 \pm 100$  kDa, consistent with the predicted molar mass of 81 853 from the gene sequence. Dynamic light scattering at 25 °C gave a translational diffusion coefficient of  $732 \times 10^{-13} \text{ m}^2 \text{ s}^{-1}$ , a hydrodynamic radius of  $3.3 \pm 0.3$  nm, and consequently a frictional ratio of 1.15, which corresponds to a prolate ellipsoid of axial ratio 3.5.

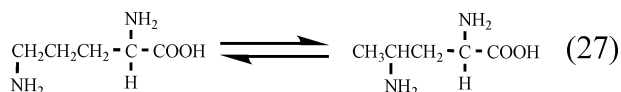
### 11.1.3. Class III Aminomutases

The aminomutases catalyze 1,2-rearrangements in which the primary amino group of lysine or ornithine exchanges places with the adjacent secondary hydrogen atom. D-Lysine-5,6-aminomutase (LAM) catalyzes the conversion of D-lysine to 2,5-diaminohexanoic acid (2,5-DAH, eq 25) and the conversion of L- $\beta$ -lysine to 3,5-diaminohexanoic acid (3,5-DAH, eq 26).



For the latter reaction the stereochemistry has been established to produce (3*S*,5*S*)-3,5-DAH. The enzyme from *Clostridium sticklandii* is an  $\alpha_2\beta_2$  heterodimer of molar mass ca. 170 kDa and undergoes rapid suicide inactivation with its normal substrates in the absence of a specific reactivating enzyme and ATP.

D-Ornithine-4,5-aminomutase (OAM) catalyzes the conversion of D-ornithine to (2*R*,4*S*)-diaminopentanoate (eq 27). The enzyme from *C. sticklandii* is also a heterodimer with a molar mass of ca. 190 kDa.



The two genes for LAM from *C. sticklandii* have now been cloned and overexpressed in *E. coli*.<sup>338</sup> The large ( $\alpha$ ) subunit has a calculated molar mass of 57.3 kDa, and the small ( $\beta$ ) subunit has a mass of 29.2 kDa, and the latter contains the consensus Asp-x-His-x-x-Gly sequence suggesting that it is the Cbl binding domain and that it binds AdoCbl in the base-off/His-on mode. The native enzyme is a heterotetramer of structure  $\alpha_2\beta_2$  and molar mass of 173 kDa. The  $K_m$  values for AdoCbl and PLP are 6.6 and 1.0  $\mu\text{M}$ , respectively. Although earlier work had suggested that ATP was an allosteric effector,<sup>339</sup> no effect of ATP (5 mM) could be found on recombinant LAM. In the presence of lysine and AdoCbl the enzyme undergoes rapid inactivation ( $k = 5.2 \times 10^{-3} \text{ s}^{-1}$ ) regardless of the presence of oxygen. With lysine but without AdoCbl the inactivation is slowed ( $t_{1/2} \approx 15$

min), but without lysine and with AdoCbl the enzyme is indefinitely stable. A base-off/His-on binding mode for cob(II)alamin was confirmed using EPR and [B1,-B3-<sup>15</sup>N<sub>2</sub>]AdoCbl, generating enzyme-bound cob(II)-alamin by treatment with hydrazine, which produces a well-resolved EPR spectrum of the reduced coenzyme with no confounding organic radical.

Frey and co-workers<sup>340</sup> studied the suicide inactivation of recombinant LAM using variety of techniques. The equilibrium constant for conversion of D-lysine to 2,5-DAH is  $1.21 \pm 0.05$  at 37 °C and pH 8.5. Incubation of LAM with D-lysine, AdoCbl, and PLP results in formation of a cob(III)alamin and 5'-deoxyadenosine (5'-dA) with about the same rate constant (ca.  $0.004 \text{ s}^{-1}$ ) as loss of activity, and the presence or absence of oxygen has no effect. The inhibition is irreversible since the cob(III)alamin product does not dissociate from the enzyme and cannot be exchanged for free AdoCbl. No deuterium isotope effect on the inactivation rate could be found regardless of whether the deuterium was in the A15 methylene of the coenzyme, the substrate, or the solvent. L-Lysine proved to be a slow substrate for LAM ( $K_m = 20 \pm 6 \text{ mM}$  and  $V_{\text{max}} = 108 \pm 7 \text{ min}^{-1}$  compared to  $K_m = 20 \pm 1 \text{ mM}$  and  $V_{\text{max}} = 800 \pm 44 \text{ min}^{-1}$  for D-lysine) but inactivated the enzyme with a rate similar to that for D-lysine. L- $\beta$ -Lysine was not a substrate, but both it and L-lysine were competitive inhibitors with  $K_i$  for L-lysine  $23 \pm 2 \text{ mM}$  but  $4.4 \pm 0.7 \mu\text{M}$  for L- $\beta$ -lysine.

Since the product from the Ado moiety of AdoCbl is 5'-dA, a heterolytic cleavage of AdoCbl to form the cob(III)alamin product can be ruled out, implicating the intermediacy of mechanism-based radicals and the possibility of an electron transfer from the cob(II)alamin product of Co–C bond homolysis to an intermediate radical. Such an electron transfer from the Ado• radical to cob(II)alamin would produce a carbanion which would have to be quenched by solvent to form 5'-dA. However, when the inactivation reaction was run in D<sub>2</sub>O, no deuterium was incorporated into 5'-dA, while the use of D,L-lysine-*d*<sub>8</sub> in H<sub>2</sub>O produced trideuterio 5'-dA exclusively, demonstrating that the putative Ado• radical obtains its hydrogens from substrate or product and is not involved in an electron transfer with cob(II)alamin. However, when D,L-lysine-*d*<sub>8</sub> was the substrate the recovered substrate/product mixture showed a slight enrichment in lysine/DAH-*d*<sub>7</sub>, but this enrichment decreased if [A15-<sup>2</sup>H<sub>2</sub>]AdoCbl was the coenzyme. Decreasing the ratio of D,L-lysine-*d*<sub>8</sub> to LAM doubled the enrichment in lysine/DAH-*d*<sub>7</sub>, but in D<sub>2</sub>O, the enrichment is decreased, confirming that the substrate/product mixture incorporates protons from solvent. In a similar experiment with tritiated water both recovered substrate and product contained tritium but the protein, 5'-dA, and PLP were unlabeled, indicating that substrate and product intermediates are involved in the suicide inhibition. The authors consequently propose that either a substrate radical or a product radical undergoes electron transfer with cob(II)alamin to form a substrate or product carbanion, which is quenched with a solvent-derived protein and cob(III)alamin, resulting in the observed suicide

inactivation.

The two genes encoding *C. sticklandii* OAM have also been cloned and expressed in *E. coli*.<sup>341</sup> The enzyme is a  $\alpha_2\beta_2$  heterotetramer with subunit molar masses of 12.8 ( $\alpha$ ) and 82.9 kDa ( $\beta$ ). The Asp-x-His-x-x-Gly consensus sequence, suggesting base-off/His-on Cbl binding, was, surprisingly, found in the large subunit, suggesting that the Cbl binding site resides on this subunit instead of the small subunit as is normally the case. The proper folding of the large subunit required the presence of the small subunit and either PLP or AdoCbl. The  $K_m$  values for D-ornithine, AdoCbl, and PLP are  $45 \pm 3$ ,  $0.43 \pm 0.04$ , and  $1.5 \pm 0.1 \mu\text{M}$ , respectively, and  $k_{\text{cat}}$  is  $6.3 \pm 0.1 \text{ s}^{-1}$ . The authors used AdoCbi<sup>+</sup> to confirm the Cbl binding mode. When wild-type OAM, but not the mutant  $\beta\text{H628G}$ , was reconstituted with AdoCbi<sup>+</sup>, the Cbl visible spectrum shifted to that of a base-on AdoCbl, suggesting that the His628 residue of the large subunit had become the axial ligand.

#### 11.1.4. Other AdoCbl-Dependent Enzymes

Two new putative AdoCbl-dependent enzymes were discovered during the period covered in this review, although neither has been significantly characterized.

Zhang and Reynolds<sup>342</sup> studied the formation of monensin analogues in *Streptomyces cinnamonensis*, in which the ratio of monensin A and monensin B depends on the ratio of the precursors methylmalonylCoA and ethylmalonylCoA. They cloned and sequenced the *meaA* gene, which encodes a 74 kDa protein with 40% sequence identity to MMCM and 36% and 53% sequence identity to the large and small subunits of ICM, respectively. The consensus sequence Asp-x-His-x-x-Gly for base-off/His-on binding occurs at near the C-terminal end, suggesting that it has Class I type base-off/His-on coenzyme binding. Unfortunately, no information on the reaction catalyzed nor any demonstration of the requirement for AdoCbl has appeared.

Conversion of magnesium protoporphyrin monomethyl ester (MPE) to protochlorophyllide (PChlide) requires the putative MPE-cyclase, BchE, to form the isocyclic ring of bacteriochlorophyll. Gough and co-workers<sup>343</sup> conducted a blast search of the sequence for *Rhodobacter capsulatus* BchE and found sequence similarities to a CH<sub>3</sub>Cbl-dependent methyl transferase from *Streptomyces hygroscopicus*. To test the possibility that BchE is a B<sub>12</sub>-dependent enzyme, mutants in the B<sub>12</sub> biosynthetic genes, *bluE* and *bluB*, which strongly inhibit the formation of bacteriochlorophyll, were studied. These mutants, when grown in the absence of B<sub>12</sub>, accumulate MPE and its 3-vinyl-8-ethyl derivative, as confirmed by mass spectroscopy and NMR analysis, as do mutants in the *BchE* gene under normal growth conditions. Although MPE-cyclase cannot yet be assayed in vitro (disruption of the cells by sonication destroys the activity), the authors developed an in-vivo assay. In a *bluE* mutant grown under conditions inhibiting protein synthesis the accumulated MPE can be used as an internal substrate for the cyclase. This activity was shown to have an absolute requirement for "B<sub>12</sub>"

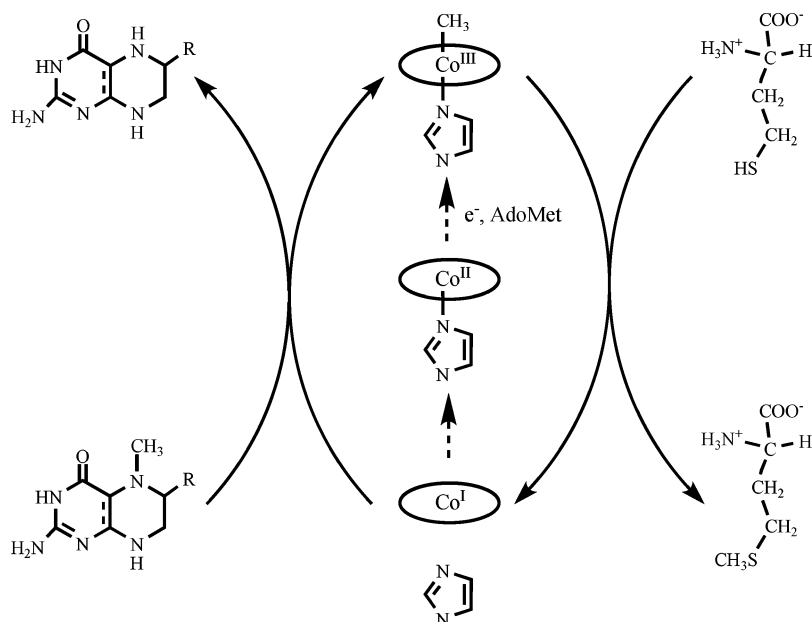
(form not specified) or AdoCbl. Since the reaction does not involve a methylation the authors speculate that the coenzyme requirement is for AdoCbl. A radical-based mechanism is proposed for the cyclization, but it is not supported by any experimentation.

## 11.2. Methyltransferases

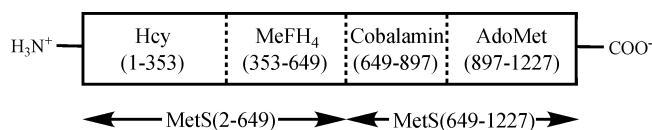
Corrinoid-dependent methyltransferases are ubiquitous in the biosphere (except for plants) and occur in organisms from mammals to simple eukaryotes to eubacteria and Archaea. The prototypical, and best studied, example is methionine synthase (MetS), which occurs in mammals and many bacteria. MetS catalyzes the transfer of a methyl group from N<sup>5</sup>-methyl-tetrahydrofolate (MeFH<sub>4</sub>) to homocysteine (Hcy) to form methionine with CH<sub>3</sub>Cbl as an enzyme-bound intermediate. The enzyme is thus a classical "ping-pong" enzyme in which two methyl transfer half-reactions, the transfer of a methyl group from MeFH<sub>4</sub> to cob(I)alamin to form enzyme-bound CH<sub>3</sub>-Cbl and the transfer of the methyl group of CH<sub>3</sub>Cbl to Hcy to form the product and regenerate cob(I)-alamin, constitute the reaction cycle (Scheme 21). Occasionally, the highly reactive cob(I)alamin intermediate becomes oxidized to cob(II)alamin, and the enzyme must be reactivated by reductive methylation with a ferridoxin reducing agent and S-adenosylmethionine (AdoMet). The enzyme from *E. coli* is a single polypeptide chain of 1227 amino acids with a calculated molar mass of 135 996 Da (not including the initiating Met residue which is removed in posttranslational processing) and containing a single, essential zinc ion. However, it has a very interesting modular structure in which binding domains for its various ligands are arranged sequentially across the amino acid sequence (Scheme 22). N-Terminal residues 2–353 constitute the Hcy binding domain, which contains the essential zinc ion ligated by three Cys residues (Cys247, Cys310, Cys311). This fragment has been expressed independently, and it catalyzes the methylation of Hcy by exogenous CH<sub>3</sub>-Cbl. Residues 354–649 make up the folate binding domain, which has not been independently expressed. However, the N-terminal half of the molecule, MetS-(2–649), catalyzed both methyl transfer half-reactions with exogenous cobalamins. Residues 650–896 make up the cobalamin binding domain, which can be generated by digestion of the protein with trypsin. The X-ray crystal structure of this fragment, the first ever determined for a Cbl-dependent protein, led to the discovery of the base-off/His-on binding mode.<sup>242</sup> Residues 897–1227 contain the AdoMet binding site and represent the activation domain of MetS. A fragment containing residues 2–896 catalyzes the overall reaction as well as full-length enzyme initially but slowly loses activity and cannot be reactivated by addition of AdoMet and a reducing agent. An X-ray structure of the activation domain has also appeared.<sup>344</sup>

Rat MetS has been expressed in insect cells using a baculovirus expression system.<sup>345</sup> The 140 kDa enzyme was purified 71-fold to homogeneity in 8% yield in five steps. The recombinant enzyme had a specific activity similar to that of purified rat liver

Scheme 21



Scheme 22



MetS and a UV-vis spectrum that resembled cob-(II)alamin. Incubation with Ti(III) citrate and AdoMet generated a  $\text{CH}_3\text{Cbl}$ -like spectrum.  $K_m$ 's for  $\text{MeFH}_4$  and Hcy were 89 and  $2.6 \mu\text{M}$ , respectively, and  $k_{\text{cat}}$  was  $4.5 \text{ s}^{-1}$ . The reaction depended absolutely on the presence of a reducing system ( $\text{H}_2\text{OCbl}^+/\text{DTT}$  or Ti(III) citrate) but not on the presence of AdoMet. However, in the absence of AdoMet the enzyme becomes inactivated ( $k_{\text{inact}} = 2.7 \times 10^{-3} \text{ s}^{-1}$ ). When the recombinant insect cells were cultured in the absence of added  $\text{B}_{12}$ , most (>90%) of the enzyme in the crude extract was apoenzyme. When this apoenzyme was incubated at  $37^\circ\text{C}$  for 15 min with no added  $\text{B}_{12}$ , >85% of the enzyme was unable to form holoenzyme with added  $\text{CH}_3\text{Cbl}$ . Apoenzyme reconstituted with  $\text{CH}_3\text{Cbl}^+$  had very little activity (4% of that of  $\text{CH}_3\text{Cbl}$ ), and incubation of the enzyme at  $37^\circ\text{C}$  for 5 min with a high concentration of  $\text{CH}_3\text{Cbl}^+$  (and no reducing agent) caused the loss of all activity. Methylcobinamide methyl phosphate, on the other hand, had 14% of the catalytic activity of  $\text{CH}_3\text{Cbl}$  but a  $K_m$  of  $2.5 \mu\text{M}$  (compared to  $0.34 \mu\text{M}$  for  $\text{CH}_3\text{Cbl}$ ). Apoenzyme reconstituted with  $\text{CH}_3\text{Cbl}$  or  $\text{H}_2\text{OCbl}^+$  reduced with Ti(III)-citrate had high activity, indicating that reduced Cbl's bind well to the apoenzyme. Several reconstitution experiments were performed in which the apoenzyme was incubated with a coenzyme analogue for 15 min at  $37^\circ\text{C}$  and then assayed for activity using the  $\text{H}_2\text{OCbl}^+/\text{DTT}$  reductant.  $\text{CH}_3\text{Cbl}$  was most effective at reconstituting holoenzyme,  $\text{H}_2\text{OCbl}^+$ -reconstituted enzyme was only slightly active, and  $\text{CNCbl}$ -reconstituted enzyme was inactive.  $\text{CH}_3\text{CH}_2\text{Cbl}$ ,  $\text{CH}_3\text{CH}_2\text{CH}_2\text{Cbl}$ , and  $\text{AdoCbl}$  failed to reconstitute active enzymes, but the activity was restored to the  $\text{CH}_3\text{CH}_2\text{Cbl}$ - and  $\text{CH}_3\text{CH}_2\text{CH}_2$ -

Cbl-reconstituted enzyme (but not to the  $\text{AdoCbl}$ -reconstituted enzyme) upon photolysis. The latter result suggests that  $\text{AdoCbl}$  does not bind to the enzyme.

While the  $\text{MetS}(2-649)$  fragment containing the Hcy and  $\text{MeFH}_4$  binding sites can catalyze both of the methyl transfer half-reactions with exogenous Cbl, these reactions are first order in Cbl and in enzyme and, consequently, cannot be directly compared to the zero order methyl transfers observed in intact MetS. Bandarian and Matthews<sup>346</sup> consequently constructed a fragment representing the other half of the enzyme,  $\text{MetS}(649-1227)$ , which contains the Cbl and AdoMet binding sites, and studied the interaction between these two "half" enzymes. Incubation of both fragments together reconstitutes the activity of MetS, and the rate of reaction is first order in each fragment with a second-order rate constant of  $4.7 \pm 0.4 \times 10^4 \text{ M}^{-1} \text{ s}^{-1}$ . To determine if both half-reactions can occur in a single encounter complex a  $\text{Cys310Ala}$  mutant of  $\text{MetS}(2-649)$ , which is impaired in catalyzing methyl transfer between Hcy and exogenous  $\text{CH}_3\text{Cbl}$  but not in catalyzing methyl transfer from  $\text{MeFH}_4$  to cob(I)-alamin, and an  $\text{Asp522Asn}$  mutant of  $\text{MetS}(2-649)$ , which is impaired in  $\text{MeFH}_4$  folate binding and cannot transfer methyl groups between cob(I)alamin and  $\text{MeFH}_4$  but has normal activity for the  $\text{CH}_3\text{Cbl}/\text{Hcy}$  methyl transfer, were employed. Equimolar mixtures of both mutants with the  $\text{MetS}(649-1227)$  fragment had the same MetS activity as mixtures of wild-type  $\text{MetS}(2-649)$  and  $\text{MetS}(649-1227)$ , but no activity could be observed when either mutant was omitted, demonstrating that the activity requires two encounters.

To determine the second-order rate constants for the two half-reactions, steady-state kinetics were measured in reaction mixtures containing  $\text{MetS}(649-1227)$  plus the  $\text{Asp522Asn}$  and  $\text{Cys310Ala}$   $\text{MetS}(2-649)$  mutants, one of which was fixed in concentration and the other varied. Thus, the rate

constant for demethylation of endogenous CH<sub>3</sub>Cbl by Hcy was determined to be  $1.34 \pm 0.2 \times 10^5 \text{ M}^{-1} \text{ s}^{-1}$ , and that for methylation of endogenous cob(I)alamin by MeFH<sub>4</sub> was determined to be  $7.0 \pm 0.6 \times 10^4 \text{ M}^{-1} \text{ s}^{-1}$ . These rate constants are 60- and 120-fold, respectively, larger than the rate constants for the two half-reactions with exogenous Cbl catalyzed by the MetS(2–649) fragment. A double-labeling experiment demonstrated that methylation of inactivated MetS(649–1227) by AdoMet had little effect on the measured rate constants. Comparing these results to nonenzymatic model systems shows that MetS(2–649) catalyzes demethylation of CH<sub>3</sub>Cbl by Hcy by some 10<sup>5</sup>–10<sup>9</sup>-fold and catalyzes the remethylation of cob(I)alamin by some 10<sup>5</sup>-fold.

During the catalytic cycle of MetS the highly reactive cob(I)alamin intermediate is occasionally oxidized to cob(II)alamin to form an inactive enzyme. Reduction by a flavodoxin and remethylation by AdoMet regenerates active enzyme, but this activity must be tightly controlled as there is strong discrimination against methylation by AdoMet, which results in a futile cycle hydrolyzing ATP rather than catalyzing the net synthesis of methionine. In the reactivation reaction the rate-determining step is the dissociation of the His759 axial ligand, which is followed by binding of flavodoxin, reduction of cob(II)alamin to cob(I)alamin, methylation by AdoMet, and re-coordination of His759.<sup>347</sup> This process has now been shown to be associated with a large protein conformational change that generates a structure capable of undergoing the reactivation reaction.<sup>348</sup> The C-terminal fragment, MetS(651–1227), which contains the Cbl and AdoMet binding domains and in which the axial ligand His759 has been mutated to Gly, has been crystallized in the cob(II)alamin form and subjected to X-ray diffraction. This mutant fragment, MetS(651–1227)His759Gly, dubbed the “activation complex”, is inactive in turnover but active in methylation of Cbl by AdoMet. In this structure the four-helix bundle that caps the Cbl in the structure of the Cbl binding fragment<sup>242</sup> moves 26 Å and rotates 63° to form a new interface between the Cbl and AdoMet binding domain, and the Cbl is displaced in a manner which would force the dissociation of its axial ligand. The corrin ring lifts, tilts, and slides, four hydrogen bonds between corrin side chain amides and the His759 loop are lost, and seven new hydrogen bonds are formed to the activation domain. Residues 1170–1174 act as a wedge to pry the Cbl from its normal binding site and the His759 loop so that the distance from His759 C<sub>α</sub> to the cobalt is increased by 2.3 Å. While crystallizations of the mutant fragment containing AdoMet were unsuccessful, addition of AdoMet to the crystals provided enough difference density to model its fit into the activation domain. However, crystal cracking and loss of resolution lead to a poor structure in which the methyl group of AdoMet is 6 Å from the cobalt. The authors suggest that AdoMet binding will induce further conformational changes in the protein that cannot be resolved in these crystals. The results provide excellent evidence for the major protein reorganizations that presumably must occur in order

for the Cbl to be able to react with three different substrates during the normal catalytic cycle and the reactivation process.

Since the Cbl in MetS must be able to react with three different substrates, a minimal model of the reaction cycle requires four conformational states, three for catalysis and one for reactivation by reductive methylation. The four-helix bundle that caps the Cbl binding site (state 1) must be displaced to allow the Hcy binding domain access to CH<sub>3</sub>Cbl to allow methyl transfer to form methionine (state 3). In turn, the Hcy binding domain must move away to allow access to the MeFH<sub>4</sub> binding domain for remethylation of cob(I)alamin (state 2). Finally, when cob(II)alamin is formed by oxidation, the AdoMet binding domain must be juxtaposed with the Cbl for reductive remethylation (state 4).

To study conformational equilibria in MetS, Bandarian, Ludwig, and Matthews<sup>349</sup> studied the state of axial ligation of the Cbl in various mutants and as a function of added protein ligands. In the wild-type C-terminal fragment of MetS (residues 649–1227) the axially coordinated His759 is hydrogen bonded to the carboxyl of Asp757 which in turn is hydrogen bonded to the hydroxyl of Ser810 (the so-called “ligand triad”). While the His759Gly mutant is inactive in substrate turnover, mutations in Asp757 and Ser810 decrease the rate of turnover by 27- and 1.5-fold, respectively. The UV–vis spectrum of wild-type MetS(649–1227) shows minimal changes with temperature, and comparison with spectra of base-on and base-off CH<sub>3</sub>Cbl gives an approximate value for the ligand equilibrium constant,  $K_{\text{eq}} = [\text{base-off}]/[\text{base-on}]$ , of 0.20 at 37 °C. The Asp757Glu mutant, however, undergoes a complete red/yellow spectral shift between 15 and 40 °C and has  $K_{\text{eq}} \approx 1$ , suggesting that it favors the base-off conformation and hence the reactivation conformation. However, the UV–vis spectrum of full-length MetS is not temperature dependent, and that of the full-length Asp757Glu mutant suggests a  $K_{\text{eq}}$  of about 0.14. The MetS(649–1227)Asp757Glu mutant does support methionine synthesis and reacts with the MetS(2–649) fragment (see above)<sup>346</sup> with a second-order rate constant of ca. 600, about 78-fold lower than that for wild-type MetS(649–1227).

The reactivation methylation by AdoMet leads to the formation of *S*-adenosylhomocysteine (AdoHcy). Binding of AdoHcy to MetS(649–1227)Asp757Glu and to “full-length” (actually residues 2–1227) MetSAsp757Glu increases the amount of base-off Cbl in a saturable manner as expected if AdoHcy binds preferentially to the reactivation conformation. The shift to the base-off species is less pronounced in the full-length mutant, suggesting that the additional conformations available in the full-length version are base-on when the Cbl is methylated. Addition of AdoHcy to the wild-type MetS(649–1227) fragment, but not to full-length wild-type enzyme, also shifts the Cbl to the base-off form. This again supports the presence of base-on states in the additional conformations available to the full-length protein. In contrast, and as expected due to the steric repulsions between the two methyl groups, addition of AdoMet

to the MetS(649–1227)Asp757Glu fragment with bound CH<sub>3</sub>Cbl leads to an increase in the base-on form ( $K_{\text{eq}}$  ca. 0.33). Thus, for the 649–1227 fragment the conformation can be shifted toward the reactivation conformation by AdoHcy and toward the base-on form by AdoMet.

Similarly, steric interactions between the methyl groups of MeFH<sub>4</sub> and CH<sub>3</sub>Cbl were expected to destabilize the state in which the MeFH<sub>4</sub> and Cbl binding domains are in close proximity. While neither AdoHcy alone nor MeFH<sub>4</sub> changed the spectrum of CH<sub>3</sub>Cbl bound to full-length wild-type MetS, when bound together the on/off equilibrium shifted to  $K_{\text{eq}} \approx 0.25$ . In contrast, the fraction of base-off species was increased both by AdoHcy and MeFH<sub>4</sub>, and when bound together ca. 62% of the base-off species was observed, the free energy changes associated with each of these ligands being additive.

Under the assumption that the ratio of states 1 and 4 is the same in full-length MetS and the C-terminal fragment 649–1227, approximate populations of the various states in wild-type and the Asp757Glu mutants in the presence and absence of MeFH<sub>4</sub> can be calculated. States 1 (ca. 25%) and 2 (ca. 58%) dominate in both wild-type and mutant MetS, as would be expected during turnover. Thus, MetS appears to be an ensemble of interconverting states, the distribution of which is altered by its various ligands, the oxidation and alkylation states of the Cbl, and the coordination state and strength of coordination of the His759 axial ligand to the cobalt.

The role of the axial ligand of CH<sub>3</sub>Cbl in the MetS reaction has been further investigated by comparison of the rates of both methyl transfer half-reactions catalyzed by the MetS(2–649) fragment with CH<sub>3</sub>Cbl and CH<sub>3</sub>Cbi<sup>+</sup>.<sup>350</sup> The reaction of cob(I)alamin with MeFH<sub>4</sub> was 2.7-fold faster than the reaction of cob(I)inamide, while the reaction of CH<sub>3</sub>Cbi<sup>+</sup> with FH<sub>4</sub> was 35-fold faster than the reaction of CH<sub>3</sub>Cbl. Thus, the free energy change for transfer of a methyl group from MeFH<sub>4</sub> to cob(I)alamin is 2.8 kcal mol<sup>-1</sup> more favorable than that for transfer to cob(I)inamide and the axial Bzm ligand contributes 0.6 kcal mol<sup>-1</sup> stabilization for the forward methyl group transfer and 2.2 kcal mol<sup>-1</sup> destabilization for the reverse reaction. Thus, the base-on/base-off switching seen during the catalysis of methyl group transfer by MetS probably does not play a major role in catalysis but may be much more important in controlling the distribution of enzyme conformations needed for catalysis.

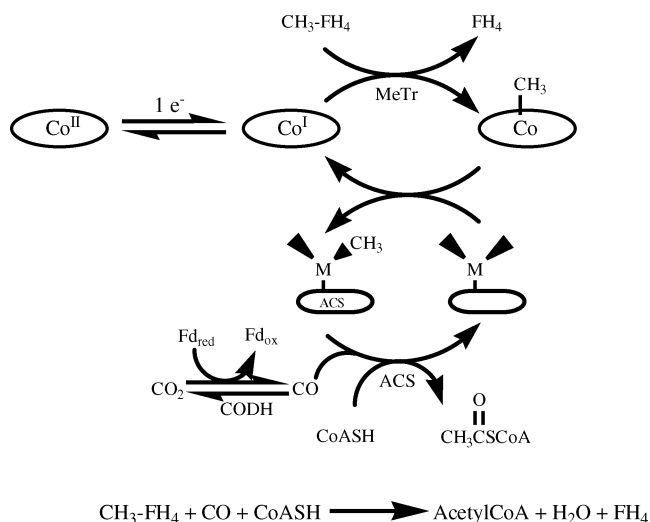
At some point during the demethylation of MeFH<sub>4</sub> the folate N5 must become protonated. Protonation prior to methyl group transfer would provide substantial activation for this reaction since nucleophilic methyl group transfer from tertiary amines is unknown and the folate anion is a very poor leaving group ( $\text{p}K_{\text{a}} > 30$ ). Smith and Matthews<sup>351</sup> used DEPT NMR to determine that MeFH<sub>4</sub> is protonated at N5 in solution and not at the conjugated carbon positions (C8a or C2) with a  $\text{p}K_{\text{a}}$  of  $5.3 \pm 0.1$ . Using phenol red as an indicator MetS(2–649) was shown not to release a proton upon binding of MeFH<sub>4</sub> at pH 7.6, as already known for full-length MetS.<sup>352</sup> Protonation

of MeFH<sub>4</sub> in solution is accompanied by the formation of a shoulder at 264 nm and a decrease in absorption at 290 nm. Very different spectral changes (a small red shift and a modest increase in absorbance at 308 nm) accompany the binding of MeFH<sub>4</sub> to MetS(2–649) which are instead similar to those accompanying the transfer of MeFH<sub>4</sub> from aqueous solution to 80% acetonitrile at pH 7.2. Hence, MeFH<sub>4</sub> is not protonated upon binding to MetS. The absorbance changes upon binding MeFH<sub>4</sub> to MetS(2–649), which are nil at low pH, show a titration curve with a  $\text{p}K_{\text{a}}$  of 5.1, slightly lower than the  $\text{p}K_{\text{a}}$  of free MeFH<sub>4</sub>, and indicate that MetS preferentially binds deprotonated MeFH<sub>4</sub>.

The authors propose that in the absence of prior protonation of MeFH<sub>4</sub> at N5 for activation for nucleophilic substitution the methylation of cob(I)alamin at the active site actually occurs via an oxidative addition of MeFH<sub>4</sub> to cob(I)alamin, which requires the formation of a three-centered bond between N5, the MeFH<sub>4</sub> methyl carbon, and the cobalt and leads to an intermediate which is a six-coordinate Co(III) complex but with no  $\alpha$  axial ligand (presumably, the His residue which is not coordinated in the cob(I)alamin state remains uncoordinated) and two  $\beta$  face ligands. This is clearly problematic from a steric point of view. Assuming that the protein can avoid steric complications due to the axially “upward” projecting  $\alpha$ ,  $c$ , and  $g$  side chains, considerable flexibility of the corrin ring would be needed to accommodate the three-centered intermediate as well as the intermediate with two  $\beta$  face ligands. Although molecular dynamics simulations<sup>89</sup> show that the corrin ring of Cbl’s is very flexible indeed, it is not clear that such flexibility is maintained when a Cbl is tightly bound to an enzyme active site. In addition, as the authors point out, chiral methyl analysis has shown that the overall MetS reaction occurs with net retention of the methyl group configuration,<sup>353</sup> which has generally been assumed to indicate two sequential inversions resulting from an S<sub>N</sub>2 mechanism for both methyl transfer steps. Since the oxidative addition of MeFH<sub>4</sub> to cob(I)alamin would occur with net retention of the methyl configuration, this would require that the demethylation of CH<sub>3</sub>Cbl by Hcy also occurs with retention (presumably via another oxidative addition). The question could thus be answered unambiguously by use of chiral methyl analysis on either MetS half-reaction.

MetS is known to contain an essential zinc ion liganded to three cysteine residues (Cys310, Cys311, Cys247) and a fourth ligand believed to be a water molecule.<sup>354</sup> Addition of Hcy leads to a zinc ion liganded by four sulfur ligands and is accompanied by release of a proton at pH 7.8,<sup>352</sup> suggesting that Hcy binds as its thiolate and that the zinc ion acts as a Lewis acid catalyst. The binding of Hcy to MetS(2–649) has now been shown to occur with a large increase in molar absorptivity at 236 nm at pH 8.5, indicating that it is indeed bound as its thiolate.<sup>355</sup> Below pH 7.5 the binding constant for Hcy increases with increasing pH, consistent with the release of a proton, but above this pH the binding constant is pH

Scheme 23



independent, indicating that a group on the protein has become deprotonated, consistent with the ionization of a zinc-bound water molecule. The pK<sub>a</sub> of the zinc-bound Hcy must be below 6, so that it is present as its reactive thiolate form at neutral pH.

While MetS does not bind protonated MeFH<sub>4</sub>, MeFH<sub>4</sub> has now been found to be protonated in the ternary complex of MetS(2–649) with cob(D)alamin and MeFH<sub>4</sub>.<sup>355</sup> While the reaction of MetS(2–649) with exogenous cob(D)alamin is first order in both Cbl and protein, it shows saturating behavior with respect to MeFH<sub>4</sub>, and similarly, the reaction of MetS(2–649) with CH<sub>3</sub>Cbl and FH<sub>4</sub> is first order in protein and CH<sub>3</sub>Cbl but saturates with respect to FH<sub>4</sub>. In saturating MeFH<sub>4</sub> the second-order rate constant for CH<sub>3</sub>Cbl formation decreases from about 9000 M<sup>-1</sup> s<sup>-1</sup> at low pH to about 100 M<sup>-1</sup> s<sup>-1</sup> at pH 9, and the reverse reaction has the opposite pH–rate profile, increasing to about 95 M<sup>-1</sup> s<sup>-1</sup> at high pH. These results show that the pH dependence arises in the ternary complex prior to or along with release of the first product, although they do not distinguish between a proton bound to MeFH<sub>4</sub> or a general acid catalyst on the protein.

A corrinoid-dependent methyl transferase, the corrinoid iron–sulfur protein (CoFeSP) in *C. thermoacetatum*, an 88 kDa heterodimeric protein containing a 5-methoxybenzimidazolylcobamide cofactor, participates in two methyl transfer steps in the Wood–Ljungdahl pathway which allows the organism to form three molecules of acetylCoA from a single glucose molecule. In the first reaction MeFH<sub>4</sub> is demethylated to form a CoFeSP-bound methylcobalt corrinoid (CH<sub>3</sub>–CoFeSP) in a reaction catalyzed by MeFH<sub>4</sub>/CoFeSP methyltransferase (MeTr). The corrinoid methyl group is then transferred from CoFeSP to carbon monoxide dehydrogenase/acetylCoA synthase (CODH/ACS), where acetylCoA is formed from this methyl group, CO, and coenzyme A (CoASH) (Scheme 23). It was suspected that the Co<sup>I</sup> corrinoid intermediate would occasionally oxidize and need to be re-reduced for activity to continue. The large (55 kDa) subunit of CoFeSP contains a [4Fe–4S] cluster which in the Cys20Ala mutant of CoFeSP<sup>356</sup> is converted to a 3Fe cluster with a substantially less

negative midpoint potential (–31 compared to –523 mV). The mutant's ability to be activated by reductants including CODH/ACS and ferredoxin was severely reduced, leading to the suggestion that reductive reactivation of Co<sup>II</sup>FeSP occurs via its iron–sulfur cluster. When the synthesis of acetylCoA from MeFH<sub>4</sub>, CO, and CoASH was studied using methylated, wild-type CoFeSP, the reaction continues linearly until the limiting reagent (CO) is consumed.<sup>357</sup> However, the Cys20AlaCoFeSP mutant initially catalyzes acetylCoA synthesis at the same rate as wild type, but its activity then decreases and becomes negligible after ca. 100 turnovers. Inactivation rate constants were inversely proportional to [CoFeSP], and the reactivation rate constant for the mutant protein (1.5 × 10<sup>-3</sup> s<sup>-1</sup>) was 4000-fold slower than that for wild type (0.88 s<sup>-1</sup>), demonstrating that reductive reactivation is required to maintain activity and that the mutant, due to its high potential Fe–S cluster, cannot accept reducing equivalents from the physiological electron donors.

Methyl group transfer from CoFeSP leads to methylation of a low potential metal center believed to be a nickel ion<sup>358</sup> on ACS. In single-turnover experiments with CODH/ACS, CoASH, and CO<sup>359</sup> the Cys20AlaCoFeSP mutant in the methyl–Co<sup>III</sup> corrinoid form underwent spectral changes indicating complete conversion to the Co<sup>I</sup>–corrinoid form, suggesting that the methyl transfer is not a radical process with the mutant protein.

Like all corrinoid-dependent methyl transferases, the CoFeSP/CODH/ACS system can utilize methyl groups from exogenous methylcorrinoids. However, unlike many such proteins, the CoFeSP's lack the consensus Asp-x-His-x-x-Gly sequence indicating base-off/His-on binding and apparently bind the corrinoid base-off.<sup>356,360</sup> Ragsdale and co-workers<sup>361</sup> have now studied the influence of the axial base on the reaction with exogenous methylcorrinoid methyl donors. In the presence of CoASH, CO, and CODH/ACS, exogenous CH<sub>3</sub>Cbl proved to be a poor methyl donor with a second-order rate constant for acetylCoA formation of <0.12 M<sup>-1</sup> s<sup>-1</sup>. In contrast, CH<sub>3</sub>Cbi<sup>+</sup> and methyl-(3,5,6-trimethylbenzimidazolyl)cobamide (CH<sub>3</sub>Me<sub>3</sub>BzmCbl, Figure 1), in which the axial Bzm ligand is methylated at NB3 and incapable of coordinating to the metal, were at least 1500-fold more reactive (*k*<sub>2</sub> = 200 and 190 M<sup>-1</sup> s<sup>-1</sup>, respectively). Compared to methylated CoFeSP, exogenous CH<sub>3</sub>Cbl transfers its methyl group to CODH/ACS 10<sup>5</sup>-fold more slowly, with 10<sup>3</sup> of this apparently due to the base-off conformation of the protein-bound methylcorrinoid. In addition, the rate constant for reduction of exogenous cob(II)inamide by CODH (CO is the reducing agent), 1.3 × 10<sup>5</sup> M<sup>-1</sup> s<sup>-1</sup>, is 10<sup>4</sup>-fold larger than that for cob(II)alamin (11 M<sup>-1</sup> s<sup>-1</sup>) and 2-fold larger than the rate of reduction of Co<sup>II</sup>FeSP.

Ragsdale and co-workers<sup>362</sup> also studied the kinetics of the methyl transfer from (6S)-MeFH<sub>4</sub> to the CoFeSP protein catalyzed by the methyl transferase (MeTr). While the pH dependence of *k*<sub>cat</sub>/*K*<sub>m</sub> for each of the substrates of MeTr show apparent pK<sub>a</sub>'s of 5.0–5.3, the pK<sub>a</sub> of MeFH<sub>4</sub> bound to MeTr is 5.8,<sup>363</sup> suggesting a rate-limiting ionization of MeTr rather

than MeFH<sub>4</sub>. Consistent with this was the previous demonstration of pH-dependent fluorescence quenching of MeTr with an apparent pK<sub>a</sub> of 5.0, suggesting a pH-dependent conformational change.<sup>364</sup> Measurement of the steady-state kinetics with saturating [MeFH<sub>4</sub>] and varying [CoFeSP] showed that K<sub>m</sub> was pH independent but that k<sub>cat</sub> and k<sub>cat</sub>/K<sub>m</sub> had pH dependencies with apparent pK<sub>a</sub>'s of 5.6 and 5.1, respectively, demonstrating that the pH dependence of the reaction is due to ionizations in the ternary complex. The dissociation constant for CoFeSP, 8 μM, measured by single-turnover stopped flow experiments, is very close to K<sub>m</sub> for CoFeSP. Since this is also the case for MeFH<sub>4</sub>, the substrates bind to MeTr independently. Product inhibition studies showed that the substrates bind randomly and that dead-end complexes, MeTr–MeFH<sub>3</sub>–CH<sub>3</sub>–CoFeSP and MeTr–CoFeSP–FH<sub>4</sub>, are not formed. Single-turnover stopped flow measurements in the forward (Co<sup>I</sup>-FeSP disappearance) and reverse (CH<sub>3</sub>–CoFeSP disappearance) directions as a function of pH gave rate constants and pK<sub>a</sub> values for the pre-steady-state phases of the reaction. These were consistent with a pH-dependent conformational change in the ternary complex and suggested that substrate binding raises the pK<sub>a</sub> for this conformational change slightly. In addition, the amplitudes for the forward reaction decrease with pH while those of the reverse reaction increase with pH, consistent with protonation of bound MeFH<sub>4</sub> in the forward reaction and deprotonation of bound FH<sub>4</sub> in the reverse reaction. Individual rate constants from the single-turnover experiments were used to simulate steady-state progress curves and evaluate all of the rate constants for the reaction.

An X-ray crystal structure of the MeTr from *C. thermoacetivum* has now appeared.<sup>365</sup> The protein, crystallized with no ligands, is a homodimer of 28 kDa subunits, each of which is organized as a TIM barrel. The tertiary structure is very similar to those of dihydropteroate synthases despite the less than 20% amino acid identity between these proteins and MeTr. The structural homology allows the MeFH<sub>4</sub> binding site to be modeled. The main difference between the dihydropteroate synthases and the MeTr is in the loop structure above the barrel, which contains the active site. In MeTr there is a solvent-exposed 3<sub>10</sub> helix and a wider open space, which has been modeled as the binding site for exogenous cobalamin or the corrinoid of CoFeSP. In the ternary complex model the corrin binds at the C-terminal opening of the barrel and closes off the active site.

The acetylCoA synthase (ACS) of *C. thermoacetivum* is a Ni–Fe–S-containing protein that undergoes the reversible methyl group transfer with CH<sub>3</sub>–CoFeSP shown in eq 28. The product CH<sub>3</sub>–ACS<sub>ox</sub> goes on to react with CO and CoASH to form acetylCoA. A novel Ni–X–Fe<sub>4</sub>S<sub>4</sub> site (the A cluster) accepts the methyl group.<sup>366</sup> It has been proposed that a redox-active Cys pair (the D-site) must be reduced for methylation to occur. There is considerable evidence that ACS becomes methylated on the nickel ion of the A cluster,<sup>358</sup> so that ACS<sub>red</sub> is likely to be {Ni<sup>2+</sup>D<sub>red</sub>} and CH<sub>3</sub>–ACS<sub>ox</sub> is likely to be {CH<sub>3</sub>–

Ni<sup>2+</sup>D<sub>ox</sub>}. Lindahl and co-workers<sup>367</sup> have now reported a thorough stopped flow kinetic study of the reaction in eq 28 using various reductants (Ti(III) citrate, dithionite, and CO) to reduce ACS to ACS<sub>red</sub>. The simplest mechanism consistent with the data involves formation of the binary complex [CH<sub>3</sub>–CoFeSP:ACS<sub>red</sub>] followed by methyl group transfer to form the product binary complex and then product complex dissociation along with the formation of a nonproductive state, [ACS<sub>red</sub>–CO], by binding of CO with a K<sub>d</sub> of about 180 μM. The nonnatural reductants, Ti(III) citrate and dithionite, inhibited the reaction, possibly by reducing the D-site of CH<sub>3</sub>ACS<sub>ox</sub>, which is oxidized by 2 e<sup>–</sup> when the methyl group is received and reduced by 2 e<sup>–</sup> in the reverse process. Values for the dissociation constants for the reactant and product binary complexes were 0.12 and 0.3 μM, respectively, and the rate constants for the forward and reverse methyl group transfer within the binary complexes (6.9 and 3.0 s<sup>–1</sup>, respectively) give an equilibrium constant for intracomplex methyl transfer of 2.3 ± 0.9. The latter value implies that the {Ni<sup>2+</sup>D<sub>red</sub>} reagent is as nucleophilic as cob(I)alamin.



The N<sup>5</sup>-methyltetrahydromethanopterin (CH<sub>3</sub>–H<sub>4</sub>-MPT):coenzyme M (CoMSH) methyltransferase of *Methanobacterium thermoautotrophicum* is a membrane-bound complex of eight proteins (MtrA–H) which couples the exergonic methyl group transfer to the establishment of a sodium ion gradient across the cytoplasmic membrane.<sup>368</sup> The complex contains tightly bound 5'-hydroxybenzimidazolylcobamide and catalyzes its methylation by CH<sub>3</sub>–H<sub>4</sub>MPT and the subsequent demethylation by CoMSH. It also catalyzes the methylation and demethylation of exogenous cob(I)alamin, the demethylation being stimulated 5-fold by sodium ions with a K<sub>m</sub> of 50 μM.<sup>369</sup> MtrA, a 23 kDa protein, contains the corrinoid cofactor, which is bound in the base-off/His-on mode, with His84 as the axial ligand, although it lacks the consensus Asp-x-His-x-x-Gly sequence characteristic of this binding mode.<sup>370</sup> Hippler and Thauer<sup>371</sup> have now reported that the 34 kDa subunit MtrH contains the CH<sub>3</sub>–H<sub>4</sub>MPT binding site and catalyzes the methylation of the MtrA corrinoid cofactor. The methyltransferase complex was purified from the membrane fraction of *M. thermoautotrophicum* with the MtrA–G complex and MtrH purifying separately. The MtrA–G complex could not catalyze the overall reaction but could catalyze the transfer of a methyl group from CH<sub>3</sub>Cbl to CoMSH. The MtrH subunit catalyzed the methylation of cob(I)alamin but could not catalyze the other half-reaction or the overall reaction. However, the purified MtrH subunit catalyzed the methylation of cob(I)alamin with CH<sub>3</sub>–H<sub>4</sub>-MPT at a significantly lower rate than did the MtrA–H complex, possibly due to a cooperative effect of the other subunits, as shown for other such methyltransferase complexes (see below).

The methylation of coenzyme M (CoMSH) by methanol is the first step in the fermentation of methanol by the methanogenic archaean *Methanosa-*

*rscina barkeri*, which can grow on methanol as a sole energy source. The methanol/CoMSH methyltransferase of *M. barkeri* consists of three proteins, MtaA, MtaB, and MtaC, the latter of which is a 27.9 kDa corrinoid protein containing 1 equiv of bound 5-hydroxybenzimidazolylcobamide. The corrinoid protein MtaC is methylated by methanol in a reaction catalyzed by MtaB, and the methylated MtaC (CH<sub>3</sub>-MtaC) is subsequently demethylated by CoMSH in a reaction catalyzed by MtaA.<sup>372</sup> In MtaC the corrinoid is bound in the base-off/His-on mode with His136 supplying the axial ligand. MtaB, a 50.7 kDa zinc protein, can also catalyze the reversible methylation of exogenous cob(I)alamin by methanol,<sup>373</sup> and MtaA, a 35.9 kDa zinc protein, can also catalyze the methylation of CoMSH by exogenous CH<sub>3</sub>Cbl.<sup>374</sup> Sauer and Thauer<sup>375</sup> have now shown that exogenous Cbl can substitute for MtaC in the complex and that both MtaB and MtaA are involved in binding exogenous Cbl. The kinetics of the net formation of CoMSCH<sub>3</sub> from methanol and CoMSH in the presence of MtaB, MtaA, and cob(I)alamin (from reduction of H<sub>2</sub>OCbl<sup>+</sup> with Ti(III) citrate) followed Michaelis-Menton kinetics with an apparent  $K_m$  for cob(I)alamin of <100 nM (approximately the same as that for MtaC). At saturation the  $V_{max}$  with cob(I)alamin was about one-half that with MtaC and the  $K_m$  for methanol was about 40 mM with either. In reactions with cob(I)alamin, methanol, and MtaB the specific activity of MtaB increased linearly with increasing [cob(I)alamin], so that the apparent  $K_m$  was >0.2 mM for cob(I)alamin. When MtaA was added, the apparent  $K_m$  for cob(I)alamin was reduced to 2.5 μM, although  $V_{max}$  and the  $K_m$  for methanol were unchanged. The effect of MtaA on the catalytic efficiency of MtaB saturated at an MtaA concentration such that the molar ratio of MtaB to MtaA was about 2:1. This half-reaction required the presence of Ti(III) citrate. Similarly, in reactions containing CoMSH, CH<sub>3</sub>Cbl, and MtaA the activity of MtaA increased linearly with [cob(I)alamin] concentration, so that the apparent  $K_m$  for cob(I)alamin is >0.2 mM. However, with added MtaB and methanol the  $K_m$  for cob(I)alamin decreased to 3 μM. Again, maximal MtaA activity was attained when the MtaB concentration gave a molar ratio of MtaB to MtaA of about 2:1. This half-reaction did not require Ti(III) citrate but was stimulated by it, and the effect was due to a decrease in the  $K_m$  for CH<sub>3</sub>Cbl rather than an increase in  $V_{max}$ . Consequently, it appears that both MtaA and MtaB are required for actual binding of exogenous Cbl's.

Cob(D)inamide was completely inactive in the overall methylation of CoMSH with methanol catalyzed by MtaB and MtaA unless imidazole (Im) was present, with half-maximal activity occurring at [Im] ca. 1mM. Similar results were obtained for the MtaB-catalyzed half-reaction, i.e., the methylation of cob(I)inamide by methanol, and its reverse. However, the results were completely different with the other half-reaction, the MtaA-catalyzed demethylation of CH<sub>3</sub>Cbl<sup>+</sup> by CoMSH. Here, CH<sub>3</sub>Cbl<sup>+</sup> was active without added Im, and in fact, Im inhibited the reaction with half-maximal inhibition occurring at about 0.2 mM Im. In fact, the specific activity of MtaA with CH<sub>3</sub>Cbl<sup>+</sup>

was about 40-fold higher than that with CH<sub>3</sub>Cbl. However, at these concentrations of Im UV-vis spectroscopy confirmed that only a few percent of CH<sub>3</sub>Cbl<sup>+</sup> was present as CH<sub>3</sub>(Im)Cbl<sup>+</sup>, and so the observed inhibition is difficult to rationalize.

Thus, in the MtaABC complex cob(I)alamin can substitute for MtaC and both the MtaA and MtaB subunits contribute to Cbl binding, each individual subunit being incapable of binding Cbl but reacting with it in a first-order manner. This suggests that the MtaAB complex interacts with exogenous Cbl in the same way it interacts with the corrinoid of the MtaC subunit.

*Methanosarcina barkeri* can also generate methane from other substrates, including methylated thiols and methylamines. In all cases the substrate methyl group is transferred to CoMSH and then converted to methane using reducing equivalents obtained by oxidation of the methyltrophic substrate to CO<sub>2</sub>. Trimethylamine is sequentially demethylated to form dimethylamine and methylamine as intermediates, both of which can serve as sole carbon and energy sources. The methylation of CoMSH for all of the methylamines is catalyzed by MtbA, a 37 kDa methylcorrinoid:CoMSH methyltransferase, which does not contain a corrinoid cofactor.<sup>376</sup> Krzycki and co-workers<sup>377</sup> reported the isolation of a corrinoid-containing protein, MtbC, which stimulates methyl transfer from dimethylamine to CoMSH in cell free extracts. MtbC co-purifies with MtbA from *M. barkeri* cells grown on trimethylamine but is separable on a hydrophobic interaction column. The 24 kDa protein, purified aerobically, contained 1 equiv of corrinoid and had a UV-vis spectrum characteristic of H<sub>2</sub>OCbl<sup>+</sup>. Addition of MtbC to cell-free extracts stimulated the methylation of CoMSH by dimethylamine but not that by trimethylamine or methylamine. MtbC and MtbA were used in an assay to purify a specific dimethylamine:MtbC methyltransferase, dubbed MtbB1, from extracts of trimethylamine-grown cells. MtbB1 was purified 35-fold to homogeneity in 19% yield as a 51 kDa polypeptide on SDS-PAGE (with a native mass of 230 kDa on size exclusion chromatography) devoid of a corrinoid cofactor. MtbB1 supported methylation of CoMSH by dimethylamine but not by trimethylamine or methylamine in the presence of MtbA, MtbC, and a Ti(III) citrate/methyl viologen activating system, and MtbC could not be replaced by HOCbl. However, MtbB1 was found to methylate exogenous cob(I)alamin (from HOCbl + Ti(III) citrate) as well as the corrinoid cofactor of MtbC with dimethylamine as the methylating agent. The methyl transfer system for dimethylamine is thus analogous to that for methylamine; each utilizes MtbA, the methylcorrinoid:CoMSH methyltransferase, but a methylamine-specific methyltransferase and a corrinoid protein. Thus, only the use of MtbB1 and MtbC (with MtbA) gave methylation of CoMSH with dimethylamine as the methyl donor, and only the combination of the analogous methylamine proteins, MtmB and MtmC<sup>378</sup> (along with MtbB), allowed CoMSH methylation by methylamine. Similarly, there was no cross-reactivity for the methylation of the corrinoid pro-

teins, MtbC or MtmC, with their methylamine substrates catalyzed by MtbB1 or MtmB.

*Methanosarcina* species are also capable of methanogenesis from methylated thiols including dimethyl sulfide and methylmercaptopropionate. As with other methanogenic substrates, the *S*-methyl group is transferred to CoMSH. In *M. barkeri* a 480 kDa corrinoid-containing protein comprised of 40 kDa (MtsA) and 30 kDa (MtsB) subunits catalyzes the transfer of methyl groups from methylated thiol to CoMSH.<sup>379</sup> Activity staining experiments demonstrated that MtsA catalyzes the transfer of methyl groups from CH<sub>3</sub>Cbl to CoMSH while MtsB is the suspected corrinoid protein.<sup>380</sup> This two-component system contrasts with the three-component systems (i.e., a corrinoid protein and two methyltransferases) involved in the methylation of CoMSH with methanol, dimethylamine, or methylamine. However, the two components of the methylthiol:CoMSH methyltransferase have not been successfully separated as active proteins. Consequently, Krzycki and co-workers<sup>381</sup> cloned *M. barkeri* MtsA in *E. coli*. The purified protein has a molar mass of 77 kDa (by size exclusion chromatography) and a subunit mass of 41 kDa (by SDS-PAGE), indicating a homodimeric configuration. It contains 1.06 equiv of zinc, no detectable corrinoid cofactor by UV-vis spectroscopy, and no detectable Co by plasma emission spectroscopy. It catalyzes the transfer of a methyl group from exogenous CH<sub>3</sub>Cbl to CoMSH, but unlike other such methyltransferases, the kinetics are not first order in CH<sub>3</sub>Cbl. Instead, CH<sub>3</sub>Cbl displayed an apparent  $K_m$  of 5.5 mM, and the  $K_m$  for CoMSH was 11 mM. MtsA also catalyzed the methylation of cob(I)alamin (from Ti(III) citrate reduction of HOCbl) by dimethyl sulfide with the concomitant formation of methanethiol. The apparent  $K_m$  for dimethyl sulfide was 33 mM, although the kinetics were first order with respect to cob(I)alamin up to 2.5 mM. The equilibrium constant for the conversion of dimethyl sulfide and cob(I)alamin to CH<sub>3</sub>Cbl and methanethiol was  $5.4 \pm 0.4 \times 10^{-4}$ . There was no cross-reactivity with the methylamine-specific CH<sub>3</sub>Cbl:CoMSH methyltransferase, which did not catalyze methyl transfer from dimethyl sulfide to cob(I)alamin. MtsA also catalyzed the methylation of CoMSH with dimethyl sulfide in the presence of cob(I)alamin, but the methylamine-specific CoMSH methyltransferase, MtbA, was unable to do so. Dimethyl sulfide was found to be a competitive inhibitor of the methylation of CoMSH by CH<sub>3</sub>Cbl with a  $K_i$  value of 14.2 mM, suggesting that dimethyl sulfide and CoMSH compete for a single active site.

Some acetogenic bacteria can also grow on methoxyaromatics, such as vanillate and syringate, derived from the depolymerization of lignin. These organisms do not utilize the aromatic ring but transfer the methoxy methyl group to FH<sub>4</sub> and subsequently oxidize it to acetylCoA via the Wood-Ljungdahl pathway. *Moorella thermoacetica*, an organism that can metabolize at least 20 such substrates, expresses a 22 kDa protein with aromatic *O*-demethylase activity when grown on these compounds.<sup>382</sup> Naidu and Ragsdale<sup>383</sup> found that extracts

of *M. thermoacetica* cells grown on dicamba (3,6-dichloro-2-methoxybenzoate) could demethylate dicamba but also vanillate (3-methoxy-4-hydroxybenzoate), which is converted to protocatechuate (which is subsequently converted to catechol). Purification of the *O*-methyltransferase resulted in the copurification of three proteins, dubbed MtvA, MtvB, and MtvC. The demethylation reaction requires a reductant, such as Ti(III) citrate, and FH<sub>4</sub> and had maximal activity at 55 °C and pH 6.6, and exogenous HOCbl or CH<sub>3</sub>Cbl could substitute for the MtvC protein. The apparent  $K_m$  values for dicamba and vanillate were 9.0 mM and 85 μM, and the maximal activity with vanillate was three times as high as that for dicamba, leading to a 350-fold  $V_{max}/K_m$  preference for vanillate, despite the fact that the cells were grown on dicamba.

Purified MtvB is a homodimer with a subunit molar mass of 48 kDa and is a colorless protein lacking any metal cofactors. It catalyzes the transfer of the methyl group of vanillate to cob(I)alamin with the concomitant formation of protocatechuate. MtvC is a monomeric 22 kDa protein containing 0.8 equiv of cob(II)alamin as purified. The EPR spectrum of this form displayed triplet superhyperfine coupling indicative of axial coordination of a nitrogen donor, but it is not known if this results from base-on binding or from substitution of an N-donor axial ligand from a protein amino acid residue. Reduction of MtvC with Ti(III) citrate leads to the formation of protein-bound cob(I)alamin, as identified by its characteristic UV-vis spectrum. MtvA is a 29.5 kDa protein based on SDS-PAGE which lacks any detectable chromophores. It catalyzed the demethylation of CH<sub>3</sub>Cbl by FH<sub>4</sub> but had no activity for the demethylation of vanillate or dicamba by cob(I)alamin. Surprisingly, the spectroscopically identified product of the demethylation of CH<sub>3</sub>Cbl is cob(II)alamin, which the authors attribute to oxidation of the anticipated cob(I)alamin product, but clearly on the bases of these experiments, a radical mechanism for this methyl transfer cannot be ruled out.

A similar, but distinct, *O*-demethylase, which demethylates 1,2-dimethoxybenzene (veratrol) and 3-methoxyphenol, can be obtained from *Acetobacterium dehalogenans*, another acetogenic methylotrophic bacterium which can metabolize the methyl groups of lignin-derived aromatic methyl ethers via MeFH<sub>4</sub> to acetylCoA. Extracts of cells grown on vanillate or 3-methoxyphenol showed a different pattern of *O*-demethylase activity with various methoxybenzene substrates, suggesting that more than one inducible *O*-demethylase could be produced.<sup>384</sup> In particular, 1,2-dimethoxybenzene, which is not a substrate for the vanillate-*O*-demethylase from *A. dehalogenans*,<sup>385</sup> was rapidly demethylated by extracts of the 3-methoxyphenol-grown cells. The veratrol *O*-demethylase purified from these cells required three proteins, CP1 (corrinoid protein 1), MTI<sub>ver</sub> (methyltransferase 1, veratrol demethylating), and Odm-RF (*O*-demethylase reconstituting fraction) plus ATP and reducing equivalents in order to catalyze the methyl transfer from 1,2-dimethoxybenzene to FH<sub>4</sub>. CP1 was a corrinoid-containing protein apparently distinct from the

corrinoïd protein from the vanillate *O*-demethylase system, although the latter could be (and was due to the small amount of CP1 in the cell extract) substituted for CP1 in the 1,2-dimethoxybenzene *O*-demethylase assay. A third distinct corrinoïd protein, CP2, was also isolated and purified to homogeneity, but it could not replace CP1 in either the veratrol or vanillate *O*-demethylase assays. MTI<sub>ver</sub> is a 32 kDa protein devoid of any cofactors which can catalyze the transfer of a methyl group from 1,2-dimethoxybenzene to CP1 or the corrinoïd protein from the vanillate *O*-demethylase. It catalyzed the demethylation of 1,2-dimethoxybenzene, 2- and 3-methoxyphenol, 3,4-dimethoxybenzoate, and 1-chloro-2-methoxybenzene at comparable rates but did not demethylate vanillate or 2- or 3-methoxybenzoate.

*Methylobacterium* sp. strain CM4 can grow on chloromethane as both a sole carbon and energy source. Leisinger and co-workers<sup>386</sup> sequenced two DNA fragments to which the transposon insertion sites of six mutants of this strain, which cannot grow in chloromethane, mapped. Using sequence analysis, the properties of various mutants, and enzymatic activities in cell-free extracts, the authors defined a pathway for the conversion of chloromethane to formate. The CmuA protein catalyzes the methylation of a corrinoïd-containing protein by chloromethane. Subsequently, the transfer of the corrinoïd-bound methyl group to FH<sub>4</sub> is catalyzed by CmuB. Both proteins show sequence similarities to methyltransferases of other methanogenic archaea. The C-terminal part of CmuA also shares similarities with corrinoïd binding proteins, suggesting it is a bifunctional protein with two domains that are generally expressed as separate proteins in other methanogens.

The *cmuB* gene was subsequently cloned and overexpressed in *E. coli*, and the recombinant CmuB protein was purified 4.3-fold to homogeneity in 39% yield by a combination of hydrophobic and anion-exchange chromatography.<sup>387</sup> The purified protein had an apparent molar mass of 66 kDa, suggesting a homodimer of the 33.3 kDa protein predicted from the *cmuB* gene sequence. CmuB catalyzes the conversion of exogenous CH<sub>3</sub>Cbl and FH<sub>4</sub> to cob(I)alamin and MeFH<sub>4</sub> with an apparent  $K_m$  for FH<sub>4</sub> (at 0.2 mM CH<sub>3</sub>Cbl) of  $240 \pm 10 \mu\text{M}$  and the reverse reaction with an apparent  $K_m$  (at 0.2 mM cob(I)alamin) for MeFH<sub>4</sub> of  $12.5 \pm 1 \text{ mM}$ . In both directions the reaction was first order in exogenous Cbl (up to 2 mM), suggesting that the physiological substrate is actually a corrinoïd protein as in other corrinoïd-dependent methyltransferases.

This was subsequently shown to be correct by the purification of the CmuA protein.<sup>388</sup> *Methylobacterium* sp. strain CM4 grown on chloromethane and [<sup>57</sup>Co]CoCl<sub>2</sub> was shown to contain endogenous corrinoïds, the majority co-chromatographing with CNCbl. CmuA was purified 29-fold to apparent homogeneity in 3.7% yield by a combination of ammonium sulfate precipitation and hydrophobic and anion-exchange chromatography. The purified protein had a native molar mass of 67 kDa (by gel filtration), migrated as a single band on SDS-PAGE

with an apparent mass of 66 kDa, and had a calculated mass of 66 988 deduced from the sequence of the *cmuA* gene. MALDI-TOF MS showed a prominent peak at 1329.3 amu, corresponding to CNCbl, and ICP-MS showed 0.68 mol of cobalt and 0.89 mol of zinc per mol of purified protein. The UV-vis spectrum of the purified protein resembled that of cob(II)alamin and on reduction with Ti(III) citrate converted to a cob(I)alamin-like spectrum.

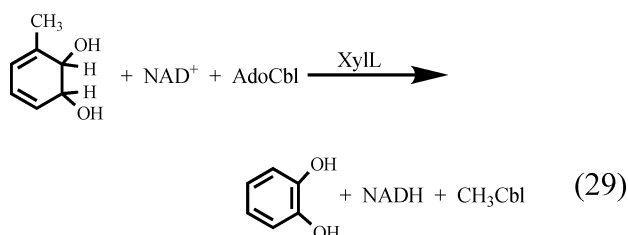
Purified CmuA and CmuB, only in combination, catalyzed the transfer of a methyl group from chloromethane to FH<sub>4</sub>. However, the rate of MeFH<sub>4</sub> formation was not proportional to the amount of CmuA employed. Exposure to oxygen inactivated the CmuA completely, but its activity could be restored by incubation with Ti(III) citrate under anaerobic conditions. Despite the sequence similarity of the N-terminal half of CmuA to that of archaea methylcobamide:CoMSH methyltransferases, CoMSH was not a methyl acceptor from CmuA.

While the rate of the overall reaction catalyzed by CmuA and CmuB increased linearly with the concentration of CmuB up to at least a 35 molar excess over CmuA, variation of CmuA concentration gave Michealis-Menton behavior with an apparent  $K_m$  for CmuA of 0.27  $\mu\text{M}$ , suggesting that CmuA and not CH<sub>3</sub>Cbl is the specific, physiological substrate for CmuB. CmuA also showed slight activity (5% of the chloromethane:FH<sub>4</sub> methyltransferase activity) as a chloromethane:halide methyltransferase (see below).

A facultative methylotroph isolated from the litter layer of a woodland soil, strain CC495, also grows on chloromethane and expresses a novel corrinoïd-dependent halomethane:bisulfide/halide ion methyltransferase.<sup>389</sup> The enzyme was purified 20-fold to apparent homogeneity in 46% yield by a combination of ion-exchange chromatography and gel filtration. The enzyme had a native molar mass of ca. 68 kDa (by gel filtration) and migrated on SDS-PAGE as a single band with an apparent molar mass of 66 kDa, suggesting a single polypeptide chain. The purified enzyme contained ca. 1 mol of a corrinoïd, apparently in the Co<sup>II</sup> oxidation state from its absorption spectrum, per mol of protein. After activation with chloromethane and DTT, which abolishes a lag phase in the kinetics, the UV-vis spectrum resembled that of a methylcorrinoïd with a nitrogenous axial ligand. The activated enzyme catalyzed the transfer of a methyl group from chloromethane, bromomethane, or iodomethane (with apparent  $K_m$ 's of 7, 30, and 36  $\mu\text{M}$ , respectively, and similar  $V_{\text{max}}$ 's) to a variety of anions including I<sup>-</sup> (0.37 mM), Cl<sup>-</sup> (11.6 mM), HS<sup>-</sup> (1.7 mM), Br<sup>-</sup> (5.1 mM), NO<sub>2</sub><sup>-</sup>, CN<sup>-</sup>, and SCN<sup>-</sup> (in order of decreasing activity with CH<sub>3</sub>Cl as the methyl donor, apparent  $K_m$ 's in parentheses). The authors suggest that bisulfide ion is the physiological acceptor since cell extracts of the organism contain methanethiol oxidase and formaldehyde dehydrogenase activities, which would provide a pathway to formate. The authors propose a nucleophilic substitution mechanism in which the protein-bound corrinoïd cycles between a CH<sub>3</sub>-Co and Co<sup>I</sup> state. However, no evidence for the intermediacy of a Co<sup>I</sup> state is presented, nucleophilic displacements of Co<sup>I</sup>-corrinoïds

by halide ions seem unlikely, and the DTT reductant should not be capable of reducing  $\text{Co}^{\text{II}}$ -corrinoids to the  $\text{Co}^{\text{I}}$  oxidation state. Consequently, a radical mechanism seems more likely.

A novel corrinoid-dependent methyltransferase that requires AdoCbl and generates  $\text{CH}_3\text{Cbl}$  has been described.<sup>390</sup> The enzyme is a *cis*-dihydrodiol dehydrogenase which converts benzene *cis*-dihydrodiols to catechols but has a lax substrate specificity and reacts with toluene *cis*-dihydrodiols and *p*-xylene *cis*-dihydrodiols. The conversion of one of the toluene *cis*-dihydrodiols, 3-methyl-4,5-cyclohexadiene-*cis*-1,2-diol, to catechol requires a demethylation. The enzyme, XylL, from the TOL plasmid pMM0 from a recombinant *Pseudomonas* strain<sup>391</sup> was cloned and overexpressed in *E. coli*, purified 85-fold to homogeneity, and had a molar mass of 28 kDa. Crude extracts catalyzed the reduction of the 3-methyl-4,5-cyclohexadiene-*cis*-1,2-diol to catechol by  $\text{NAD}^+$  with no other cofactor requirement. However, the purified enzyme converted the 3-methyl-4,5-cyclohexadiene-*cis*-1,2-diol to 3-methylcatechol in the presence of  $\text{NAD}^+$  alone. Addition of AdoCbl led to catechol as the product, as confirmed by mass spectrometry.  $\text{CNCbl}$  and  $\text{H}_2\text{OCbl}^+$  did not confer the demethylation activity on purified XylL. The Cbl product was identified as  $\text{CH}_3\text{Cbl}$  by comparison of its mass spectrum to that of an authentic sample. Thus, the reaction catalyzed appears to be that shown in eq 29. Unfortunately, the fate of the Ado ligand of AdoCbl was not determined. Oddly, 4-methyl-3,5-cyclohexadiene-*cis*-1,2-diol-1-carboxylic acid, a normal substrate for XylL, was converted to 4-methylcatechol in both the presence and the absence of AdoCbl.



The picture that emerges of the corrinoid-dependent methyltransferases is thus one of diversity. While some methyl transferases bind corrinoids with a His residue as the lower axial ligand, others probably bind corrinoids with altered axial nucleotides such as 5-hydroxy- or 5-methoxybenzimidazole, base-on, and still others appear to bind the corrinoid in a base-off mode, with no axial donor from an amino acid residue. While all Cbl-dependent methyl transferases react with exogenous Cbl, all also react with endogenous, protein-bound corrinoids, but there is substantial diversity in the methyltransferase systems. In some systems independent methyltransferases are used to alternately methylate and then demethylate a corrinoid-containing protein, while in others the corrinoid cofactor resides in the same protein as one of the methyl transferase activities. Alternatively, a single methyl transferase catalyzes both the methylation and demethylation of a separate corrinoid protein. The only known system in which both methyltransferase activities and the corrinoid bind-

ing protein (and the reactivating protein as well) reside on the same protein is methionine synthase.

### 11.3. Reductive Dehalogenases

A number of anaerobic bacteria are capable of reductively dechlorinating aliphatic and aromatic chlorinated hydrocarbons as part of their energy metabolism.<sup>392</sup> A variety of reductive dehalogenases have been purified from these organisms, including those which dehalogenate tetrachloroethene (PCE) and trichloroethene (TCE), those that dehalogenate chlorinated aromatics, and some that can dehalogenate both aliphatic and aromatic substrates. With one possible exception, all of these enzymes contain one bound corrinoid and two Fe/S clusters. The tetrachloroethene reductive dehalogenase (PCE-RD) from *Dehalospirillum multivorans*, a monomeric protein of molar mass 58 kDa,<sup>393</sup> catalyzes the dechlorination of PCE and TCE to *cis*-1,2-dichloroethene (DCE) using Ti(III) citrate reduced methyl viologen as the reductant (the natural reductant is unknown).<sup>394</sup> With Ti(III) citrate alone the turnover number was reduced by 14-fold.<sup>395</sup> Both *trans*- and *cis*-1,3-dichloropropene (DCP) were dechlorinated to a mixture of *cis*-1-chloropropene, *trans*-1-chloropropene, and 3-chloropropene, but the rate was lower for *cis*-1,3-DCP, and this isomer inhibited the enzyme. In addition, 2,3-dichloropropene was converted to 2-chloropropene and 1,1,3-trichloropropene was converted to 1,1-dichloropropene. Other compounds tested were neither substrates nor inhibitors. Apparent  $K_m$ 's for all substrates were similar and on the order of 250  $\mu\text{M}$ . A number of halogenated acetates and acetamides as well as hexachloroethane were also substrates for this enzyme. However, as  $\text{CNCbl}/\text{Ti(III)}$  reductants are also known to catalyze reductive dehalogenation of chlorinated compounds nonenzymatically, the corrinoid cofactor of PCE-RD was tested (after heat denaturation of the enzyme) and proved to catalyze the reductive dehalogenation of many of these substrates (but not the chlorinated ethenes and propenes) more efficiently than the enzyme. In fact, the native corrinoid cofactor of PCE-RD was 20–100 times more efficient at such “abiotic” reductive dehalogenation than  $\text{CNCbl}$ . However, as this corrinoid cofactor has subsequently been identified as  $\text{norpseudoB}_{12}$ ,<sup>82</sup> the analogue of  $\text{pseudoB}_{12}$  (*Co* $\beta$ -cyano-7'-adeninylcobamide, Figure 1) missing the Pr3 methyl group on the nucleotide loop 2-propanolamine moiety, these observations are very hard to rationalize.

Enzymes capable of dehalogenating chlorinated aromatics have been found in several species.<sup>396–398</sup> The first molecular characterization of a chloroaryl reductive dehalogenase, the *ortho*-chlorophenol reductive dehalogenase (*o*-CPDH) from *Desulfitobacterium dehalogenans*, has appeared.<sup>399</sup> The enzyme was purified 90-fold to apparent homogeneity in 46% yield under anaerobic conditions from *D. dehalogenans* grown on 3-chloro-4-hydroxyphenylacetate (Cl-OHPA). The purified enzyme had maximal activity at pH 8.1 and 52 °C, and the  $K_m$  for Cl-OHPA was 20  $\mu\text{M}$  at 30 °C when assayed with reduced methyl viologen as the electron donor. The enzyme was

active with 2-chlorophenol, 2,3-, 2,4-, and 2,6-dichlorophenol, pentachlorophenol, and 2-bromo-4-chlorophenol but not with 2-fluoro-4-chlorophenol. There was no activity with PCE or TCE. The enzyme has a molar mass of 48 kDa by SDS-PAGE and contains 0.7 equiv of cobalt and 7 equiv of iron per monomer unit.

Determination of the N-terminal sequence allowed cloning and sequencing of the *cprA* locus, which included the *cprA* gene, a predicted 405 amino acid polypeptide with a molar mass of 45 305 Da (after loss of a 42 residue leader sequence), which lacked the consensus Asp-x-His-x-x-Gly sequence, and a second open reading frame, *cprB*, which encoded a predicted 11.5 kDa polypeptide that appears to be a membrane-spanning protein. The situation is analogous to the PCE-RD of *Dehalospirillum multivorans*, a gene which also contains an additional open reading frame coding for an 8 kDa membrane-spanning protein.<sup>393</sup>

The EPR spectrum of *o*-CPDH, reduced by a light-induced deazaflavin/EDTA reductant, had signals at *g* values of 2.05, 1.93, and 1.87 which rapidly broaden above 20 K, indicating a [4Fe-4S]<sup>+</sup> cluster, as well as a base-off cob(II)alamin-like signal and a trace of a base-on cob(II)alamin-like signal. After addition of the substrate, Cl-OHPA, the spectrum resembled that of the enzyme as isolated and clearly showed base-off cob(II)alamin. Simulations of the EPR signal gave *g* values of 1.99, 2.35, and 2.35 and cobalt hyperfine parameters of 14, 7.5, and 7.5 millitesla and indicated a minor component of base-on cob(II)alamin. These parameters are close to those found for the PCE dehalogenase from *D. restrictus*.<sup>400</sup> Addition of potassium ferricyanide results in formation of a nearly isotropic signal near *g* = 2, typical of a [3Fe-4S]<sup>+</sup> cluster. The authors conclude that the enzyme contains one [4Fe-4S] cluster, one [3Fe-4S] cluster, and one corrinoid per protein monomer. Redox titrations gave midpoint potential values of -440, +70, and -370 mV, respectively, for these redox-active centers.

## 12. Acknowledgment

The author's work in this area is supported by grant GM 48858 from the National Institute of General Medical Sciences.

## 13. References

- Rickes, E. L.; Brink, N. G.; Koniuszy, F. R.; Wood, T. R.; Folkers, K. *Science* **1948**, *107*, 396.
- Smith, E. L. *Nature (London)* **1948**, *162*, 144.
- Smith, E. L.; Parker, L. F. *Proc. Biochem. Soc.* **1948**, *43*, viii.
- Chemistry and Biochemistry of B<sub>12</sub>*; Banerjee, R., Ed; Wiley: New York, 1999.
- Mulliez, E.; Fontecave, M. *Coord. Chem. Rev.* **1999**, *185-186*, 775.
- Chemaly, S. M. *S. Afr. J. Sci.* **1999**, *95*, 125.
- Marsh, E. N. G. *Essays Biochem.* **1999**, *34*, 139.
- Toraya, T. *Cell. Mol. Life Sci.* **2000**, *57*, 106.
- Toraya, T. *J. Mol. Catal. B: Enzym.* **2000**, *10*, 87.
- Marsh, E.; Neil, G. *Bioorg. Chem.* **2000**, *28*, 176.
- Xu, Y.; Grissom, C. B. *Compr. Nat. Prod. Chem.* **1999**, *5*, 263.
- Licht, S.; Stubbe, J. *Compr. Nat. Prod. Chem.* **1999**, *5*, 163.
- Marsh, E. N. G.; Holloway, D. E. *Subcell. Biochem.* **2000**, *35*, 351.
- Banerjee, R. *Biochemistry* **2001**, *40*, 6191.
- Matthews, R. G. *Acc. Chem. Res.* **2001**, *34*, 681.
- Marsh, E. N. G.; Drennan, C. L. *Curr. Opin. Chem. Biol.* **2001**, *5*, 499.
- Gruber, K.; Kratky, C. *Curr. Opin. Chem. Biol.* **2002**, *6*, 598.
- Toraya, T. *Chem. Record* **2002**, *2*, 352.
- Banerjee, R. *Chem. Rev.* **2003**, *103*, 2083.
- Banerjee, R.; Ragsdale, S. W. *Annu. Rev. Biochem.* **2003**, *72*, 209.
- Reed, G. H.; Mansoorabadi, S. O. *Curr. Opin. Struct. Biol.* **2003**, *13*, 716.
- Raux, E.; Schubert, H. L.; Roper, J. M.; Wilson, Ke. S.; Warren, M. J. *Bioorg. Chem.* **1999**, *27*, 100.
- Scott, A. I.; Roessner, C. A. *Biochem. Soc. Trans.* **2002**, *30*, 613.
- Warren, M. J.; Raux, E.; Schubert, H. L.; Escalante-Semerena, J. C. *Nat. Prod. Rep.* **2002**, *19*, 390.
- Scott, A. I. *J. Org. Chem.* **2003**, *68*, 2529.
- Riether, D.; Mulzer, J. *Eur. J. Org. Chem.* **2003**, *30*.
- Marques, H. M.; Brown, K. L. *Coord. Chem. Rev.* **1999**, *190-192*, 127.
- Marques, H. M.; Brown, K. L. *Coord. Chem. Rev.* **2002**, *225*, 123.
- Hisaeda, Y.; Nishioka, T.; Inoue, Y.; Asada, K.; Hayashi, T. *Coord. Chem. Rev.* **2000**, *198*, 21.
- Marzilli, L. G. In *Bioinorganic Catalysis*, 2nd ed.; Reedijk, J., Bouwman, E. R., Eds; Marcel Dekker: New York, 1999; p 423.
- Kräutler, B.; Ostermann, S. In *Porphyrin Handbook*; Kadish, K. M., Smith, K. M., Guilard, R., Eds.; Elsevier Science: San Diego, 2003; Vol 11, p 229.
- Vitamin B<sub>12</sub> and B<sub>12</sub> Proteins*; Kräutler, B., Arigoni, D., Golding, B. T., Eds.; Wiley-VCH: Weinheim, 1998.
- Cheng, S.; Zang, E.; Brown, K. L. *Synth. Commun.* **1999**, *29*, 891.
- Brown, K. L.; Xia, Z. *J. Labelled Compd. Radiopharm.* **2000**, *43*, 635.
- Walker, T. E.; Hogenkamp, H. P. C.; Needham, T. E.; Matwiyoff, N. A. *Biochemistry* **1974**, *13*, 2650.
- Fonseca, M. V.; Escalante-Semerena, J. C. *J. Biol. Chem.* **2001**, *276*, 32101.
- Kontaxis, G.; Riether, D.; Hannak, R.; Tollinger, M.; Kräutler, B. *Helv. Chim. Acta* **1999**, *82*, 848.
- Brown, K. L.; Cheng, S.; Marques, H. M. *Polyhedron* **1998**, *17*, 2213.
- Fieber, W.; Hoffmann, B.; Schmidt, W.; Stupperich, E.; Konrat, R.; Krautler, B. *Helv. Chim. Acta* **2002**, *85*, 927.
- White, W. T.; Finke, R. G. *J. Inorg. Biochem.* **2002**, *91*, 371.
- Hay, B. P.; Finke, R. G. *Polyhedron* **1988**, *7*, 1469. Doll, K. M.; Fleming, P. E.; Finke, R. G. *J. Inorg. Biochem.* **2002**, *91*, 338.
- Hogenkamp, H. P. C. *J. Biol. Chem.* **1963**, *238*, 477.
- Brown, K. L.; Zou, X.; Li, J.; Chen, G. *Inorg. Chem.* **2001**, *40*, 5942.
- Kräutler, B.; Konrat, R.; Stupperich, E.; Fäber, G.; Gruber, K.; Kratky, C. *Inorg. Chem.* **1994**, *33*, 4128.
- Weigl, U.; Heimerger, M.; Pierik, A. J.; Rétey, J. *Chem. Eur. J.* **2003**, *9*, 652.
- Magnusson, O. Th.; Frey, P. A. *J. Am. Chem. Soc.* **2000**, *122*, 8807.
- Magnusson, O. Th.; Reed, G. H.; Frey, P. A. *J. Am. Chem. Soc.* **1999**, *121*, 9764.
- Suh, S. J.; Escalante-Semerena, J. C. *J. Bacteriol.* **1995**, *177*, 921.
- Mitchell, A. M.; Bayomi, A.; Natarajan, E.; Barrows, L. R.; West, F. G.; Grissom, C. B. *Biomed. Health Res.* **1999**, *27*, 150.
- Wilbur, D. S.; Pathare, P. M.; Hamlin, D. K.; Rothenberg, S. P.; Quadros, E. V. *Bioconjugate Chem.* **1999**, *10*, 912.
- McEwan, J. F.; Veitch, H. S.; Russell-Jones, G. J. *Bioconjugate Chem.* **1999**, *10*, 1131.
- Marques, H. M.; Brown, K. L.; Jacobsen, D. W. *J. Biol. Chem.* **1988**, *263*, 12378.
- Marchaj, A.; Jacobsen, D. W.; Savon, S. R.; Brown, K. L. *J. Am. Chem. Soc.* **1995**, *117*, 11640.
- Horton, R. A.; Bagnato, J. D.; Grissom, C. B. *J. Org. Chem.* **2003**, *68*, 7108.
- Hogenkamp, H. P. C.; Collins, D. A.; Live, D.; Benson, L. M.; Naylor, S. *Nucl. Med. Biol.* **2000**, *27*, 89.
- Jacobsen, D. W.; Huennekens, F. M. *Methods Enzymol.* **1986**, *123*, 28.
- Smeltzer, C. C.; Cannon, M. J.; Pinson, P. R.; Munger, J. D., Jr.; West, F. G.; Grissom, C. B. *Org. Lett.* **2001**, *3*, 799.
- Wagner, F.; Bernhauer, K. *Ann. N. Y. Acad. Sci.* **1964**, *112*, 580.
- Jacobsen, D. W.; Lee-Denison, C.; Luce, K.; Green, R. *Fed. Proc.* **1987**, *46*, 1005.
- Brasch, N. E.; Hsu, T.-L. C.; Doll, K. M.; Finke, R. G. *J. Inorg. Biochem.* **1999**, *76*, 197.
- Suto, R. K.; Brasch, N. E.; Anderson, O. P.; Finke, R. G. *Inorg. Chem.* **2001**, *40*, 2686.
- Sun, F.; Darbre, T.; Keese, *Tetrahedron* **1999**, *55*, 9777.
- Sun, F.; Darbre, T. *Helv. Chim. Acta* **2002**, *85*, 3002.
- Darbre, T.; Keese, R.; Silegovic, A.; Wolleb-Gygi, A. *Helv. Chim. Acta* **1996**, *79*, 2100.
- Fraga, R.; Keese, R., *Synlett* **2000**, 1694.
- Ariga, K.; Tanaka, K.; Katagiri, K.; Kikuchi, J.-i.; Ohshima, E.; Hisaeda, Y. *Colloids Surf., A* **2000**, *169*, 47.

- (67) Shimakoshi, H.; Inaoka, T.; Hisaeda, Y. *Tetrahedron Lett.* **2003**, *44*, 6421.
- (68) Brink-Shoemaker, C.; Cruickshank, D. W. J.; Hodgkin, D. C.; Kamper, J.; Pilling, D. *Proc. R. Soc. London, Ser. A* **1964**, *278*, 1–26.
- (69) DeRidder, D. J. A.; Zangrando, E.; Büergi, H.-B. *J. Mol. Struct.* **1996**, *374*, 63.
- (70) Garau, G.; Geremia, S.; Marzilli, L. G.; Nardin, G.; Randaccio, L.; Tazher, G. *Acta Crystallogr. Sect. B* **2003**, *B59*, 51.
- (71) Randaccio, L.; Geremia, S.; Nardin, G.; Slouf, M.; Srnova, I. *Inorg. Chem.* **1999**, *38*, 4087.
- (72) Perry, C. B.; Fernandes, M. A.; Brown, K. L.; Zou, X.; Valente, E. J.; Marques, H. M. *Eur. J. Inorg. Chem.* **2003**, 2095.
- (73) Randaccio, L.; Furlan, M.; Geremia, S.; Slouf, M.; Srnova, I.; Toffoli, D. *Inorg. Chem.* **2000**, *39*, 3403.
- (74) Brown, K. L.; Zou, X.; Savon, S. R.; Jacobsen, D. W. *Biochemistry* **1993**, *32*, 8421.
- (75) Rossi, M.; Glusker, J. P.; Randaccio, L.; Summers, M. F.; Toscano, P. J.; Marzilli, L. G. *J. Am. Chem. Soc.* **1985**, *107*, 1729.
- (76) Glusker, J. P. In *B<sub>12</sub>*; Dolphin, D., Ed.; Wiley: New York, 1982; Vol. 1, p 23.
- (77) Gruber, K.; Jögl, G.; Klintsher, G.; Kratky, C. In *Vitamin B<sub>12</sub> and B<sub>12</sub>-Proteins*; Kräutler, B., Arigoni, D., Golding, B. T., Eds.; Wiley-VCH: Weinheim, 1998; p 335.
- (78) Wagner, T.; Afshar, C. E.; Carrell, H. L.; Glusker, J. P.; Englert, U.; Hogenkamp, H. P. C. *Inorg. Chem.* **1999**, *38*, 1785.
- (79) Zou, X.; Brown, K. L. *Inorg. Chim. Acta* **1998**, *267*, 305.
- (80) McCauley, K. M.; Wilson, S. R.; van der Donk, W. *J. Am. Chem. Soc.* **2003**, *125*, 4410.
- (81) Boupuiere, J. P.; Finney, J. L.; Savage, H. F. J. *Acta Crystallogr.* **1994**, *B50*, 566. Boupuiere, J. P.; Finney, J. L.; Lehmann, M. S.; Lindley, P. F.; Savage, H. F. J. *Acta Crystallogr.* **1993**, *B49*, 79. Savage, H. F. J. *J. Biophys.* **1986**, *50*, 947. Savage, H. F. J.; Finney, J. L. *Nature* **1986**, *322*, 717.
- (82) Kräutler, B.; Färber, W.; Ostermann, S.; Fasching, M.; Ongania, K.; Gruber, K.; Kratky, C.; Mikl, C.; Siebert, A.; Diekert, G. *Helv. Chim. Acta* **2003**, *86*, 3698.
- (83) Kopf, J.; Bieganski, R.; Friedrich, W.; Vondeuten, K. *Z. Naturforsch.* **1981**, *C36*, 506.
- (84) Langan, P.; Lehmann, M.; Wilkinson, C.; Jögl, G.; Kratky, C. *Acta Crystallogr., Sect. D: Biol. Crystallogr.* **1999**, *D55*, 51.
- (85) Kräutler, B.; Keller, W.; Kratky, C. *J. Am. Chem. Soc.* **1989**, *111*, 8936.
- (86) Hoffmann, B.; Oberhuber, M.; Stupperich, E.; Bothe, H.; Buckel, W.; Konrat, R.; Kräutler, B. *J. Bacteriol.* **2000**, *182*, 4773.
- (87) Marques, H. M.; Zou, X.; Brown, K. L. *J. Mol. Struct.* **2000**, *520*, 75.
- (88) Tollinger, M.; Konrat, R.; Kräutler, B. *Helv. Chim. Acta* **1999**, *82*, 1596.
- (89) Brown, K. L.; Zou, X.; Marques, H. M. *J. Mol. Struct. (THEOCHEM)* **1998**, *453*, 209.
- (90) Forbes, C. L.; Franck, R. W. *J. Org. Chem.* **1999**, *64*, 1424.
- (91) Brodie, J. D. *Proc. Nat. Acad. Sci. U.S.A.* **1969**, *62*, 461.
- (92) Grate, J. H.; Schrauzer, J. *Am. Chem. Soc.* **1979**, *101*, 4601.
- (93) Kleban, M.; Kautz, U.; Greul, J.; Hilgers, P.; Kugler, R.; Dong, H.-Q.; Jäger, V. *Synthesis* **2000**, 1027.
- (94) Petrovic, Z. D.; Anđelkovic, D.; Stevanovic, L. *J. Serbian Chem. Soc.* **2003**, *68*, 719; *Chem. Abstr.* **2003**, *140*, 303935.
- (95) Petrovic, Z.; Bugarcic, Z.; Marjanovic, L.; Konstantinovic, S. *J. Mol. Catal. A: Chem.* **1999**, *142*, 393.
- (96) Njue, C. K.; Nuthakki, B.; Vaze, A.; Bobbitt, J. M.; Rusling, J. F. *Electrochem. Commun.* **2001**, *3*, 733.
- (97) Zhou, D.-L.; Njue, C. K.; Rusling, J. F. *J. Am. Chem. Soc.* **1999**, *121*, 2909.
- (98) Njue, C. K.; Rusling, J. F. *Electrochem. Commun.* **2002**, *4*, 340.
- (99) Shimakoshi, H.; Nakazato, A.; Tokunaga, M.; Katagiri, K.; Ariga, K.; Kikuchi, J.-I.; Hisaeda, Y. *Dalton Trans.* **2003**, 2308.
- (100) Grodkowski, J.; Neta, P. *J. Phys. Chem. A* **2000**, *104*, 1848.
- (101) Vilakazi, S. L.; Nyokong, T. *Electrochim. Acta* **2000**, *46*, 453.
- (102) Lexa, D.; Saveant, J. M.; Zickler, J. *J. Am. Chem. Soc.* **1980**, *102*, 2654.
- (103) Shey, J.; van der Donk, W. A. *J. Am. Chem. Soc.* **2000**, *122*, 12403.
- (104) Kim, Y.-H.; Carraway, E. R. *Environ. Technol.* **2002**, *23*, 1135.
- (105) Shey, J.; McGinley, C. M.; McCauley, K. M.; Dearth, A. S.; Young, B. T.; van der Donk, W. A. *J. Org. Chem.* **2002**, *67*, 837.
- (106) Brown, K. L.; Zou, X. *J. Inorg. Biochem.* **1999**, *77*, 185.
- (107) Hay, B. P.; Finke, R. G. *J. Am. Chem. Soc.* **1986**, *108*, 4820.
- (108) Brown, K. L.; Marques, H. M. *Polyhedron* **1996**, *15*, 2187.
- (109) Sirovatka, J. M.; Finke, R. G. *J. Inorg. Biochem.* **2000**, *78*, 149.
- (110) Sirovatka, J. M.; Finke, R. G. *Inorg. Chem.* **1999**, *38*, 1697.
- (111) Sirovatka, J. M.; Finke, R. G. *Inorg. Chem.* **2001**, *40*, 1082.
- (112) Garr, C. D.; Sirovatka, J. M.; Finke, R. G. *J. Am. Chem. Soc.* **1996**, *118*, 11142.
- (113) Sirovatka, J. M.; Finke, R. G. *J. Am. Chem. Soc.* **1997**, *119*, 3057.
- (114) Garr, C. D.; Finke, R. G. *J. Am. Chem. Soc.* **1992**, *114*, 10440.
- (115) Trommel, J. S.; Warncke, K.; Marzilli, L. G. *J. Am. Chem. Soc.* **2001**, *123*, 3358.
- (116) Koenig, T. W.; Hay, B. P.; Finke, R. G. *Polyhedron* **1988**, *7*, 1499.
- (117) Jensen, M. P.; Halpern, J. *J. Am. Chem. Soc.* **1999**, *121*, 2181.
- (118) Hogenkamp, H. P. C.; Rush, J. E.; Swenson, C. A. *J. Biol. Chem.* **1965**, *240*, 3641.
- (119) Brasch, N. E.; Haupt, R. *J. Inorg. Chem.* **2000**, *39*, 5469.
- (120) Brasch, N. E.; Cregan, A. G.; Vanselow, M. E. *J. Chem. Soc., Dalton Trans.* **2002**, 1287.
- (121) Hamza, M. S. A.; Cregan, A. G.; Brasch, N. E.; van Eldik, R. *Dalton Trans.* **2003**, 596.
- (122) Hung, R. R.; Grabowski, J. J. *J. Am. Chem. Soc.* **1999**, *121*, 1359.
- (123) Martin, B. D.; Finke, R. G. *J. Am. Chem. Soc.* **1990**, *112*, 2419.
- (124) Chen, H.; Li, G.; Zhang, F. F.; Sun, L.; Chen, H. L.; Zhang, S. Y. *Spectrochim. Acta* **2003**, *59A*, 2767.
- (125) Chen, H. L.; Yan, H.; Luo, L. B.; Cui, X. X.; Tang, W. X. *J. Inorg. Biochem.* **1997**, *66*, 219.
- (126) Luo, L. B.; Li, G.; Chen, H. L.; Fu, S. W.; Zhang, S. Y. *J. Chem. Soc., Dalton Trans.* **1998**, 2103.
- (127) Zheng, D.; Darbre, T.; Keese, R. *J. Inorg. Biochem.* **1999**, *73*, 273.
- (128) Darbre, T.; Zheng, D.; Fraga, R.; Keese, R. *Proc. Electrochem. Soc.* **2000**, *2000-15*, 53.
- (129) Wedemeyer-Exl, C.; Darbre, T.; Keese, R. *Helv. Chim. Acta* **1999**, *82*, 1173.
- (130) Zakharyan, R. A.; Aposhian, H. V. *Toxicol. Appl. Pharmacol.* **1999**, *154*, 287.
- (131) Mosimann, H.; Kräutler, B. *Angew. Chem., Int. Ed.* **2000**, *39*, 393.
- (132) Grate, J. H.; Grate, J. W.; Schrauzer, G. N. *J. Am. Chem. Soc.* **1982**, *104*, 1588.
- (133) Brown, K. L.; Hakimi, J. M.; Nuss, D. M.; Montejano, Y. D.; Jacobsen, D. W. *Inorg. Chem.* **1984**, *23*, 1463.
- (134) Brown, K. L. *J. Am. Chem. Soc.* **1987**, *109*, 2277.
- (135) Hamza, M. S. A.; Zou, X.; Brown, K. L.; van Eldik, R. *Eur. J. Inorg. Chem.* **2003**, 268.
- (136) Hamza, M. S. A.; Zou, X.; Brown, K. L.; van Eldik, R. *Dalton Trans.* **2003**, 2986.
- (137) Firth, R. A.; Hill, H. A. O.; Mann, B. E.; Pratt, J. M.; Thorp, R. G.; Williams, R. J. P. *J. Chem. Soc. A* **1968**, 2419.
- (138) Brown, K. L.; Wu, G.-Z. *Inorg. Chem.* **1994**, *33*, 4122.
- (139) Wirt, M. D.; Chance, M. R. *J. Inorg. Biochem.* **1993**, *49*, 265.
- (140) Hamza, M. S. A.; Van Eldik, R.; Harper, P. L. S.; Pratt, J. M.; Betterton, E. A. *Eur. J. Inorg. Chem.* **2002**, 580.
- (141) Drljaca, A.; Hubbard, C. D.; van Eldik, R.; Asano, T.; Basilevsky, M. V.; Noble, W. J. *Chem. Rev.* **1998**, *98*, 2167.
- (142) Hamza, M. S. A.; Zou, X.; Brown, K. L.; van Eldik, R. *Inorg. Chem.* **2001**, *40*, 5440.
- (143) Hamza, M. S. A.; Zou, X.; Brown, K. L.; van Eldik, R. *J. Chem. Soc., Dalton Trans.* **2002**, 3832.
- (144) Brodie, S. J.; Cregan, A. G.; van Eldik, R.; Brasch, N. E. *Inorg. Chim. Acta* **2003**, *348*, 221.
- (145) Dorweiler, J. S.; Matthews, R. G.; Finke, R. G. *Inorg. Chem.* **2002**, *41*, 6217.
- (146) Wolak, M.; Stochel, G.; Hamza, M.; van Eldik, R. *Inorg. Chem.* **2000**, *39*, 2018.
- (147) Marques, H. M.; Knapton, L. *J. Chem. Soc., Dalton Trans.* **1997**, 3827.
- (148) Zheng, D.; Birke, R. L. *J. Am. Chem. Soc.* **2001**, *123*, 4637.
- (149) Wolak, M.; Zahl, A.; Schnepfenseper, T.; Stochel, G.; van Eldik, R. *J. Am. Chem. Soc.* **2001**, *123*, 9780.
- (150) Zheng, D.; Yan, L.; Birke, R. L. *Inorg. Chem.* **2002**, *41*, 2548.
- (151) Sharma, V. S.; Pilz, R. B.; Boss, G. R.; Magde, D. *Biochemistry* **2003**, *42*, 8900.
- (152) Brown, K. L.; Hakimi, J. M.; Jacobsen, D. W. *J. Am. Chem. Soc.* **1984**, *106*, 7894.
- (153) Hayward, G. C.; Hill, H. A. O.; Pratt, J. M.; Vanston, N. J.; Williams, R. J. P. *J. Chem. Soc.* **1965**, 6485.
- (154) Cregan, A. G.; Brasch, N. E.; van Eldik, R. *Inorg. Chem.* **2001**, *40*, 1430.
- (155) Marques, H. M.; Knapton, L.; Zou, X.; Brown, K. L. *J. Chem. Soc., Dalton Trans.* **2002**, 3195.
- (156) Reenstra, W. W.; Jencks, W. P. *J. Am. Chem. Soc.* **1979**, *101*, 5780.
- (157) Lexa, D.; Savéant, J. M. *J. Am. Chem. Soc.* **1978**, *100*, 3220.
- (158) Brown, K. L.; Zou, X. *Inorg. Chem.* **1991**, *30*, 4185.
- (159) Ngandu, L.; Robin, D.; El Kasmi, A.; Lexa, D. *Inorg. Chim. Acta* **1999**, *292*, 204.
- (160) Mimica, D.; Bedioui, F.; Zagal, J. H. *Electrochim. Acta* **2002**, *48*, 323.
- (161) Meskers, S. C. J.; Dekkers, H. P. J. M. *Spectrochim. Acta, Part A* **1999**, *55A*, 1837.
- (162) Meskers, S. C. J.; Dekkers, H. P. J. M. *J. Phys. Chem. A* **2001**, *105*, 4589.
- (163) Huskowska, E.; Riehl, J. P. *Inorg. Chem.* **1995**, *34*, 5615.
- (164) Meskers, S. C. J.; Dekkers, H. P. J. M. *Spectrochim. Acta, Part A* **1999**, *55A*, 1857.
- (165) Haglund, J.; Rafiq, A.; Ehrenberg, L.; Golding, B. T.; Toernqvist, M. *Chem. Res. Toxicol.* **2000**, *13*, 253.
- (166) Wolak, M.; Stochel, G.; van Eldik, R. *J. Am. Chem. Soc.* **2003**, *125*, 1334.

- (167) Hisaeda, Y.; Ohshima, E.; Arimura, M. *Colloids Surf., A* **2000**, *169*, 143.
- (168) Murakami, Y.; Hiseada, Y.; Ohno, T. *J. Chem. Soc., Perkin Trans. 2* **1991**, 405.
- (169) Sun, F.; Darbre, T. *Org. Biomol. Chem.* **2003**, *1*, 3154.
- (170) Hannak, R. B.; Konrat, R.; Schuler, W.; Kräutler, B.; Auditor, M.-T. M.; Hilvert, D. *Angew. Chem., Int. Ed.* **2002**, *41*, 3613.
- (171) Brown, K. L.; Marques, H. M.; Jacobsen, D. W. *J. Biol. Chem.* **1988**, *263*, 1872.
- (172) Shiang, J. J.; Walker, L. A., II; Anderson, N. A.; Cole, A. G.; Sension, R. J. *J. Phys. Chem. B* **1999**, *103*, 10532.
- (173) Yoder, L. M.; Cole, A. G.; Walker, L. A., II; Sension, R. J. *J. Phys. Chem. B* **2001**, *105*, 12180.
- (174) Cole, A. G.; Yoder, L. M.; Shiang, J. J.; Anderson, N. A.; Walker, L. A., II; Banaszak Holl, M. M.; Sension, R. J. *J. Am. Chem. Soc.* **2002**, *124*, 434.
- (175) Endicott, J. F.; Netzel, T. L. *J. Am. Chem. Soc.* **1979**, *101*, 4000.
- (176) Chagovitz, A. M.; Grissom, C. B. *J. Am. Chem. Soc.* **1993**, *115*, 12152.
- (177) Walker, L. A.; Shiang, J. J.; Anderson, N. A.; Pullen, S. H.; Sension, R. J. *J. Am. Chem. Soc.* **1998**, *120*, 7286.
- (178) Bussandri, A. P.; Kiarie, C. W.; van Willigen, H. *Res. Chem. Intermed.* **2002**, *28*, 697.
- (179) Medek, A.; Frydman, L. *J. Am. Chem. Soc.* **2000**, *122*, 684.
- (180) Brink-Shoemaker, C.; Cruikshank, D. W. J.; Hodgkin, D. C.; Kamper, M. J.; Pilling, D. *Proc. R. Soc. A* **1964**, *278*, 1.
- (181) Hodgkin, D. C.; Lindsey, J.; Sparks, R. A.; Trueblood, K. N.; White, J. G. *Proc. R. Soc. A* **1962**, *266*, 494.
- (182) Brasch, N. E.; Finke, R. G. *J. Inorg. Biochem.* **1999**, *73*, 215.
- (183) van Doorslaer, S.; Schweiger, A.; Kräutler, B. *J. Phys. Chem. B* **2001**, *105*, 7554.
- (184) Hohenester, E.; Kratky, C.; Kräutler, B. *J. Am. Chem. Soc.* **1991**, *113*, 4523.
- (185) Harmer, J.; Van Doorslaer, S.; Gromov, I.; Schweiger, A. *Chem. Phys. Lett.* **2002**, *358*, 8.
- (186) Van Doorslaer, S.; Jeschke, G.; Epel, B.; Goldfarb, D.; Eichel, R.-A.; Kräutler, B.; Schweiger, A. *J. Am. Chem. Soc.* **2003**, *125*, 5915.
- (187) Kräutler, B.; Keller, W.; Hughes, M.; Caderas, C.; Kratky, C. *J. Chem. Soc., Chem. Commun.* **1987**, 1678.
- (188) Mancia, F.; Keep, N. H.; Nakagawa, A.; Leadlay, P. F.; McSweeney, S.; Rasmussen, B.; Bösecke, P.; Diat, O.; Evans, P. R. *Structure* **1996**, *4*, 339.
- (189) Shibata, N.; Masuda, J.; Tobimatsu, T.; Toraya, T.; Suto, K.; Morimoto, Y.; Yasuoka, N. *Structure* **1999**, *7*, 997.
- (190) Cockle, S.; Hill, H. A. O.; Ridsdale, S.; Williams, R. J. P. *J. Chem. Soc., Dalton Trans.* **1972**, 297.
- (191) Champloy, F.; Gruber, K.; Jögl, G.; Kratky, C. *J. Synchrotron Radiat.* **2000**, *7*, 267.
- (192) Scheidt, W. R. *J. Am. Chem. Soc.* **1974**, *96*, 84.
- (193) Stich, T. A.; Brooks, A. J.; Buan, N. R.; Brunold, T. C. *J. Am. Chem. Soc.* **2003**, *125*, 5897.
- (194) Hay, B. P.; Finke, R. G. *J. Am. Chem. Soc.* **1987**, *109*, 8012.
- (195) Andruniow, T.; Zgierski, M. Z.; Kozlowski, P. M. *Chem. Phys. Lett.* **2000**, *331*, 509.
- (196) Andruniow, T.; Zgierski, M. Z.; Kozlowski, P. M. *J. Phys. Chem. B* **2000**, *104*, 10921.
- (197) Jensen, K. P.; Sauer, S. P. A.; Liljefors, T.; Norrby, P.-O. *Organometallics* **2001**, *20*, 550.
- (198) Randaccio, L.; Geremia, S.; Stener, M.; Toffoli, D.; Zangrando, E. *Eur. J. Inorg. Chem.* **2002**, 93.
- (199) Jensen, K. P.; Mikkelsen, K. V. *Inorg. Chim. Acta* **2001**, *323*, 5.
- (200) Andruniow, T.; Zgierski, M. Z.; Kozlowski, P. M. *J. Am. Chem. Soc.* **2001**, *123*, 2679.
- (201) Dölker, N.; Maseras, F.; Lledos, A. *J. Phys. Chem. B* **2001**, *105*, 7564.
- (202) Jensen, K. P.; Ryde, U. *THEOCHEM* **2002**, *585*, 239.
- (203) Jensen, K. P.; Ryde, U. *J. Phys. Chem. A* **2003**, *107*, 7539.
- (204) Dybala-Defratyka, A.; Paneth, P. *J. Inorg. Biochem.* **2001**, *86*, 681.
- (205) Dölker, N.; Maseras, F.; Lledos, A. *J. Phys. Chem. B* **2003**, *107*, 306.
- (206) Jensen, K. P.; Ryde, U. *J. Am. Chem. Soc.* **2003**, *125*, 13970.
- (207) Banerjee, R. V.; Frasca, V.; Ballou, D. P.; Matthews, G. R. *Biochemistry* **1990**, *29*, 11101.
- (208) Andruniow, T.; Kozlowski, P. M.; Zgierski, M. Z. *J. Chem. Phys.* **2001**, *115*, 7522.
- (209) Ouyang, L.; Randaccio, L.; Rulis, P.; Kurmaev, E. Z.; Moewes, A.; Ching, W. Y. *THEOCHEM* **2003**, *622*, 221.
- (210) Kurmaev, E. Z.; Moewes, A.; Ouyang, L.; Randaccio, L.; Rulis, P.; Ching, W. Y.; Bach, M.; Neumann, M. *Europhys. Lett.* **2003**, *62*, 582.
- (211) Andruniow, T.; Zgierski, M. Z.; Kozlowski, P. M. *Chem. Phys. Lett.* **2000**, *331*, 502.
- (212) Andruniow, T.; Zgierski, M. Z.; Kozlowski, P. M. *J. Phys. Chem. A* **2002**, *106*, 1365.
- (213) Torrent, M.; Musaev, D. G.; Morokuma, K.; Ke, S.-C.; Warncke, K. *J. Phys. Chem. B* **1999**, *103*, 8618.
- (214) Rovira, C.; Kunc, K.; Hutter, J.; Parrinello, M. *Inorg. Chem.* **2001**, *40*, 11.
- (215) Scheidt, W. R.; Turowska-Tyrk, I. *Inorg. Chem.* **1994**, *33*, 1314.
- (216) Jansen, K. P.; Ryde, U. *ChemBioChem* **2003**, *4*, 413.
- (217) Benciu, A. C. *Rev. Roum. Chim.* **2002**, *46*, 1265, CA 138:401861.
- (218) Marques, H. M.; Brown, K. L. *J. Mol. Struct. (THEOCHEM)* **1995**, *340*, 97.
- (219) Brown, K. L.; Marques, H. M. *J. Inorg. Biochem.* **2001**, *83*, 121.
- (220) Sirovatka, J. M.; Rappe, A. K.; Finke, R. G. *Inorg. Chim. Acta* **2000**, *300–302*, 545.
- (221) Brown, K. L.; Li, J. *J. Am. Chem. Soc.* **1998**, *37*, 9466.
- (222) Chowdhury, S.; Banerjee, R. *Biochemistry* **2000**, *39*, 7998.
- (223) Marques, H. M.; Ngoma, B.; Egan, T. J.; Brown, K. L. *J. Mol. Struct.* **2001**, *561*, 71.
- (224) Baker, S. A.; Miller-Ihli, N. J. *Spectrochim. Acta, Part B* **2000**, *55B*, 1823.
- (225) Linn, D. E.; Gould, E. S. *Inorg. Chem.* **1988**, *27*, 1625.
- (226) Sahni, M. K.; Spanos, S.; Wahrman, M. Z.; Sharma, G. M. *Anal. Biochem.* **2001**, *289*, 68.
- (227) Bain, B.; Broom, G. N.; Woodside, J.; Litwinczuk, R. A.; Wick-ansingh, S. N. *J. Clin. Pathol. London* **1982**, *35*, 1110.
- (228) Fedosov, S. N.; Berglund, L.; Nexø, E.; Petersen, T. E. *J. Biol. Chem.* **1999**, *274*, 26015.
- (229) Fedosov, S. N.; Fedosova, N. U.; Nexø, E.; Petersen, T. E. *J. Biol. Chem.* **2000**, *275*, 11791.
- (230) Platiga, O.; Janeczko, R.; Quadros, E. V.; Regec, A.; Romain, R.; Rothenberg, S. P. *J. Biol. Chem.* **1991**, *266*, 7860.
- (231) Fedosov, S. N.; Berglund, L.; Fedosova, N. U.; Nexø, E.; Petersen, T. E. *J. Biol. Chem.* **2002**, *277*, 9989.
- (232) Sussman, D.; Greensides, D.; Reilly, K.; Wilson, C. *Acta Crystallogr., Sect. D* **1999**, *D55*, 326.
- (233) Sussman, D.; Nix, J. C.; Wilson, C. *Nat. Struct. Biol.* **2000**, *7*, 53.
- (234) Sussman, D.; Wilson, C. *Structure (London)* **2000**, *8*, 719.
- (235) Lorsch, J. R.; Szostak, J. W. *Biochemistry* **1994**, *33*, 973.
- (236) Gulati, S.; Brody, L. C.; Banerjee, R. *Biochem. Biophys. Res. Commun.* **1999**, *259*, 436.
- (237) Lundrigan, M. D.; Kadner, R. J. *J. Bacteriol.* **1989**, *171*, 154.
- (238) Nou, X.; Kadner, R. J. *Proc. Natl. Acad. Sci. U.S.A.* **2000**, *97*, 7190.
- (239) Nahvi, A.; Sudarsan, N.; Ebert, M. S.; Zou, X.; Brown, K. L.; Breaker, R. R. *Chem. Biol.* **2002**, *9*, 1043.
- (240) Buckel, W.; Golding, B. T. *Chem. Soc. Rev.* **1996**, 329.
- (241) Golding, B. T.; Buckel, W. In *Comprehensive Biochemical Catalysis*; Sinnott, M. L., Ed.; Academic Press: London, 1997; Vol. 3, pp 239–259.
- (242) Drennan, C. L.; Huang, S.; Drummond, J. T.; Matthews, R. G.; Ludwig, M. L. *Science* **1994**, *266*, 1669.
- (243) Brown, K. L.; Zou, X.; Chen, G.; Xia, Z.; Marques, H. M. *J. Inorg. Biochem.* **2004**, *98*, 287.
- (244) Switzer, R. L. In *B<sub>12</sub>*; Dolphin, D., Ed.; Wiley: New York, 1982; Vol. 2, p 289.
- (245) Bothe, H.; Bröker, G.; Müller, U.; Schall, I.; Texter, S.; Golding, B. T.; Buckel, W. In *Vitamin B<sub>12</sub> and B<sub>12</sub> Proteins*; Kräutler, B., Arigoni, D., Golding, B. T., Eds.; Wiley-VCH: Weinheim, 1998; p 237.
- (246) Scheuring, E.; Padmakumar, R.; Banerjee, R.; Chance, M. R. *J. Am. Chem. Soc.* **1997**, *119*, 12192.
- (247) Fonda, E.; Michalowicz, A.; Randaccio, L.; Tazher, G.; Vlaic, G. *Eur. J. Inorg. Chem.* **2001**, 1269.
- (248) Miyamoto, E.; Watanabe, F.; Yamaji, R.; Inui, H.; Sato, K.; Nakano, Y. *J. Nutr. Sci. Vitaminol.* **2002**, *48*, 242.
- (249) Mancia, F.; Smith, G. A.; Evans, P. R. *Biochemistry* **1999**, *38*, 7999.
- (250) Mancia, F.; Evans, P. R. *Structure* **1998**, *6*, 711.
- (251) Dong, S.; Padmakumar, R.; Banerjee, R.; Spiro, T. G. *J. Am. Chem. Soc.* **1999**, *121*, 7063.
- (252) Padmakumar, R.; Padmakumar, R.; Banerjee, R. *Biochemistry* **1997**, *36*, 3713.
- (253) Chowdhury, S.; Banerjee, R. *J. Am. Chem. Soc.* **2000**, *122*, 5417.
- (254) Wetmore, S. D.; Smith, D. M.; Golding, B. T.; Radom, L. *J. Am. Chem. Soc.* **2001**, *123*, 7963.
- (255) Doll, K. M.; Bender, B. R.; Finke, R. G. *J. Am. Chem. Soc.* **2003**, *125*, 10877.
- (256) Doll, K. M.; Finke, R. G. *Inorg. Chem.* **2003**, *42*, 4849.
- (257) Brown, K. L.; Brooks, H. B. *Inorg. Chem.* **1991**, *30*, 3420.
- (258) Waddington, M. D.; Finke, R. G. *J. Am. Chem. Soc.* **1993**, *115*, 4629.
- (259) Chowdhury, S.; Banerjee, R. *Biochemistry* **1999**, *38*, 15287.
- (260) Padmakumar, R.; Taoka, S.; Padmakumar, R.; Banerjee, R. *J. Am. Chem. Soc.* **1995**, *117*, 7033.
- (261) Chowdhury, S.; Thomas, M. G.; Escalante-Semerena, J. C.; Banerjee, R. *J. Biol. Chem.* **2001**, *276*, 1015.
- (262) Vlasie, M.; Chowdhury, S.; Banerjee, R. *J. Biol. Chem.* **2002**, *277*, 18523.
- (263) Chen, H. P.; Marsh, E. N. *Biochemistry* **1997**, *36*, 7884.
- (264) Vlasie, M. D.; Banerjee, R. *J. Am. Chem. Soc.* **2003**, *125*, 5431.
- (265) Reitzer, R.; Gruber, K.; Jögl, G.; Wagner, U. G.; Bothe, H.; Buckel, W.; Kratky, C. *Structure (London)* **1999**, *7*, 891.

- (266) Champloy, F.; Jögl, G.; Reitzer, R.; Buckel, W.; Bothe, H.; Beatrix, B.; Broecker, G.; Michalowicz, A.; Meyer-Klaucke, W.; Kratky, C. *J. Am. Chem. Soc.* **1999**, *121*, 11780.
- (267) Grubber, K.; Reitzer, R.; Kratky, C. *Angew. Chem., Int. Ed.* **2001**, *40*, 3377.
- (268) Rétey, J. *Angew. Chem., Int. Ed. Engl.* **1990**, *29*, 355.
- (269) Hoffmann, B.; Konrat, R.; Bothe, H.; Buckel, W.; Kräutler, B. *Eur. J. Biochem.* **1999**, *263*, 178.
- (270) Tollinger, M.; Eichmüller, C.; Konrat, R.; Huhta, M. S.; Marsh, E. N. G.; Kräutler, B. *J. Mol. Biol.* **2001**, *309*, 777.
- (271) Hoffmann, B.; Tollinger, M.; Konrat, R.; Huhta, M. S.; Marsh, E. N. G.; Kräutler, B. *ChemBioChem* **2001**, *2*, 643.
- (272) Tollinger, M.; Konrat, B. H.; Hilbert, B. H.; Marsh, E. N. G.; Kräutler, B. *Structure* **1998**, *6*, 1021.
- (273) Poppe, L.; Bothe, H.; Bröker, G.; Buckel, W.; Stupperich, E.; Rétey, J. *J. Mol. Catal. B: Enzym.* **2000**, *10*, 345.
- (274) Huhta, M. S.; Chen, H.-P.; Hemann, C.; Hille, C. R.; Marsh, E. N. G. *Biochem. J.* **2001**, *355*, 131.
- (275) Chih, H.-W.; Marsh, E. N. G. *Biochemistry* **2001**, *40*, 13060.
- (276) Essenberg, M. K.; Frey, P. A.; Abeles, R. H. *J. Am. Chem. Soc.* **1971**, *93*, 1242.
- (277) Weisblat, D. A.; Babior, B. M. *J. Biol. Chem.* **1971**, *246*, 6064.
- (278) Roymoulik, I.; Chen, H.-P.; Marsh, E. N. G. *J. Biol. Chem.* **1999**, *274*, 11619.
- (279) Marsh, E. N. G. *Biochemistry* **1995**, *34*, 7542.
- (280) Huhta, M. S.; Ciceri, D.; Golding, B. T.; Marsh, E. N. G. *Biochemistry* **2002**, *41*, 3200.
- (281) Leutbecher, U.; Bocher, R.; Linder, D.; Buckel, W. *Eur. J. Biochem.* **1992**, *205*, 759.
- (282) Madhavapeddi, P.; Ballou, D. P.; Marsh, E. N. G. *Biochemistry* **2002**, *41*, 15803.
- (283) Marsh, E. N. G.; Ballou, D. P. *Biochemistry* **1998**, *37*, 11864.
- (284) Ratnatilleke, A.; Vrijbloed, J. W.; Robinson, J. A. *J. Biol. Chem.* **1999**, *274*, 31679.
- (285) Masuda, J.; Yamaguchi, T.; Tobimatsu, T.; Toraya, T.; Suto, K.; Shibata, N.; Morimoto, Y.; Higuchi, Y.; Yasuoka, N. *Acta Crystallogr., Sect. D* **1999**, *D55*, 907.
- (286) Masuda, J.; Shibata, N.; Morimoto, Y.; Toraya, T.; Yasuoka, N. *Structure (London)* **2000**, *8*, 775.
- (287) Shibata, N.; Masuda, J.; Morimoto, Y.; Yasuoka, N.; Toraya, T. *Biochemistry* **2002**, *41*, 12607.
- (288) Kratky, C.; Kräutler, B. In *Chemistry and Biochemistry of B<sub>12</sub>*; Banerjee, R., Ed; Wiley: New York, 1999; p 9.
- (289) Masuda, J.; Shibata, N.; Morimoto, Y.; Toraya, T.; Yasuoka, N. *J. Synchrotron Radiat.* **2001**, *8*, 1182.
- (290) Yamanishi, Ma.; Yunoki, M.; Tobimatsu, T.; Sato, H.; Matsui, J.; Dokiya, A.; Iuchi, Y.; Oe, K.; Suto, K.; Shibata, N.; Morimoto, Y.; Yasuoka, N.; Toraya, T. *Eur. J. Biochem.* **2002**, *269*, 4484.
- (291) Liao, D.-I.; Dotsen, G.; Turner, I.; Reiss, L.; Emptage, M. *J. Inorg. Biochem.* **2003**, *93*, 84.
- (292) Ushio, K.; Honda, S.; Toraya, T.; Fukui, S. *J. Nutr. Sci. Vitam. 1982*, *28*, 225.
- (293) Mori, K.; Tobimatsu, T.; Hara, T.; Toraya, T. *J. Biol. Chem.* **1997**, *272*, 32034.
- (294) Tobimatsu, T.; Kajiura, H.; Yunoki, M.; Azuma, M.; Toraya, T. *J. Bacteriol.* **1999**, *181*, 4110.
- (295) Toraya, T.; Mori, K. *J. Biol. Chem.* **1999**, *274*, 3372.
- (296) Kajiura, H.; Mori, K.; Tobimatsu, T.; Toraya, T. *J. Biol. Chem.* **2001**, *276*, 36514.
- (297) Mori, K.; Toraya, T. *Biochemistry* **1999**, *38*, 13170.
- (298) Magnusson, O. Th.; Frey, P. A. *Biochemistry* **2002**, *41*, 1695.
- (299) Poppe, L.; Hull, W. E.; Nitsche, R.; Graf, T.; Stupperich, E.; Rétey, J. *Helv. Chim. Acta* **1999**, *82*, 1250.
- (300) Fukuoka, M.; Yamada, S.; Miyoshi, S.; Yamashita, K.; Yamanishi, M.; Zou, X.; Brown, K. L.; Toraya, T. *J. Biochem. (Tokyo, Japan)* **2002**, *132*, 935.
- (301) Wagner, O. W.; Lee, H. A. J.; Frey, P. A.; Abeles, R. H. *J. Biol. Chem.* **1966**, *249*, 1751.
- (302) Abend, A.; Bandarian, V.; Reed, G. H.; Frey, P. A. *Biochemistry* **2000**, *39*, 6250.
- (303) Sauvageot, N.; Pichereau, V.; Louarme, L.; Hartke, A.; Auffray, Y.; Laplace, J.-M. *Eur. J. Biochem.* **2002**, *269*, 5731.
- (304) Poppe, L.; Stupperich, E.; Hull, W. E.; Buckel, T.; Rétey, J. *Eur. J. Biochem.* **1997**, *250*, 303.
- (305) Abend, A.; Bandarian, V.; Nitsche, R.; Stupperich, E.; Rétey, J.; Reed, G. H. *Arch. Biochem. Biophys.* **1999**, *370*, 138.
- (306) Abend, A.; Nitsche, R.; Bandarian, V.; Stupperich, E.; Rétey, J. *Angew. Chem., Int. Ed. Engl.* **1998**, *37*, 625.
- (307) Ke, S.-C.; Torrent, M.; Museav, D. G.; Morokuma, K.; Warncke, K. *Biochemistry* **1999**, *38*, 12681.
- (308) Babior, B. M.; Moss, T. H.; Orme-Johnson, W. H.; Benert, H. J. *J. Biol. Chem.* **1974**, *249*, 4537.
- (309) Warncke, K.; Schmidt, J. C.; Ke, S.-C. *J. Am. Chem. Soc.* **1999**, *121*, 10522.
- (310) Ke, S.-C.; Warncke, K. *J. Am. Chem. Soc.* **1999**, *121*, 9922.
- (311) Ke, S. C. *Biochim. Biophys. Acta* **2003**, *1620*, 267.
- (312) Canfield, J. M.; Warncke, K. *J. Phys. Chem. B* **2002**, *106*, 8831.
- (313) LoBrutto, R.; Bandarian, V.; Magnusson, O. Th.; Chen, X.; Schramm, V. L.; Reed, G. H. *Biochemistry* **2001**, *40*, 9.
- (314) Anderson, M. A.; Xu, Y.; Grissom, C. B. *J. Am. Chem. Soc.* **2001**, *123*, 6720.
- (315) Harkins, T. T.; Grissom, C. B. *Science* **1994**, *263*, 958.
- (316) Bandarian, V.; Reed, G. H. *Biochemistry* **2000**, *39*, 12069.
- (317) Bandarian, V.; Reed, G. H. *Biochemistry* **1999**, *38*, 12394.
- (318) Bandarian, V.; Poyner, R. R.; Reed, G. H. *Biochemistry* **1999**, *38*, 12403.
- (319) Booker, S.; Stubbe, J. *Proc. Nat. Acad. Sci. U.S.A.* **1993**, *90*, 8352.
- (320) Booker, S.; Licht, S.; Broderick, J.; Stubbe, J. *Biochemistry* **1994**, *33*, 12676.
- (321) Licht, S.; Gerfen, G. J.; Stubbe, J. *Science* **1996**, *271*, 477.
- (322) Licht, S. S.; Booker, S.; Stubbe, J. *Biochemistry* **1999**, *38*, 1221.
- (323) Chen, D.; Abend, A.; Stubbe, J.; Frey, P. A. *Biochemistry* **2003**, *42*, 4578.
- (324) Licht, S. S.; Lawrence, C. C.; Stubbe, J. *Biochemistry* **1999**, *38*, 1234.
- (325) Tamao, T.; Blakley, R. L. *Biochemistry* **1973**, *12*, 24.
- (326) Suto, R. K.; Whalen, M. A.; Finke, R. G. *Prepr. Biochem. Biotechnol.* **1999**, *29*, 273.
- (327) Brown, K. L.; Zou, X.; Li, J.; Chen, G. *Inorg. Chem.* **2001**, *40*, 5942.
- (328) Singh, D.; Tamao, Y.; Blakley, R. L. *Adv. Enzyme Regul.* **1977**, *15*, 81.
- (329) Licht, S. S.; Lawrence, C. C.; Stubbe, J. *J. Am. Chem. Soc.* **1999**, *121*, 7463.
- (330) Lawrence, C. C.; Gerfen, G. J.; Samano, V.; Nitsche, R.; Robins, M. J.; Rétey, J.; Stubbe, J. *J. Biol. Chem.* **1999**, *274*, 7039.
- (331) Suto, R. K.; Poppe, L.; Rétey, J.; Finke, R. G. *Bioorg. Chem.* **1999**, *27*, 451.
- (332) Poppe, L.; Rétey, J. *Eur. J. Biochem.* **1997**, *245*, 389.
- (333) Poppe, L.; Rétey, J. *Arch. Biochem. Biophys.* **1995**, *316*, 541.
- (334) Sintchak, M. D.; Arjara, G.; Kellogg, B. A.; Stubbe, J.; Drennan, C. L. *Nat. Struct. Biol.* **2002**, *9*, 293.
- (335) Gerfen, G. J.; Licht, S.; Willems, J. P.; Hoffman, B. M.; Stubbe, J. *J. Am. Chem. Soc.* **1996**, *118*, 8192.
- (336) Suto, R. K.; Whalen, M. A.; Finke, R. G. *Prepr. Biochem. Biotechnol.* **1999**, *29*, 273.
- (337) Suto, R. K.; Whalen, M. A.; Bender, B. R.; Finke, R. G. *Nucleosides Nucleotides* **1998**, *17*, 1453.
- (338) Chang, C. H.; Frey, P. A. *J. Biol. Chem.* **2000**, *275*, 106.
- (339) Morley, C. G. D.; Stadtman, T. C. *Biochemistry* **1970**, *9*, 4890.
- (340) Tang, K.-H.; Chang, C. H.; Frey, P. A. *Biochemistry* **2001**, *40*, 5190.
- (341) Chen, H.-P.; Wu, S.-H.; Lin, Y.-L.; Chen, C.-M.; Tsay, S.-S. *J. Biol. Chem.* **2001**, *276*, 44744.
- (342) Zhang, W.; Reynolds, K. A. *J. Bacteriol.* **2001**, *183*, 2071.
- (343) Gough, S. P.; Petersen, B. O.; Duus, J. O. *Proc. Natl. Acad. Sci. U.S.A.* **2000**, *97*, 6908.
- (344) Dixon, M. M.; Huang, S.; Matthews, R. G.; Ludwig, M. *Structure* **1996**, *4*, 1263.
- (345) Yamada, K.; Yamada, S.; Tobimatsu, T.; Toraya, T. *J. Biol. Chem.* **1999**, *274*, 35571.
- (346) Bandarian, V.; Matthews, R. G. *Biochemistry* **2001**, *40*, 5056.
- (347) Jarrett, J. T.; Hoover, D. M.; Ludwig, M. L.; Matthews, R. G. *Biochemistry* **1998**, *37*, 12649.
- (348) Bandarian, V.; Patridge, K. A.; Lennon, B. W.; Huddler, D. R.; Matthews, R. G.; Ludwig, M. L. *Nat. Struct. Biol.* **2002**, *9*, 53.
- (349) Bandarian, V.; Ludwig, M. L.; Matthews, R. G. *Proc. Natl. Acad. Sci. U.S.A.* **2003**, *100*, 8156.
- (350) Dorweiler, J. S.; Finke, R. G.; Matthews, R. G. *Biochemistry* **2003**, *42*, 14653.
- (351) Smith, A. E.; Matthews, R. G. *Biochemistry* **2000**, *39*, 13880.
- (352) Jarrett, J. T.; Choi, C. Y.; Matthews, R. G. *Biochemistry* **1997**, *36*, 15739.
- (353) Zydowski, T. M.; Courtney, L. F.; Frasca, V.; Kobayashi, K.; Shimizu, H.; Yuen, L.-D.; Matthews, R. G.; Benkovic, S. J.; Floss, H. G. *J. Am. Chem. Soc.* **1986**, *108*, 3152.
- (354) Goulding, C. W.; Matthews, R. G. *Biochemistry* **1997**, *50*, 88052.
- (355) PEARISO, K.; Goulding, C. W.; Huang, S.; Matthews, R. G.; Penner-Hahn, J. E. *J. Am. Chem. Soc.* **1998**, *120*, 8410.
- (356) Matthews, R. G.; Smith, A. E.; Zhou, Z. S.; Taugro, R. E.; Bandarian, V.; Evans, J. C.; Ludwig, M. *Helv. Chim. Acta* **2003**, *86*, 3939.
- (357) Ragsdale, S. W.; Lindahl, P. A.; Münch, E. *J. Biol. Chem.* **1987**, *262*, 14289.
- (358) Menon, S.; Ragsdale, S. W. *J. Biol. Chem.* **1999**, *274*, 11513.
- (359) Barondeau, D. P.; Lindahl, P. A. *J. Am. Chem. Soc.* **1997**, *119*, 3959.
- (360) Kumar, M.; Qiu, D.; Spiro, T. G.; Ragsdale, S. W. *Science* **1995**, *270*, 628.
- (361) Wirt, M. D.; Wu, J.-J.; Scheuring, E. M.; Kumar, M.; Ragsdale, S. W.; Chance, M. R. *Biochemistry* **1995**, *34*, 5269.
- (362) Seravalli, J.; Brown, K. L.; Ragsdale, S. W. *J. Am. Chem. Soc.* **2001**, *123*, 1786.
- (363) Seravalli, J.; Zhao, S.; Ragsdale, S. W. *Biochemistry* **1999**, *38*, 5728.
- (364) Seravalli, J.; Shoemaker, R. K.; Sudbeck, M. J.; Ragsdale, S. W. *Biochemistry* **1999**, *38*, 5736.

- (364) Zhao, S.; Roberts, D. L.; Ragsdale, S. W. *Biochemistry* **1995**, *34*, 15075.
- (365) Doukov, T.; Seravalli, J.; Stezowski, J. J.; Ragsdale, S. W. *Structure (London)* **2000**, *8*, 817.
- (366) Russell, W. K.; Stålhandske, C. M. V.; Xia, J. Q.; Scott, R. A.; Lindahl, P. A. *J. Am. Chem. Soc.* **1998**, *120*, 7502.
- (367) Tan, X. S.; Sewell, C.; Lindahl, P. A. *J. Am. Chem. Soc.* **2002**, *124*, 6277.
- (368) Deppenmeier, U.; Müller, V.; Gottschalk, G. *Arch. Microbiol.* **1996**, *165*, 149.
- (369) Weiss, D. S.; Gärtner, P.; Thauer, R. K. *Eur. J. Biochem.* **1994**, *226*, 799.
- (370) Harms, U.; Thauer, R. K. *Eur. J. Biochem.* **1997**, *250*, 783.
- (371) Hippler, B.; Thauer, R. K. *FEBS Lett.* **1999**, *449*, 165.
- (372) Sauer, K.; Thauer, R. K. *Eur. J. Biochem.* **1998**, *253*, 653.
- (373) Sauer, K.; Thauer, R. K. *Eur. J. Biochem.* **1997**, *249*, 280.
- (374) Grahame, D. A. *J. Biol. Chem.* **1989**, *264*, 12890.
- (375) Sauer, K.; Thauer, R. K. *Eur. J. Biochem.* **1999**, *261*, 674.
- (376) Yeliseev, A.; Gärtner, P.; Harms, U.; Linder, D.; Thauer, R. K. *Arch. Microbiol.* **1993**, *159*, 530.
- (377) Ferguson, D. J., Jr.; Gorlatova, N.; Grahame, D. A.; Krzycki, J. A. *J. Biol. Chem.* **2000**, *275*, 29053.
- (378) Burke, S. A.; Krzycki, J. A. *J. Biol. Chem.* **1997**, *272*, 16570.
- (379) Kremer, J. D.; Cao, X.; Krzycki, J. *J. Bacteriol.* **1993**, *175*, 4824.
- (380) Tallant, T. C.; Krzycki, J. A. *J. Bacteriol.* **1996**, *178*, 1295.
- (381) Tallant, T. C.; Paul, L.; Krzycki, J. A. *J. Biol. Chem.* **2001**, *276*, 4485.
- (382) Daniel, S. L.; Wu, Z.; Drake, H. L. *FEMS Microbiol. Lett.* **1988**, *52*, 25.
- (383) Naidu, D.; Ragsdale, S. W. *J. Bacteriol.* **2001**, *183*, 3276.
- (384) Engelmann, T.; Kaufmann, F.; Diekert, G. *Arch. Microbiol.* **2001**, *175*, 376.
- (385) Kaufmann, F.; Wohlfarth, G.; Diekert, G. *Arch. Microbiol.* **1997**, *168*, 136.
- (386) Vannelli, T.; Messmer, M.; Studer, A.; Vuilleumier, S.; Leisinger, T. *Proc. Natl. Acad. Sci. U.S.A.* **1999**, *96*, 4615.
- (387) Studer, A.; Vuilleumier, S.; Leisinger, T. *Eur. J. Biochem.* **1999**, *264*, 242.
- (388) Studer, A.; Stupperich, E.; Vuilleumier, S.; Leisinger, T. *Eur. J. Biochem.* **2001**, *268*, 2931.
- (389) Coulter, C.; Hamilton, J. T. G.; McRoberts, W. C.; Kulakov, L.; Larkin, M. J.; Harper, D. B. *Appl. Environ. Microbiol.* **1999**, *65*, 4301.
- (390) Lee, J.-Y.; Park, H.-S.; Kim, H.-S. *J. Bacteriol.* **1999**, *181*, 2953.
- (391) Lee, J. Y.; Jung, K. H.; Choi, S. H.; Kim, H. S. *Appl. Environ. Microbiol.* **1995**, *61*, 2211.
- (392) Wohlfarth, G.; Diekert, G. *FEMS Microbiol. Rev.* **1998**, *22*, 383.
- (393) Neumann, A.; Wohlfarth, G.; Diekert, G. *J. Biol. Chem.* **1996**, *271*, 16515.
- (394) Neumann, A.; Siebert, A.; Diekert, G. *Biol. Abwasserreinigung* **2001**, *15*, 137.
- (395) Neumann, A.; Siebert, A.; Trescher, T.; Reinhardt, S.; Wohlfarth, G.; Diekert, G. *Arch. Microbiol.* **2002**, *177*, 420.
- (396) Ni, S.; Fredrickson, J. K.; Xun, L. *J. Bacteriol.* **1995**, *177*, 5135.
- (397) Löffler, F. E.; Sanford, R. A.; Tiedje, J. M. *Appl. Environ. Microbiol.* **1996**, *62*, 3809.
- (398) Christiansen, N.; Ahring, B. K.; Wohlfarth, G.; Diekert, G. *FEBS Lett.* **1998**, *436*, 159.
- (399) Van de Pas, B. A.; Smidt, H.; Hagen, W. *J. Biol. Chem.* **1999**, *274*, 20287.
- (400) Schmacer, W.; Holliger, C.; Zehnder, A. J. B.; Hagen, W. R. *FEBS Lett.* **1997**, *409*, 42.

CR030720Z

